Unravelling the signaling cascade mediating microglial pro-inflammatory responses in Parkinsonian Syndrome

by

Souvarish Sarkar

A dissertation submitted to the graduate faculty
in partial fulfillment of the requirements for the degree of

DOCTOR OF PHILOSOPHY

Co-majors: Molecular, Cellular, & Developmental Biology; Toxicology

Program of Study Committee:

Anumantha Kanthasamy, Co-major Professor
Arthi Kanthasamy, Co-major Professor
Jeffery Essner
Marian Kohut
Thimmasettappa Thippeswamy

The student author, whose presentation of the scholarship herein was approved by the program of study committee, is solely responsible for the content of this dissertation. The Graduate College will ensure this dissertation is globally accessible and will not permit alterations after a degree is conferred.

Iowa State University

Ames, Iowa

2018

TABLE OF CONTENTS Page

ABSTRACT

In vitro cell culture, *ex vivo* brain slice culture, and *in vivo* model systems of Parkinson's disease (PD), as well as postmortem brains from PD patients, have implicated microglial hyperactivation, mediated by inflammatory ligands, in the loss of dopaminergic neurons in the substantia nigra region of the brain. The signaling pathways leading to this chronic, sustained microglial activation in response to environmental stressors or disease-associated molecular patterns (DAMPs) are not clearly understood. We show herein the role of mitochondrial dysfunction in mediating pro-inflammatory signaling cascades in microglial cells in response to environmental factors such as pesticides and metals. Exposure to the pesticides rotenone and tebufenpyrad as well as the neurotoxic divalent metal manganese (Mn) leads to the activation of the NLRP3 pro-inflammatory signaling cascade in microglial cells. Mitochondrial superoxide generation plays a key role in activation of the NLRP3 inflammasome. Furthermore, activation of NLRP3 produces neurotoxic factors, like IL-1β and IL-18, that lead to neurodegeneration. The novel mitochondria-targeted antioxidant mito-apocynin was able to reduce mitochondrial superoxide generation and NLRP3 inflammasome activation. We also demonstrated that Mn leads to mitochondrial dysfunction by downregulation of mitochondrial fusion protein (Mfn2). Lastly, we show that Mn exposure leads to the propagation of the NLRP3 inflammasome through the mechanism of exosomal release of ASC, an inflammasome component. This finding has high translational relevance since exosomes isolated from welder cohorts known to have been exposed to Mn fumes

carry a higher exosomal load of ASC. Collectively, we demonstrated the gene-environment crosstalk which modulates neuroinflammation and neurodegeneration.

Alpha-synuclein aggregates are a major component of Lewy bodies and neurites, which are pathological hallmarks of PD. Classical activation of microglial cells has been shown to be mediated by pre-formed fibrillar α-synuclein (αSyn_{Agg}), but the signaling mechanism is not well understood. We sought to identify the role of microglial potassium channels in regulating αSyn_{Agg}-induced neuroinflammation. We show conclusively, in both cell culture and animal models of PD, that αSyn_{Agg}-induced neuroinflammation is associated with upregulation of the voltage-gated potassium channel Kv1.3. Remarkably, Kv1.3 was also highly induced in post-mortem PD patient tissues, as well as in peripheral blood mononuclear cells (PBMC) isolated from PD patients. We show that Fyn kinase, a src family kinase, regulates Kv1.3 transcriptionally through the p38 MAPK and NFκB pathways. Fyn was also observed to directly bind to Kv1.3, phosphorylating tyrosine 139 to modulate the channel's activity. Lastly, we demonstrate that Kv1.3 inhibition reduces neuroinflammation and neurodegeneration *in vitro* and in preclinical setups. Overall, we identify key mechanistic pathways in response to both environmental stressors and DAMPs which strongly contribute to the chronic microglial pro-inflammatory responses that characterize PD-associated neuroinflammation.

CHAPTER I

GENERAL INTRODUCTION

Thesis Layout & Organization

The alternative format was chosen for this thesis and consists of manuscripts that have been formatted for submission to peer-reviewed journals. The dissertation contains a general introduction, three research papers, general conclusions, future directions charting out where the research story will be taken next, and two appendices which have also been prepared for publication. Because of the Dissertation's journal format, each manuscript chapter includes a list of references cited. However, references pertaining to the background and literature review, as well as those used in the general conclusions are listed separately at the end of the dissertation. The Introduction in Chapter 1 provides a background and overview of Parkinson's disease (PD). Chapter 2 covers current evidence implicating a pathogenic role for reactive microgliosis in mediating progressive dopaminergic neuron loss in PD, and concentrates on the effect of environmental stressors in activating glial cells that leads to neuroinflammation. This provides an overview of the research objectives pertaining to Chapters 4 and 5. Chapter 3 pertains to Chapter 6 and gives a brief introduction of the different microglial ion channels with respect to their role in inflammation and their potential as drug targets. The manuscript from Chapter 2 was recently published in *Npj Parkinson's Disease*. It elucidates the role of mitochondrial complex-I inhibitors in activating the NLRP3 inflammasome signaling pathway in cell culture and animal models of PD. Chapter 3 explores how neurotoxic manganese (Mn^{2+}) can induce and propagate the NLRP3 inflammasome. This manuscript is

currently under preparation for submission in *Science Signaling*. Chapter 4 studies how the voltage-gated potassium channel Kv1.3 contributes to microgliosis and inflammasome activation in cell culture and animal models of PD as well as in human post-mortem PD brain tissues. Chapter 4 is being prepared for submitting for publication. Chapter 5 is a general conclusion of the findings and provides future directions.

Apart from the five chapters, this thesis consists of two appendices. Appendix 1 is on developing a faster method for isolating primary microglial cells used for most of the studies in Chapter 2. This method was published in the *Journal of Visualized Experiments*. Appendix 2, is under revision in *Neurotoxicology,* is a comparative analysis and characterization of a recently developed microglial cell line that was used for conducting the studies in Chapters 3 and 4.

All of the research described by the author in this thesis was performed during the course of his doctoral studies at Iowa State University under the guidance of his major professors, Drs. Anumantha G. Kanthasamy and Arthi Kanthasamy.

Introduction

Parkinson's names a disease whose symptomology has been known about since ancient times. The ancient Indian medical system of Ayurveda refers to it as “Kampavata.” In Western medical literature, it was described in AD 175 by the Greek physician Galen as the "shaking palsy". However, it was not until 1817 that a detailed medical article, "An Essay on the Shaking Palsy", was published by the London doctor James Parkinson, thereby “paralysis agitans” as a recognized medical condition. Parkinson’s essay arose from the examination or interview of six people who manifested the symptoms. In 1872, after an even more detailed study of its full clinical spectrum, the French neurologist Jean Martin Charcot renamed it Parkinson's disease since there was much more to the disease than just paralysis and tremor.

Symptoms of the disease are progressive and degenerative and it tends to more often afflict older individuals. Although a dopamine deficiency in the brain is what triggers the most recognizable motor symptoms, why this initially occurs is less clear. Though PD has been known for more than a century there is no cure for PD. L-dopa is a dopamine replacement therapy which is the gold standard for PD treatment till date. In Ayurvedic literature, and a current study showed that *Mucuna pruriens* extract can reduce PD like symptoms in a rodent model of PD and contains L-dopa and other unknown anti-parkinsonian compound (Manyam, 1990).

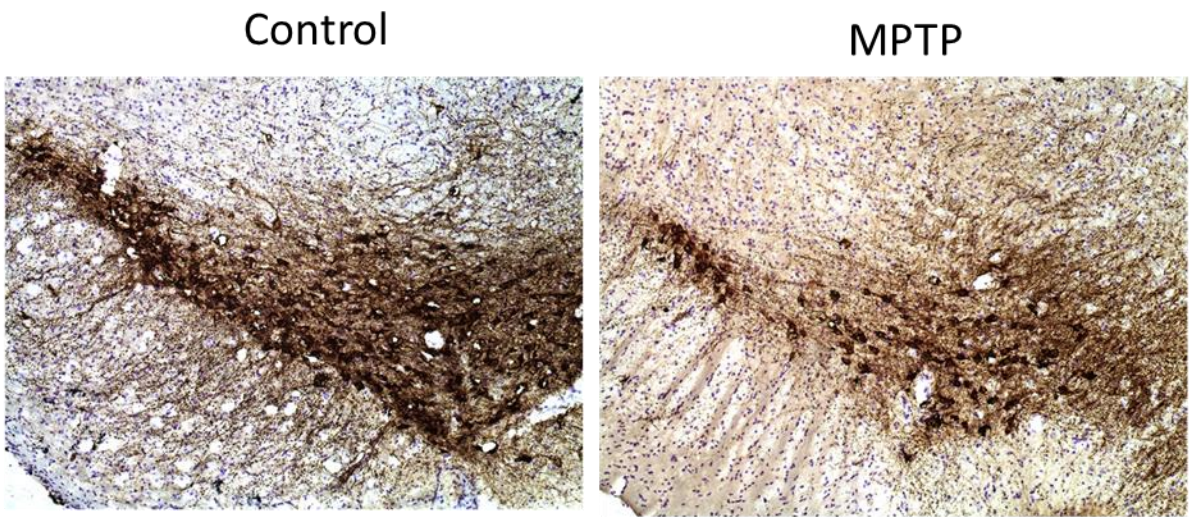

Fig 1. Loss of dopaminergic neurons in substantia nigra region in MPTP mouse model of PD

Parkinson's disease (PD) is the most common neurodegenerative movement disorder affecting around 2% of the population over the age of 60, and its incidence is expected to rise dramatically with the advancing median age of the population, worsening the substantial socioeconomic burden on patients, their families, and society. The main pathological hallmark of this disease is the degeneration of dopaminergic (DAergic) neurons within the nigrostriatal tract that project from the substantia nigra (SN) to the striatum, resulting in a severe depletion of striatal DA that clinically manifests as a range of debilitating motor symptoms (Lotharius and Brundin, 2002; Wolters, 2009). The underlying mechanism of the neuronal degeneration is not well understood but mitochondrial dysfunction, chronic inflammation, and oxidative stress have been implicated in different animal models of PD (Goldman, 2014; Mullin and Schapira, 2015). The role of inflammation in PD was first suggested in 1988 when major histocompatibility complex molecules were shown to be upregulated in PD patients (Whitton, 2007). Various pro-inflammatory factors like tumor necrosis factor

α (TNF-α) and IL-1β have been shown to be upregulated in cerebrospinal fluid (CSF) and different regions of the brain in PD patients (Nagatsu et al., 2000). Moreover, in animal models of PD, such as the 6-OHDA, MPTP, and rotenone models, selective loss of dopaminergic neurons is accompanied by chronic inflammation (Ghosh et al., 2016; Kosloski et al., 2013; Panicker et al., 2015). Treatment with non-steroidal anti-inflammatory drugs (NSAIDs), like ibuprofen, can be effective against PD-related inflammation (Rees et al., 2011).

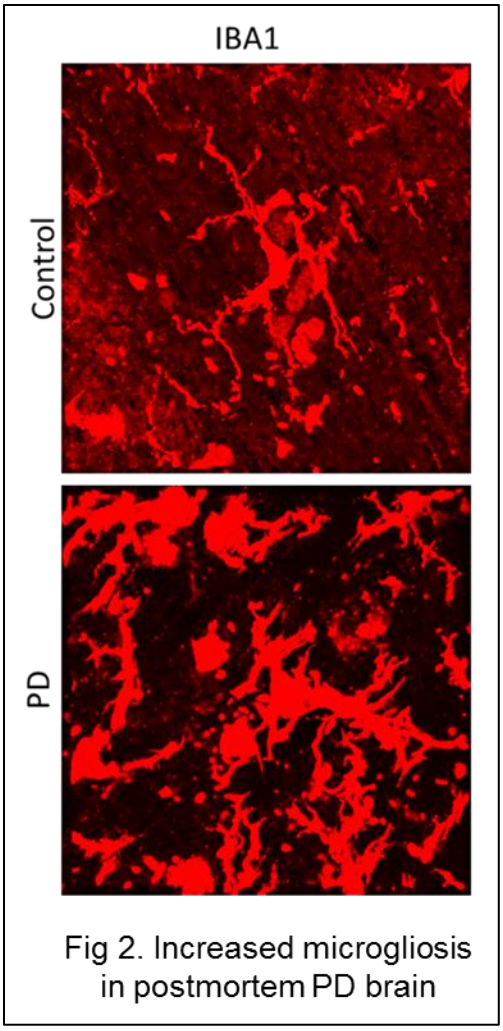

Fig 2. Increased microgliosis in postmortem PD brain

Microglia are resident immune cells of the brain that primarily mediate brain inflammation (Gammon, 2013; Liu and Hong, 2003). Depending on the stimuli, microglia secrete both anti-inflammatory and pro-inflammatory factors, as well as growth factors, thereby tightly controlling neuronal survival (Mosley et al., 2012). Glial activation leading to inflammation have been well documented both in peripheral and central nervous system in PD (Table 1). Though microglia have been identified as key modulators of chronic neuroinflammation, the underlying mechanisms remain equivocal. Hence, understanding the mechanisms driving this chronic inflammation in the brain may lead to a better understanding of disease pathogenesis and progression.

Table 1: Inflammatory Markers found in PD patients

Method	**Inflammatory marker**	**Sample**	**Reference**
PET scan	[^{11}C]-(*R*)-PK11195-PET Activated microglia	Live patient	(Gerhard, 2016)
Immuno-histochemistry	HLADR Activated Microglia	Post Mortem Brain	(McGeer et al., 1988)
Protein detection	TNFα	Cerebrospinal fluid	(Mogi et al., 1994)
Luminex, and qPCR	TNFα, IL-1β and other pro-inflammatory factor	Peripheral blood monocytes	(Grozdanov et al., 2014)

Table 2: List of genes associated with Parkinsonian Syndrome

Symbol	**Gene Name**	**Inheritance**	**Disease**
PARK 1	SNCA	Autosomal Dominant	Early Onset PD
PARK 2	Parkin	Autosomal Recessive	Early Onset PD
PARK 3	Unknown	Autosomal Dominant	Classical PD
PARK 4	SNCA	Autosomal Dominant	Early Onset PD
PARK 5	UCHL1	Autosomal Dominant	Classical PD
PARK 6	PINK1	Autosomal Recessive	Early Onset PD
PARK 7	DJ1	Autosomal Recessive	Early Onset PD
PARK 8	LRRK2	Autosomal Dominant	Classical PD
PARK 9	ATP13A2	Autosomal Recessive	Atypical PD
PARK 10	Unknown	Risk Factor	Classical PD
PARK 11	Unknown	Autosomal Dominant	Late Onset PD
PARK 12	Unknown	Risk Factor	Classical PD
PARK 13	HTRA1	Autosomal Dominant	Classical PD
PARK 14	PLA2G6	Autosomal Recessive	Early-onset dystonia-parkinsonism
PARK 15	FBXO7	Autosomal Recessive	Early-onset parkinsonian-pyramidal syndrome
PARK 16	Unknown	Risk Factor	Classical PD
PARK 17	VPS35	Autosomal Dominant	Classical PD

Table 2. (continued)

PARK 18	EIF4G1	Autosomal Dominant	Classical PD
PARK 19	DNAJC6	Autosomal Recessive	Early Onset PD
PARK 20	SYNJ1	Autosomal Recessive	Early Onset PD
PARK 21	DNAJC13	Autosomal Dominant	Classical PD
PARK 22	CHCD2	Autosomal Dominant	Late Onset PD
PARK 23	VPS13C	Autosomal Recessive	Early Onset PD

PD is a multifactorial disease with several associated genes as mentioned in Table 1. having diverse roles with regards to the neuroinflammation contributing to PD pathology. Microglial cells can be classically activated by αSyn_{Agg}, leading to the production of proinflammatory factoras like TNFα, IL-1β, nitrites, and others (Kim, C. et al., 2013; Lee et al., 2010; Su et al., 2008). *LRRK2*, a gene associated with autosomal dominant disease, activates microglial pro-inflammatory signaling pathways (Moehle et al., 2012). Loss of function in *PINK1* and *DJ1* induces microglial activation through activation of the NF-κB pathway (Kim, J. et al., 2013) and the hyperactivation of STAT1, respectively (Kim, J.H. et al., 2013). More than 90% of PD cases are sporadic and the effect of environment in PD pathogenesis cannot be overlooked. Exposure to environmental toxicants, such as pesticides and metals, have been linked to a higher risk of developing PD. These environmental stressors have

been shown to induce microglial activation and neuroinflammation. Rotenone, a classical PD toxicant, activates microglial cells leading to the production of proinflammatory neurotoxic factors (Sarkar et al., 2017). Overexposure to the divalent metal manganese (Mn) activates the proinflammatory signaling cascade in microglial and astroglial cells (Dodd and Filipov, 2011; Filipov et al., 2005; Kirkley et al., 2017). Recently, diesel exhaust particles (DEP) have also been implicated in microglial activation (Levesque et al., 2013). The cellular events triggered by environmental stressors suggest a crosstalk between genes and the environment. Thus, mapping out the novel signaling pathways underlying the hyperactivation of microglia would serve to identify attractive drug targets with the potential to slow or halt the progression of PD.

CHAPTER II

THE ROLE OF ENVIRONMENTAL TOXICANTS IN REGULATING NEUROINFLAMMATION IN PARKINSONIAN SYNDROME: GENE X ENVIRONEMENT

Manuscript to be submitted to *Toxicological Sciences*

Souvarish Sarkar, Emir Malovic, Huajun Jin, Vellareddy Anantharam, Arthi Kanthaasamy, Anumantha Kanthasamy.

Parkinson Disorders Research Laboratory, Iowa Center for Advanced Neurotoxicology, Department of Biomedical Sciences, 2062 Veterinary Medicine Building, Iowa State University, Ames, IA 50011

*To whom correspondence should be addressed: Anumantha Kanthasamy, Ph.D. Distinguished Professor and Chair, Department of Biomedical Sciences, Iowa State University, Ames, IA 50011, Telephone: (515) 294-2516; Fax: (515) 294-2315, Email: akanthas@iastate.edu

Abstract

Parkinson's disease is the most prevalent motor disorder and is characterized by loss of dopaminergic neurons in the substantia nigra pars compacta (SNpc) region of the brain. Though the pathology of PD is well established the cause of this cell death is not well understood. 90% of PD is sporadic and environment plays a major role in disease pathogenesis. The etiology of PD is complex. Neuroinflammation is one of the key factors that have been implicated in neuronal loss. Non-steroidal anti-

inflammatory drugs (NSAID's) have been shown to reduce risk of developing PD. But the signaling mechanism underlying neuroinflammation is equivocal. Astroglia and microglia are the two key immune cells which play an important role in maintain the neurons. Recently, astroglial and microglial activation have been linked to PD. Exposure to environmental stressors from various sources have been shown to affect these glial cells. Exposure to complex I-inhibiting pesticides rotenone have been shown to induce inflammation and neurodegeneration in animal models. Further rotenone, can induce NLRP3 inflammasome activation, leading to chronic inflammation, in microglial cells. Paraquat, the most widely used herbicide, have been shown to directly induce microglial NOX2 leading to oxidative stress and inflammation. Moreover, overexposure to neurotoxic metals like Manganese (Mn) have been implicated in a PD-like disease manganism. Occupational exposure to Mn have been shown to induce microglial activation. Mn can cause mitochondrial dysfunction in astroglial cells leading to inflammation. Mn can further potentiate the effect of LPS on microglial cells. This neurotoxic metal has been shown to induce the pro-inflammatory pathway nuclear factor κB (Nfκb). Moreover, recent studies have shown that diesel fume exhaust leads to microglial activation in mouse model. In this review, we discuss the recent advances in our knowledge, the mechanism of microglial response and activation to changes in extracellular milieu.

Introduction

Glial hyper-activation and inflammation have been linked to multiple neurodegenerative disorders including Alzheimer's disease (AD), Parkinson's disease (PD) among others (Block et al., 2007; Halle et al., 2008; Heneka et al., 2013). But the mechanism underlying glial activation is still under active research. Multiple signaling proteins like NADPH oxidase (NOX), Nuclear factor kb (NFκb), and the inflammasomes have been linked to glial inflammation (Panicker et al., 2015; Langley et al., 2017a; Sarkar et al., 2017b).

Environment plays a major role in pathogenesis of PD, with around 90% PD cases being sporadic. Exposure to metals, pesticides, traumatic brain injury among others have been linked to higher incidence of PD (Rokad et al., 2016; Harischandra et al., 2017; Sarkar et al., 2017a). These environmental factors play a key role in glial inflammation (Lawana et al., 2017). This review summarizes some of the key signaling pathways involved in glial inflammation and the crosstalk of environmental factors with these signaling proteins leading to sustained inflammation in a neurodegenerative environment.

Signaling Pathways

NOX enzyme complex

NADPH oxidase is a membrane bound enzyme complex which are involved in generating superoxide. The cellular localization of NOX varies depending on the NOX catalytic subunit (Fig. 1). Till date, 7 NOX catalytic units, namely Nox1 (Banfi et al., 2000), Nox2 (Cheng et al., 2001; Segal, 2005) , NOX3 (Cheng et al., 2001), NOX4 (Geiszt et al., 2000), NOX5 (Banfi et al., 2001), Duox1 (Edens et al., 2001), and Duox2

(Edens et al., 2001) have been identified. In microglia NOX2 plays an important role in regulating inflammation. Phosphorylation of a subunit of NOX2, p47phox, leads to activation of this enzyme complex in glial cells (Roepstorff et al., 2008). Multiple kinases including MAPK, PKC isoforms and others have been shown to phosphorylate NOX2 in glial cells (Belarbi et al., 2017). LPS treatment induced NOX2 activation in microglial cells leading to inflammation. Reduction of NOX2 activation has been shown to reduce inflammation in glial cells (Langley et al., 2017a). NOX2 have been shown to play a critical role in PD pathogenesis. NOX2 deficient mice fail to induce dopaminergic neuronal loss and inflammation in MPTP mouse model of PD (Wu et al., 2003). Furthermore, inhibition of NOX2 using a derivative of Apocynin, mito-apocynin was shown to protect neuronal loss in MPTP and Mitopark mouse model of PD (Ghosh et al., 2016; Langley et al., 2017a). Recently, NOX4 have been shown to be upregulated in PD patients suggesting a probable role of NOX4 activation in PD pathogenesis (Zawada et al., 2015). Given the mitochondrial localization of NOX4, the activation of this catalytic unit may drive the glial inflammation as recent studies have linked mitochondrial superoxide generation in regulating glial inflammation (Sarkar et al., 2017b). Further studies looking into the possible mechanism of NOX4 induced inflammation may lead to identification of key anti-inflammatory targets.

Nfκb pro-inflammatory pathways

Nuclear factor kb (NFκb) activation in microglia cells have been termed as the “holy grail” for anti-inflammatory drug targets (Lawrence, 2009). The NFκb transcription factor consist of various subunits like p50, p65 and others. Inhibitor of Nfκb (Iκb) binds to the subunits of NFκb and inhibits its translocation into the nucleus.

Under inflammagen stress, Iκb gets phosphorylated by Iκb kinase (IKK) and marked for degradation, which leads to the translocation of p50-p65 heterodimer into the nucleus and transcription of pro-inflammatory factors like IL-1β, TNFα and NOS2 (Panicker et al., 2015). This activation of NFκb is termed as the classical activation or the canonical pathway of NFκb. Alternative activation of NFκb leads to translocation of RelB-p52 to nucleus. Though the role of this type of NFκb activation is not clear in inflammation, alternative activation plays a role in B-lymphocyte function (Bonizzi et al., 2004). Recently, another alternative activation of NFκb have been discovered which leads to nuclear translocation of p50-p50 homodimer leading to production of anti-inflammatory factors. P50 KO mice were more susceptible to endotoxemia. Further, p50 was shown to regulate anti-inflammatory factor IL-10 suggesting its role in antiinflammation (Cao et al., 2006). Activation of classical NFκb pathway have been linked to neuroinflammation in glial cells leading to secondary neurodegeneration in AD, PD and other neurodegenerative disease (Block et al., 2007; Shih et al., 2015).

Inflammasomes

Inflammasomes were first described by Tschopp in the early 2000s, as large, cytosolic multimeric assembly platforms, that effect the activation of pro-inflammatory caspases such as Caspase-1. Recently, studies on microglial cells have shown that rotenone can induce NLRP3 inflammasome activation by regulating mitochondrial dysfunction and autophagy (Lawana et al., 2017; Martinez et al., 2017; Sarkar et al., 2017b). In the last decade, inflammasome activation have been implicated as a key molecular mechanism regulating inflammation in immune cells. NLRP3 inflammasome is one of the major functional inflammasome in microglial which has

been implicated in neurodegenerative disorders including AD (Halle et al., 2008; Heneka et al., 2013). Inflammasomes are tightly regulated processes in cells which require two signals for activation. Signal I generally activate the Nfκb activation leading to transcription of NLRP3, pro-IL-18 and pro-IL-1β. Signal II, which can be disease associated molecular patterns, and pathogen associated molecular patterns, through some unknown mechanism leads to the assembly of NLRP3 inflammasome complex and cleavage of pro-IL-18 and pro-IL-1β to its matured form and secreted. Potassium efflux have also been implicated in activation of inflammasomes. The inflammasome complex consist of NLR3, the adapter protein ASC, and pro-Caspase 1. Upon activation caspase-1 is cleaved by autolytic cleavage (Freeman and Ting, 2016) which in turn cleaves pro-IL-1β and pro-IL-18 to its active matured form (Fig. 2).

Environmental Factors

Pesticides

Rotenone

Rotenone is a classical PD toxicant and is a mitochondrial complex I inhibitor. Rotenone have been shown to cause dopaminergic neuronal loss *in vitro* and *in vivo* (Sherer et al., 2007; Cannon et al., 2009; Inden et al., 2011; Charli et al., 2016). Further analysis showed that microglia are activated by rotenone to produce superoxide, which is selectively toxic to dopaminergic neurons, and dependent on NOX2, as genetic deletion of NOX2 was neuroprotective against rotenone (Gao et al., 2003). Rotenone exposure in rodent models have been shown to induce microglial activation (Sarkar et al., 2017b). Mount *et al.* , further demonstrated that microglia

isolated from IFNγ deficient microglia, did not induce dopaminergic neuronal death in response to rotenone treatment (Mount et al., 2007).

Our group along with others have recently shown the importance of mitochondrial dynamics in regulating glial inflammation (Zhou et al., 2011; Sarkar et al., 2017a; Sarkar et al., 2017b). A recent report suggested that rotenone induced neuroinflammation can be reduced by opening of ATP-dependent mitochondrial potassium channel, K_{ATP}. The opening of this channel reduced p38 MAPK activity thereby reducing inflammation in microglial cells (Zhou et al., 2008).

Rotenone have been shown to induce microglial activation in BV2 microglial cell line leading to production of iNos, and other proinflammatory factors like TNFα and IL-1β. N-acetylcysteine, an ROS scavenger, was shown to reduce this rotenone-induced inflammation by reducing Nfκb and p38 MAPK activation. This suggests the probable role of rotenone-induced ROS in activating the abovementioned inflammatory signaling cascade in microglial cells (Gao et al., 2013). Rotenone has further been shown to directly interact with membrane bound NOX2, the catalytic subunit of NOX2 enzyme complex, thereby playing an important role in superoxide and ROS generation. Diphenyleneiodonium, a NOX inhibitor, reduced the interaction of rotenone with this enzyme complex (Zhou et al., 2012).

Recent studies by Zhao *et al.* showed that exposure to rotenone lead to induction of NLRP3 inflammasome in macrophage (Zhou et al., 2011). Our group have demonstrated that rotenone exposure leads to NLRP3 inflammasome activation in microglial cells in cell culture and animal models. We have further shown that mitochondrial superoxide formation plays an important role in rotenone induced

inflammasome activation. Treatment with mitochondrially targeted derivative of anti-oxidant of apocynin, mito-apocynin, reduced NLRP3 inflammasome assembly and dopaminergic neuronal death by reducing rotenone-induced superoxide generation (Sarkar et al., 2017b). Lawana *et al.* further demonstrated that c-abl tyrosine kinase regulates rotenone-induced NLRP3 inflammasome activation by modulating the priming step of inflammasome and by reducing the dysregulation of mitochondrial dynamics (Lawana et al., 2017). Rifampicin, an antibacterial drug used in tuberculosis, has been further shown to reduce microglial activation by reducing rotenone-induced NLRP3 inflammasome activation (Liang et al., 2015).

Paraquat

Paraquat (N,N′ -dimethyl-4,4′-bipyridinium dichloride), one of the widely used herbicides, have been linked to higher PD risk (Hertzman et al., 1990; Cicchetti et al., 2005; Costello et al., 2009), and selective loss of DA neurons in substantia nigra region in rodent models (Cicchetti et al., 2005). Apart from having direct neurotoxic activity, paraquat can activate microglial cells by activating NOX2 in culture (Bonneh-Barkay et al., 2005). PHOX -/- mice , lacking the catalytic subunit of NOX2 have attenuated neurotoxicity and glial activation post paraquat exposure (Wu et al., 2005). NADPH oxidase inhibitor, apocynin, have been shown to reduce paraquat induced glial activation (Miller et al., 2007). Furthermore, a novel isoform of PKC, PKCδ, have been shown to play a role in paraquat mediated toxicity. Treatment with PKCδ specific inhibitor, rottlerin, inhibited paraquat induced NOX2 activation and ROS generation (Miller et al., 2007). Recent studies by Castello et al. suggested that mitochondria are a key source of paraquat induced H_2O_2 production. This study further showed that

mitochondrial complex III, and mitochondrial transmembrane potential is a key player in the ROS generation and acts as a redox modulator (Castello et al., 2007). Our studies in microglia suggested that mitochondrial ROS drives inflammasome activation (Sarkar et al., 2017b). But further studies looking the role of redox modulation by paraquat leading to inflammasome activation is required. These studies further show that paraquat leads to glial activation by interacting with NOX2 and leading to ROS generation.

Other Pesticides

Other than rotenone and paraquat, other pesticides like dieldrin, tebufenpyrad and organophosphates have been shown to modulate microglial inflammation and proliferation. Exposure to dieldrin, an organochloride, have been shown to cause dopaminergic neuronal loss (Song et al., 2010). Dieldrin was shown to induce generation of ROS in microglial cells (Mao and Liu, 2008) which have been shown to cause neuronal damage. NOX inhibitors reduced the microglia generated ROS post dieldrin exposure (Mao et al., 2007). Tebufenpyrad, a complex 1 inhibitor have been shown to induce dopaminergic neuronal death in cell culture (Charli et al., 2016). Our group further showed that tebufenpyrad induced NLRP3 inflammasome activation in microglial cells leading to release of IL-1β (Sarkar et al., 2017b). Organophosphate pesticide diisopropylflurophosphate (DFP) have been shown to neurotoxic. A recent study showed that DFP can also activate microglial cells in the hippocampus leading to production of proinflammatory factors like IL-1β and TNFα (Li et al., 2015). These studies together suggest that pesticide exposure can lead to glial inflammation through crosstalk with known inflammatory mediators like NOX and NFκb.

Metals

Prolonged exposure to heavy metals at occupational sites has revealed much about the environmental linkages to the etiology of neurodegenerative disorders such as Alzheimer's (AD) and Parkinson's (PD)(Rokad et al., 2016).

Manganese

Aerial overexposure to the transition metal manganese (Mn) was first noted in miners(Archibald and Tyree, 1987), and subsequently in industrial workers like welders (Kwakye et al., 2015). Although Mn has a multitude of physiological functions (e.g., enzyme cofactor for superoxide dismutase and arginase, immunity, bone development, and reproduction)(Karki et al., 2015), accruing toxic levels will predominately localize to the globus pallidus, but also to the striatum and substantia nigra, leading to manganism, which is phenotypically similar to PD(Milatovic et al., 2007; Kwakye et al., 2015). Excluding occupation as a factor, diets including grains, legumes, and nuts represent the main source of Mn, of which less than 5% is intestinally absorbed(Karki et al., 2013; Kwakye et al., 2015). On the other hand, 30-40% of inhaled Mn is absorbed into the bloodstream, where it travels primarily bound to albumin and β-globulin as Mn^{+2} (refer Mn as Mn^{+2} unless otherwise noted) (Karki et al., 2013). This oxidation state of Mn is facilitated into and within the central nervous system (CNS) by transporters such as divalent metal ion transporter 1 (DMT1) found on cell membranes (Sidoryk-Wegrzynowicz and Aschner, 2013; Karki et al., 2015).

As the most numerous constituent of the CNS, astrocytes are the glue whose physiological roles are indispensable for cellular homeostatic maintenance(Volterra

and Meldolesi, 2005). Astrocytes regulate extracellular glutamate amongst neurons in tripartite synapses(Popoli et al., 2011; Karki et al., 2013). Disruption of this regulation by Mn is possible by the induction of tumor necrosis factor-α (TNFα). This inflammatory response leads to increased yin yang-1 expression that can inhibit the production of excitatory amino acid transporter-2, which is necessary for glutamate reuptake(Karki et al., 2014; Karki et al., 2015). By way of this mechanism, it is observable that Mn neurotoxicity can be understood as a secondary dysfunction brought on by astrocytic inflammation.

Along with pericytes, the end-feet of astrocytes envelope blood vessels to regulate blood-brain barrier trafficking(Pekny and Pekna, 2014). Interestingly, astrocytes have been demonstrated to have an increased affinity for Mn, with concentrations up to 50-fold greater than in neurons(Aschner et al., 1992; Gonzalez et al., 2008). Once internalized, the Mn is sequestered by mitochondria via the calcium (Ca^{+2}) uniporter(Gunter et al., 2006). Kinetical analyses reveal the influx of Mn over this mitochondrial uniporter is slower than Ca^{+2} itself, but Mn efflux is far slower(Gavin et al., 1990; Martinez-Finley et al., 2013). Although the atomic charge properties and size of Mn are quite analogous to Ca^{+2}, which explains the sequestration of Mn by the Ca^{+2} uniporter, the two Ca^{+2} efflux mechanisms are poor exporters of Mn(Gunter et al., 1975; Gunter and Sheu, 2009; Martinez-Finley et al., 2013). Specifically, Na^{+}-independent Ca^{+2} efflux does transport Mn; however, Na^{+}-dependent Ca^{+2} efflux, the predominant mechanism in CNS mitochondria, has not been reported to export Mn(Gavin et al., 1990; Gunter and Sheu, 2009; Martinez-Finley et al., 2013). This

extremely sluggish efflux of Mn both explains the prolonged CNS clearance and the source of toxicity(Martinez-Finley et al., 2013). Indeed, Mn can competitively inhibit both efflux pathways, raising the intramitochondrial Ca^{+2} concentration that can impair aerobic respiration and elicit reactive oxygen species(Gavin et al., 1990; Tjalkens et al., 2006; Martinez-Finley et al., 2013; Streifel et al., 2013).

Mn toxicity has been well documented in neurodegeneration and glial biology (Hazell et al., 1999; Filipov et al., 2005a; Milatovic et al., 2007; Sidoryk-Wegrzynowicz et al., 2009; Dodd and Filipov, 2011; Sarkar et al., 2017a). More specifically, Mn induces TNF-α and inducible nitrogen synthase (iNOS) in astrocytes (Moreno et al., 2008; Moreno et al., 2009), causes mitochondrial dysfunction by its accumulation in mitochondria (Yin et al., 2008), and it was shown to induce neurotoxicity in a rat model of manganism by modulating microgliosis (Zhao et al., 2009). Mn exposure has been shown to induce classical activation in microglial cells (Chang and Liu, 1999) as well as astrocytes(Sarkar et al., 2017a) in the central nervous system, leading to production of pro-inflammatory cytokines. The plethora of pro-inflammatory factors have been shown to cause neuronal damage (Filipov et al., 2005b). Furthermore, Mn has been shown to enhance, LPS-induced production of pro-inflammatory factors in microglial cells (Dodd and Filipov, 2011). Langley *et al.* recently illustrated that Mn potentiates the activation of microglial cells in MitoPark mouse model of PD, suggesting a probable crosstalk between gene and environment in regulating microglial homeostasis (Langley et al., 2017b).

Though Mn has been shown to induce microglial activation, the mechanism underlying this inflammation has been equivocal. A recent study has shown that Mn

induces NLRP3 inflammasome activation in BV2 microglial cell line. This inflammasome activation was accompanied by modulation in autophagy dysfunction and lysosomal dysfunction (Wang et al., 2017). Lysosomal cathepsin B played a major role in activating Mn-induced inflammasome (Wang et al., 2017). Our study showed that Mn can lead to mitochondrial dysfunction in microglial cells which drives the inflammasome activation. Moreover, we showed that Mn leads to propagation of inflammasome by regulating the exosomal release of inflammasome component ASC.

Other Metals

Other than Mn, other metals like Copper (Cu), Lead (Pb), Zinc (Zn), and Iorn (Fe) have been linked to glial activation. Modulation Cu homeostasis have been implicated in change in microglial phenotype in AD mouse models (Zheng et al., 2010). Further, exposure to Cu has been shown to reduce amyloid β clearance in AD by microglia, as well as production of proinflammatory factors like TNFα and IL-6 (Kitazawa et al., 2016). Moreover, Cu exposure have further been linked to S-nitrosothiol signaling dysfunction and NO metabolism in microglial cells (Rossi-George and Guo, 2016).

Pb exposure have been linked to astrogliosis and microgliosis in brain (Chibowska et al., 2016). Pb exposure increased the levels of IL-6 and TGF-β1 by modulation of MAPK (Kasten-Jolly et al., 2011). Pb further increases the level of pro-inflammatory cytokine IL-18, IL-1β, and IL-1α by induction of p38 MAPK (Conti et al., 1999; Wheeler et al., 2003; Cordova et al., 2004). Furthermore, Pb exposure reduces the level of anti-inflammatory factor IL-10 in rodent models (Kasten-Jolly et al., 2012). Pb further, induced the expression of Caspase 1 and Nos 2 in rodent model of lead

toxicity (Kasten-Jolly et al., 2012). Though the mechanism of Pb-induced activation of glia is still not clear, the potential of inflammasome activation by Pb is immense given the fact that Pb induces both the end products of inflammasome activation, IL-1β and IL-18, as well as cleavage of caspase 1. Zinc treatment have also been shown to potentiate LPS-induced microglial inflammation and production of inflammatory factors like IL-1β and IL-6. Further, this potentiation was blocked using a cell permeable Zinc chelator. P2X7 receptor antagonist also reduced the effect of Zinc on microglial activation suggesting the role of this receptor in zinc-induced microglial activation (Higashi et al., 2017). All these studies taken together confirms the role of environmental metals in regulating glial inflammation.

Diesel Exhaust Particle

Another environmental stressor affecting dopaminergic neurons are diesel particle extract. Block *et al.* demonstrated that diesel exhaust particle induced a dose-dependent loss of dopaminergic neurons (Block et al., 2004). Interestingly, diesel exhaust particle did not elicit this neurotoxic effect in neuron rich culture lacking microglia, suggesting the probable role of microglia in diesel exhaust particle-induced neurotoxicity. These particles were shown to be taken up by the microglial cells, thereby generating superoxide, which were neurotoxic. Moreover, NADPH oxidase have been shown to play an important role in diesel particle-induced microglial activation. NADPH oxidase knockout mice failed to induce superoxide generation and neuronal loss post diesel exhaust particle exposure (Block et al., 2004). Rats exposed to diesel exhaust further had increased level of pro-inflammatory factor, IL-6, nitrated proteins, and IBA1. Midbrain region has been shown to be mostly affected by diesel

exhaust with increase in inflammatory factors, TNFα, IL-1β, IL-6, and MIP-1α (Levesque et al., 2011). Surprisingly, in HAPI microglial cell line diesel exhaust did not induce the production of these inflammatory cytokines, but potentiated the release of these factors on LPS treatment (Levesque et al., 2011). This diesel particle-induced microglial activation is regulated by MAC1. Pretreatment with MAC1 antibody have been shown to reduce microglial activation post diesel extract treatment. Moreover, MAC1 knockout neuron glia culture were protected from diesel exhaust induced neurotoxicity and H_2O_2 production (Levesque et al., 2013). Exposure to diesel exhaust particles leading to neuroinflammation and microglial activation leading to neurotoxicity is more pronounced in males compared to females(Cole et al., 2016). These studies in summary indicate the probable role of lung-brain axis in regulating microglial activation in neurodegenerative disorders. Further understanding underlying the mechanism of diesel exhaust particle induced microgliosis may unravel key insights in the role of air pollution in regulating brain functions.

Conclusion and Future Directions

As discussed in this review glial activation leading to inflammation is regulated by multiple signaling proteins and cascade, including NOX2, NfκB, inflammasome and others. Environmental exposures to metals, pesticides and air pollution regulates the glial inflammation through crosstalk with the these signaling molecules. Pesticides like rotenone and tebufenpyrad, environmental metals like manganese leads to microglial activation by regulating inflammasome activation (Fig. 3). Paraquat induces oxidative stress and microglial ROS generation by modulating NOX activity. These gene-environment cross talks have been linked to multiple neurodegenerative disorders like

AD and PD. Understanding the mechanism underlying this interrelationship between the signaling proteins and our environment will give us key insights into probable cause of these sporadic disease which are associated with neuroinflammation.

References

Archibald FS, Tyree C (1987) Manganese poisoning and the attack of trivalent manganese upon catecholamines. Arch Biochem Biophys 256:638-650.

Aschner M, Gannon M, Kimelberg HK (1992) Manganese uptake and efflux in cultured rat astrocytes. J Neurochem 58:730-735.

Banfi B, Molnar G, Maturana A, Steger K, Hegedus B, Demaurex N, Krause KH (2001) A Ca(2+)-activated NADPH oxidase in testis, spleen, and lymph nodes. J Biol Chem 276:37594-37601.

Banfi B, Maturana A, Jaconi S, Arnaudeau S, Laforge T, Sinha B, Ligeti E, Demaurex N, Krause KH (2000) A mammalian H+ channel generated through alternative splicing of the NADPH oxidase homolog NOH-1. Science 287:138-142.

Belarbi K, Cuvelier E, Destee A, Gressier B, Chartier-Harlin MC (2017) NADPH oxidases in Parkinson's disease: a systematic review. Mol Neurodegener 12:84.

Block ML, Zecca L, Hong JS (2007) Microglia-mediated neurotoxicity: uncovering the molecular mechanisms. Nat Rev Neurosci 8:57-69.

Block ML, Wu X, Pei Z, Li G, Wang T, Qin L, Wilson B, Yang J, Hong JS, Veronesi B (2004) Nanometer size diesel exhaust particles are selectively toxic to dopaminergic neurons: the role of microglia, phagocytosis, and NADPH oxidase. FASEB J 18:1618-1620.

Bonizzi G, Bebien M, Otero DC, Johnson-Vroom KE, Cao Y, Vu D, Jegga AG, Aronow BJ, Ghosh G, Rickert RC, Karin M (2004) Activation of IKKalpha target genes depends on recognition of specific kappaB binding sites by RelB:p52 dimers. EMBO J 23:4202-4210.

Bonneh-Barkay D, Reaney SH, Langston WJ, Di Monte DA (2005) Redox cycling of the herbicide paraquat in microglial cultures. Brain Res Mol Brain Res 134:52-56.

Cannon JR, Tapias V, Na HM, Honick AS, Drolet RE, Greenamyre JT (2009) A highly reproducible rotenone model of Parkinson's disease. Neurobiol Dis 34:279-290.

Cao S, Zhang X, Edwards JP, Mosser DM (2006) NF-kappaB1 (p50) homodimers differentially regulate pro- and anti-inflammatory cytokines in macrophages. J Biol Chem 281:26041-26050.

Castello PR, Drechsel DA, Patel M (2007) Mitochondria are a major source of paraquat-induced reactive oxygen species production in the brain. J Biol Chem 282:14186-14193.

Chang JY, Liu LZ (1999) Manganese potentiates nitric oxide production by microglia. Brain Res Mol Brain Res 68:22-28.

Charli A, Jin H, Anantharam V, Kanthasamy A, Kanthasamy AG (2016) Alterations in mitochondrial dynamics induced by tebufenpyrad and pyridaben in a dopaminergic neuronal cell culture model. Neurotoxicology 53:302-313.

Cheng G, Cao Z, Xu X, van Meir EG, Lambeth JD (2001) Homologs of gp91phox: cloning and tissue expression of Nox3, Nox4, and Nox5. Gene 269:131-140.

Chibowska K, Baranowska-Bosiacka I, Falkowska A, Gutowska I, Goschorska M, Chlubek D (2016) Effect of Lead (Pb) on Inflammatory Processes in the Brain. Int J Mol Sci 17.

Cicchetti F, Lapointe N, Roberge-Tremblay A, Saint-Pierre M, Jimenez L, Ficke BW, Gross RE (2005) Systemic exposure to paraquat and maneb models early Parkinson's disease in young adult rats. Neurobiol Dis 20:360-371.

Cole TB, Coburn J, Dao K, Roque P, Chang YC, Kalia V, Guilarte TR, Dziedzic J, Costa LG (2016) Sex and genetic differences in the effects of acute diesel exhaust exposure on inflammation and oxidative stress in mouse brain. Toxicology 374:1-9.

Conti B, Park LC, Calingasan NY, Kim Y, Kim H, Bae Y, Gibson GE, Joh TH (1999) Cultures of astrocytes and microglia express interleukin 18. Brain Res Mol Brain Res 67:46-52.

Cordova FM, Rodrigues AL, Giacomelli MB, Oliveira CS, Posser T, Dunkley PR, Leal RB (2004) Lead stimulates ERK1/2 and p38MAPK phosphorylation in the hippocampus of immature rats. Brain Res 998:65-72.

Costello S, Cockburn M, Bronstein J, Zhang X, Ritz B (2009) Parkinson's disease and residential exposure to maneb and paraquat from agricultural applications in the central valley of California. Am J Epidemiol 169:919-926.

Dodd CA, Filipov NM (2011) Manganese potentiates LPS-induced heme-oxygenase 1 in microglia but not dopaminergic cells: role in controlling microglial hydrogen peroxide and inflammatory cytokine output. Neurotoxicology 32:683-692.

Edens WA, Sharling L, Cheng G, Shapira R, Kinkade JM, Lee T, Edens HA, Tang X, Sullards C, Flaherty DB, Benian GM, Lambeth JD (2001) Tyrosine cross-linking of extracellular matrix is catalyzed by Duox, a multidomain oxidase/peroxidase with homology to the phagocyte oxidase subunit gp91phox. J Cell Biol 154:879-891.

Filipov NM, Seegal RF, Lawrence DA (2005a) Manganese potentiates in vitro production of proinflammatory cytokines and nitric oxide by microglia through a nuclear factor kappa B-dependent mechanism. Toxicol Sci 84:139-148.

Filipov NM, Seegal RF, Lawrence DA (2005b) Manganese potentiates in vitro production of proinflammatory cytokines and nitric oxide by microglia through a nuclear factor kappa B-dependent mechanism. Toxicol Sci Oxford University Press 84.

Freeman LC, Ting JP (2016) The pathogenic role of the inflammasome in neurodegenerative diseases. J Neurochem 136 Suppl 1:29-38.

Gao F, Chen D, Hu Q, Wang G (2013) Rotenone directly induces BV2 cell activation via the p38 MAPK pathway. PLoS One 8:e72046.

Gao HM, Liu B, Hong JS (2003) Critical role for microglial NADPH oxidase in rotenone-induced degeneration of dopaminergic neurons. J Neurosci 23:6181-6187.

Gavin CE, Gunter KK, Gunter TE (1990) Manganese and calcium efflux kinetics in brain mitochondria. Relevance to manganese toxicity. Biochem J 266:329-334.

Geiszt M, Kopp JB, Varnai P, Leto TL (2000) Identification of renox, an NAD(P)H oxidase in kidney. Proc Natl Acad Sci U S A 97:8010-8014.

Ghosh A, Langley MR, Harischandra DS, Neal ML, Jin H, Anantharam V, Joseph J, Brenza T, Narasimhan B, Kanthasamy A, Kalyanaraman B, Kanthasamy AG (2016) Mitoapocynin Treatment Protects Against Neuroinflammation and Dopaminergic Neurodegeneration in a Preclinical Animal Model of Parkinson's Disease. J Neuroimmune Pharmacol 11:259-278.

Gonzalez LE, Juknat AA, Venosa AJ, Verrengia N, Kotler ML (2008) Manganese activates the mitochondrial apoptotic pathway in rat astrocytes by modulating the expression of proteins of the Bcl-2 family. Neurochem Int 53:408-415.

Gunter RE, Puskin JS, Russell PR (1975) Quantitative magnetic resonance studies of manganese uptake by mitochondria. Biophys J 15:319-333.

Gunter TE, Sheu SS (2009) Characteristics and possible functions of mitochondrial Ca(2+) transport mechanisms. Biochim Biophys Acta 1787:1291-1308.

Gunter TE, Gavin CE, Aschner M, Gunter KK (2006) Speciation of manganese in cells and mitochondria: a search for the proximal cause of manganese neurotoxicity. Neurotoxicology 27:765-776.

Halle A, Hornung V, Petzold GC, Stewart CR, Monks BG, Reinheckel T, Fitzgerald KA, Latz E, Moore KJ, Golenbock DT (2008) The NALP3 inflammasome is involved in the innate immune response to amyloid-beta. Nat Immunol 9:857-865.

Harischandra DS, Ghaisas S, Rokad D, Zamanian M, Jin H, Anantharam V, Kimber M, Kanthasamy A, Kanthasamy AG (2017) Environmental neurotoxicant manganese regulates exosome-mediated extracellular miRNAs in cell culture

model of Parkinson's disease: Relevance to alpha-synuclein misfolding in metal neurotoxicity. Neurotoxicology.

Hazell AS, Desjardins P, Butterworth RF (1999) Chronic exposure of rat primary astrocyte cultures to manganese results in increased binding sites for the 'peripheral-type' benzodiazepine receptor ligand 3H-PK 11195. Neurosci Lett 271:5-8.

Heneka MT, Kummer MP, Stutz A, Delekate A, Schwartz S, Vieira-Saecker A, Griep A, Axt D, Remus A, Tzeng TC, Gelpi E, Halle A, Korte M, Latz E, Golenbock DT (2013) NLRP3 is activated in Alzheimer's disease and contributes to pathology in APP/PS1 mice. Nature 493:674-678.

Hertzman C, Wiens M, Bowering D, Snow B, Calne D (1990) Parkinson's disease: a case-control study of occupational and environmental risk factors. Am J Ind Med 17:349-355.

Higashi Y, Aratake T, Shimizu S, Shimizu T, Nakamura K, Tsuda M, Yawata T, Ueba T, Saito M (2017) Influence of extracellular zinc on M1 microglial activation. Sci Rep 7:43778.

Inden M, Kitamura Y, Abe M, Tamaki A, Takata K, Taniguchi T (2011) Parkinsonian rotenone mouse model: reevaluation of long-term administration of rotenone in C57BL/6 mice. Biol Pharm Bull 34:92-96.

Karki P, Lee E, Aschner M (2013) Manganese neurotoxicity: a focus on glutamate transporters. Ann Occup Environ Med 25:4.

Karki P, Smith K, Johnson J, Jr., Aschner M, Lee E (2015) Role of transcription factor yin yang 1 in manganese-induced reduction of astrocytic glutamate

transporters: Putative mechanism for manganese-induced neurotoxicity. Neurochem Int 88:53-59.

Karki P, Webb A, Smith K, Johnson J, Jr., Lee K, Son DS, Aschner M, Lee E (2014) Yin Yang 1 is a repressor of glutamate transporter EAAT2, and it mediates manganese-induced decrease of EAAT2 expression in astrocytes. Mol Cell Biol 34:1280-1289.

Kasten-Jolly J, Heo Y, Lawrence DA (2011) Central nervous system cytokine gene expression: modulation by lead. J Biochem Mol Toxicol 25:41-54.

Kasten-Jolly J, Pabello N, Bolivar VJ, Lawrence DA (2012) Developmental lead effects on behavior and brain gene expression in male and female BALB/cAnNTac mice. Neurotoxicology 33:1005-1020.

Kitazawa M, Hsu HW, Medeiros R (2016) Copper Exposure Perturbs Brain Inflammatory Responses and Impairs Clearance of Amyloid-Beta. Toxicol Sci 152:194-204.

Kwakye GF, Paoliello MM, Mukhopadhyay S, Bowman AB, Aschner M (2015) Manganese-Induced Parkinsonism and Parkinson's Disease: Shared and Distinguishable Features. Int J Environ Res Public Health 12:7519-7540.

Langley M, Ghosh A, Charli A, Sarkar S, Ay M, Luo J, Zielonka J, Brenza T, Bennett B, Jin H, Ghaisas S, Schlichtmann B, Kim D, Anantharam V, Kanthasamy A, Narasimhan B, Kalyanaraman B, Kanthasamy AG (2017a) Mito-Apocynin Prevents Mitochondrial Dysfunction, Microglial Activation, Oxidative Damage, and Progressive Neurodegeneration in MitoPark Transgenic Mice. Antioxid Redox Signal.

Langley MR, Ghaisas S, Ay M, Luo J, Palanisamy BN, Jin H, Anantharam V, Kanthasamy A, Kanthasamy AG (2017b) Manganese exposure exacerbates progressive motor deficits and neurodegeneration in the MitoPark mouse model of Parkinson's disease: Relevance to gene and environment interactions in metal neurotoxicity. Neurotoxicology.

Lawana V, Singh N, Sarkar S, Charli A, Jin H, Anantharam V, Kanthasamy AG, Kanthasamy A (2017) Involvement of c-Abl Kinase in Microglial Activation of NLRP3 Inflammasome and Impairment in Autolysosomal System. J Neuroimmune Pharmacol.

Lawrence T (2009) The nuclear factor NF-kappaB pathway in inflammation. Cold Spring Harb Perspect Biol 1:a001651.

Levesque S, Taetzsch T, Lull ME, Johnson JA, McGraw C, Block ML (2013) The role of MAC1 in diesel exhaust particle-induced microglial activation and loss of dopaminergic neuron function. J Neurochem 125:756-765.

Levesque S, Taetzsch T, Lull ME, Kodavanti U, Stadler K, Wagner A, Johnson JA, Duke L, Kodavanti P, Surace MJ, Block ML (2011) Diesel exhaust activates and primes microglia: air pollution, neuroinflammation, and regulation of dopaminergic neurotoxicity. Environ Health Perspect 119:1149-1155.

Li Y, Lein PJ, Ford GD, Liu C, Stovall KC, White TE, Bruun DA, Tewolde T, Gates AS, Distel TJ, Surles-Zeigler MC, Ford BD (2015) Neuregulin-1 inhibits neuroinflammatory responses in a rat model of organophosphate-nerve agent-induced delayed neuronal injury. J Neuroinflammation 12:64.

Liang Y, Jing X, Zeng Z, Bi W, Chen Y, Wu X, Yang L, Liu J, Xiao S, Liu S, Lin D, Tao E (2015) Rifampicin attenuates rotenone-induced inflammation via suppressing NLRP3 inflammasome activation in microglia. Brain Res 1622:43-50.

Mao H, Liu B (2008) Synergistic microglial reactive oxygen species generation induced by pesticides lindane and dieldrin. Neuroreport 19:1317-1320.

Mao H, Fang X, Floyd KM, Polcz JE, Zhang P, Liu B (2007) Induction of microglial reactive oxygen species production by the organochlorinated pesticide dieldrin. Brain Res 1186:267-274.

Martinez-Finley EJ, Gavin CE, Aschner M, Gunter TE (2013) Manganese neurotoxicity and the role of reactive oxygen species. Free Radic Biol Med 62:65-75.

Martinez EM, Young AL, Patankar YR, Berwin BL, Wang L, von Herrmann KM, Weier JM, Havrda MC (2017) Editor's Highlight: Nlrp3 Is Required for Inflammatory Changes and Nigral Cell Loss Resulting From Chronic Intragastric Rotenone Exposure in Mice. Toxicol Sci 159:64-75.

Milatovic D, Yin Z, Gupta RC, Sidoryk M, Albrecht J, Aschner JL, Aschner M (2007) Manganese induces oxidative impairment in cultured rat astrocytes. Toxicol Sci 98:198-205.

Miller RL, Sun GY, Sun AY (2007) Cytotoxicity of paraquat in microglial cells: Involvement of PKCdelta- and ERK1/2-dependent NADPH oxidase. Brain Res 1167:129-139.

Moreno JA, Sullivan KA, Carbone DL, Hanneman WH, Tjalkens RB (2008) Manganese potentiates nuclear factor-kappaB-dependent expression of nitric oxide synthase 2 in astrocytes by activating soluble guanylate cyclase and

extracellular responsive kinase signaling pathways. J Neurosci Res 86:2028-2038.

Moreno JA, Streifel KM, Sullivan KA, Legare ME, Tjalkens RB (2009) Developmental exposure to manganese increases adult susceptibility to inflammatory activation of glia and neuronal protein nitration. Toxicol Sci 112:405-415.

Mount MP, Lira A, Grimes D, Smith PD, Faucher S, Slack R, Anisman H, Hayley S, Park DS (2007) Involvement of interferon-gamma in microglial-mediated loss of dopaminergic neurons. J Neurosci 27:3328-3337.

Panicker N, Saminathan H, Jin H, Neal M, Harischandra DS, Gordon R, Kanthasamy K, Lawana V, Sarkar S, Luo J, Anantharam V, Kanthasamy AG, Kanthasamy A (2015) Fyn Kinase Regulates Microglial Neuroinflammatory Responses in Cell Culture and Animal Models of Parkinson's Disease. J Neurosci 35:10058-10077.

Pekny M, Pekna M (2014) Astrocyte reactivity and reactive astrogliosis: costs and benefits. Physiol Rev 94:1077-1098.

Popoli M, Yan Z, McEwen BS, Sanacora G (2011) The stressed synapse: the impact of stress and glucocorticoids on glutamate transmission. Nat Rev Neurosci 13:22-37.

Roepstorff K, Rasmussen I, Sawada M, Cudre-Maroux C, Salmon P, Bokoch G, van Deurs B, Vilhardt F (2008) Stimulus-dependent regulation of the phagocyte NADPH oxidase by a VAV1, Rac1, and PAK1 signaling axis. J Biol Chem 283:7983-7993.

Rokad D, Ghaisas S, Harischandra DS, Jin H, Anantharam V, Kanthasamy A, Kanthasamy AG (2016) Role of neurotoxicants and traumatic brain injury in alpha-synuclein protein misfolding and aggregation. Brain Res Bull.

Rossi-George A, Guo CJ (2016) Copper disrupts S-nitrosothiol signaling in activated BV2 microglia. Neurochem Int 99:1-8.

Sarkar S, Malovic E, Harischandra DS, Ngwa HA, Ghosh A, Hogan C, Rokad D, Zenitsky G, Jin H, Anantharam V, Kanthasamy AG, Kanthasamy A (2017a) Manganese exposure induces neuroinflammation by impairing mitochondrial dynamics in astrocytes. Neurotoxicology.

Sarkar S, Malovic E, Harishchandra DS, Ghaisas S, Panicker N, Charli A, Palanisamy BN, Rokad D, Jin H, Anantharam V, Kanthasamy A, Kanthasamy AG (2017b) Mitochondrial impairment in microglia amplifies NLRP3 inflammasome proinflammatory signaling in cell culture and animal models of Parkinson's disease. NPJ Parkinsons Dis 3:30.

Segal AW (2005) How neutrophils kill microbes. Annu Rev Immunol 23:197-223.

Sherer TB, Richardson JR, Testa CM, Seo BB, Panov AV, Yagi T, Matsuno-Yagi A, Miller GW, Greenamyre JT (2007) Mechanism of toxicity of pesticides acting at complex I: relevance to environmental etiologies of Parkinson's disease. J Neurochem 100:1469-1479.

Shih RH, Wang CY, Yang CM (2015) NF-kappaB Signaling Pathways in Neurological Inflammation: A Mini Review. Front Mol Neurosci 8:77.

Sidoryk-Wegrzynowicz M, Aschner M (2013) Role of astrocytes in manganese mediated neurotoxicity. BMC Pharmacol Toxicol 14:23.

Sidoryk-Wegrzynowicz M, Lee E, Albrecht J, Aschner M (2009) Manganese disrupts astrocyte glutamine transporter expression and function. J Neurochem 110:822-830.

Song C, Kanthasamy A, Anantharam V, Sun F, Kanthasamy AG (2010) Environmental neurotoxic pesticide increases histone acetylation to promote apoptosis in dopaminergic neuronal cells: relevance to epigenetic mechanisms of neurodegeneration. Mol Pharmacol 77:621-632.

Streifel KM, Miller J, Mouneimne R, Tjalkens RB (2013) Manganese inhibits ATP-induced calcium entry through the transient receptor potential channel TRPC3 in astrocytes. Neurotoxicology 34:160-166.

Tjalkens RB, Zoran MJ, Mohl B, Barhoumi R (2006) Manganese suppresses ATP-dependent intercellular calcium waves in astrocyte networks through alteration of mitochondrial and endoplasmic reticulum calcium dynamics. Brain Res 1113:210-219.

Volterra A, Meldolesi J (2005) Astrocytes, from brain glue to communication elements: the revolution continues. Nat Rev Neurosci 6:626-640.

Wang D, Zhang J, Jiang W, Cao Z, Zhao F, Cai T, Aschner M, Luo W (2017) The role of NLRP3-CASP1 in inflammasome-mediated neuroinflammation and autophagy dysfunction in manganese-induced, hippocampal-dependent impairment of learning and memory ability. Autophagy 13:914-927.

Wheeler RD, Brough D, Le Feuvre RA, Takeda K, Iwakura Y, Luheshi GN, Rothwell NJ (2003) Interleukin-18 induces expression and release of cytokines from

murine glial cells: interactions with interleukin-1 beta. J Neurochem 85:1412-1420.

Wu DC, Teismann P, Tieu K, Vila M, Jackson-Lewis V, Ischiropoulos H, Przedborski S (2003) NADPH oxidase mediates oxidative stress in the 1-methyl-4-phenyl-1,2,3,6-tetrahydropyridine model of Parkinson's disease. Proc Natl Acad Sci U S A 100:6145-6150.

Wu XF, Block ML, Zhang W, Qin L, Wilson B, Zhang WQ, Veronesi B, Hong JS (2005) The role of microglia in paraquat-induced dopaminergic neurotoxicity. Antioxid Redox Signal 7:654-661.

Yin Z, Aschner JL, dos Santos AP, Aschner M (2008) Mitochondrial-dependent manganese neurotoxicity in rat primary astrocyte cultures. Brain Res 1203:1-11.

Zawada WM, Mrak RE, Biedermann J, Palmer QD, Gentleman SM, Aboud O, Griffin WS (2015) Loss of angiotensin II receptor expression in dopamine neurons in Parkinson's disease correlates with pathological progression and is accompanied by increases in Nox4- and 8-OH guanosine-related nucleic acid oxidation and caspase-3 activation. Acta Neuropathol Commun 3:9.

Zhao F, Cai T, Liu M, Zheng G, Luo W, Chen J (2009) Manganese induces dopaminergic neurodegeneration via microglial activation in a rat model of manganism. Toxicol Sci 107:156-164.

Zheng Z, White C, Lee J, Peterson TS, Bush AI, Sun GY, Weisman GA, Petris MJ (2010) Altered microglial copper homeostasis in a mouse model of Alzheimer's disease. J Neurochem 114:1630-1638.

Zhou F, Yao HH, Wu JY, Ding JH, Sun T, Hu G (2008) Opening of microglial K(ATP) channels inhibits rotenone-induced neuroinflammation. J Cell Mol Med 12:1559-1570.

Zhou H, Zhang F, Chen SH, Zhang D, Wilson B, Hong JS, Gao HM (2012) Rotenone activates phagocyte NADPH oxidase by binding to its membrane subunit gp91phox. Free Radic Biol Med 52:303-313.

Zhou R, Yazdi AS, Menu P, Tschopp J (2011) A role for mitochondria in NLRP3 inflammasome activation. Nature 469:221-225.

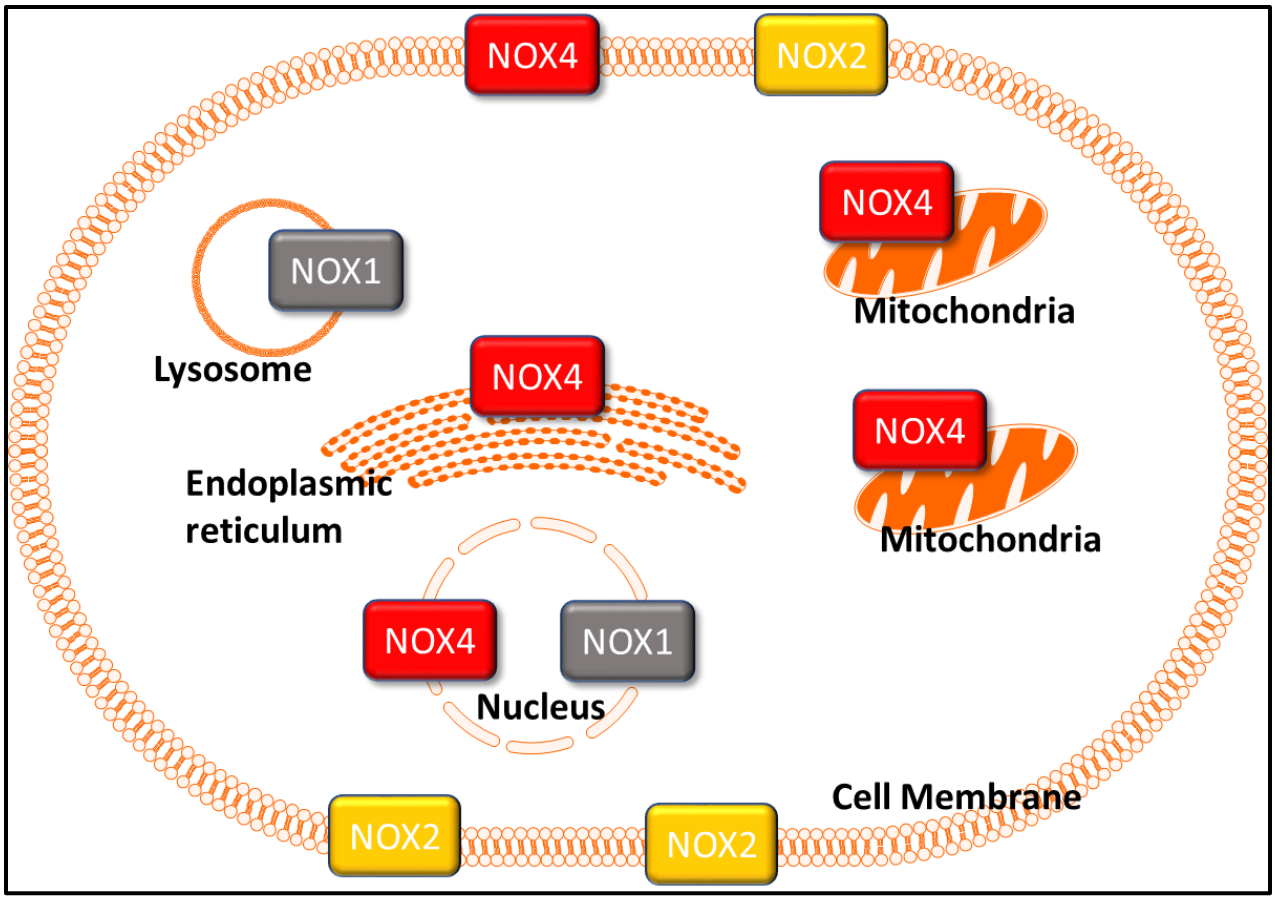

Fig. 1: Cellular localization of various NADPH oxidase (NOX) isoforms. NOX1 is localized on lysosomal and nuclear membrane. NOX2 is localized on plasma membrane. NOX4 is localized on plasma membrane, mitochondrial membrane, endoplasmic reticulum, and nuclear membrane.

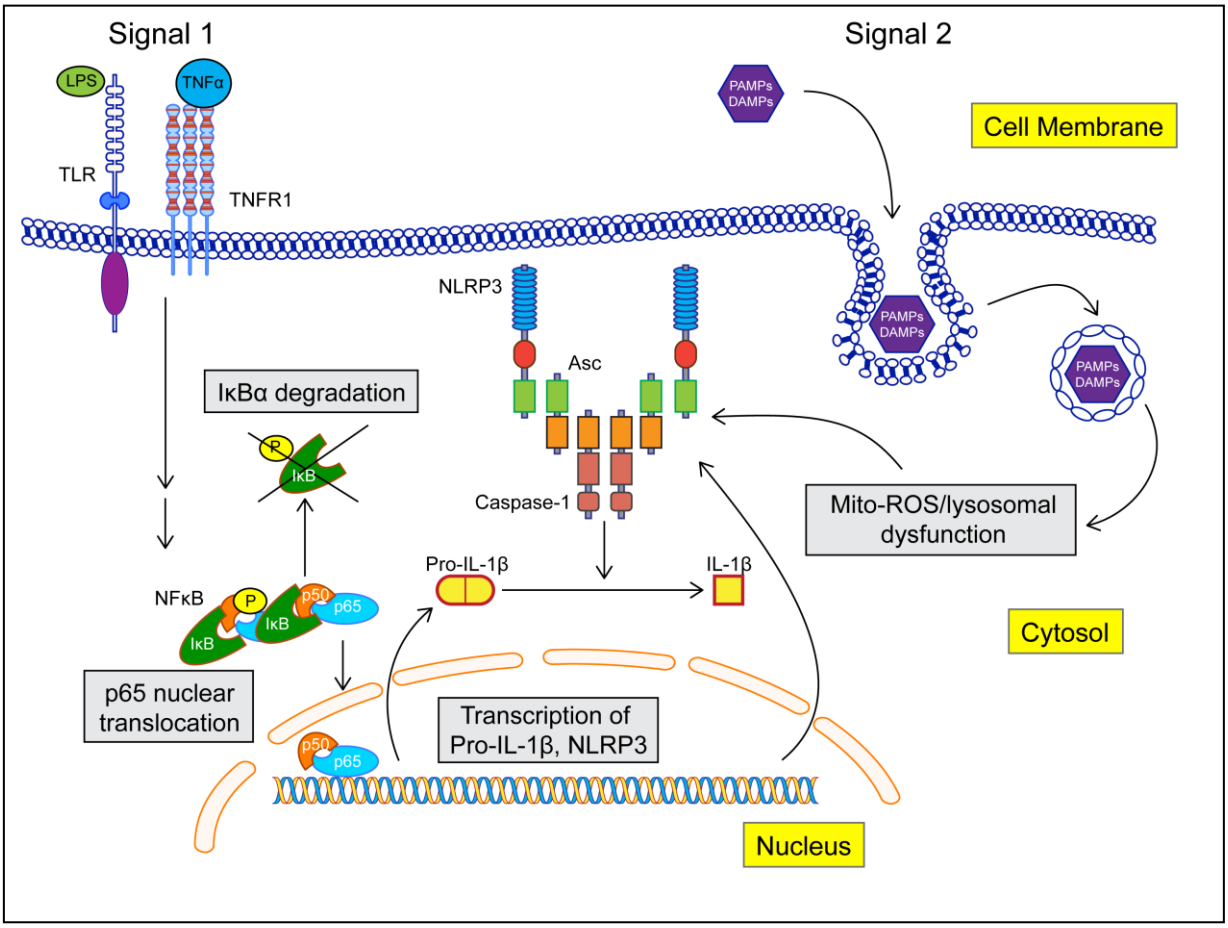

Fig. 2. Mechanism of NLRP3 inflammasome activation in glial cells (Adopted from *Panicker et al. 2016*)

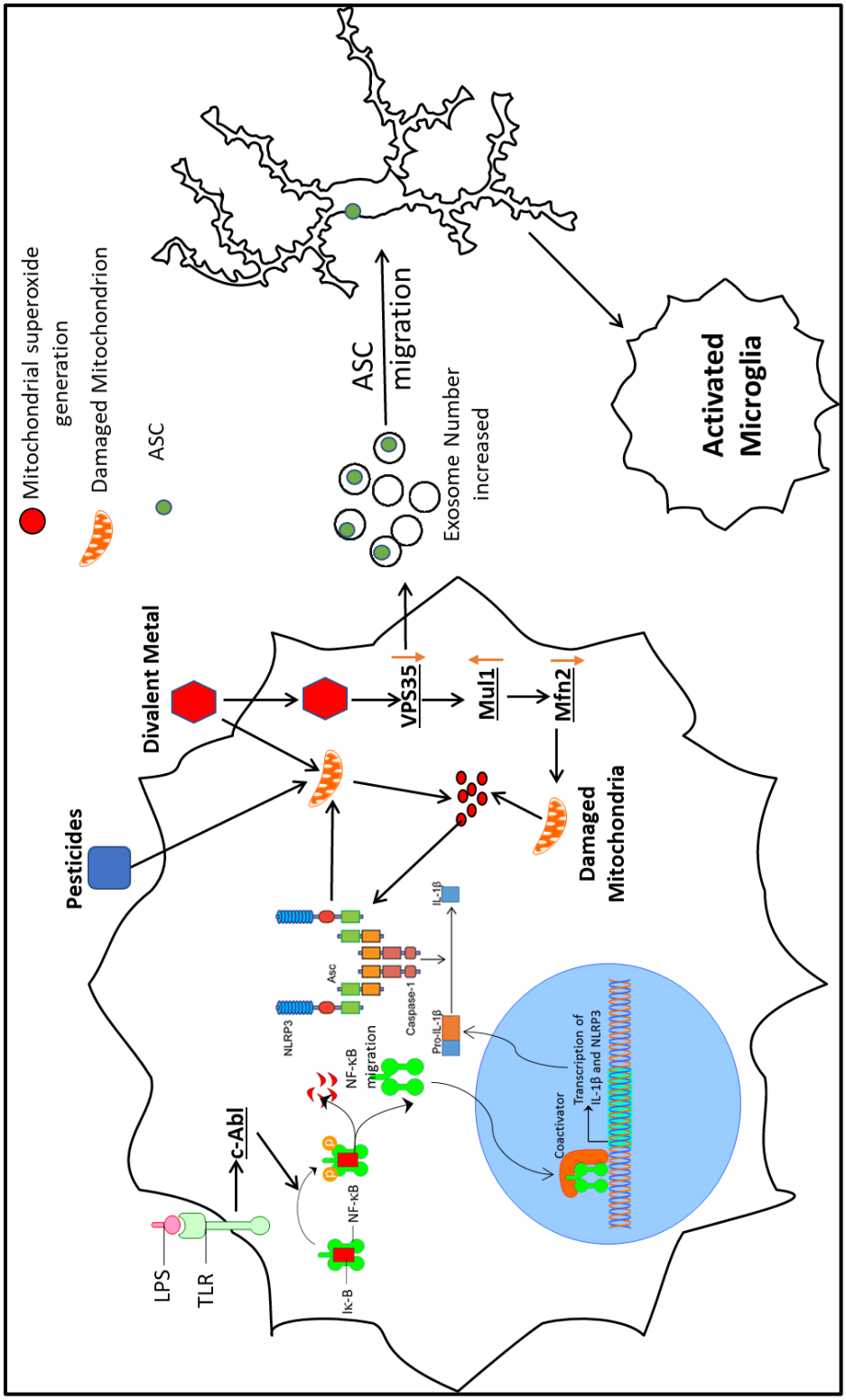

Fig. 3. Schematic representation of mechanism of pesticide and Metal induced inflammasome activation and propagation in microglial cells

CHAPTER III

MICROGLIAL ION CHANNELS: A KEY PLAYER IN NEURODEGENERATIVE DISORDERS

Manuscript to be submitted to *Glia*

Souvarish Sarkar[1], Emir Malovic[1], Huajun Jin[1], Heike Wulff[2], Anumantha Kanthasamy[1].

1-Parkinson Disorders Research Laboratory, Iowa Center for Advanced Neurotoxicology, Department of Biomedical Sciences, 2062 Veterinary Medicine Building, Iowa State University, Ames, IA 50011

2-University of California, Davis

*To whom correspondence should be addressed: Anumantha Kanthasamy, Ph.D. Distinguished Professor and Chair, Department of Biomedical Sciences, Iowa State University, Ames, IA 50011, Telephone: (515) 294-2516; Fax: (515) 294-2315, Email: akanthas@iastate.edu

Abstract

Neuroinflammation is one of the major key pathophysiological hallmark of neurodegenerative disorders including Alzheimer's disease (AD), Parkinson's disease (PD) and traumatic brain injury (TBI). Microglia, the first responders of the brain, are the drivers of this neuroinflammation. Microglial activation, leading to induction of pro-inflammatory factors, like IL-1β, TNFα, nitrites and others, have been shown to induce neurodegeneration. Non-steroidal anti-inflammatory drugs (NSAID's) have been

shown to reduce risk of developing PD. But the mechanism underlying the microglial activation is still under active research. Recently, microglial ion channels have come to the forefront as potential drug targets for in multiple neurodegenerative disorders including AD and PD. Microglia expresses a variety of ion channels including potassium channels, calcium channels, chloride channels, sodium channels, and proton channels. The diversity of channels present on microglia is responsible for the dynamic nature of these immune cells of the brain. These ion channels regulate microglial proliferation, chemotaxis, phagocytosis, antigen recognition and presentation, apoptosis, and cell signaling leading to inflammation, among other key critical functions. Understanding the role of these ion channels and the signaling mechanism these channels regulate under pathological conditions is an active area of research. This review will be focusing on the roles of different microglial ion channels, and their potential role in regulating microglial functions in neurodegenerative disorders.

Introduction

Microglia, the first responders of the brain, are key players in shaping up the neural circuit during development, as well as maintaining the neuronal health (Paolicelli et al. 2011). Hyperactivation of microglial cells have been linked to multiple disease including epilepsy (Sharma et al. 2017), Parkinson's disease (PD) (Panicker et al. 2015), Alzheimer's disease (AD) (Halle et al. 2008), and Traumatic brain injury (TBI) (Turtzo et al. 2014). Microglia derived proinflammatory factors have been shown to be neurotoxic and can lead to neuronal loss (Sarkar et al. 2017). Hence, anti-inflammatory drugs targeting microglial activation, and proliferation have gained importance in recent years.

Microglial ion channels perform a diverse set of functions which leads to microglia-induced inflammation, proliferation and migration (Feske et al. 2015). In neurodegenerative disease conditions multiple of these ion channels have been shown to be upregulated, which make them lucrative drug targets. In this review, we discuss the major ion channels involved in microglial function and their mechanism of action.

Potassium Channels

Kv1.3

Kv1.3 is one of the 40 voltage gated channel in human genome. Kv1.3 channel was identified in T cells following its cloning (DeCoursey et al. 1985; Grissmer et al. 1990; Matteson and Deutsch 1984). It is composed of 4 α subunits and each of the subunits has 1 P loop and 6 transmembrane segments (S1-S6). 4 Arginine residues in S4 segment are responsible for the opening of this channel due to polarization.

Other than T cells, Kv1.3 channels have been identified in lymphocytes, RGC's, microglia and various other cell types. Kv1.3 knock out mice have been shown to be resistant to diet induced obesity (Upadhyay et al. 2013; Xu et al. 2004), immune to experimental autoimmune encephalomyelitis (EAE)(Gocke et al. 2012) and also improved sense of smell(Fadool et al. 2004) showing the diverse function of this voltage gated channel. The role of this channel has been studied in mostly autoimmune disease and also ischemia and in development in RGC's. The N-terminal end of this channel has a proline-rich sequence which has been shown to bind to src-homology domain of src-family kinase (SFK).

First sequenced and cloned by Chandy in 1991 (Chandy 1991), the transcript of Kv1.3 in microglial cells was first discovered in 1993 by Norenberg *et al* (Norenberg et al. 1993). Since then the role of Kv1.3 in microglial function and activation have been implicated. A study by Schlichter *et al.* demonstrated that primary microglia in culture do express functional Kv1.3 outward rectifier channels but following prolonged culturing, these microglia loose the channel function (Schlichter et al. 1996). Kv1.3 plays an important role in driving LPS-induced inflammation in microglial cells. Fordyce *et al.* demonstrated that Kv1.3 channel activity in microglial cells is necessary to kill hippocampal neurons using a co-culture system. This study further showed that Kv1.3 inhibitors reduced the respiratory burst and free radical production in microglial cells hence reducing the formation of peroxynitrite, a key inflammatory molecule (Fordyce et al. 2005). A recent study by Rangaraju *et al.* further elucidated the Kv1.3 dependent pathways in microglial cells post LPS treatment (Rangaraju et al. 2017). This study used a Kv1.3 inhibitor, Shk, to inhibit the channel activity post LPS

treatment and performed whole cell proteomics to determine the Kv1.3 dependent pathways involved during in an inflammagen insult. Interestingly, blocking Kv1.3 reduced phosphorylation of STAT1 which is an immediate downstream signaling of LPS-TLR signaling cascade. Blocking of Kv1.3 further reduced the microglial phagocytic activity, and also modulated microglial chemotaxis and migration. Kv1.3 was further shown to be regulating MHC-1 antigen presentation pathways in microglia by regulating TAP1 and EHD1. Interestingly, Kv1.3 inhibition also altered one of the subunits of GA binding protein (GABP) which has been involved in mitochondrial DNA replication, and oxidative phosphorylation (Quiros et al. 2016). Interestingly, Kv1.3 is also present on the mitochondrial membrane, and has been linked to cytochrome c release and apoptosis in lymphocytes (Gulbins et al. 2010; Szabo et al. 2008). But till date, no studies have looked into the probable role of mitochondrial Kv1.3 in microglia and its role in microglial function. Recently, our group along with others have shown the importance of mitochondrial dynamics in driving inflammation in microglial cells (Lawana et al. 2017; Sarkar et al. 2017). Hence, studies on mitochondrial Kv1.3 and its role in regulating mitochondrial health in glial cells may provide key mechanistic insights.

Microglial Kv1.3 have been shown to be induced in multiple disease models like stroke, AD, HIV induced dementia, radiation induced brain injury, and status epilepticus. Menteyne *et al.* showed that Kv1.3 is the predominant potassium channels in the kainate mouse model of epilepsy in microglial cells. In this study, post kainate treatment in CX3CR1(eGFP/+) mice, whole-cell-patch clamp was performed on GFP-microglial cells, which demonstrated an increase of Kv1.3 current in the activated

microglia. Treatment with Kv1.3 inhibitor, agitoxin-2 and margatoxin inhibited this current (Menteyne et al. 2009). Microglial cells have been also shown to play a critical role in HIV induced neuropathology. HIV-1 regulatory protein, Tat, induced microglial inflammation, by induction of Kv1.3 and classical activation of Nfκb (Visentin et al. 2001). siRNA knockdown of Kv1.3 in microglial cells reduced the neurotoxicity induced by Tat by reducing the release of pro-inflammatory factors in microglial cells. Also, Kv1.3 inhibition lead to a decrease in activation of ERK1/2 MAPK pathway induced by Tat (Liu et al. 2013). Also, the gp-120 subunit of HIV-1 virus have been shown to activate microglial cells. Gp-120 further induced Kv1.3 channel activity in the glial cells. Furthermore, inhibition of Kv1.3 reduced microglial activation by reduction of p38 MAPK pathway (Liu et al. 2012). Methamphetamine drug abuse have been also linked to higher risk of HIV-1 induced neurotoxicity. Liu *et al.* further demonstrated that methamphetamine exacerbates gp-120-induced microglial Kv1.3 current activity, leading to hyperactivation of microglial cells and neurodegeneration (Liu et al. 2017).

Kv1.3 was also increased in a mouse model of radiation induced brain injury. Further, Shk, a peptide inhibitor of Kv1.3, reduced microglial inflammation, and neurotoxicity, and promoted proliferation of neural stem cells and neurogenesis (Peng et al. 2014). Furthermore, Reeves *et al.* demonstrated that in a model of TBI, Clofazimine, a Kv1.3 inhibitor, treatment reduced microglial activation and microgliosis, hence reducing the white matter pathology of the disease (Reeves et al. 2016).

Microgliosis and neuroinflammation have been shown to be an important factor contributing to neuronal loss in AD (Halle et al. 2008). Kv1.3 is has been shown to be

highly expressed in microglial cells in AD brains. Moreover, the Kv1.3 positive glial cells were shown to be associated with amyloid β (Aβ) tangles in the frontal cortex of AD patients (Rangaraju et al. 2015). A recent study further demonstrated that Aβ induced microglial activation and Kv1.3 upregulation in microglial cells. Furthermore, Kv1.3 was also induced in the transgenic mouse model APP/PS1 of AD. Pharmacological inhibition of Kv1.3 channel *in vivo* in this mouse model of AD, resulted in reduced inflammation as well as rescue of disease phenotype. Also, Kv1.3 inhibition resulted in higher uptake of Aβ and reduced cerebral amyloid load. PAP1, the Kv1.3 inhibitor further, improved hippocampal neuronal plasticity, behavioral and cognitive deficits in mouse model of AD (Maezawa et al. 2017). Though the importance of microglial Kv1.3 in AD has been elucidated, further studies looking into the downstream signaling mechanism of Kv1.3 in microglia may identify some novel pathways in regulating microglial function in disease pathology. Furthermore, the upstream signaling cascade leading to Kv1.3 activation in disease condition have not been studied.

The role of Kv1.3 is not well known in PD. We demonstrated that Kv1.3 is highly induced by aggregated α-synuclein. Furthermore, post mortem PD patients had higher microglial Kv1.3. Inhibition of Kv1.3 reduced microglial activation and neurodegeneration in multiple PD models *in vitro* and *in vivo*. Kv1.3 is regulated by p38 MAPK pathway and Nfκb pathway. We also showed that Fyn, a src family kinase can modulate the function of this potassium channel by directly binding to Kv1.3 and phosphorylating it. The significant number of studies suggesting the role of this channel in disease pathology and inflammation and its diverse role in regulating

microglial signaling cascade in various disease models makes it an interesting target for a drug. But further studies, understanding the role of mitochondrial Kv1.3 in microglia, in disease condition, may give key insights in understanding the role of mitochondria in regulating microglial function.

Kca3.1

First identified by György Gárdos in 1958 (Gardos 1958), Kca3.1 is a voltage independent potassium channel activated by intracellular calcium. The activation of this channel leads to hyperpolarization of the membrane leading to calcium influx (Joiner et al. 1997; Wei et al. 2005). Kaushal *et al.* demonstrated that Kca3.1 inhibition reduced microglial activation and pro-inflammatory cytokine release by regulating p38 MAPK pathway but not Nfκb signaling cascade. Moreover, TRAM-34, a Kca3.1 blocker, reduced degeneration of retinal ganglion cells in an optic nerve transection mouse model (Kaushal et al. 2007). A study by Maezawa and colleagues, further demonstrated that oligomeric Aβ-induced microglial activation and proliferation *in vitro* and activated this voltage independent potassium channel. TRAM-34 treatment inhibited the activation of microglia and oligomeric Aβ-induced neurotoxicity further suggesting a role of Kca3.1 in regulating neuroinflammation and neurodegeneration (Maezawa et al. 2011). The expression of Kca3.1 was shown to be induced in microglial cells surrounding infarction areas in a stroke mouse model. Treatment with TRAM-34, further reduced the microglial activation and infarction area in this stroke model (Chen et al. 2011). Kca3.1 expression was highly induced in microglial cells in a spinal cord injury mouse model. Inhibition of this channel not only reduced production of inflammatory cytokines TNFα and IL-1β but also improved locomotor

deficits and tissue protection (Bouhy et al. 2011). Kca3.1 also plays an important role in regulating glioblastoma invasiveness, and activation and propagation of microglia (D'Alessandro et al. 2013). Surprisingly, LPS did not elicit Kca3.1 channel activity, but ATP and IFNγ elicited moderate amount of Kca3.1 channel activity (Nguyen et al. 2017).

KATP

ATP sensitive-K_{ATP} channels were first identified in cardiac myocytes (Noma 1983), and are composed of eight protein subunits, four subunits of inward rectifier, Kir6.1 or Kir6.2 and four subunits of sulfonylurea receptors (Inagaki et al. 1995). These channels act as metabolic sensors and have a variety of physiological functions, including insulin secretion, and inflammation (Quan et al. 2011). Glial K_{ATP} channels have been implicated in various disorders including stroke, multiple sclerosis and PD. Iptakalim, a K_{ATP} channel opener, was able to reduce glial activation, production of proinflammatory factors like TNFα and p38 MAPK activation in MPP model of PD. Furthermore, these protective effects were reversed when a K_{ATP} channel blocker, hydroxydecanoate, was used (Yang et al. 2009). Moreover, opening of K_{ATP} channel reduced neuroinflammation induced by rotenone in BV2 microglial cell line by reducing p38/JNK MAPK pathway (Zhou et al. 2008). This ATP sensitive potassium channel is further involved in NOS2 production from microglial cells in response to LPS (Kurland et al. 2016). Taken together, most of the current literature suggest a prominent anti-inflammatory role of K_{ATP} in regulating microglial activation in neurodegenerative disorders. Further studies, looking into the potential signaling cascades involved in

regulating K_{ATP} will give leads to potential anti-inflammatory strategies in disease condition.

Other Potassium Channels

Various potassium channels including the ones discussed above play important roles in regulating microglial functions by modulating signaling cascades. Kir2.1, an inward rectifier channel, has been shown to be induced upon alternative activation of microglial cells (Lam et al. 2017). Furthermore, Kir2.1 inhibition reduced microglial proliferation upon anti-inflammatory stimulus (Lam et al. 2017). Kir2.1 further modulates microglial chemotaxis, migration, and intracellular calcium signaling at resting and alternative activation states (Lam and Schlichter 2015). Kv1.5 have also been shown to be induced in classically activated microglial cells (Jou et al. 1998). Furthermore, Kv1.5 knockout microglia have reduced production of NO and proliferation post inflammatory insult (Pannasch et al. 2006) suggesting the role of this outward potassium channel in multiple microglial functions. Further Kv1.5 channel expression was also highly induced in amyloid β treated microglial cells (Chung et al. 2001). Together, the role of potassium channels in microglia is diverse in physiological and disease condition (Fig. 1). Modulation of these ion channels may lead to discovery of key drug targets for neurodegenerative disorders but further mechanistic study to understand the downstream signaling of these channels are necessary.

Sodium Channels

First identified in jellyfish, sodium channels play a major role in diverse physiological functions including cognition, locomotion, and depolarization (Marban et

al. 1998). Sodium channels were the first voltage gated channels to be cloned in 1984 (Noda et al. 1984), but the role of sodium channel in microglial channels is not well studied.

Primary rat microglia isolated from prenatal pups expressed different isoform of sodium channels including Nav1.1, Nav1.5, and Nav1.6 (Black et al. 2009). These channels control a range of microglial functions. Sodium channel inhibition lead to reduced phagocytosis in LPS-activated microglial cells. Further, these channels play an important role in regulating the proinflammatory cytokine release from microglial cells. Phenytoin, a sodium channel inhibitor, reduced the production of IL-1α, IL-1β, and TNFα, induced by LPS but had minimal effect on the other secretory cytokines and chemokines. Furthermore, sodium channel inhibition, reduced ATP-induced microglial chemotaxis and migration (Black et al. 2009).

Deng *et al.* identified the key role of sodium channels in microglial cells in hypoxic environment. This study showed that activated microglia express higher level of sodium channels. Further, these activated microglial cells induced the production of proinflammatory factors including, TNFα and IL-1β, which resulted in the loss of neurons and also linked to periventricular white matter damage associated with hypoxic environment in brain (Deng et al. 2011).

ATP release in extracellular space, leading to neuronal damage and inflammation have been linked to multiple neurodegenerative disorders (Gan et al. 2015; Jun et al. 2007; Rodrigues et al. 2015; Shin et al. 2016). Persson *et al.* demonstrated that inhibition of Nav1.6 modulates the ERK1/2 MAPK pathway thereby regulating the accumulation of Rac1 in response to extracellular ATP in microglial

cells. This study further showed that Nv1.6 directly regulates the cellular polarization, spatial arrangement and microglial movement in response to ATP (Persson et al. 2014).

Microglial sodium channels have been shown to be upregulated in multiple disease models including spinal cord injury and multiple sclerosis. Sodium channel blockage lead to a decreased microglial activation and production of proinflammatory cytokines in spinal cord injury model. Inhibiting sodium channels lead to reduced activation of classical Nfκb, pro-inflammatory pathway, and p38 MAPK pathway but did not alter the activation of JNK pathway (Jung et al. 2013). In animal model of experimental autoimmune encephalopathy, Nav1.6 was found to be highly upregulated in activated microglial cells (Craner et al. 2005). But recent studies looking into specific inhibition of sodium channels have shown that Nv1.2, Na1.4, and Nav1.6 blockage exacerbates experimental autoimmune encephalomyelitis (Stevens et al. 2013). These studies suggest that sodium channel plays a complex role in regulating microglial function. Further studies, understanding the modulation of these diverse channels in disease condition and the signaling pathway is necessary.

Other Channels

Another key channel affecting microglial function in disease model is the unique voltage gated proton channel, Hv1. Microglia, but not astrocytes and neurons, have been shown to express Hv1 current. Interestingly, Hv1 knockout mice have reduced neuronal loss in an ischemic stroke mouse model. Hv1 was shown to play an important role in NADPH oxidase mediated ROS generation in glial cells, which was shown to play an important role in neurodegeneration in stroke model (Wu et al. 2012).

This voltage-gated proton channel compensates cellular loss of electrons with protons hence activating NADPH oxidase (Wu 2014). Dextromethorphan which has an anti-inflammatory activity have been shown to reduce proton channels in microglial cell line, BV2 (Song and Yeh 2012). Moreover Hv1 knockout microglia had lower NOX activation in a cell culture model of periventricular leukomalacia (Yu et al. 2017). Tian *et al.* demonstrated that this unique proton channel can be a potential target for modulating microglial activation profile in disease model. Hv1 deficient microglia was further shown to shift the microglial activation profile towards an alternative anti-inflammatory M2-like phenotype in stroke model (Tian et al. 2016). ROS generation and NADPH oxidase activation in microglial cells is one of the major inflammatory pathways in multiple neurodegenerative disorders including PD (Langley et al. 2017) and AD (Hernandes and Britto 2012; Zekry et al. 2003). NOX inhibition has been implicated as therapeutic targets in these neurodegenerative disorders (Cifuentes-Pagano et al. 2015). But the potential role of Hv1 in AD or PD, the two most prevalent neurodegenerative disorders have not been elucidated.

Other Channels

Multiple calcium channels as well as purinergic receptors have been reported to modulate various physiological functions of microglia in disease conditions (Echeverry et al. 2016; Espinosa-Parrilla et al. 2015; Sperlagh and Illes 2014). L-type voltage gated calcium channels have been implicated in microglial activation in AD and prion disease. Misfolded prion protein, a classical hallmark of prion associated disease, increased the expression of L-type calcium channels and induced microglial activation. Treatment with inhibitors of L-type voltage sensitive calcium channels

reduced the microglial activation suggesting the role of this type of channels in classical activation of glial cells (Silei et al. 1999). Cav1.2 subunit of voltage gated calcium channel was shown to be upregulated in glial cells in mouse model of AD and was related to increase in amyloid β load (Daschil et al. 2013). Moreover, Cav1.2 and Cav1.3 have been shown to be upregulated in microglial cells in a rodent model of N-methyl-D-aspartate-induced hippocampal neurodegeneration (Espinosa-Parrilla et al. 2015). Furthermore, blocking of these calcium channels reduced the production of proinflammatory factors, TNFα and NO, in BV2 microglial cell line post LPS treatment further elucidating the role if these channel in regulating microglial inflammation (Espinosa-Parrilla et al. 2015).

Transient receptor potential (TRP) channels, which are non-selective cation channels, further regulation microglial functions under physiological and disease conditions (Echeverry et al. 2016). Out of the TRPV subfamily of channels TRPV1, TRPV2, and TRPV4 has been shown to regulate major microglial functions. TRPV1 has been associated with microglial inflammation. Induction of TRPV1 lead to increased ROS production and NOX activity leading to inflammation (Schilling and Eder 2009). Induction of TRPV1 channels have been shown to produce other proinflammatory factors, like IL-6 and NO, and activation of pro-inflammatory signaling cascade Nfκb (Sappington and Calkins 2008; Talbot et al. 2012) and MAPK (Miyake et al. 2015). TRPV1 have also been linked to microglial chemotaxis. Induction of TRPV1 lead to increased microglial chemotaxis, while TRPV1-selective blockers reversed the effect (Miyake et al. 2015). TRPV2 is predominantly present in the endoplasmic reticulum and translocate to the plasma membrane post-stress. Though

the role of glial TRPV2 is not well established, this channel may be regulating intracellular calcium signaling leading to microglial activation (Hassan et al. 2014). TRPV4, a mechanosensitive channel, have been shown to play an important role in infrasound induced glial activation and production of proinflammatory factors (Shi et al. 2013). Further, TRPV4 blockage reduced LPS-induced TNFα release and microglial activation (Konno et al. 2012).

TRPM family of non-selective calcium channels further play a role in regulating inflammation in microglial cells. TRPM2 have been shown to induce H_2O_2-induced microglial activation by modulating calcium influx. TRPM2 knockout mice have reduced inflammatory response in response to LPS/ IFN-γ and have reduction in activation of MAPK and JNK signaling cascade (Miyake et al. 2014). TRPM2 and TRPM4 channel activity have been shown to be induced under inflammatory insult and may play a critical role in monitoring microglial cytokine release (Beck et al. 2008; Haraguchi et al. 2012). TRPM7, a calcium permeable channel, have been shown to modulate microglial migration and invasion during alternative activation (Siddiqui et al. 2014). Microglial ATP sensitive purinergic receptor P2X7, have been recently implicated to play an important role in activation of NLRP3 inflammasome (Burm et al. 2016). NLRP3 inflammasome is one of the major functional inflammasome in microglial which has been implicated in neurodegenerative disorders including AD (Halle et al. 2008; Heneka et al. 2013). The microglial functions modulated by these channels are diverse. The mechanism underlying the channel dependent pathways is still under investigation.

Conclusion and Future Directions

As discussed in this review, the current literature has a wealth of information suggesting the probable role of microglial ion channels in regulating diverse physiological and disease associated microglial function (Table 1). The potential of microglial ion channels as drug target is immense keeping into consideration the diverse function of these channels. As mentioned in Fig. 2, these channels have been shown to regulate both classical and alternative microglial activation. Hence proper modulation of microglial ion channels may lead to reduced inflammation or anti-inflammatory microglial phenotype in neurodegenerative conditions. These ion channels may regulate multiple key inflammatory or anti-inflammatory signaling cascade in glial cells and hence modulate neuroinflammation in disease condition. Using one or more of these ion channels as drug targets may be beneficial in case of neurodegenerative disorders, considering the role of inflammation in these diseases. Although we have a lot evidence regarding the probable role of these channels in glial cells, the signaling pathways involved is not clearly understood. Future studies, looking into the channel dependent pathways in these glial cells may open a new avenue for a new class of drug targets for neurodegenerative disease.

References

Beck A, Penner R, Fleig A. 2008. Lipopolysaccharide-induced down-regulation of Ca2+ release-activated Ca2+ currents (I CRAC) but not Ca2+-activated TRPM4-like currents (I CAN) in cultured mouse microglial cells. J Physiol 586:427-39.

Black JA, Liu S, Waxman SG. 2009. Sodium channel activity modulates multiple functions in microglia. Glia 57:1072-81.

Bouhy D, Ghasemlou N, Lively S, Redensek A, Rathore KI, Schlichter LC, David S. 2011. Inhibition of the Ca(2)(+)-dependent K(+) channel, KCNN4/KCa3.1, improves tissue protection and locomotor recovery after spinal cord injury. J Neurosci 31:16298-308.

Burm SM, Zuiderwijk-Sick EA, Weert PM, Bajramovic JJ. 2016. ATP-induced IL-1beta secretion is selectively impaired in microglia as compared to hematopoietic macrophages. Glia 64:2231-2246.

Chandy KG. 1991. Simplified gene nomenclature. Nature 352:26.

Chen YJ, Raman G, Bodendiek S, O'Donnell ME, Wulff H. 2011. The KCa3.1 blocker TRAM-34 reduces infarction and neurological deficit in a rat model of ischemia/reperfusion stroke. J Cereb Blood Flow Metab 31:2363-74.

Chung S, Lee J, Joe EH, Uhm DY. 2001. Beta-amyloid peptide induces the expression of voltage dependent outward rectifying K+ channels in rat microglia. Neurosci Lett 300:67-70.

Cifuentes-Pagano ME, Meijles DN, Pagano PJ. 2015. Nox Inhibitors & Therapies: Rational Design of Peptidic and Small Molecule Inhibitors. Curr Pharm Des 21:6023-35.

Craner MJ, Damarjian TG, Liu S, Hains BC, Lo AC, Black JA, Newcombe J, Cuzner ML, Waxman SG. 2005. Sodium channels contribute to microglia/macrophage activation and function in EAE and MS. Glia 49:220-9.

D'Alessandro G, Catalano M, Sciaccaluga M, Chece G, Cipriani R, Rosito M, Grimaldi A, Lauro C, Cantore G, Santoro A and others. 2013. KCa3.1 channels are involved in the infiltrative behavior of glioblastoma in vivo. Cell Death Dis 4:e773.

Daschil N, Obermair GJ, Flucher BE, Stefanova N, Hutter-Paier B, Windisch M, Humpel C, Marksteiner J. 2013. CaV1.2 calcium channel expression in reactive astrocytes is associated with the formation of amyloid-beta plaques in an Alzheimer's disease mouse model. J Alzheimers Dis 37:439-51.

DeCoursey TE, Chandy KG, Gupta S, Cahalan MD. 1985. Voltage-dependent ion channels in T-lymphocytes. J Neuroimmunol 10:71-95.

Deng YY, Lu J, Ling EA, Kaur C. 2011. Role of microglia in the process of inflammation in the hypoxic developing brain. Front Biosci (Schol Ed) 3:884-900.

Echeverry S, Rodriguez MJ, Torres YP. 2016. Transient Receptor Potential Channels in Microglia: Roles in Physiology and Disease. Neurotox Res 30:467-78.

Espinosa-Parrilla JF, Martinez-Moreno M, Gasull X, Mahy N, Rodriguez MJ. 2015. The L-type voltage-gated calcium channel modulates microglial pro-inflammatory activity. Mol Cell Neurosci 64:104-15.

Fadool DA, Tucker K, Perkins R, Fasciani G, Thompson RN, Parsons AD, Overton JM, Koni PA, Flavell RA, Kaczmarek LK. 2004. Kv1.3 channel gene-targeted deletion produces "Super-Smeller Mice" with altered glomeruli, interacting scaffolding proteins, and biophysics. Neuron 41:389-404.

Feske S, Wulff H, Skolnik EY. 2015. Ion channels in innate and adaptive immunity. Annu Rev Immunol 33:291-353.

Fordyce CB, Jagasia R, Zhu X, Schlichter LC. 2005. Microglia Kv1.3 channels contribute to their ability to kill neurons. J Neurosci 25:7139-49.

Gan M, Moussaud S, Jiang P, McLean PJ. 2015. Extracellular ATP induces intracellular alpha-synuclein accumulation via P2X1 receptor-mediated lysosomal dysfunction. Neurobiol Aging 36:1209-20.

Gardos G. 1958. The function of calcium in the potassium permeability of human erythrocytes. Biochim Biophys Acta 30:653-4.

Gocke AR, Lebson LA, Grishkan IV, Hu L, Nguyen HM, Whartenby KA, Chandy KG, Calabresi PA. 2012. Kv1.3 deletion biases T cells toward an immunoregulatory phenotype and renders mice resistant to autoimmune encephalomyelitis. J Immunol 188:5877-86.

Grissmer S, Dethlefs B, Wasmuth JJ, Goldin AL, Gutman GA, Cahalan MD, Chandy KG. 1990. Expression and chromosomal localization of a lymphocyte K+ channel gene. Proc Natl Acad Sci U S A 87:9411-5.

Gulbins E, Sassi N, Grassme H, Zoratti M, Szabo I. 2010. Role of Kv1.3 mitochondrial potassium channel in apoptotic signalling in lymphocytes. Biochim Biophys Acta 1797:1251-9.

Halle A, Hornung V, Petzold GC, Stewart CR, Monks BG, Reinheckel T, Fitzgerald KA, Latz E, Moore KJ, Golenbock DT. 2008. The NALP3 inflammasome is involved in the innate immune response to amyloid-beta. Nat Immunol 9:857-65.

Haraguchi K, Kawamoto A, Isami K, Maeda S, Kusano A, Asakura K, Shirakawa H, Mori Y, Nakagawa T, Kaneko S. 2012. TRPM2 contributes to inflammatory and neuropathic pain through the aggravation of pronociceptive inflammatory responses in mice. J Neurosci 32:3931-41.

Hassan S, Eldeeb K, Millns PJ, Bennett AJ, Alexander SP, Kendall DA. 2014. Cannabidiol enhances microglial phagocytosis via transient receptor potential (TRP) channel activation. Br J Pharmacol 171:2426-39.

Heneka MT, Kummer MP, Stutz A, Delekate A, Schwartz S, Vieira-Saecker A, Griep A, Axt D, Remus A, Tzeng TC and others. 2013. NLRP3 is activated in Alzheimer's disease and contributes to pathology in APP/PS1 mice. Nature 493:674-8.

Hernandes MS, Britto LR. 2012. NADPH oxidase and neurodegeneration. Curr Neuropharmacol 10:321-7.

Inagaki N, Gonoi T, Clement JPt, Namba N, Inazawa J, Gonzalez G, Aguilar-Bryan L, Seino S, Bryan J. 1995. Reconstitution of IKATP: an inward rectifier subunit plus the sulfonylurea receptor. Science 270:1166-70.

Joiner WJ, Wang LY, Tang MD, Kaczmarek LK. 1997. hSK4, a member of a novel subfamily of calcium-activated potassium channels. Proc Natl Acad Sci U S A 94:11013-8.

Jou I, Pyo H, Chung S, Jung SY, Gwag BJ, Joe EH. 1998. Expression of Kv1.5 K+ channels in activated microglia in vivo. Glia 24:408-14.

Jun DJ, Kim J, Jung SY, Song R, Noh JH, Park YS, Ryu SH, Kim JH, Kong YY, Chung JM and others. 2007. Extracellular ATP mediates necrotic cell swelling in SN4741 dopaminergic neurons through P2X7 receptors. J Biol Chem 282:37350-8.

Jung GY, Lee JY, Rhim H, Oh TH, Yune TY. 2013. An increase in voltage-gated sodium channel current elicits microglial activation followed inflammatory responses in vitro and in vivo after spinal cord injury. Glia 61:1807-21.

Kaushal V, Koeberle PD, Wang Y, Schlichter LC. 2007. The Ca2+-activated K+ channel KCNN4/KCa3.1 contributes to microglia activation and nitric oxide-dependent neurodegeneration. J Neurosci 27:234-44.

Konno M, Shirakawa H, Iida S, Sakimoto S, Matsutani I, Miyake T, Kageyama K, Nakagawa T, Shibasaki K, Kaneko S. 2012. Stimulation of transient receptor potential vanilloid 4 channel suppresses abnormal activation of microglia induced by lipopolysaccharide. Glia 60:761-70.

Kurland DB, Gerzanich V, Karimy JK, Woo SK, Vennekens R, Freichel M, Nilius B, Bryan J, Simard JM. 2016. The Sur1-Trpm4 channel regulates NOS2 transcription in TLR4-activated microglia. J Neuroinflammation 13:130.

Lam D, Lively S, Schlichter LC. 2017. Responses of rat and mouse primary microglia to pro- and anti-inflammatory stimuli: molecular profiles, K(+) channels and migration. J Neuroinflammation 14:166.

Lam D, Schlichter LC. 2015. Expression and contributions of the Kir2.1 inward-rectifier K(+) channel to proliferation, migration and chemotaxis of microglia in unstimulated and anti-inflammatory states. Front Cell Neurosci 9:185.

Langley M, Ghosh A, Charli A, Sarkar S, Ay M, Luo J, Zielonka J, Brenza T, Bennett B, Jin H and others. 2017. Mito-Apocynin Prevents Mitochondrial Dysfunction, Microglial Activation, Oxidative Damage, and Progressive Neurodegeneration in MitoPark Transgenic Mice. Antioxid Redox Signal.

Lawana V, Singh N, Sarkar S, Charli A, Jin H, Anantharam V, Kanthasamy AG, Kanthasamy A. 2017. Involvement of c-Abl Kinase in Microglial Activation of NLRP3 Inflammasome and Impairment in Autolysosomal System. J Neuroimmune Pharmacol.

Liu J, Xu C, Chen L, Xu P, Xiong H. 2012. Involvement of Kv1.3 and p38 MAPK signaling in HIV-1 glycoprotein 120-induced microglia neurotoxicity. Cell Death Dis 3:e254.

Liu J, Xu E, Tu G, Liu H, Luo J, Xiong H. 2017. Methamphetamine potentiates HIV-1gp120-induced microglial neurotoxic activity by enhancing microglial outward K(+) current. Mol Cell Neurosci 82:167-175.

Liu J, Xu P, Collins C, Liu H, Zhang J, Keblesh JP, Xiong H. 2013. HIV-1 Tat protein increases microglial outward K(+) current and resultant neurotoxic activity. PLoS One 8:e64904.

Maezawa I, Nguyen HM, Di Lucente J, Jenkins DP, Singh V, Hilt S, Kim K, Rangaraju S, Levey AI, Wulff H and others. 2017. Kv1.3 inhibition as a potential microglia-targeted therapy for Alzheimer's disease: preclinical proof of concept. Brain.

Maezawa I, Zimin PI, Wulff H, Jin LW. 2011. Amyloid-beta protein oligomer at low nanomolar concentrations activates microglia and induces microglial neurotoxicity. J Biol Chem 286:3693-706.

Marban E, Yamagishi T, Tomaselli GF. 1998. Structure and function of voltage-gated sodium channels. J Physiol 508 (Pt 3):647-57.

Matteson DR, Deutsch C. 1984. K channels in T lymphocytes: a patch clamp study using monoclonal antibody adhesion. Nature 307:468-71.

Menteyne A, Levavasseur F, Audinat E, Avignone E. 2009. Predominant functional expression of Kv1.3 by activated microglia of the hippocampus after Status epilepticus. PLoS One 4:e6770.

Miyake T, Shirakawa H, Kusano A, Sakimoto S, Konno M, Nakagawa T, Mori Y, Kaneko S. 2014. TRPM2 contributes to LPS/IFNgamma-induced production of nitric oxide via the p38/JNK pathway in microglia. Biochem Biophys Res Commun 444:212-7.

Miyake T, Shirakawa H, Nakagawa T, Kaneko S. 2015. Activation of mitochondrial transient receptor potential vanilloid 1 channel contributes to microglial migration. Glia 63:1870-82.

Nguyen HM, Grossinger EM, Horiuchi M, Davis KW, Jin LW, Maezawa I, Wulff H. 2017. Differential Kv1.3, KCa3.1, and Kir2.1 expression in "classically" and "alternatively" activated microglia. Glia 65:106-121.

Noda M, Shimizu S, Tanabe T, Takai T, Kayano T, Ikeda T, Takahashi H, Nakayama H, Kanaoka Y, Minamino N and others. 1984. Primary structure of

Electrophorus electricus sodium channel deduced from cDNA sequence. Nature 312:121-7.

Noma A. 1983. ATP-regulated K+ channels in cardiac muscle. Nature 305:147-8.

Norenberg W, Appel K, Bauer J, Gebicke-Haerter PJ, Illes P. 1993. Expression of an outwardly rectifying K+ channel in rat microglia cultivated on teflon. Neurosci Lett 160:69-72.

Panicker N, Saminathan H, Jin H, Neal M, Harischandra DS, Gordon R, Kanthasamy K, Lawana V, Sarkar S, Luo J and others. 2015. Fyn Kinase Regulates Microglial Neuroinflammatory Responses in Cell Culture and Animal Models of Parkinson's Disease. J Neurosci 35:10058-77.

Pannasch U, Farber K, Nolte C, Blonski M, Yan Chiu S, Messing A, Kettenmann H. 2006. The potassium channels Kv1.5 and Kv1.3 modulate distinct functions of microglia. Mol Cell Neurosci 33:401-11.

Paolicelli RC, Bolasco G, Pagani F, Maggi L, Scianni M, Panzanelli P, Giustetto M, Ferreira TA, Guiducci E, Dumas L and others. 2011. Synaptic pruning by microglia is necessary for normal brain development. Science 333:1456-8.

Peng Y, Lu K, Li Z, Zhao Y, Wang Y, Hu B, Xu P, Shi X, Zhou B, Pennington M and others. 2014. Blockade of Kv1.3 channels ameliorates radiation-induced brain injury. Neuro Oncol 16:528-39.

Persson AK, Estacion M, Ahn H, Liu S, Stamboulian-Platel S, Waxman SG, Black JA. 2014. Contribution of sodium channels to lamellipodial protrusion and Rac1 and ERK1/2 activation in ATP-stimulated microglia. Glia 62:2080-95.

Quan Y, Barszczyk A, Feng ZP, Sun HS. 2011. Current understanding of K ATP channels in neonatal diseases: focus on insulin secretion disorders. Acta Pharmacol Sin 32:765-80.

Quiros PM, Mottis A, Auwerx J. 2016. Mitonuclear communication in homeostasis and stress. Nat Rev Mol Cell Biol 17:213-26.

Rangaraju S, Gearing M, Jin LW, Levey A. 2015. Potassium channel Kv1.3 is highly expressed by microglia in human Alzheimer's disease. J Alzheimers Dis 44:797-808.

Rangaraju S, Raza SA, Pennati A, Deng Q, Dammer EB, Duong D, Pennington MW, Tansey MG, Lah JJ, Betarbet R and others. 2017. A systems pharmacology-based approach to identify novel Kv1.3 channel-dependent mechanisms in microglial activation. J Neuroinflammation 14:128.

Reeves TM, Trimmer PA, Colley BS, Phillips LL. 2016. Targeting Kv1.3 channels to reduce white matter pathology after traumatic brain injury. Exp Neurol 283:188-203.

Rodrigues RJ, Tome AR, Cunha RA. 2015. ATP as a multi-target danger signal in the brain. Front Neurosci 9:148.

Sappington RM, Calkins DJ. 2008. Contribution of TRPV1 to microglia-derived IL-6 and NFkappaB translocation with elevated hydrostatic pressure. Invest Ophthalmol Vis Sci 49:3004-17.

Sarkar S, Malovic E, Harishchandra DS, Ghaisas S, Panicker N, Charli A, Palanisamy BN, Rokad D, Jin H, Anantharam V and others. 2017. Mitochondrial impairment

in microglia amplifies NLRP3 inflammasome proinflammatory signaling in cell culture and animal models of Parkinson's disease. NPJ Parkinsons Dis 3:30.

Schilling T, Eder C. 2009. Importance of the non-selective cation channel TRPV1 for microglial reactive oxygen species generation. J Neuroimmunol 216:118-21.

Schlichter LC, Sakellaropoulos G, Ballyk B, Pennefather PS, Phipps DJ. 1996. Properties of K+ and Cl- channels and their involvement in proliferation of rat microglial cells. Glia 17:225-36.

Sharma S, Carlson S, Puttachary S, Sarkar S, Showman L, Putra M, Kanthasamy AG, Thippeswamy T. 2017. Role of the Fyn-PKCdelta signaling in SE-induced neuroinflammation and epileptogenesis in experimental models of temporal lobe epilepsy. Neurobiol Dis 110:102-121.

Shi M, Du F, Liu Y, Li L, Cai J, Zhang GF, Xu XF, Lin T, Cheng HR, Liu XD and others. 2013. Glial cell-expressed mechanosensitive channel TRPV4 mediates infrasound-induced neuronal impairment. Acta Neuropathol 126:725-39.

Shin HJ, Kwon HK, Lee JH, Anwar MA, Choi S. 2016. Etoposide induced cytotoxicity mediated by ROS and ERK in human kidney proximal tubule cells. Sci Rep 6:34064.

Siddiqui T, Lively S, Ferreira R, Wong R, Schlichter LC. 2014. Expression and contributions of TRPM7 and KCa2.3/SK3 channels to the increased migration and invasion of microglia in anti-inflammatory activation states. PLoS One 9:e106087.

Silei V, Fabrizi C, Venturini G, Salmona M, Bugiani O, Tagliavini F, Lauro GM. 1999. Activation of microglial cells by PrP and beta-amyloid fragments raises

intracellular calcium through L-type voltage sensitive calcium channels. Brain Res 818:168-70.

Song JH, Yeh JZ. 2012. Dextromethorphan inhibition of voltage-gated proton currents in BV2 microglial cells. Neurosci Lett 516:94-8.

Sperlagh B, Illes P. 2014. P2X7 receptor: an emerging target in central nervous system diseases. Trends Pharmacol Sci 35:537-47.

Stevens M, Timmermans S, Bottelbergs A, Hendriks JJ, Brone B, Baes M, Tytgat J. 2013. Block of a subset of sodium channels exacerbates experimental autoimmune encephalomyelitis. J Neuroimmunol 261:21-8.

Szabo I, Bock J, Grassme H, Soddemann M, Wilker B, Lang F, Zoratti M, Gulbins E. 2008. Mitochondrial potassium channel Kv1.3 mediates Bax-induced apoptosis in lymphocytes. Proc Natl Acad Sci U S A 105:14861-6.

Talbot S, Dias JP, Lahjouji K, Bogo MR, Campos MM, Gaudreau P, Couture R. 2012. Activation of TRPV1 by capsaicin induces functional kinin B(1) receptor in rat spinal cord microglia. J Neuroinflammation 9:16.

Tian DS, Li CY, Qin C, Murugan M, Wu LJ, Liu JL. 2016. Deficiency in the voltage-gated proton channel Hv1 increases M2 polarization of microglia and attenuates brain damage from photothrombotic ischemic stroke. J Neurochem 139:96-105.

Turtzo LC, Lescher J, Janes L, Dean DD. 2014. Macrophagic and microglial responses after focal traumatic brain injury in the female rat. J Neuroinflammation 11.

Upadhyay SK, Eckel-Mahan KL, Mirbolooki MR, Tjong I, Griffey SM, Schmunk G, Koehne A, Halbout B, Iadonato S, Pedersen B and others. 2013. Selective Kv1.3 channel blocker as therapeutic for obesity and insulin resistance. Proc Natl Acad Sci U S A 110:E2239-48.

Visentin S, Renzi M, Levi G. 2001. Altered outward-rectifying K(+) current reveals microglial activation induced by HIV-1 Tat protein. Glia 33:181-90.

Wei AD, Gutman GA, Aldrich R, Chandy KG, Grissmer S, Wulff H. 2005. International Union of Pharmacology. LII. Nomenclature and molecular relationships of calcium-activated potassium channels. Pharmacol Rev 57:463-72.

Wu LJ. 2014. Microglial voltage-gated proton channel Hv1 in ischemic stroke. Transl Stroke Res 5:99-108.

Wu LJ, Wu G, Akhavan Sharif MR, Baker A, Jia Y, Fahey FH, Luo HR, Feener EP, Clapham DE. 2012. The voltage-gated proton channel Hv1 enhances brain damage from ischemic stroke. Nat Neurosci 15:565-73.

Xu J, Wang P, Li Y, Li G, Kaczmarek LK, Wu Y, Koni PA, Flavell RA, Desir GV. 2004. The voltage-gated potassium channel Kv1.3 regulates peripheral insulin sensitivity. Proc Natl Acad Sci U S A 101:3112-7.

Yang YJ, Zhang S, Ding JH, Zhou F, Hu G. 2009. Iptakalim protects against MPP+-induced degeneration of dopaminergic neurons in association with astrocyte activation. Int J Neuropsychopharmacol 12:317-27.

Yu Y, Yu Z, Xie M, Wang W, Luo X. 2017. Hv1 proton channel facilitates production of ROS and pro-inflammatory cytokines in microglia and enhances

oligodendrocyte progenitor cells damage from oxygen-glucose deprivation in vitro. Biochem Biophys Res Commun.

Zekry D, Epperson TK, Krause KH. 2003. A role for NOX NADPH oxidases in Alzheimer's disease and other types of dementia? IUBMB Life 55:307-13.

Zhou F, Yao HH, Wu JY, Ding JH, Sun T, Hu G. 2008. Opening of microglial K(ATP) channels inhibits rotenone-induced neuroinflammation. J Cell Mol Med 12:1559-70.

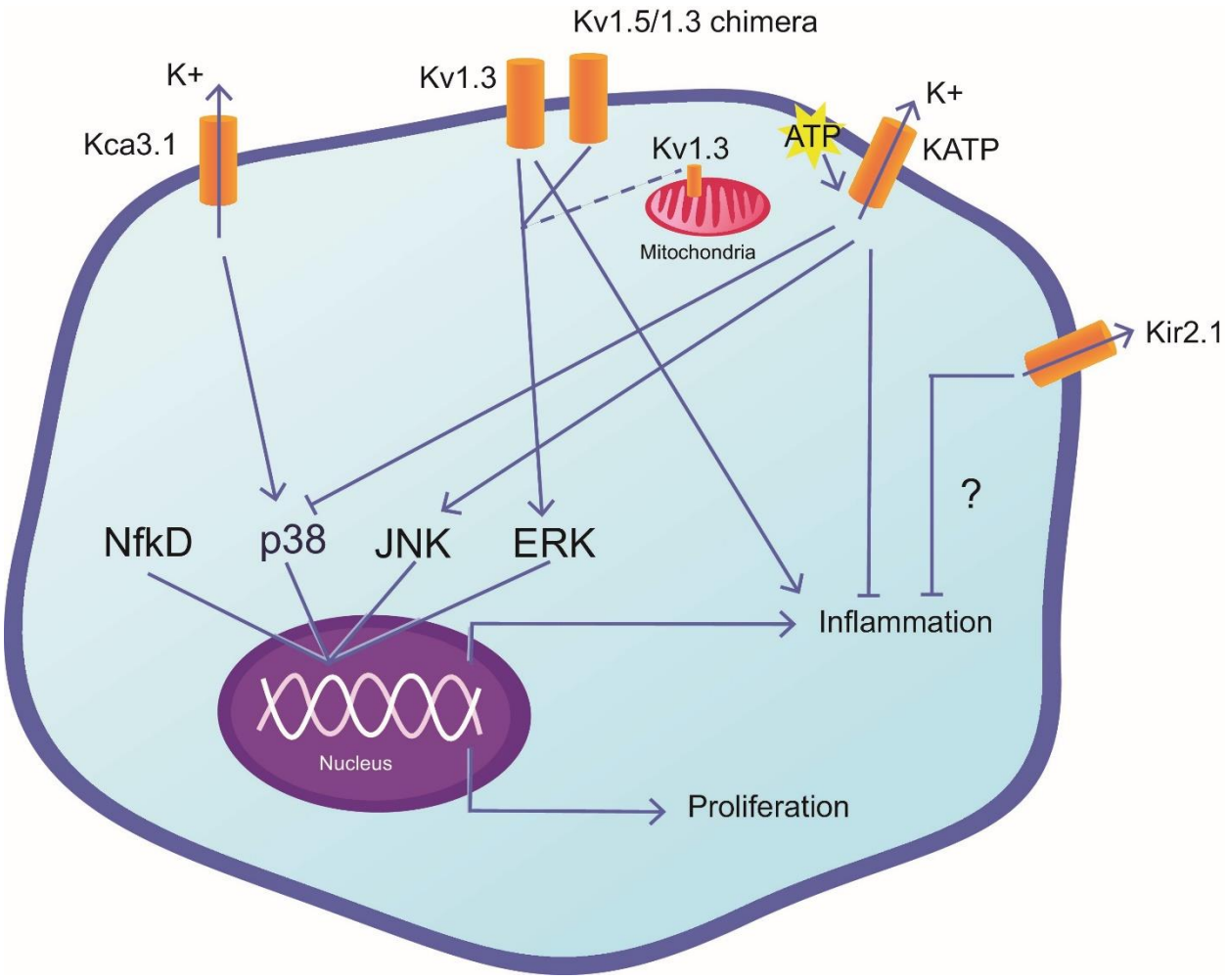

Fig. 1: Signaling pathways regulated by potassium channels in microglial cells leading to inflammation

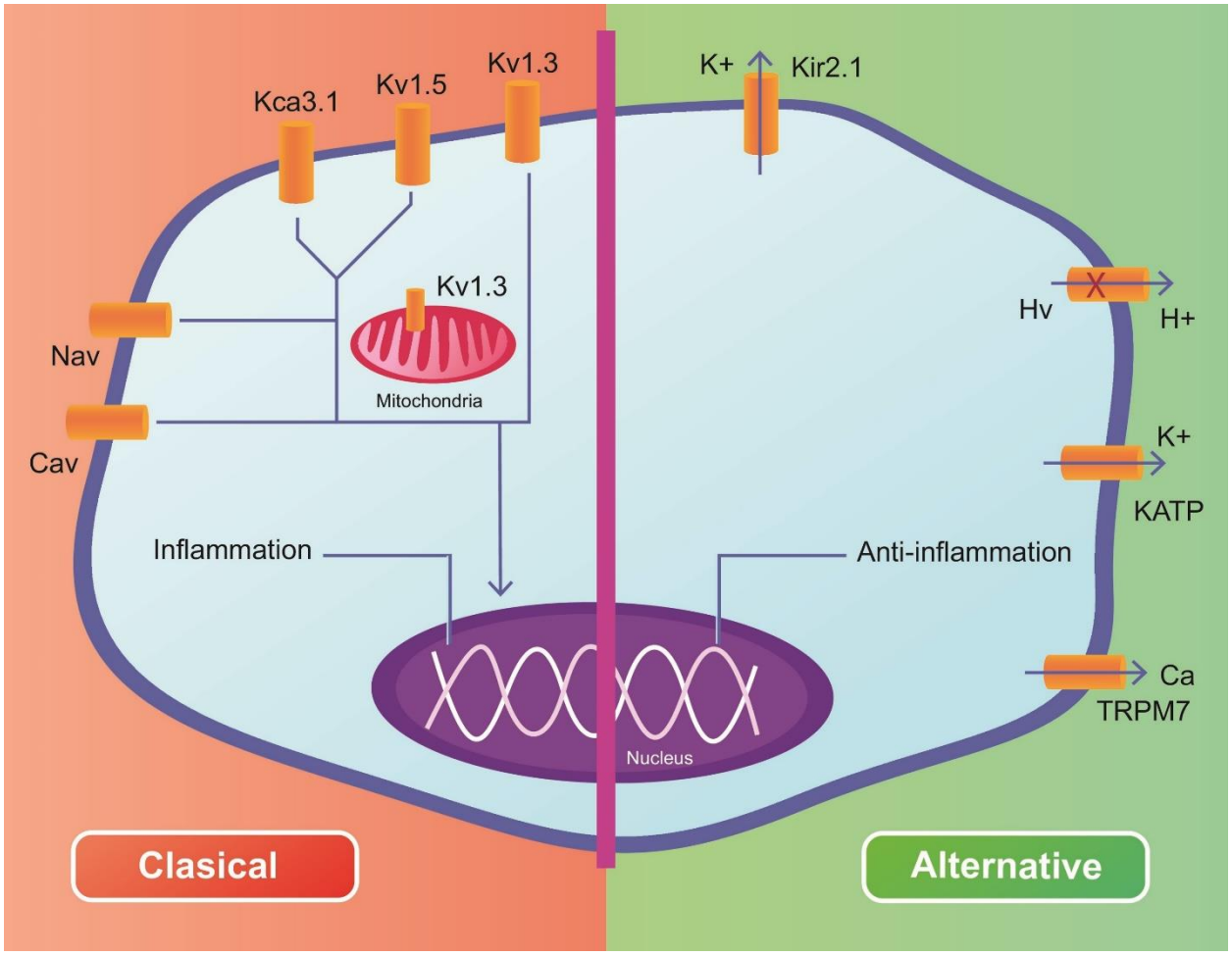

Fig. 2. Ion channels involved in classical and alternative activation of microglial cells

Table 1. Ion channel dependent microglial function in disease conditions.

Channel Name	Disease Associated	Microglial function	References
Kv1.3	AD, PD, HIV induced dementia, epilepsy, and radiation induced brain injury	Proinflammation, Phagocytosis, Antigen Presentation, Migration and Proliferation	Schlichter et al. 1996; Fordyce et al. 2005; Rangaraju et al. 2017; Visentin et al. 2001; Reeves et al. 2016; Rangaraju et al. 2015; Liu et al. 2017; Liu et al. 2013;
Kca3.1	optic nerve transection mouse model, AD, stroke	Proinflammation, Migration, and Proliferation	Maezawa et al. 2011; Chen et al. 2011; Bouhy et al. 2011; D'Alessandro et al. 2013; Nguyen et al. 2017;
Kv1.5	AD	Inflammation	Jou et al. 1998; Pannasch et al. 2006; Chung et al. 2001;
K_{ATP}	MS, Stroke, PD	Anti-inflammation	Yang et al. 2009; Zhou et al. 2008; Kurland et al. 2016;

Table 1. (continued)

Kir2.1	IL-4 and IL-10 treatment	Anti-inflammation; Migration, and proliferation	Lam et al. 2017; Lam and Schlichter 2015;
Nav	Hypoxia, spinal cord injury, multiple sclerosis, stroke	Inflammation, phagocytosis, cellular polarization, spatial arrangement and microglial movement	Black et al. 2009; Deng et al. 2011; Gan et al. 2015; Jun et al. 2007; Rodrigues et al. 2015; Shin et al. 2016; Jung et al. 2013; Craner et al. 2005; Stevens et al. 2013;
Hv	Stroke, PD, AD	Anti-inflammation	Hernandes and Britto 2012; Zekry et al. 2003; Cifuentes-Pagano et al. 2015; Tian et al. 2016;
L-type calcium channels	AD, Hippocampal neurodegeneration	Proinflammation	Silei et al. 1999; Daschil et al. 2013; Espinosa-Parrilla et al. 2015;

Table 1. (continued)

TRPV	Inflammatory stress condition	Proinflammation, Chemotaxis	Echeverry et al. 2016; Schilling and Eder 2009; Sappington and Calkins 2008; Talbot et al. 2012; Miyake et al. 2015; Hassan et al. 2014; Shi et al. 2013; Konno et al. 2012;
TRPM	Inflammatory stress condition	Proinflammation, chemotaxis, migration, Anti-inflammation*	Miyake et al. 2014; Beck et al. 2008; Haraguchi et al. 2012; Siddiqui et al. 2014;

*TRPM7 has an anti-inflammatory function leading to alternative activation of glial cells. Other know TRPM induce classical activation of microglia.

CHAPTER IV

MITOCHONDRIAL IMPAIRMENT IN MICROGLIA AMPLIFIES NLRP3 INFLAMMASOME PROINFLAMMATORY SIGNALING IN CELL CULTURE AND ANIMAL MODELS OF PARKINSON'S DISEASE

Manuscript published in *Nature Parkinson's Disease*

Souvarish Sarkar[1], Emir Malovic[1], Dilshan Harishchandra[1†], Shivani Ghaisas[1†], Nikhil Panicker[1§], Adhithiya Charli[1], Bharathi Palanisamy[1], Dharmin Rokad[1], Huajun Jin[1], Vellareddy Anantharam[1], Arthi Kanthasamy[1], Anumantha Kanthasamy[1*]

[1]Department of Biomedical Science, Iowa State University, Ames, Iowa 50011

[†]Current address: Perelman School of Medicine, Abramson Family Cancer Research Institute, University of Pennsylvania, 421 Curie Boulevard, 642 BRB II/III, Philadelphia PA, 19104

[§]Current address: Institute for Cell Engineering, The Johns Hopkins School of Medicine, 733 North Broadway, Baltimore, MD 21210

*To whom correspondence should be addressed: Anumantha Kanthasamy, Ph.D. Distinguished Professor and Chair, Department of Biomedical Sciences, Iowa State University, Ames, IA 50011, Telephone: (515) 294-2516; Fax: (515) 294-2315, Email: akanthas@iastate.edu

Abstract

The NLRP3 inflammasome signaling pathway is a major contributor to the neuroinflammatory process in the central nervous system. Oxidative stress and mitochondrial dysfunction are key pathophysiological processes of many chronic neurodegenerative diseases, including Parkinson's disease (PD). However, the inter-relationship between mitochondrial defects and neuroinflammation is not well understood. In the present study, we show that impaired mitochondrial function can augment the NLRP3 inflammasome-driven proinflammatory cascade in microglia. Primary mouse microglia treated with the common inflammogen, LPS, increased NLRP3 and pro-IL-1β expression. Interestingly, exposure of LPS-primed microglial cells to the mitochondrial complex-I inhibitory pesticides, rotenone and tebufenpyrad, specifically potentiated the NLRP3 induction, ASC speck formation and pro-IL-1β processing to IL-1β in a dose-dependent manner, indicating that mitochondrial impairment heightened the NLRP3 inflammasome-mediated proinflammatory response in microglia. The neurotoxic pesticide-induced NLRP3 inflammasome activation was accompanied by bioenergetic defects and lysosomal dysfunction in microglia. Furthermore, the pesticides enhanced mitochondrial ROS generation in primary microglia, while amelioration of mitochondria-derived ROS by the mitochondria-targeted antioxidant mito-apocynin completely abolished IL-1β release, indicating mitochondrial ROS drives the potentiation of NLRP3 inflammasome in microglia. Exposure to conditioned media obtained from mitochondrial inhibitor-treated, LPS-primed microglial cells, but not unprimed cells, induced dopaminergic neurodegeneration in cultured primary mesencephalic and human dopaminergic

neuronal cells (LUHMES). Notably, our *in vivo* results with chronic rotenone rodent models of PD further support the activation of proinflammatory NLRP3 inflammasome signaling due to mitochondrial dysfunction. Collectively, our results demonstrate that mitochondrial impairment in microglia can amplify NLRP3 inflammasome signaling, which augments dopaminergic neurodegenerative process.

Keywords: Mitochondria, mitochondrial dysfunction, microglia, microglial activation, NLRP3 inflammasome, proinflammatory signaling, Parkinson's Disease, rotenone, pesticides

Introduction

Parkinson's disease (PD) is the most common neurodegenerative movement disorder affecting around 2% of the US population over age 60. Its incidence is expected to rise dramatically with the advancing median age of the population, worsening the substantial socioeconomic burden on patients, their families and society. The main pathological hallmark of this disease is degenerating dopaminergic (DAergic) neurons within the nigrostriatal tract that project from the substantia nigra (SN) to the striatum, resulting in severely depleted striatal DA that clinically manifests as a range of debilitating motor symptoms[1,2]. The underlying mechanisms of the neuronal degeneration are not well understood, but mitochondrial dysfunction, chronic inflammation, and oxidative stress have been implicated in different animal models of PD[3-5]. The role of inflammation in PD was first suggested in 1988 when major histocompatibility complex molecules were shown to be upregulated in PD patients[6]. Furthermore, various proinflammatory factors like tumor necrosis factor α (TNF-α) and IL-1β were found to be upregulated in cerebrospinal fluid (CSF) and different regions of the brain in PD patients[7]. In various animal models of PD, including nigrostriatal lesions with 6-OHDA, MPTP, and rotenone, a selective loss of DAergic neurons is accompanied by chronic neuroinflammation[8-12], partly mediated by microglia, the resident immune cells in the brain[5,13-15]. Since, depending on stimuli, microglia secrete both anti-inflammatory and pro-inflammatory factors, as well as growth factors, they are critical for regulating neuronal survival[16,17]. Though various inflammogens have been shown to stimulate microglia-mediated neuroinflammatory processes, the precise mechanisms underlying neuroinflammation remain equivocal. Understanding

the mechanism driving chronic brain inflammation may lead to a better understanding of PD pathogenesis and progression.

Mitochondrial dysfunction and perturbations in mitochondrial dynamics in DAergic neurons are well established causes of neuronal degeneration in PD[18-24]. Despite this, the link between mitochondrial impairment in microglia *per se* and neuroinflammation is not well characterized. Recent studies have implicated inflammasome activation in inflammatory neurodegenerative disorders[25,26] like Alzheimer's disease (AD), multiple sclerosis and traumatic brain injury (TBI)[25,27]. Inflammasomes are multiprotein oligomers mainly formed by ASC, caspase-1, and the inflammasome component (e.g., NLRP3, NLRP1, NLRC4, AIM2). Multiple *inflammasomes* have been identified in microglia, astrocytes and neurons. The major function of an inflammasome is to cleave pro-IL-1β to IL-1β, or to produce IL-18 to enhance and sustain inflammation. Both NLRP3 and NLRP1 inflammasomes have been implicated in AD pathogenesis[28,29]. NLRP3 inflammasome activation normally requires two signals for its function. Signal 1 activates the NFκB pathway facilitating pro-IL-1β and NLRP3 transcription and translation. Signal 2 forms the inflammasome complex comprising NLRP3, ASC, and caspase-1, which in turn cleaves pro-IL-1β to IL-1β. Signal 2 can vary from pathogens to aggregated proteins to ATP. Mechanisms underlying inflammasome complex formation remain unresolved[30].

The current study addresses the putative link between mitochondrial impairment and inflammasome activation in microglial cells, which may help identify a mechanism behind chronic inflammation-driven neurodegeneration. Recently, we demonstrated in a DAergic neuronal cell culture model that mitochondria-impairing

pesticides compromise mitochondrial dynamics (structure and function) by inhibiting mitochondrial complex-I[21]. Here, we demonstrate that impairing mitochondrial function in primary microglial cells, which had been treated with the classical PD mitochondrial neurotoxicant rotenone and the acaricide tebufenpyrad, may play an important role in inducing the NLRP3 inflammasome. Furthermore, we demonstrate the activation of NLRP3 inflammasome in a chronic rotenone animal model of PD. We also demonstrate that mitochondrial derived ROS contributes to inflammasome activation by utilizing a mitochondrially targeted derivative of apocynin.

Results

Rotenone and tebufenpyrad activate NLRP3 inflammasome in primary microglia

We utilized two mitochondrial complex-1 inhibitors, rotenone and tebufenpyrad, to confirm cross-talk between mitochondrial dysfunction and microglial NLRP3 inflammasome signaling. Exposure of LPS-primed (1 μM for 3 h) or unprimed primary mouse microglia cells to a concentration (1 μM for 24 h) of rotenone or tebufenpyrad sufficient to inhibit mitochondrial complex-1[31] did not induce cell death, as measured by MTS assay (Fig. 1a). Next, Luminex multiplex cytokine assays revealed a dramatic increase in the levels of IL-1β, but not that of TNF-α, confirming that the rotenone and tebufenpyrad treatments of primed cells induced release of the pro-inflammatory cytokine that is mediated by inflammasome signaling (Fig. 1b). Pesticide treatments alone did not increase either IL-1β or TNF-α in unprimed primary microglia (Fig. 1b).

Next, LPS-primed or unprimed primary microglia were exposed to rotenone and tebufenpyrad for 3 and 6 h. Western blotting (Fig. 1c) revealed a time-dependent increase in cleaved caspase-1 levels when compared to LPS-primed and unprimed

microglia, although cleaved caspase-1 did increase slightly in LPS-primed microglia. Both the enhanced release of IL-1β and cleavage of caspase-1, suggesting the induction and activation of inflammasome signaling following mitochondrial complex-1 inhibition. Next, ICC analysis revealed that NLRP3 immunoreactivity is indeed induced in rotenone- and tebufenpyrad-treated, LPS-primed microglia, but not in control microglia (Supplementary Fig. 1). As expected, NLRP3 induction also occurred in the LPS-priming alone group. Exposure of LPS-primed microglia to a secondary stimulus like rotenone or tebufenpyrad after NLRP3 induction resulted in the association of NLPR3 with ASC[32], as revealed by the proximal ligation Duolink assay (Fig. 1d). Furthermore, both rotenone- and tebufenpyrad-treated primed microglial exhibited inflammasome activation-linked ASC speck formation[33] (Fig. 1e). These data collectively support the two-pronged approach of inflammasome activation as previously described[27,32]. Signal 1, which in our study is LPS, induces the expression of NLRP3 and pro-IL-1β, but not the cleavage of pro-IL-1β to its active form IL-1β. Signal 2, which in our study are the mitochondrial inhibitors, leads to formation of the inflammasome complex consisting of NLRP3, ASC and caspase-1. This complex formation leads to activation of caspase-1, which in-turn cleaves pro-IL-1β to IL-1β. That is why we observed increased IL-1β release only in the LPS+Rot and LPS+Tebu groups.

Wilson et al.[34] have shown that NLRP3 inflammasome activation also induces IL-18 release along with IL-1β. Thus, we treated LPS-primed mouse microglia with either tebufenpyrad or rotenone for 2 h and then measured pro-IL-18 by qRT-PCR mRNA analysis. In line with previous reports[32],both pro-IL-1β mRNA levels, and pro-

IL-18 levels, increased significantly in LPS-primed and pesticide treatment groups, (Supplementary Fig. 2A-B).

A study by *Sherer et al.* [35] reported that the IC50 for complex I inhibition is in nano molar range for both rotenone and tebufenpyrad, the cell type used in their study is of neuronal lineage which is more susceptible to complex I inhibitors than macrophage-like cells, including microglial cells used in our study. A much higher dose of rotenone (10 µM) has been previously used in inflammasome studies[32]. High micro-molar doses of rotenone are known to induce acetylation of tubulin [36]. Microtubule acetylation has also recently been linked to NLRP3 inflammasome activation [37]. Misawa et al. [37] reported that SIRT2 downregulation leads to acetylation of α-tubulin, which modulates NLRP3 inflammasome activation. Hence, to confirm if our micro-molar dose of pesticides affects microtubule assembly and inflammasome activation, primary microglial cells were treated with 1 µM rotenone and tebufenpyrad for 3 h following LPS priming. ICC analysis revealed that SIRT2 and acetylated α-tubulin levels did not change significantly following pesticide exposure (Supplementary Fig 3). These data suggest that pesticide-induced inflammasome activation is not dependent on microtubule assembly at early time points.

Next, we utilized a neuron-microglia co-culture system to see if pesticide exposure alone can prime the microglial cells. Mouse MN9D dopaminergic neuronal cells were grown on inserts placed in wells growing microglial cells. The cells were treated with 1 µM rotenone for 6 h, after which q-RT-PCR analysis revealed that pesticide exposure induced NLRP3 (Supplementary Fig. 4A) and pro-IL-β (Supplementary Fig. 4B) in the co-cultured microglial cells. To further validate our *in*

vitro study *in vivo,* we made use of the rotenone mouse model of PD[38]. Mice were gavaged daily for 28 days with 30 mg/kg rotenone. Rotenone significantly increased NLRP3 gene expression as revealed by qPCR analysis of striatal lysates (Fig. 1f). Immunoblot analysis showed that rotenone also significantly increased inflammasome markers such as NLRP3, cleaved caspase 1 p20, pro-IL-1β and cleaved IL-1β (Fig. 1g-l).

Next, we also utilized the rat model of rotenone. Rats were injected with 2.8 mg of rotenone for 4 days, and sacrificed after 3 months[11], q-RT-PCR analysis revealed that, like in the mouse model, rotenone induced NLRP3 expression in rats (Supplementary Fig. 5A). Moreover, immunohistochemical analysis revealed that rotenone exposure upregulated NLRP3 in the IBA1-positive microglial cells (Supplementary Fig. 5B). We wanted to clarify that the LPS priming used in the *in vitro* model acts as signal 1 to activate the NFκB pathway. However, in the *in vivo* models, LPS priming is not necessary since the rotenone-induced neuronal stress can itself act as signal 1[30]. Furthermore, including LPS priming step *in vivo* will make the model more complex as LPS can induce inflammasome activation[39]. Also, unlike an LPS priming step for *in vitro* models, it is not possible to get rid of the LPS *in vivo* after a certain time. These results collectively showed that mitochondrial complex-1 inhibition can lead to NLRP3 inflammasome activation in an environmental pesticide toxicant-driven mouse model of PD. Together, these findings indicate that rotenone and tebufenpyrad can activate the NLRP3 inflammasome in primary mouse microglia.

Mitochondrial complex-1 inhibition induces a dose-dependent release of IL-1β in primed microglia through the NLRP3 inflammasome pathway

To test if the effects of rotenone and tebufenpyrad on inflammasome activation are dose-dependent, we exposed LPS-primed primary mouse microglia to 10-1000 nM of rotenone or 50-1000 nM of tebufenpyrad for 24 h and then the medium was used for determining the levels of extracellularly released IL-1β. Luminex assays revealed both rotenone (Fig. 2a) and tebufenpyrad (Fig. 2b) induced a dose-dependent release of IL-1β from LPS-primed cells. Indeed, even doses as low as 50 nM induced NLRP3 inflammasome-mediated IL-1β release.

To further confirm whether the rotenone- and tebufenpyrad-induced IL-1β release is due to the activation of NLRP3 inflammasome, LPS-primed and unprimed primary microglial cells were pretreated with 100 nM MCC-950, a potent NLRP3 inflammasome inhibitor [40], for 1 h followed by co-treatment with rotenone or tebufenpyrad for 6h. An MTS assay revealed that 100 nM MCC-950, tested alone or in combination with the pesticides, did not lead to cell death, confirming that the NLRP3 inhibitor's effect was not due to cytotoxicity (Supplementary Fig. 6). Also, the MCC-950 pre-treatment almost completely blocked the rotenone-induced secretion of IL-1β (Fig. 2c) and tebufenpyrad (Fig. 2d). As a negative control, MCC-950 does not block the rotenone- or tebufenpyrad-induced release of IL-12, which is not dependent on NLRP3 activation (Fig. c-d, right panels).

The other NLRP family members AIM2 and NLRC4 can also mediate the release of IL-1β [41]. Thus, we treated LPS-primed mouse primary microglia with the mitochondrial inhibitors for 2 h and then measured various inflammasomes by qRT-

PCR mRNA analysis. We observed a huge induction in NLRP3 mRNA levels only in LPS-primed microglia without changes in AIM2 or NLRC4 levels (Fig. 2e), again suggesting specificity towards NLRP3 induction in primary microglia. Together, these results strongly suggest that the complex-1 inhibitor-induced release of IL-1β is indeed mediated by NLRP3 activation.

Mitochondrial complex-1 inhibitors induce structural and functional changes in microglia

Next, we characterized the microglial structural and functional changes underlying cross-talk between mitochondrial dysfunction and NLRP3 inflammasome activation. We first treated LPS-primed primary microglial cells with 1 μM rotenone or tebufenpyrad for 3 h. Exposure of LPS-primed cells to both complex-1 inhibitors impaired mitochondrial bioenergetics as indicated by compromised basal respiration, ATP-linked respiration, and spare respiratory capacity, which were measured using a Seahorse Bioscience XFe24 analyzer (Fig. 3a). Next, we treated LPS-primed primary microglia for 2 h with rotenone or tebufenpyrad and then stained them with TMRM, a dye which is readily sequestered into active mitochondria and stains them according to their potential. Pesticide-treated primed microglia exhibited reduced TMRM fluorescence (Fig. 3b) compared to unprimed cells, suggesting inflammasome-related mitochondrial dysfunction. Furthermore, an ATP assay (Fig. 3c) revealed that the pesticide-treated primed microglia produced less ATP when compared to unprimed cells, suggesting that their mitochondria were functionally damaged at an early stage of inflammasome activation. We tested for additional markers of pesticide-induced mitochondrial structural damage in primed primary microglial cells treated with 1 μM

rotenone or tebufenpyrad by staining them for 6 h with MitoTracker Red. Quantification of fluorescence revealed that mitochondria in pesticide-treated, LPS-primed microglial cells exhibited greater fission-related circularity and solidity than did non-treated cells (Fig. 3d-e).

To identify if the mitochondrial dysfunction is an effect of inflammasome activation, we co-treated primary microglial cells with the NLRP3-specific inhibitor MCC-950 (100 nM) and 1 μM rotenone or tebufenpyrad for 3 h. The mitochondrial stress assay revealed that inhibiting the NLRP3 inflammasome did not reverse the mitochondrial defects (Supplementary Fig. 7a-b). These data indicate the probable role of mitochondria upstream of inflammasome activation.

Together with inflammasome results, these findings indicate that complex-1 inhibition-associated NLRP3 inflammasome activation is accompanied by mitochondrial structural and functional dysfunction in microglial cells.

Mitochondrial superoxide generation plays a role in rotenone- and tebufenpyrad-induced NLRP3 inflammasome activation

Damaged mitochondria release superoxide (O2-), which not only causes oxidative damage to cells [42], but also activates inflammasome signaling in peripheral immune cells [43,44]. To decipher the role of superoxide in complex-1 inhibition-associated NLRP3 inflammasome activation, we treated primed microglia with rotenone or tebufenpyrad for 3 h and then stained with MitoSox dye to detect mitochondrial superoxide generation. The pesticide-treated primed microglia exhibited intense MitoSox staining, but unprimed and primed-only cells did not (Fig. 4a). Next, real-time images taken every 1 h of primed wild-type microglial cells treated with

tebufenpyrad or rotenone revealed intense MitoSox fluorescence in the pesticide-treated groups within 2 h (Supplementary Video. 1-3).

Previous studies by Dr. Jorg Tschopp [32] and others[45] have shown that blocking mitophagy increases superoxide generation, which leads to NLRP3 inflammasome activation. Furthermore, upon activation, NLRP3 redistributes and colocalizes with the mitochondria. Mitochondrial prion-like proteins called MAVS mediate this redistribution of NLRP3 to mitochondria [45]. Since NLRP3 has been shown to translocate to mitochondria upon inflammasome activation [32], we next examined whether NLRP3 co-localizes with superoxide generated by damaged mitochondria. LPS-primed or unprimed primary mouse microglia treated with rotenone or tebufenpyrad for 3 and 6 h were stained for MitoSox and NLRP3. A marked increase in NLRP3 immunoreactivity overlapping with the increased MitoSox Red fluorescence was observed in pesticide-treated cells (Fig. 4b), suggesting that the NLRP3 mitochondrial translocation depends on mitochondrial superoxide generated from damaged mitochondria. The degree of co-localization was further visualized as a shift in the 3D color plot (Fiji plugin), signifying that MitoSox and NLRP3 overlap, merging along the diagonal on the red and green channel axes.

We also hypothesized that reducing mitochondrial superoxide levels would decrease inflammasome activation and in turn lower IL-1β release. For this study, we pretreated primary microglia for 1 h with 40 μM of mito-apocynin (Mito-Apo), a mitochondria-targeted derivative of apocynin that was previously shown by our group to reduce oxidative stress and superoxide generation [9,46]. This was followed by a 3 h rotenone or tebufenpyrad treatment of primed microglia. Mito-Apo pretreatment

significantly reduced superoxide generation as evidenced by reduced MitoSox staining (Fig. 4e). Furthermore, Luminex assays revealed that Mito-Apo significantly reduced rotenone- and tebufenpyrad-induced IL-1β release in primed cells (Fig. 4c-d). Mito-Apo was more effective in reducing inflammasome activation than its precursor, apocynin.

Interestingly, ICC analysis further revealed that Mito-Apo not only reduced the superoxide generation, but also reduced the NLRP3 colocalization, with the superoxide-generating mitochondria indicating the probable upstream role of mitochondria in NLRP3 inflammasome activation (Fig. 4b). These findings suggest that inhibition of mitochondrial superoxide generation can reduce NLRP3 inflammasome activation and that the mitochondrial ROS plays a central role in the functional interaction between mitochondrial dysfunction and NLRP3 inflammasome activation.

Lysosomal dysfunction enhances rotenone- and tebufenpyrad-induced NLRP3 inflammasome activation in microglia

Healthy cells degrade damaged mitochondria through a lysosomal mechanism called mitophagy[47]. Since blocking mitophagy has already been shown to induce inflammasome activation [32], we hypothesized that lysosomal dysfunction may add to the accumulation of damaged mitochondria and more superoxide. We treated primary microglia with rotenone or tebufenpyrad for 6 h following LPS priming. Staining with LysoTracker dye revealed markedly reduced LysoTracker fluorescence in pesticide-treated primed cells relative to unprimed cells, indicating the occurrence of lysosomal dysfunction in pesticide-treated primed microglial cells (Fig. 5a).

Next, to determine the extent of lysosomal damage, we stained the primary cells with LAMP2, a lysosomal marker, and found a significant reduction of LAMP2 immunoreactivity in rotenone- and tebufenpyrad-treated groups (Fig. 5b). High magnification imaging of primary microglia double-stained with LAMP2 and the autophagy marker LC3 revealed that LAMP2 forms large vesicle-like structures in response to tebufenpyrad and rotenone (Fig. 5c). Western blot analysis further revealed that 1 µM pesticides induced LC3-II in primed microglial cells after 3 h (Fig. 5d). Lysosomal membrane rupture leads to cathepsin release and activation, which have been shown to further modulate NLRP3 inflammasome activation [48]. Since our ICC analysis showed reduced LAMP2, we performed a Cathepsin D assay (Fig. 5e). This assay revealed that 1 µM rotenone or tebufenpyrad induced the activity of this lysosomal enzyme, further indicating lysosomal dysfunction in microglia. Collectively, these findings indicate that the loss of lysosomal activity may lead to the accumulation of damaged mitochondria which can result in the overproduction of superoxide leading to enhanced, persistent inflammasome activation.

Conditioned medium from complex-1 inhibitor-treated primed microglia induce DAergic neurodegeneration in primary mesencephalic cultures and human DAergic cells

To investigate the functional importance of complex-1 inhibition-induced microglial NLRP3 inflammasome activation, we used both mouse primary neuronal culture and differentiated LUHMES cells and conditioned medium from complex-1 inhibitor-treated primary microglial cells. Media collected from primed and unprimed microglial cells treated with tebufenpyrad or rotenone for 6 h was used to treat mouse

primary nigral neurons to induce neuronal damage. TH-ICC analysis revealed significantly reduced neurite length of TH-positive neurons treated with medium from both rotenone and tebufenpyrad-treated primed cells, but not from unprimed cells (Fig. 6a). Interestingly, TH-negative neurite length did not significantly decrease, suggesting that these pesticides are specifically toxic to TH-positive neurons (Supplementary Fig. 8). This evidence suggests that complex-1 inhibition-triggered NLRP3 inflammasome activation in microglia is capable of inducing DAergic neuronal loss. The conditioned medium from the unprimed cells exposed to pesticides also caused neuronal damage. Hence, to further determine that the DAergic neuronal injury results from pesticide-induced inflammasome activation and not the pesticides present in the conditioned medium, we washed the LPS-primed cells to completely remove all the pesticides following a 6-h pesticide treatment and then kept the cells in 2% fresh medium for 18 h. Cells were also co-treated with MCC-950 (100 nM) during the 6-h pesticide exposure. When the pesticide-free medium was used to treat LUHMES cells, only cells incubated with conditioned medium from pesticide-treated, LPS-primed microglia, exhibited a significant loss of TH^+ cells (Fig. 6b). Conditioned medium co-treated with MCC-950 protected against the loss of neurite length (Fig. 6b). A Luminex bioassay of the cytokine profile further revealed that the conditioned medium collected from pesticide-treated, primed microglial cells, but not from the LPS-priming alone cells, contained IL-1β (Fig. 6c). These results further support the hypothesis that inflammasome activation resulting from mitochondrial dysfunction in microglia contributes to DAergic degeneration.

Discussion

Recent studies suggest that the NLRP3 inflammasome plays an important role in mediating neuroinflammation[41]; however, the key upstream signaling mechanisms that govern inflammasome activation have yet to be elucidated. Despite ample evidence that mitochondrial dysfunction is a key player in neurodegeneration, the link between mitochondrial dysfunction and neuroinflammation is much weaker. Our study bridges that gap in the field with a major focus on understanding the role of mitochondrial complex-1 inhibition in microglial cells and its relevance to inflammation, more specifically to NLRP3 inflammasome signaling. Here, we demonstrate that the complex-1 inhibitors rotenone and tebufenpyrad induce NLRP3 inflammasome activation in primary microglial cells by modulating mitochondrial dynamics in microglia itself. We also show that mitochondrial superoxide generation in microglia plays an important role in NLRP3 inflammasome activation. Furthermore, mito-apocynin, a derivative of mitochondria-targeted apocynin, attenuates inflammasome activation by decreasing superoxide generation. Finally, we demonstrate activation of the NLRP3 inflammasome in a chronic rotenone mouse model of PD.

A recent study by Zhou et al.[32] has linked NLRP3 inflammasome activation to mitochondrial dysfunction in macrophages. The authors reported that upon activation, the NLRP3 complex migrates to the mitochondria, though its role in mitochondria is not well understood. In our present study, we show that the potent complex-1 inhibitors rotenone and tebufenpyrad both induce NLRP3 inflammasome activation in LPS-primed primary mouse microglia. As early as 3 h, both rotenone and tebufenpyrad induced a proteolytic conversion of pro-caspase-1 to active caspase-1 in LPS-primed

primary microglia (Fig. 1), the first step in inflammasome activation. Rotenone and tebufenpyrad also induced the next step in the inflammasome activation process, namely caspase-1-mediated conversion of pro-IL-1β to IL-1β. Tebufenpyrad is more potent than rotenone at the same dose and leads to more caspase-1 p20 production and IL-1β secretion (Fig. 1b-c). ASC, the adapter protein for the NLRP3 inflammasome, forms spec-like structures and propagates in a “prionoid” fashion to propagate the inflammasome [33,49]. As expected, both rotenone and tebufenpyrad treatments led to the formation of ASC specs (Fig. 1e). Furthermore, our results indicate that these complex-1 inhibitors induced the release of IL-1β in a dose-dependent manner, beginning at an extremely low dose of 50 nM (Fig. 2). To determine which inflammasome is mediating the generation and release of IL-1β, we used the NLRP3-specific inhibitor MCC950 [40]. MCC950 completely abolished the rotenone- and tebufenpyrad-induced release of IL-1β from LPS-primed microglia, thus confirming that NLRP3 is the major inflammasome activated by complex-1 inhibition. In terms of understanding the role of these environmental toxicants in sustained inflammation, our study demonstrates that pesticides can activate the NLRP3 inflammasome in primary microglial cells, thereby contributing to chronic inflammation.

Recent studies have focused on the role of mitochondria in NLRP3 inflammasome activation[50,51] in different immune cells like bone marrow-derived macrophages (BMDMs). Shimada *et al*.[52] revealed that mitochondrial DNA can activate the NLRP3 inflammasome. Inhibition of mitophagy has been shown to induce NLRP3 inflammasome activation. Furthermore, upon activation, NLRP3 translocates

to the mitochondria. Recent studies have further shown that during activation the mitochondrial adaptor MAVS, through a prion-like mechanism, facilitates this translocation and activation of the NLRP3 inflammasome [45]. Other studies revealed that mitochondrially generated reactive oxygen species (mROS) can activate macrophagic NLRP3 inflammasomes in response to alum or Nigericin[50,53]. Mitochondrial dysfunction and mROS are druggable targets for reducing inflammasome activation[54].Apart from mounting evidence that mitochondrial dysfunction is a major regulator signal for inflammasome activation in non-neuronal systems[32,50,51,54,55], our study further strengthens the role of mitochondrial impairment in NLRP3 inflammasome activation in microglial cells. We show that NLRP3 inflammasome activation is associated with altered mitochondrial dynamics, including functional and structural damage, as well as mitochondrial membrane potential changes (Fig. 3). Also, mitochondrial capacity for ATP generation was diminished when LPS-primed microglia were treated with complex-1-inhibiting pesticides. After prolonged exposure, structural damage to the mitochondria was manifested as increased mitochondrial circularity. Inhibiting inflammasome activation did not alter the mitochondrial dysfunction induced by the pesticides, indicating that the mitochondrial damage may be upstream of inflammasome activation. Superoxide generation preceded discernible mitochondrial damage [32], and interestingly, our studies show that NLRP3 translocates to and co-localizes with damaged mitochondria. These findings agree with Zhou et al. [32], who suggested NLRP3 localizes to superoxide-concentrated domains. Recently, we demonstrated that a mitochondria-targeted derivative of apocynin, mito-apocynin, reduces neuroinflammation and prevents

DAergic neurodegeneration in an MPTP mouse model of PD [9]. In the present study, mito-apocynin pre-treatment attenuated rotenone- and tebufenpyrad-induced superoxide generation, which in turn reduced secretion of IL-1β in primed microglia. Furthermore, reducing the superoxide generation reduces the translocation of NLRP3, indicating the probable upstream role of mitochondrial superoxide in NLRP3 inflammasome activation.

Although we observed in the Seahorse Mito Stress test that rotenone and tebufenpyrad could diminish mitochondrial activity in unprimed microglia, at other endpoints the effect of the pesticides in unprimed cells was not that dramatic. This could be due to the high sensitivity of the Seahorse assay compared to other tests. Another possible reason is that, unlike neuronal cells, microglial cells may compensate the bioenergy deficits from extra-mitochondrial energy sources. Future studies will address this issue. Sherer et al. [35] reported the loss of ATP in tebufenpyrad treated cells at 6 h. In this study, most of the functional assays were performed at the 2-h to 3 h time point. Also, rotenone activates the p-38 MAPK and NFκB pathways in microglial cells [56], which may lead to proliferation of microglia. Further research needs to be performed to delineate the molecular mechanism that makes glial cells more resistant to mitochondrial inhibitors.

Lysosomal dysfunction and dysregulation of autophagy have been linked to PD [57]. Downregulation of lysosomal function may lead to accumulation of misfolded proteins like α-synuclein, which has been linked to PD pathology. Recent studies have shown that lysosomal dysfunction and destabilization can lead to inflammasome activation in macrophages in Gaucher disease models[58,59]. Furthermore, a

compromised lysosomal membrane leads to release of lysosomal cathepsins, which can induce NLRP3 inflammasome activation [48]. Here, we demonstrate that prolonged exposure to both rotenone and tebufenpyrad induced lysosomal dysfunction in primed microglial cells, pointing out a probable role for lysosome dysfunction in regulating neuroinflammation.

Neuroinflammation and mitochondria-derived superoxide generation play key roles in degeneration of DAergic neurons in PD[15,16,60,61]. Inflammasome activation in glial cells has been shown to contribute to disease pathology in AD [28,62] and TBI, wherein treatment with anti-ASC antibody after TBI was beneficial in a mouse model [63]. Furthermore, induction of IL-1β and IL-18 was linked to higher susceptibility and progression of multiple sclerosis [25]. Here, we show that conditioned media from primed microglial cells treated with complex-1 inhibitors triggered DAergic neurotoxicity in both primary mesencephalic cultures and differentiated LUHMES cells, suggesting that NLRP3 inflammasome activation in glial cells can potentially lead to neurodegeneration (Fig. 6). Furthermore, MCC-950, the NLRP3 inflammasome inhibitor, reduced the loss of TH-positive neurite length, suggesting the inflammasome's probable role in neurodegeneration. The mouse model of rotenone (30 mg/kg, gavaged daily for 28 days) exhibits motor deficits, selective loss of nigrostriatal DAergic neurons and increased α-synuclein in DAergic neurons [64]. The rotenone mouse model was re-evaluated by Inden et al. [38] who used two doses (30 and 100 mg/kg) of rotenone for 56 days. But 100 mg/kg of rotenone for 28 days did not cause any change in DAergic neurons. Hence, for this study, we utilized the rotenone model and were able to demonstrate activation of the NLRP3 inflammasome

in vivo (Fig. 1F-K) during mitochondrial impairment. The major source of NLRP3 activation leading to inflammation in brain are the microglial cells [65]. In this study, we have also shown that rotenone exposure leads to increased NLRP3 in microglial cells in rats further solidifying the activation of NLRP3 in microglial cells *in vivo.*

In various neurodegenerative disorders including PD, the underlying mechanism behind sustained chronic inflammation has still not been deciphered. In this study, we propose a mechanism for regulating chronic inflammation in PD. All our findings collectively show that microglial mitochondria play an important role in regulating the NLRP3 inflammasome pathway in PD models (Fig. 6d). In this study, we show that LPS priming induce NLRP3 and pro-IL-1β production but not capase-1 cleavage or assembly of the inflammasome complex in microglia, which is consistent with the current literature on the NLRP3 inflammasome signaling pathway. Pesticide exposure leads to the inflammasome assembly and secretion of IL-1β. Furthermore, we show that the superoxides generated by mitochondrial dysfunction leads to NLRP3 translocation. Reducing this superoxide generation lowers the translocation and inflammasome activation, but inhibiting the activation of NLRP3 does not reduce the mitochondrial damage, indicating that mitochondrial dysfunction is upstream of inflammasome formation. Additionally, the inflammatory cascade is intensified by lysosomal dysfunction, leading to the accumulation of more damaged mitochondria and thus greater superoxide generation. Collectively, our study points to the existence of a complex interplay between microglial mitochondrial impairment and NLRP3 inflammasome signaling and its role in sustained neuroinflammation in DAergic neurodegenerative processes in PD.

Materials and Methods

Chemicals and reagents

Rotenone (95–98% purity), oligomycin, FCCP and antimycin were purchased from Sigma, and tebufenpyrad (96% purity) was purchased from AK Scientific Inc. DMSO was purchased from Fisher Scientific. We purchased DMEM-F12, fetal bovine serum (FBS), L-glutamine, penicillin, streptomycin, MitoTracker Red, LysoTracker Green, and MitoSox Red stains from Invitrogen. The CellTiter 96 AQueous Non-Radioactive Cell Proliferation Assay kit and CellTiter Glo Luminescent Cell Viability Assay kit were obtained from Promega. ASC, NLRP3 and Caspase-1 antibodies were purchased from Adipogen, and the TH antibody was obtained from Millipore. The CD11b magnetic separation kit was purchased from STEMCELL Technologies. LCIII, AIM2 and NLRC4 antibodies were purchased from Cell Signaling Technologies. IL-1β antibody was purchased from R&D Technologies, while LAMP2 antibody was from Santa Cruz Biotechnology. Acetylated α-tubulin antibody and Duolink PLA red were obtained from Sigma. The MAP2 and Tuj1 antibodies and Cathepsin D activity kit were obtained from Abcam. All the standards used for Luminex assay were purchased from PeproTech Inc. Streptavidin-biotin and biotinylated antibodies used for Luminex were purchased from eBioSciences. MCC950 was obtained from Dr. Trent Woodruff's lab University of Queensland, Brisbane, Australia. Mito-Apocynin was obtained from Dr. Balaraman Kalyanaraman's lab at the Medical College of Wisconsin in Milwaukee.

Cell cultures and treatments

For primary microglial culture, one-day-old C57BL/6 pups were sacrificed, their brains dissected out, and a single cell suspension was prepared. After growing in

culture for 16 days, the microglia were separated using a magnetic bead separation technique as previously described[66,67]. Primary microglial cells were cultured in DMEM-F12, 10% FBS, 5% sodium pyruvate, 5% glutamine, 5% penicillin-streptavidin, and 5% non-essential amino acids. We also obtained a wild-type microglial cell line as a kind donation from Dr. D.T. Golenbock (University of Massachusetts Medical School, Worcester, MA). The wild-type microglial cell line was characterized by Halle et al. [28] and cultured in DMEM medium, 10% FBS, 5% glutamine, and 5% penicillin-streptavidin. The DAergic Lund human mesencephalic (LUHMES) cell line was differentiated and maintained as described in our recent publication [68].Treatments were done in 2% FBS-containing medium. For LPS-priming treatments, cells were treated with LPS (1 µg/mL) for 3 h. Next, the cells were triple-washed with full serum medium to remove any LPS, and then mitochondrial complex-1 inhibitors were added to the cells (50 nM to 1 µM) for 2 to 24 h.

Primary mesensephalic neurons were isolated from gestational 15-day-old mouse embryos as described previously[69]. These plated cells have a viability ranging from 70-80%. The primary cultures used were enriched in neurons. Briefly, mesencephalic tissues from E15 mouse embryos were dissected and maintained in ice-cold DMEM media and then dissociated in 10 mls of trypsin-0.25% EDTA (TE) for 15 min in a 37°C water bath with sporadic shaking. The action of TE was stopped using 20 mls DMEM containing 10% FBS. the trypsinized tissue was further washed twice in 10% DMEM followed by a final wash in Neurobasal media. Tissue was titurated using a 10 ml sterile pipette and the resulting suspension was passed through a 70 micron filter. The dissociated cells were then plated at an equal density of 0.1

million cells per well on 12-mm coverslips precoated with 0.1 mg/ml poly-D-lysine. Cultures were maintained in neurobasal media fortified with B-27 supplement, 500 mM L-glutamine, 100 IU/ml penicillin, and 100 µg/ml streptomycin. The cells were maintained in a humidified CO2 incubator (5% CO2 and 37°C) for 24 h. One-half of the culture media was replaced every other day. 6-7 day old cultures were used for experiments. These cells were maintained in neurobasal medium which selectively inhibits glial proliferation. Cells were treated with conditioned medium from primed and unprimed microglial cells for 24 h. For neurite length analysis, NeuronJ plugin in ImageJ was utilized. Only neurites in contact with the cell body were measured; neurites without cell body contacts were not measured.

Animal studies

Eight-week-old male C57BL/6N mice (3-4 animals per group), obtained from Charles River, were housed under standard conditions: constant temperature (22 ± 1°C), humidity (relative, 30%), and a 12-h light/dark cycle. From the *in vitro data,* we estimated 3-4 animals per group as sufficient to detect significant biochemical changes. All mice were pre-screened for normal baseline performance during behavioral assessments conducted before randomly assigning animals to experimental groups. Investigators involved with data collection and analysis were not blinded to group allocation. After acclimating for 3 days, mice were gavaged daily with 30 mg/kg of rotenone for 28 days, after which the mice were sacrificed. This protocol for chronic administration of rotenone has been reported to cause a significant loss of nigrostriatal DAergic neurons and behavioral impairment in mice [38,64]. Sixteeen rats, age 6-7 months old, were purchased from Hilltop Lab Animals (Scottdale, PA). These

animals were administered either rotenone (2.8 mg/kg/day, n = 8) or vehicle (n = 8) for 4 consecutive days via intraperitoneal (i.p) injection. The rotenone solution was first prepared as a 50× stock in 100% dimethyl sulfoxide (DMSO) and diluted in the medium-chain triglyceride Miglyol 812 N. Vortexing the solution created a stable emulsion with a final concentration of 2.8 mg/mL rotenone in 98% Miglyol 812 N and 2% DMSO. After the final injection, the animals were housed for 3 months. The animals were randomly assigned to treatment using an online randomization tool (random.org). Experimenters were blinded to each rat's treatment allocation.

Use of the animals and protocol procedures were approved by the Institutional Animal Care and Use Committee (IACUC) at Iowa State University (Ames, IA, USA) and all methods were performed in accordance with relevant guidelines and regulations.

Western blotting

Following the treatment of rotenone or tebufenpyrad for 3-6 h, primed or unprimed microglial cell pellets were lysed using modified RIPA buffer and sonicated. The proteins were normalized and 20-30 µg of protein was loaded in each lane and separated using a 12-15% SDS polyacrylamide gel as discussed previously [70,71]. After transferring, nitro-cellulose membranes were blocked with LI-COR blocking buffer and washed with PBS mixed with 0.05% Tween. The membranes were then treated with the indicated primary antibodies, followed by incubation with IR-680 anti-mouse and IR-800 anti-rabbit secondary antibodies. The membranes were scanned using the Odyssey LI-COR Imaging System. The primary antibodies used for immunoblotting were NLRP3 (1:1000) (AB_2490202), Caspase-1 p20 (1:1000) (AB_2490248), and IL-1β (1:1000) (AB_416684). β-actin was used as a loading control.

Immunocytochemistry (ICC)

Cells were plated on PDL-coated coverslips. After treatment for 2-6 h with a pesticide, primed or unprimed cells were fixed in 4% paraformaldehyde (PFA) for 30 min followed by blocking with 1.5% BSA, 0.05% Tween, and 0.5% Triton for 1 h. Primary antibodies were prepared in 1% BSA and incubated overnight at 4°C. The following primary antibodies were used: ASC (1:400, AB_2490440), NLRP3 (1:500, AB_2490202), TH (1: 2000, AB_2201528), TH (1:1000, AB_696697), MAP2 (1:1000, AB_448205), Tuj1 (1:1000, AB_444319), LC3 (1:400, AB_2137716), acetylated α-tubulin (1:400, AB_477585), SIRT2 (1:500, AB_1142864) and LAMP2 (1:400). After primary antibody incubation, each well was washed with PBS five times and then incubated with secondary antibody for 1 h. Cell nuclei were stained with Hoechst (1:5000) and mounted on slides using the Fluoromount mounting medium (Sigma). Slides were dried overnight and then imaged using a Nikon Eclipse C1 microscope. For co-localization, a 3D color plotter (Fiji image analysis software) was used to plot all the different colors seen in the RGB images. Briefly, RGB images were opened using Fiji and then analyzed using its 3D color plotter plug-in, which plots every colored pixel it picks up in the RGB image along x, y and z axes representing red, green and blue, respectively. For co-localization between the green and red channel, it plots the pixels along the diagonal of the red and green axes to visualize the co-localization. Furthermore, the resulting intensity from merging the red and green signals can also be quantified in this analysis.

Luminex assays

Cytokine levels were assessed via Luminex assays according to a protocol by Panicker et al. [8]. Briefly, primary microglial cells were treated in 96-well plates (Fig. 2, 4 and 6) or 6-well plates (Fig 1) with 100-900 μL of 2% FBS-containing DMEM-F12 medium for 6-24 h. After treatment, 40 μl of treatment medium was collected and added to 40 μL of primary antibody conjugated to magnetic microspheres and incubated overnight at 4°C in a clear-bottom, black 96-well plate. After incubation, each well was triple-washed using a magnetic washer and then incubated for 1 h with secondary antibodies. Lastly, samples were incubated for 30 min with streptavidin/phycoerythrin. A Bio-Plex reader was used to read the 96-well plates. A standard curve of all the cytokines was prepared using standard cytokines.

q-RT-PCR

RNA was isolated using TRIzol extraction methods as previously described [72]. Following treatment for 2 h with the pesticides, RNA concentration was measured using NanoDrop. One microgram of RNA was used to convert RNA into cDNA using the High Capacity cDNA Reverse Transcription Kit (Applied Biosystems #4368814) following the manufacturers' protocol. For qPCR, 10 μL of SYBR Green Mastermix (Qiagen Cat #208056), 1-2 μL of primers, 6-7 μL of water and 1-2 μL of cDNA were used. The following genes were used for q-RT-PCR: NLRP3 (primer sequences: forward-TGCTCTTCACTGCTATCAAGCCCT, and reverse-ACAAGCCTTTGCTCCAGACCCTAT, synthesized at Iowa State University's DNA Facility), IL-1β, IL-18, NLRC4, and AIM2 (QuantiTect Primers, Qiagen). The house keeping gene 18S rRNA (Qiagen Cat #PPM57735E) was used in all qPCR

experiments. No-template controls (NTCs) and dissociation curves were run for all experiments to exclude cross-contamination.

Live cell staining

Cells were stained following the manufacturer's protocol using tetramethylrhodamine methyl ester perchlorate (TMRM) (2-h treatment), MitoSox Red (3- to 6-h treatment), MitoTracker Red (6-h treatment), and LysoTracker Green (6-h treatment), all obtained from Molecular Probes and used according to our previous publication [21]. Briefly, cells were treated either on PDL-coated coverslips or in 96-well plates. Following treatment, cells were washed twice with HBSS and then the dye was added according to the dilution recommended by manufacturer. After staining, cells were washed and then either fixed for ICC or imaged directly. Following 2-h pesticide exposure for TMRM, non-fixed cells were imaged under the FLoid Cell Imaging system (Thermo Fisher Scientific). For MitoSox Red imaging, a Cytation 3 real-time imaging system (BioTek) was used to take hourly images. Changes in mitochondrial structure were quantified using the ImageJ plugin "mitochondrial morphology," developed by Ruben K Dagda (2010). We selected parameters for quantifying damage to mitochondrial structure based on recent studies [21,31,73].

ATP assay

Cells were plated in opaque-walled 96-well plates and treated with the toxicants for 2 h. After treatment, 100 μl of CellTiter-Glo Reagent was added to each well containing 100 μl treatment media and incubated for 5 min. Readings were taken using a luminometer.

MTS mitochondrial activity assay

Cells were plated in 96-well plates, and after treatment for 3-24 h, 10 μl of MTS dye (Promega) was added to each well and incubated for 1.5 h. After incubation, a plate reader was used to take excitation and background (subtracted) readings at 490 and 660 nm, respectively.

Mitochondrial dynamics analysis

A Seahorse XFe24 Analyzer was used to measure mitochondrial oxygen consumption rates (OCR) and extracellular acidification rates (ECAR) using the Mito Stress test following a previously published protocol [31]. Primary mouse microglia were plated 90,000 cells/well on a Seahorse 24-well plate. The calibration plate was hydrated overnight in a non-CO_2 incubator. All treatments were done in serum-free medium. Cells were primed with LPS for 3 h followed by pesticide exposure for 3 h. For the Mito-Stress test, 0.75 μM oligomycin, 1 μM FCCP, and 0.5 μM rotenone/antimycin were used. Mito-Stress report generator was used for analysis.

Duolink Proximal Ligation Assay (PLA)

Duolink PLA assay was performed following the manufacturer's protocol [74]. Briefly, 15 k primary microglial cells were plated on PDL-coated coverslips in 96-well cell culture plates. Following treatment for 3 h, cells were washed and fixed using 4% poly-D-lysine, blocked with blocking buffer, and incubated in primary antibodies overnight. After primary antibody incubation, the Duolink *in situ* Detection Reagents Red (Sigma) was used according to manufacturer's protocol. Confocal imaging was performed on these coverslips at the Iowa State University Microscope Facility using

a Leica DMEIR2 confocal microscope with 63X oil objective. For z-stacking, each image consisted of 0.5-µm sections and 5 slices.

Cathepsin D assay

One million primary microglial cells were plated in PDL-coated, 12-well cell culture plates. Following a 6-h treatment of rotenone or tebufenpyrad, cells were collected and the cathepsin activity assay was performed following manufacturer's protocol (Abcam).

Statistical Analysis

All *in vitro* data were determined from three to eight biological replicates. GraphPad 5.0 was used for statistical analysis with $p \leq 0.05$ considered statistically significant. Two-way ANOVA was used for comparing multiple groups. In most cases, Bonferroni post analysis was applied. For comparing 2 groups, Student's t-test was used. Where the normality assumption was violated, we conducted nonparametric tests, however, in no case did the nonparametric results change the overall interpretation of parametric results.

Data Availability

Raw data supporting the results reported in this article are in the figure source data files available upon request.

Acknowledgements

This study was supported by NIH grants NS088206, ES026892, and ES027245. Special thanks to Dr. Woodruff, Dr. Golenbock and Dr. Kalyanaraman for supplying key resources and reagents for the study. We thank Sarah Mientka for her assistance in formatting figures and Gary Zenitsky for proofreading the manuscript.

Conflict of interest

A.G.K. and V.A. are shareholders of PK Biosciences Corporation (Ames, IA), which is interested in identifying novel biomarkers and potential therapeutic targets for PD. A.G.K and V.A do not have any commercial interests in the present work.

Contributions

S.S., A.K., and A.G.K. designed research; S.S., E.M., D.S.H., N.P., A.C., D.R, B.N.P, and S.G performed research; S.S., H.J., and A.G.K. analyzed data; S.S., H.J., V.A., and A.G.K. wrote the paper.

Supplementary Materials

Supplementary information is available at Nature Parkinson Disease's website

References

1 Lotharius, J. & Brundin, P. Pathogenesis of Parkinson's disease: dopamine, vesicles and alpha-synuclein. *Nat Rev Neurosci* **3**, 932-942, doi:10.1038/nrn983 (2002).

2 Wolters, E. Non-motor extranigral signs and symptoms in Parkinson's disease. *Parkinsonism Relat Disord* **15 Suppl 3**, S6-12, doi:10.1016/S1353-8020(09)70770-9 (2009).

3 Goldman, S. M. Environmental toxins and Parkinson's disease. *Annu Rev Pharmacol Toxicol* **54**, 141-164, doi:10.1146/annurev-pharmtox-011613-135937 (2014).

4 Mullin, S. & Schapira, A. H. Pathogenic mechanisms of neurodegeneration in Parkinson disease. *Neurol Clin* **33**, 1-17, doi:10.1016/j.ncl.2014.09.010 (2015).

5 Block, M. L., Zecca, L. & Hong, J. S. Microglia-mediated neurotoxicity: uncovering the molecular mechanisms. *Nat Rev Neurosci* **8**, 57-69, doi:10.1038/nrn2038 (2007).

6 Whitton, P. S. Inflammation as a causative factor in the aetiology of Parkinson's disease. *Br J Pharmacol* **150**, 963-976, doi:10.1038/sj.bjp.0707167 (2007).

7 Nagatsu, T., Mogi, M., Ichinose, H. & Togari, A. Cytokines in Parkinson's disease. *J Neural Transm Suppl*, 143-151 (2000).

8 Panicker, N. *et al.* Fyn Kinase Regulates Microglial Neuroinflammatory Responses in Cell Culture and Animal Models of Parkinson's Disease. *J Neurosci* **35**, 10058-10077, doi:10.1523/JNEUROSCI.0302-15.2015 (2015).

9 Ghosh, A. *et al.* Mitoapocynin Treatment Protects Against Neuroinflammation and Dopaminergic Neurodegeneration in a Preclinical Animal Model of Parkinson's Disease. *J Neuroimmune Pharmacol* **11**, 259-278, doi:10.1007/s11481-016-9650-4 (2016).

10 Kosloski, L. M., Kosmacek, E. A., Olson, K. E., Mosley, R. L. & Gendelman, H. E. GM-CSF induces neuroprotective and anti-inflammatory responses in 1-methyl-4-phenyl-1,2,3,6-tetrahydropyridine intoxicated mice. *J Neuroimmunol* **265**, 1-10, doi:10.1016/j.jneuroim.2013.10.009 (2013).

11 Cannon, J. R. *et al.* A highly reproducible rotenone model of Parkinson's disease. *Neurobiol Dis* **34**, 279-290 (2009).

12 Barnum, C. J. *et al.* Peripheral administration of the selective inhibitor of soluble tumor necrosis factor (TNF) XPro(R)1595 attenuates nigral cell loss and glial activation in 6-OHDA hemiparkinsonian rats. *J Parkinsons Dis* **4**, 349-360, doi:10.3233/JPD-140410 (2014).

13 Liu, B. & Hong, J. S. Role of microglia in inflammation-mediated neurodegenerative diseases: mechanisms and strategies for therapeutic intervention. *J Pharmacol Exp Ther* **304**, 1-7, doi:10.1124/jpet.102.035048 (2003).

14 Gammon, K. Inflammation: A complex problem. *Nature* **502**, S86-87 (2013).

15 Tansey, M. G. & Goldberg, M. S. Neuroinflammation in Parkinson's disease: its role in neuronal death and implications for therapeutic intervention. *Neurobiology of disease* **37**, 510-518 (2010).

16 Mosley, R. L., Hutter-Saunders, J. A., Stone, D. K. & Gendelman, H. E. Inflammation and adaptive immunity in Parkinson's disease. *Cold Spring Harb Perspect Med* **2**, a009381, doi:10.1101/cshperspect.a009381 (2012).

17 Carson, M. J., Thrash, J. C. & Walter, B. The cellular response in neuroinflammation: The role of leukocytes, microglia and astrocytes in neuronal death and survival. *Clin Neurosci Res* **6**, 237-245, doi:10.1016/j.cnr.2006.09.004 (2006).

18 Moon, H. E. & Paek, S. H. Mitochondrial Dysfunction in Parkinson's Disease. *Exp Neurobiol* **24**, 103-116, doi:10.5607/en.2015.24.2.103 (2015).

19 Rokad, D. *et al.* Role of neurotoxicants and traumatic brain injury in alpha-synuclein protein misfolding and aggregation. *Brain Res Bull*, doi:10.1016/j.brainresbull.2016.12.003 (2016).

20 Di Maio, R. *et al.* alpha-Synuclein binds to TOM20 and inhibits mitochondrial protein import in Parkinson's disease. *Sci Transl Med* **8**, 342ra378, doi:10.1126/scitranslmed.aaf3634 (2016).

21 Charli, A., Jin, H., Anantharam, V., Kanthasamy, A. & Kanthasamy, A. G. Alterations in mitochondrial dynamics induced by tebufenpyrad and pyridaben in a dopaminergic neuronal cell culture model. *Neurotoxicology*, doi:10.1016/j.neuro.2015.06.007 (2015).

22 Abou-Sleiman, P. M., Muqit, M. M. & Wood, N. W. Expanding insights of mitochondrial dysfunction in Parkinson's disease. *Nat Rev Neurosci* **7**, 207-219, doi:10.1038/nrn1868 (2006).

23 Martinez, T. N. & Greenamyre, J. T. Toxin models of mitochondrial dysfunction in Parkinson's disease. *Antioxid Redox Signal* **16**, 920-934, doi:10.1089/ars.2011.4033 (2012).

24 Dawson, T. M. & Dawson, V. L. Mitochondrial Mechanisms of Neuronal Cell Death: Potential Therapeutics. *Annu Rev Pharmacol Toxicol* **57**, 437-454, doi:10.1146/annurev-pharmtox-010716-105001 (2017).

25 Freeman, L. C. & Ting, J. P. The pathogenic role of the inflammasome in neurodegenerative diseases. *J Neurochem*, doi:10.1111/jnc.13217 (2015).

26 Son, M. Y. *et al.* A novel human model of the neurodegenerative disease GM1 gangliosidosis using induced pluripotent stem cells demonstrates inflammasome activation. *J Pathol* **237**, 98-110, doi:10.1002/path.4551 (2015).

27 Guo, H., Callaway, J. B. & Ting, J. P. Inflammasomes: mechanism of action, role in disease, and therapeutics. *Nat Med* **21**, 677-687, doi:10.1038/nm.3893 (2015).

28 Halle, A. *et al.* The NALP3 inflammasome is involved in the innate immune response to amyloid-beta. *Nat Immunol* **9**, 857-865, doi:10.1038/ni.1636 (2008).

29 Saresella, M. *et al.* The NLRP3 and NLRP1 inflammasomes are activated in Alzheimer's disease. *Mol Neurodegener* **11**, 23, doi:10.1186/s13024-016-0088-1 (2016).

30 Latz, E., Xiao, T. S. & Stutz, A. Activation and regulation of the inflammasomes. *Nat Rev Immunol* **13**, 397-411, doi:10.1038/nri3452 (2013).

31 Charli, A., Jin, H., Anantharam, V., Kanthasamy, A. & Kanthasamy, A. G. Alterations in mitochondrial dynamics induced by tebufenpyrad and pyridaben in a dopaminergic neuronal cell culture model. *Neurotoxicology* **53**, 302-313, doi:10.1016/j.neuro.2015.06.007 (2016).

32 Zhou, R., Yazdi, A. S., Menu, P. & Tschopp, J. A role for mitochondria in NLRP3 inflammasome activation. *Nature* **469**, 221-225, doi:10.1038/nature09663 (2011).

33 Franklin, B. S. *et al.* The adaptor ASC has extracellular and 'prionoid' activities that propagate inflammation. *Nat Immunol* **15**, 727-737, doi:10.1038/ni.2913 (2014).

34 Wilson, N. S. *et al.* Inflammasome-dependent and -independent IL-18 production mediates immunity to the ISCOMATRIX adjuvant. *J Immunol* **192**, 3259-3268, doi:10.4049/jimmunol.1302011 (2014).

35 Sherer, T. B. *et al.* Mechanism of toxicity of pesticides acting at complex I: relevance to environmental etiologies of Parkinson's disease. *J Neurochem* **100**, 1469-1479, doi:10.1111/j.1471-4159.2006.04333.x (2007).

36 Wolpaw, A. J. *et al.* Modulatory profiling identifies mechanisms of small molecule-induced cell death. *Proc Natl Acad Sci U S A* **108**, E771-780, doi:10.1073/pnas.1106149108 (2011).

37 Misawa, T. *et al.* Microtubule-driven spatial arrangement of mitochondria promotes activation of the NLRP3 inflammasome. *Nat Immunol* **14**, 454-460, doi:10.1038/ni.2550 (2013).

38 Inden, M. *et al.* Parkinsonian rotenone mouse model: reevaluation of long-term administration of rotenone in C57BL/6 mice. *Biol Pharm Bull* **34**, 92-96 (2011).

39 Zhang, Z. T. *et al.* Activation of the NLRP3 inflammasome in lipopolysaccharide-induced mouse fatigue and its relevance to chronic fatigue syndrome. *J Neuroinflammation* **13**, 71, doi:10.1186/s12974-016-0539-1 (2016).

40 Coll, R. C. *et al.* A small-molecule inhibitor of the NLRP3 inflammasome for the treatment of inflammatory diseases. *Nat Med* **21**, 248-255, doi:10.1038/nm.3806 (2015).

41 Freeman, L. C. & Ting, J. P. The pathogenic role of the inflammasome in neurodegenerative diseases. *J Neurochem* **136 Suppl 1**, 29-38, doi:10.1111/jnc.13217 (2016).

42 Indo, H. P. *et al.* A mitochondrial superoxide theory for oxidative stress diseases and aging. *J Clin Biochem Nutr* **56**, 1-7, doi:10.3164/jcbn.14-42 (2015).

43 Bordt, E. A. & Polster, B. M. NADPH oxidase- and mitochondria-derived reactive oxygen species in proinflammatory microglial activation: a bipartisan affair? *Free Radic Biol Med* **76**, 34-46, doi:10.1016/j.freeradbiomed.2014.07.033 (2014).

44 Lupfer, C. *et al.* Receptor interacting protein kinase 2-mediated mitophagy regulates inflammasome activation during virus infection. *Nat Immunol* **14**, 480-488, doi:10.1038/ni.2563 (2013).

45 Subramanian, N., Natarajan, K., Clatworthy, M. R., Wang, Z. & Germain, R. N. The adaptor MAVS promotes NLRP3 mitochondrial localization and inflammasome activation. *Cell* **153**, 348-361, doi:10.1016/j.cell.2013.02.054 (2013).

46 Dranka, B. P. *et al.* A novel mitochondrially-targeted apocynin derivative prevents hyposmia and loss of motor function in the leucine-rich repeat kinase 2 (LRRK2(R1441G)) transgenic mouse model of Parkinson's disease. *Neurosci Lett* **583**, 159-164, doi:10.1016/j.neulet.2014.09.042 (2014).

47 Ivankovic, D., Chau, K. Y., Schapira, A. H. & Gegg, M. E. Mitochondrial and lysosomal biogenesis are activated following PINK1/parkin-mediated mitophagy. *J Neurochem* **136**, 388-402, doi:10.1111/jnc.13412 (2016).

48 He, Y., Hara, H. & Nunez, G. Mechanism and Regulation of NLRP3 Inflammasome Activation. *Trends Biochem Sci* **41**, 1012-1021, doi:10.1016/j.tibs.2016.09.002 (2016).

49 Baroja-Mazo, A. *et al.* The NLRP3 inflammasome is released as a particulate danger signal that amplifies the inflammatory response. *Nat Immunol* **15**, 738-748, doi:10.1038/ni.2919 (2014).

50 Alfonso-Loeches, S., Urena-Peralta, J. R., Morillo-Bargues, M. J., Oliver-De La Cruz, J. & Guerri, C. Role of mitochondria ROS generation in ethanol-induced NLRP3 inflammasome activation and cell death in astroglial cells. *Front Cell Neurosci* **8**, 216, doi:10.3389/fncel.2014.00216 (2014).

51 Gurung, P., Lukens, J. R. & Kanneganti, T. D. Mitochondria: diversity in the regulation of the NLRP3 inflammasome. *Trends Mol Med* **21**, 193-201, doi:10.1016/j.molmed.2014.11.008 (2015).

52 Shimada, K. *et al.* Oxidized mitochondrial DNA activates the NLRP3 inflammasome during apoptosis. *Immunity* **36**, 401-414, doi:10.1016/j.immuni.2012.01.009 (2012).

53 Sorbara, M. T. & Girardin, S. E. Mitochondrial ROS fuel the inflammasome. *Cell Res* **21**, 558-560, doi:10.1038/cr.2011.20 (2011).

54 Jabaut, J., Ather, J. L., Taracanova, A., Poynter, M. E. & Ckless, K. Mitochondria-targeted drugs enhance Nlrp3 inflammasome-dependent IL-1beta secretion in association with alterations in cellular redox and energy status. *Free Radic Biol Med* **60**, 233-245, doi:10.1016/j.freeradbiomed.2013.01.025 (2013).

55 Dashdorj, A. *et al.* Mitochondria-targeted antioxidant MitoQ ameliorates experimental mouse colitis by suppressing NLRP3 inflammasome-mediated inflammatory cytokines. *BMC Med* **11**, 178, doi:10.1186/1741-7015-11-178 (2013).

56 Emmrich, J. V., Hornik, T. C., Neher, J. J. & Brown, G. C. Rotenone induces neuronal death by microglial phagocytosis of neurons. *FEBS J* **280**, 5030-5038, doi:10.1111/febs.12401 (2013).

57 Lynch-Day, M. A., Mao, K., Wang, K., Zhao, M. & Klionsky, D. J. The role of autophagy in Parkinson's disease. *Cold Spring Harb Perspect Med* **2**, a009357, doi:10.1101/cshperspect.a009357 (2012).

58 Aflaki, E. *et al.* Lysosomal storage and impaired autophagy lead to inflammasome activation in Gaucher macrophages. *Aging Cell* **15**, 77-88, doi:10.1111/acel.12409 (2016).

59 Jo, E. K., Kim, J. K., Shin, D. M. & Sasakawa, C. Molecular mechanisms regulating NLRP3 inflammasome activation. *Cell Mol Immunol* **13**, 148-159, doi:10.1038/cmi.2015.95 (2016).

60 Wu, D. C. *et al.* NADPH oxidase mediates oxidative stress in the 1-methyl-4-phenyl-1,2,3,6-tetrahydropyridine model of Parkinson's disease. *Proc Natl Acad Sci U S A* **100**, 6145-6150, doi:10.1073/pnas.0937239100 (2003).

61 Zhang, F. L. *et al.* Therapeutic effects of fucoidan in 6-hydroxydopamine-lesioned rat model of Parkinson's disease: Role of NADPH oxidase-1. *CNS Neurosci Ther* **20**, 1036-1044, doi:10.1111/cns.12340 (2014).

62 Heneka, M. T. *et al.* NLRP3 is activated in Alzheimer's disease and contributes to pathology in APP/PS1 mice. *Nature* **493**, 674-678, doi:10.1038/nature11729 (2013).

63 de Rivero Vaccari, J. P. *et al.* Therapeutic neutralization of the NLRP1 inflammasome reduces the innate immune response and improves histopathology after traumatic brain injury. *J Cereb Blood Flow Metab* **29**, 1251-1261, doi:10.1038/jcbfm.2009.46 (2009).

64 Inden, M. *et al.* Neurodegeneration of mouse nigrostriatal dopaminergic system induced by repeated oral administration of rotenone is prevented by 4-phenylbutyrate, a chemical chaperone. *J Neurochem* **101**, 1491-1504, doi:10.1111/j.1471-4159.2006.04440.x (2007).

65 Gustin, A. *et al.* NLRP3 Inflammasome Is Expressed and Functional in Mouse Brain Microglia but Not in Astrocytes. *PLoS One* **10**, e0130624, doi:10.1371/journal.pone.0130624 (2015).

66 Gordon, R. *et al.* A simple magnetic separation method for high-yield isolation of pure primary microglia. *J Neurosci Methods* **194**, 287-296, doi:10.1016/j.jneumeth.2010.11.001 (2011).

67 Sarkar, S. *et al.* Rapid and Refined CD11b Magnetic Isolation of Primary Microglia with Enhanced Purity and Versatility. *J Vis Exp*, doi:10.3791/55364 (2017).

68 Ay, M. *et al.* Molecular cloning, epigenetic regulation, and functional characterization of Prkd1 gene promoter in dopaminergic cell culture models of Parkinson's disease. *J Neurochem* **135**, 402-415, doi:10.1111/jnc.13261 (2015).

69 Brenza, T. M. *et al.* Neuronal protection against oxidative insult by polyanhydride nanoparticle-based mitochondria-targeted antioxidant therapy. *Nanomedicine* **13**, 809-820, doi:10.1016/j.nano.2016.10.004 (2017).

70 Jin, H. *et al.* alpha-Synuclein negatively regulates protein kinase Cdelta expression to suppress apoptosis in dopaminergic neurons by reducing p300 histone acetyltransferase activity. *J Neurosci* **31**, 2035-2051, doi:10.1523/JNEUROSCI.5634-10.2011 (2011).

71 Sarkar, S. *et al.* Manganese exposure induces neuroinflammation by impairing mitochondrial dynamics in astrocytes. *Neurotoxicology*, doi:10.1016/j.neuro.2017.05.009 (2017).

72 Seo, J., Ottesen, E. W. & Singh, R. N. Antisense methods to modulate pre-mRNA splicing. *Methods Mol Biol* **1126**, 271-283, doi:10.1007/978-1-62703-980-2_20 (2014).

73 Mitra, K. & Lippincott-Schwartz, J. Analysis of mitochondrial dynamics and functions using imaging approaches. *Curr Protoc Cell Biol* **Chapter 4**, Unit 4 25 21-21, doi:10.1002/0471143030.cb0425s46 (2010).

74 Thymiakou, E. & Episkopou, V. Detection of signaling effector-complexes downstream of bmp4 using PLA, a proximity ligation assay. *J Vis Exp*, doi:10.3791/2631 (2011).

Figures

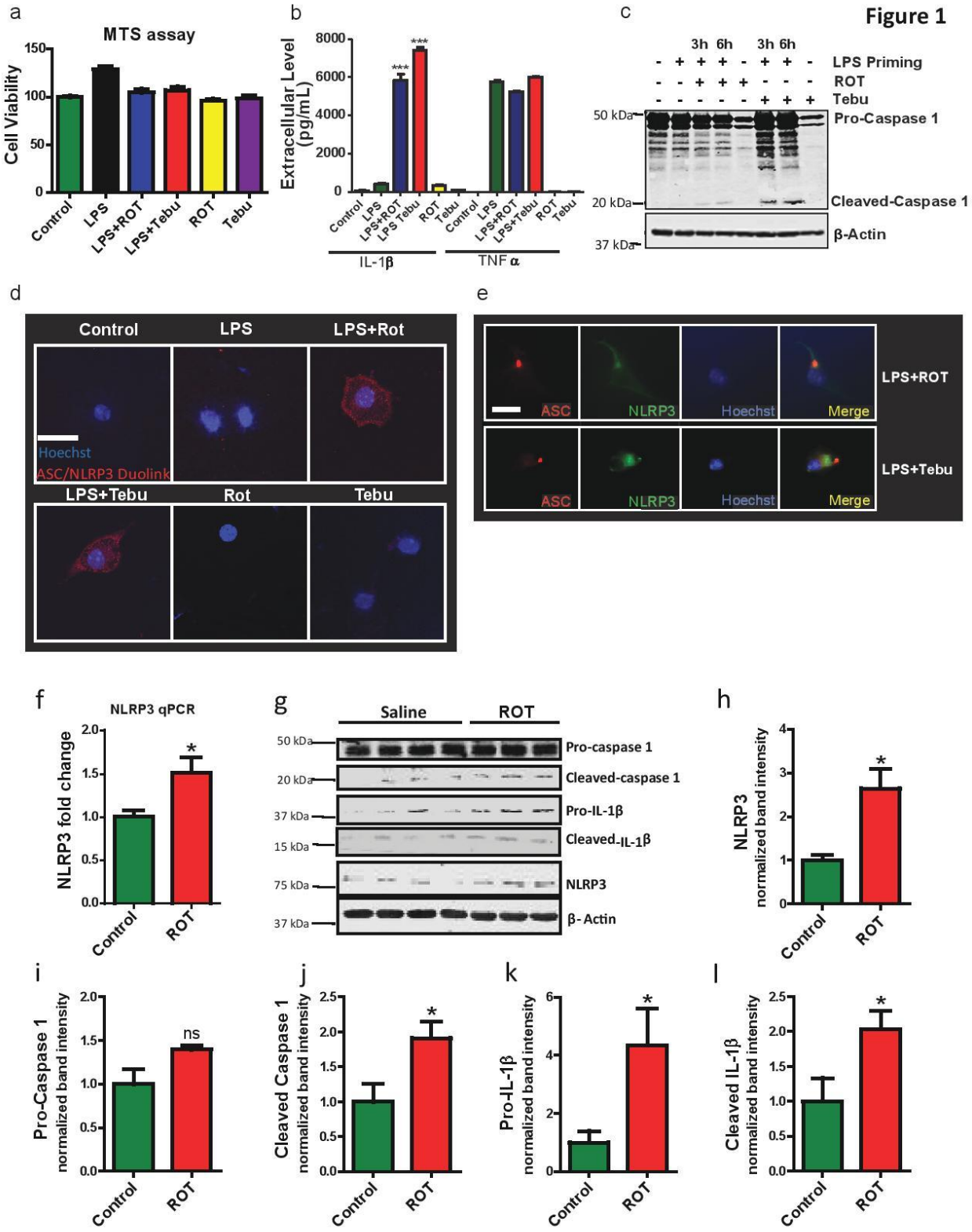
Figure 1
a
MTS assay
Cell Viability
Control
LPS
LPS+ROT
LPS+Tebu
ROT
Tebu
b
Extracellular Level (pg/mL)
IL-1β
TNF α
c
3h 6h 3h 6h
LPS Priming
ROT
Tebu
50 kDa
Pro-Caspase 1
20 kDa
Cleaved-Caspase 1
37 kDa
β-Actin
d
Control
LPS
LPS+Rot
Hoechst
ASC/NLRP3 Duolink
LPS+Tebu
Rot
Tebu
e
ASC
NLRP3
Hoechst
Merge
LPS+ROT
LPS+Tebu
f
NLRP3 qPCR
NLRP3 fold change
g
Saline
ROT
Pro-caspase 1
Cleaved-caspase 1
Pro-IL-1β
Cleaved-IL-1β
NLRP3
β-Actin
h
NLRP3 normalized band intensity
i
Pro-Caspase 1 normalized band intensity
ns
j
Cleaved Caspase 1 normalized band intensity
k
Pro-IL-1β normalized band intensity
l
Cleaved IL-1β normalized band intensity

Fig 1: **Rotenone and tebufenpyrad activate NLRP3 inflammasome in primary murine microglia.** (a) MTS assay of cell viability after treating lipopolysaccharide (LPS)-primed primary microglia with the mitochondrial complex-1 inhibiting pesticides rotenone (rot) or tebufenpyrad (tebu) (both 1 μM) for 24 h. (b) Luminex assay showing an increased IL-1β release from LPS-primed microglia after pesticide treatments for 24 h. Treatment with rotenone or tebufenpyrad did not alter TNFα release. (c) Western blot analysis of pesticide-treated primed microglial cells showing the cleavage of pro-caspase-1 to its active form caspase-1 p20. (d) Duolink proximal ligation assay reveals ASC and NLRP3 interaction in pesticide-exposed, primed microglial cells but not in unprimed cells following 3 h of pesticide exposure. Scale bar, 15 μm. (e) ICC showing ASC speck formation in pesticide-treated primed microglial cells for 2 h. Scale bar, 20 μm. (f) q-RT-PCR analysis of vehicle- and rotenone-gavaged (n=4 each group, 30 mg/kg for 28 days) mice for striatal NLRP3 gene expression. (g) Western blot analysis for vehicle- and rotenone-gavaged (30 mg/kg for 28 days) mice for NLRP3, Caspase 1 and IL-1β. (H-K) Densitometric analysis of Western blot for NLRP3 (h), Caspase 1 (i), Caspase 1 p20 (j), pro-IL-1β (k) and cleaved IL-1β (l). For all Western blots, samples derive from the same experiment and were processed in parallel. Data analyzed via Student's t test, or via two-way ANOVA with Bonferroni adjustment, *$p<0.05$, **$p<0.01$, ***$p<0.001$ and are represented as Mean±SEM with n=3-8.

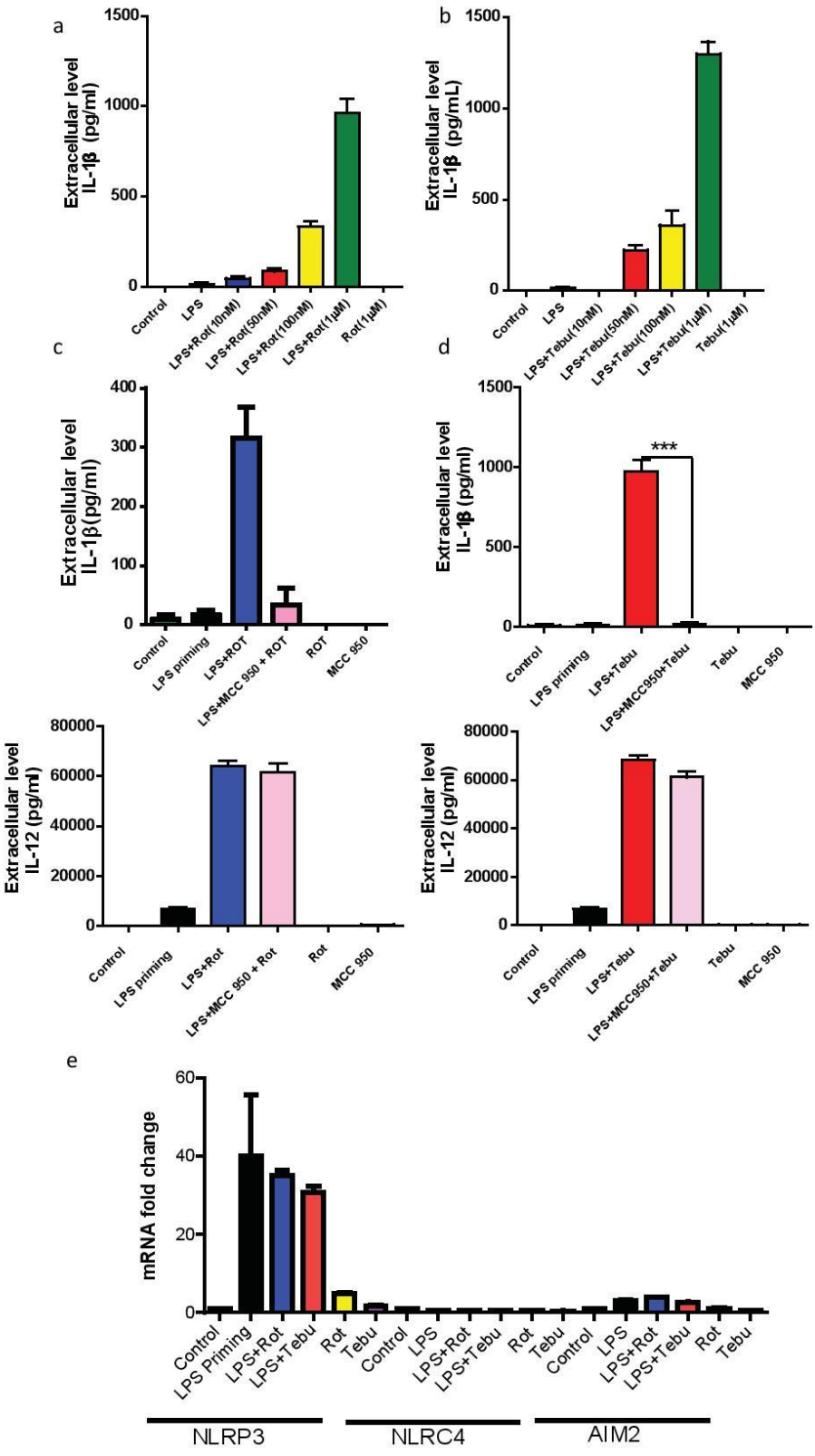
a
Extracellular level IL-1β (pg/ml)
1500
1000
500
0
Control
LPS
LPS+Rot(10nM)
LPS+Rot(50nM)
LPS+Rot(100nM)
LPS+Rot(1μM)
Rot(1μM)
b
Extracellular level IL-1β (pg/mL)
1500
1000
500
0
Control
LPS
LPS+Tebu(10nM)
LPS+Tebu(50nM)
LPS+Tebu(100nM)
LPS+Tebu(1μM)
Tebu(1μM)
c
Extracellular level IL-1β(pg/ml)
400
300
200
100
0
Control
LPS priming
LPS+ROT
LPS+MCC 950 + ROT
ROT
MCC 950
d
Extracellular level IL-1β (pg/ml)
1500
1000
500
0
***
Control
LPS priming
LPS+Tebu
LPS+MCC950+Tebu
Tebu
MCC 950
Extracellular level IL-12 (pg/ml)
80000
60000
40000
20000
0
Control
LPS priming
LPS+Rot
LPS+MCC 950 + Rot
Rot
MCC 950
Extracellular level IL-12 (pg/ml)
80000
60000
40000
20000
0
Control
LPS priming
LPS+Tebu
LPS+MCC950+Tebu
Tebu
MCC 950
e
mRNA fold change
60
40
20
0
Control
LPS Priming
LPS+Rot
LPS+Tebu
Rot
Tebu
Control
LPS
LPS+Rot
LPS+Tebu
Rot
Tebu
Control
LPS
LPS+Rot
LPS+Tebu
Rot
Tebu
NLRP3
NLRC4
AIM2

Figure 2

Fig 2: **Rotenone and tebufenpyrad induce a dose-dependent release of IL-1β in primed microglial cells through the NLRP3 inflammasome pathway.** (a-b) Luminex assay showing a dose-dependent increase in IL-1β release after treating primed primary microglial cells for 24 h with rotenone (a) and tebufenpyrad (b). (c) Luminex assay showing inhibition of IL-1β release after co-treating primed microglial cells with rotenone and MCC950, and showing no change in IL-12 release. (d) Luminex assay showing inhibition of IL-1β release after co-treating primed microglial cells with MCC950 and tebufenpyrad, and showing no change in IL-12 release. (e) q-RT-PCR analysis showing different inflammasome gene expression after treatment of LPS-primed primary mouse microglia with 1 μM rotenone and tebufenpyrad for 2 h. Data analyzed via two-way ANOVA with Bonferroni adjustment, *$p<0.05$, **$p<0.01$, ***$p<0.001$ and are represented as Mean±SEM with n=3-8.

Figure 3

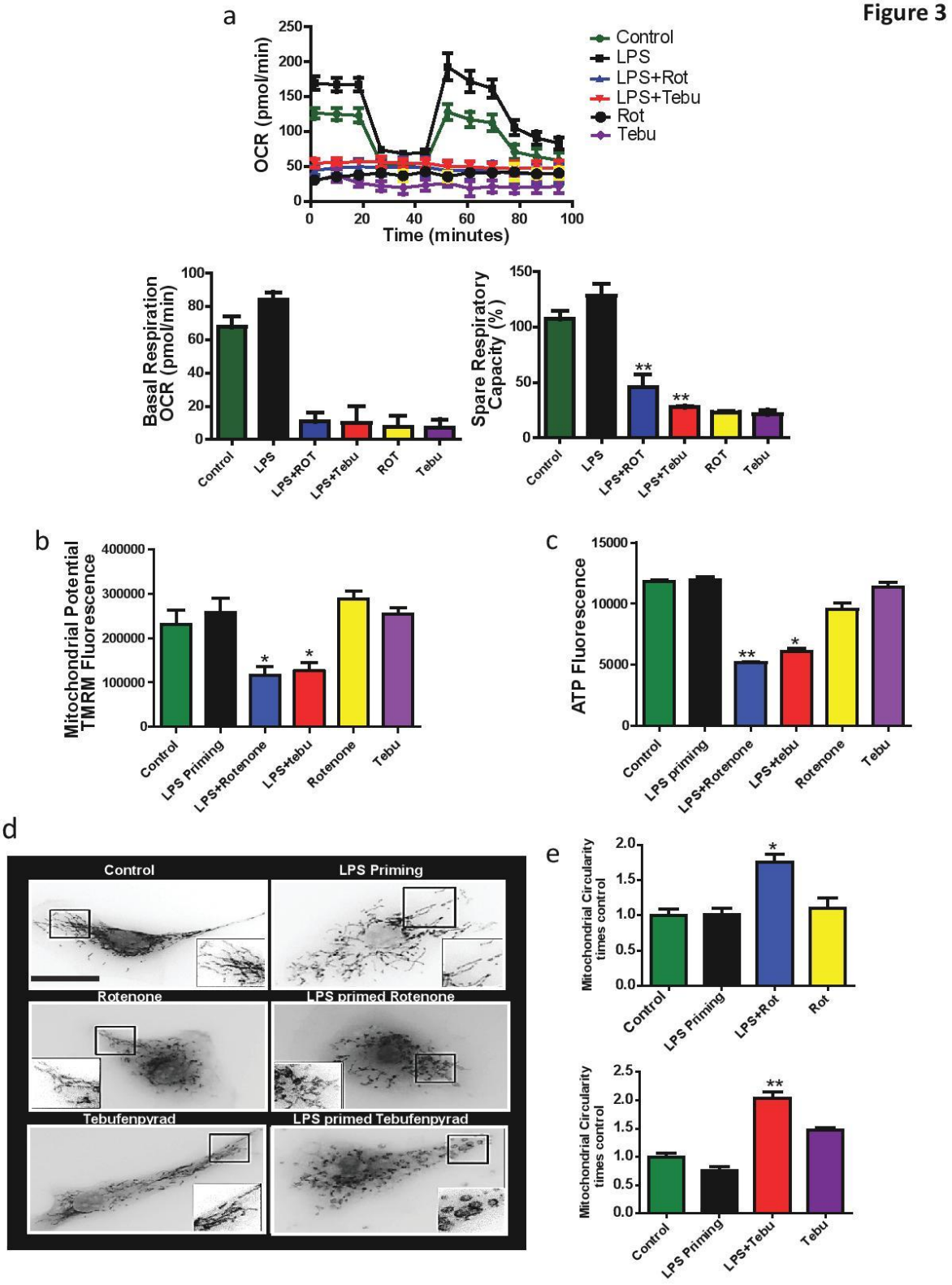
a
OCR (pmol/min)
Time (minutes)
Control
LPS
LPS+Rot
LPS+Tebu
Rot
Tebu
Basal Respiration OCR (pmol/min)
Spare Respiratory Capacity (%)
Control
LPS
LPS+ROT
LPS+Tebu
ROT
Tebu
b
Mitochondrial Potential TMRM Fluorescence
Control
LPS Priming
LPS+Rotenone
LPS+tebu
Rotenone
Tebu
c
ATP Fluorescence
Control
LPS priming
LPS+Rotenone
LPS+tebu
Rotenone
Tebu
d
Control
LPS Priming
Rotenone
LPS primed Rotenone
Tebufenpyrad
LPS primed Tebufenpyrad
e
Mitochondrial Circularity times control
Control
LPS Priming
LPS+Rot
Rot
Mitochondrial Circularity times control
Control
LPS Priming
LPS+Tebu
Tebu

Fig 3: **NLRP3 inflammasome activation is accompanied by mitochondrial functional and structural damage.** (a) Seahorse Mito-Stress assays showing impaired mitochondrial bioenergetics in LPS-primed primary microglial cells treated with pesticides. (b) Quantification of TMRM fluorescence staining showing mitochondrial potential in untreated and treated primary microglia. (c) ATP assays in LPS-primed mouse primary microglia treated with rotenone and tebufenpyrad. (d) MitoTracker assays show changes in mitochondrial morphology in LPS-primed primary microglia treated with pesticides. Scale bar, 15 μm. (e) Circularity, indicative of mitochondrial fragmentation, increased after pesticide treatment. Data analyzed via two-way ANOVA with Bonferroni adjustment, *$p<0.05$, **$p<0.01$, ***$p<0.001$ and are represented as Mean±SEM with n=3-8.

Figure 4

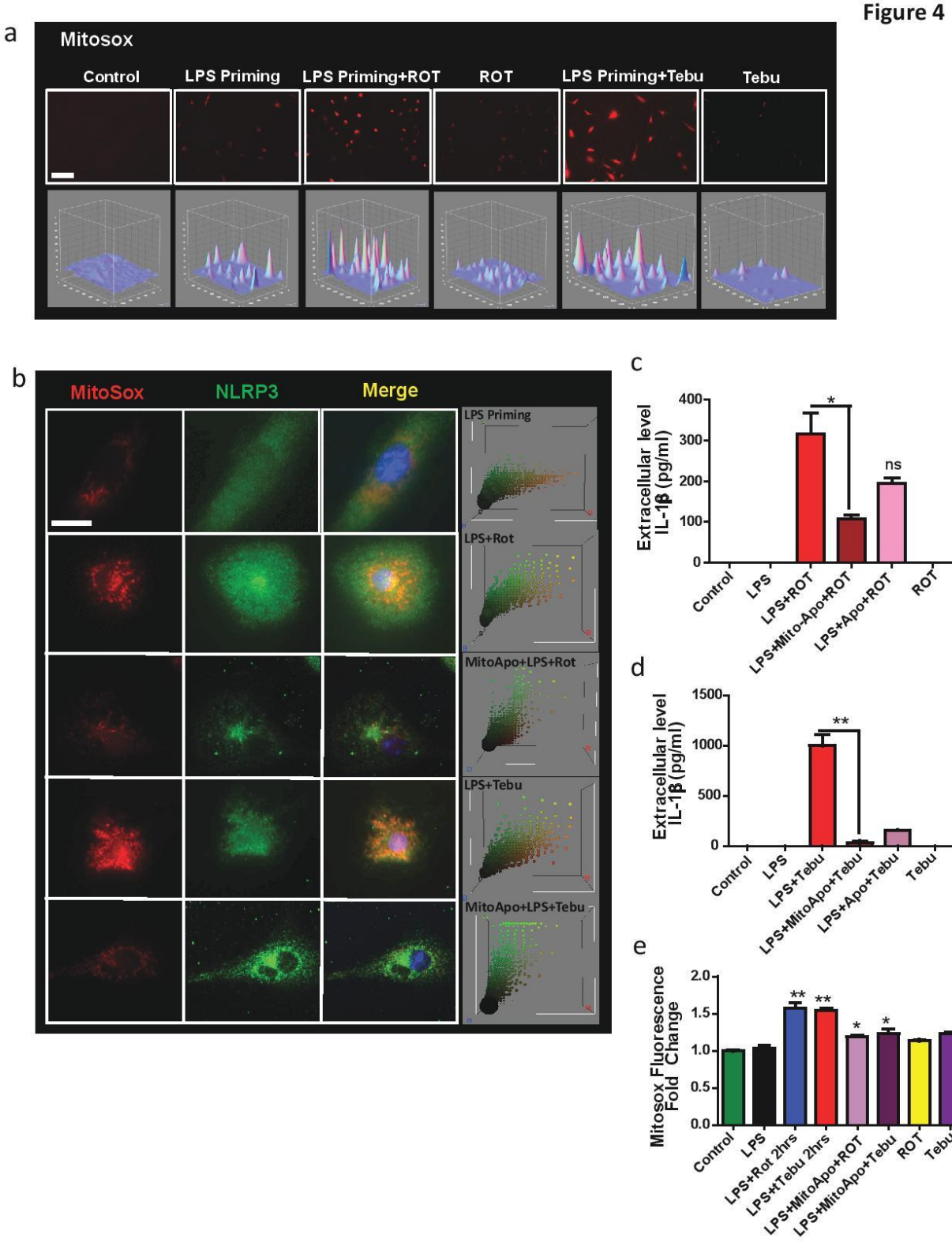
a
Mitosox
Control
LPS Priming
LPS Priming+ROT
ROT
LPS Priming+Tebu
Tebu
b
MitoSox
NLRP3
Merge
LPS Priming
LPS+Rot
MitoApo+LPS+Rot
LPS+Tebu
MitoApo+LPS+Tebu
c
Extracellular level IL-1β (pg/ml)
400
300
200
100
0
*
ns
Control
LPS
LPS+ROT
LPS+Mito-Apo+ROT
LPS+Apo+ROT
ROT
d
Extracellular level IL-1β (pg/ml)
1500
1000
500
0
**
Control
LPS
LPS+Tebu
LPS+MitoApo+Tebu
LPS+Apo+Tebu
Tebu
e
Mitosox Fluorescence Fold Change
2.0
1.5
1.0
0.5
0.0
**
**
*
*
Control
LPS
LPS+Rot 2hrs
LPS+Tebu 2hrs
LPS+MitoApo+ROT
LPS+MitoApo+Tebu
ROT
Tebu

Fig 4: **Mitochondrial superoxide generation plays a role in pesticide-induced NLRP3 inflammasome activation.** (a) ICC showing MitoSox generation from pesticide-treated primed microglial cells. Lower panel shows interactive-3D surface plot from corresponding ICC, which shows the intensity of superoxide generation. Scale bar, 100 μm. (b) ICC showing co-localization of mitochondrial superoxide generation and NLRP3. The right-most panel is the representative 3D color plot. Mito-apocynin reduced this co-localization between NLRP3 and MitoSox. Scale bar, 15 μm. (c-d) Luminex assays demonstrate that mito-apocynin reduced IL-1β secretion from primed microglial cells treated with rotenone (c) and tebufenpyrad (d). (e) MitoSox assays reveal that mito-apocynin reduced pesticide-induced superoxide generation in pesticide-treated primed microglial cells. Data analyzed via two-way ANOVA with Bonferroni adjustment, *$p<0.05$, **$p<0.01$, ***$p<0.001$ and are represented as Mean±SEM with n=3-8.

Figure 5

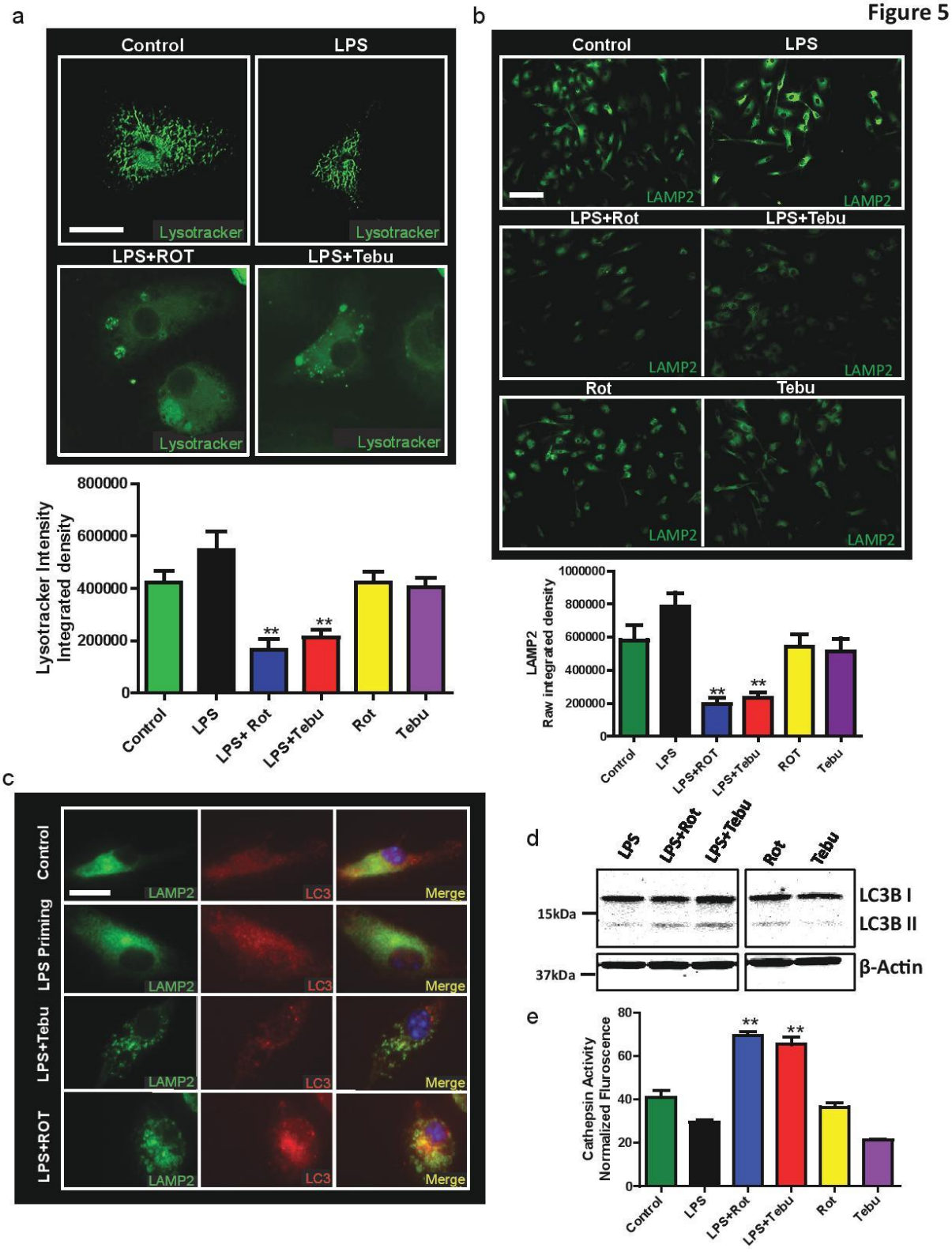
a
Control
LPS
Lysotracker
LPS+ROT
LPS+Tebu
Lysotracker Intensity
Integrated density
800000
600000
400000
200000
0
**
**
Control
LPS
LPS+ Rot
LPS+Tebu
Rot
Tebu
b
Control
LPS
LAMP2
LPS+Rot
LPS+Tebu
Rot
Tebu
LAMP2
Raw integrated density
1000000
800000
600000
400000
200000
0
ROT
c
Control
LPS Priming
LPS+Tebu
LPS+ROT
LAMP2
LC3
Merge
d
LPS
LPS+Rot
LPS+Tebu
Rot
Tebu
15kDa
37kDa
LC3B I
LC3B II
β-Actin
e
Cathepsin Activity
Normalized Fluroscence
80
60
40
20
0

Fig 5: **Lysosomal dysfunction enhances pesticide-induced NLRP3 inflammasome activation in microglia.** (a) Confocal microscopy showing a lower LysoTracker fluorescence intensity in primed microglial cells treated with pesticides (1 μM). Scale bar, 15 μm. (b) ICC for LAMP2 staining showing a lower LAMP2 immunoreactivity in primed microglial cells treated with pesticides, implying lysosomal damage. Scale bar, 100 μm. (c) 60X imaging for LAMP2 ICC showing structural changes in lysosomes in primed microglial cells treated with pesticides. Scale bar, 20 μm. (d) Western blot analysis reveals increased LC3-II in primed microglial cells exposed to 1 μM pesticides for 3 h. Samples derive from the same experiment and gels/blots were processed in parallel (e) Cathepsin activity assay revealed that 1 μM rotenone or tebufenpyrad for 6 h induced higher activity of this enzyme in primed microglial cells. Data analyzed via two-way ANOVA with Bonferroni adjustment, *$p<0.05$, **$p<0.01$, ***$p<0.001$ and are represented as Mean±SEM with n=3-8.

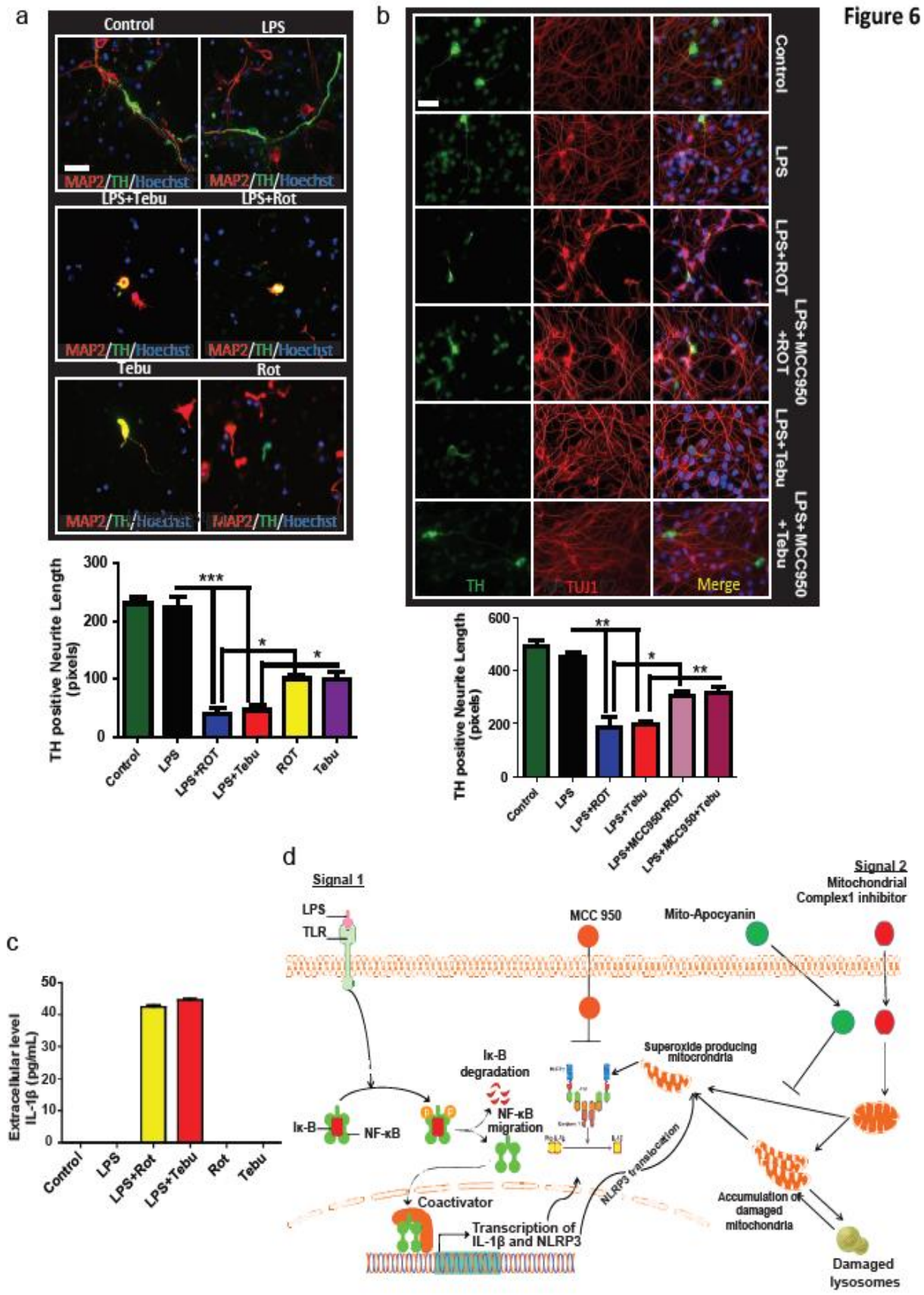
a
Control
LPS
MAP2/TH/Hoechst
LPS+Tebu
LPS+Rot
Tebu
Rot
TH positive Neurite Length (pixels)
300
200
100
0
***
*
*
Control
LPS
LPS+ROT
LPS+Tebu
ROT
Tebu
b
Control
LPS
LPS+ROT
LPS+MCC950 +ROT
LPS+Tebu
LPS+MCC950 +Tebu
TH
TUJ1
Merge
TH positive Neurite Length (pixels)
600
400
200
0
**
*
**
Control
LPS
LPS+ROT
LPS+Tebu
LPS+MCC950+ROT
LPS+MCC950+Tebu
c
Extracellular level IL-1β (pg/mL)
50
40
30
20
10
0
Control
LPS
LPS+Rot
LPS+Tebu
Rot
Tebu
d
Signal 1
LPS
TLR
MCC 950
Mito-Apocyanin
Signal 2
Mitochondrial Complex1 inhibitor
Superoxide producing mitocrondria
Ix-B degradation
Ix-B
NF-κB
NF-κB migration
Coactivator
Transcription of IL-1β and NLRP3
NLRP3 translocation
Accumulation of damaged mitochondria
Damaged lysosomes

Figure 6

Fig 6: **Conditioned medium from primary microglia treated with mitochondrial complex-1 inhibitors leads to DAergic neuronal toxicity.** (a) ICC analysis of TH^+ neurons treated with conditioned medium from primed microglial cells treated with 1 µM rotenone or tebufenpyrad for 24 h. The length of TH^+ neurites was determined using ImageJ. Conditioned medium from primed-microglial cells treated with tebufenpyrad reduced TH^+ neurite length. Scale bar, 100 µm. (b) ICC analysis of differentiated LUHMES cells treated with conditioned medium from primed microglial cells treated with 1 µM tebufenpyrad or rotenone for 24 h and cotreated with MCC-950. Scale bar, 100 µm. (c) Luminex analysis of the conditioned medium used to treat LUHMES cells. (d) A schematic representation illustrating the signaling cascade involved in pesticide-induced NLRP3 inflammasome activation in microglial cells; drawing created by S. Sarkar using biomedical PowerPoint toolkit from Motifolio. Data analyzed via two-way ANOVA with Bonferroni adjustment, *$p<0.05$, **$p<0.01$, ***$p<0.001$ and are represented as Mean±SEM with n=3-8.

Supplementary Materials

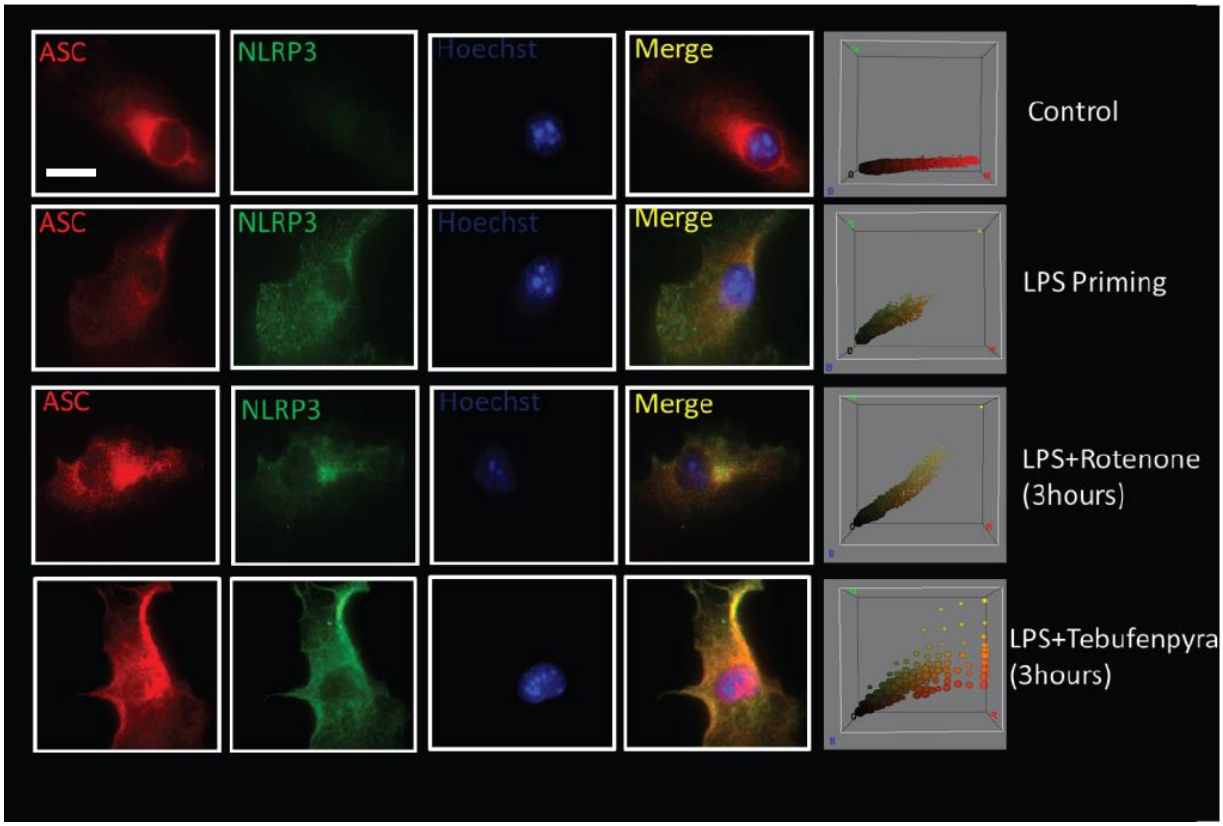

Supplementary Fig. 1: **LPS priming leads to NLRP3 upregulation in primary microglial cells.** ICC showing the upregulation of NLRP3 and co-localization with ASC after treatment with rotenone or tebufenpyrad for 2 h. The right-most panel is the representative 3D color plot. Scale bar, 20 μm.

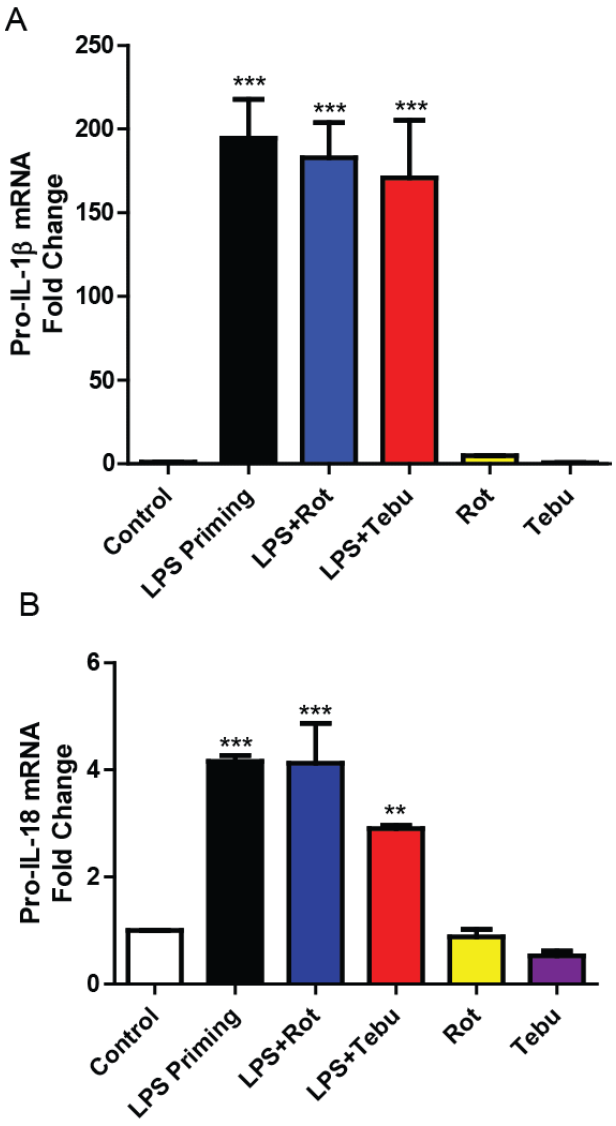

Supplementary Fig 2: **Pesticide-induced inflammasome activation induces IL-1β and pro-IL-18.** q-RT-PCR analysis showing the gene levels of pro-IL-1β and pro-IL-18 in LPS-primed primary mouse microglia treated with or without 1 µM rotenone or tebufenpyrad for 2 h. Data analyzed via two-way ANOVA with Bonferroni adjustment, *p<0.05, **p<0.01, ***p<0.001 and are represented as Mean±SEM with n=3-8.

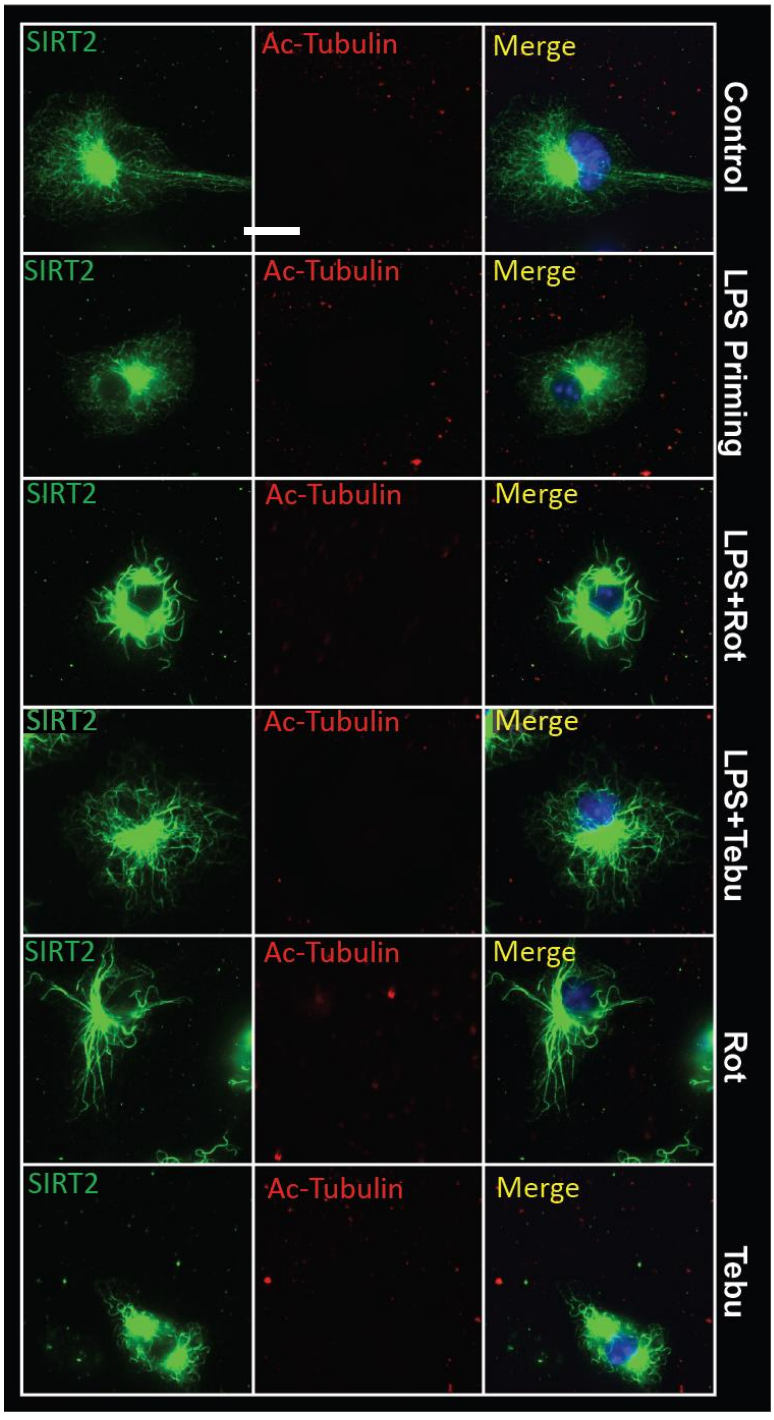

Supplementary Fig. 3: **Pesticide exposure does not induce acetylation of microtubules at early time points in microglial cells.** ICC analysis reveals that

SIRT2 levels or acetylated α-tubulin did not significantly change after 2 h of 1-μM pesticide exposure in primed and unprimed primary microglial cells. Scale bar, 20 μm.

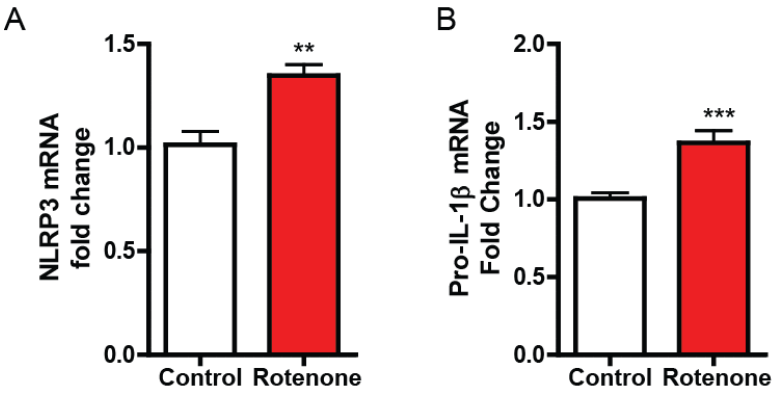

Supplementary Fig. 4: **Pesticide exposure alone induced NLRP3 and pro-IL-β in presence of neurons.** (A-B) qRT-PCR analysis showing gene level of NLRP3 (A) and pro-IL-1β (B) following 1 μM rotenone exposure for 6 h in presence of neurons. Data analyzed via two-way ANOVA with Bonferroni adjustment, *p<0.05, **p<0.01, ***<0.001 and are represented as Mean±SEM with n=3-8.

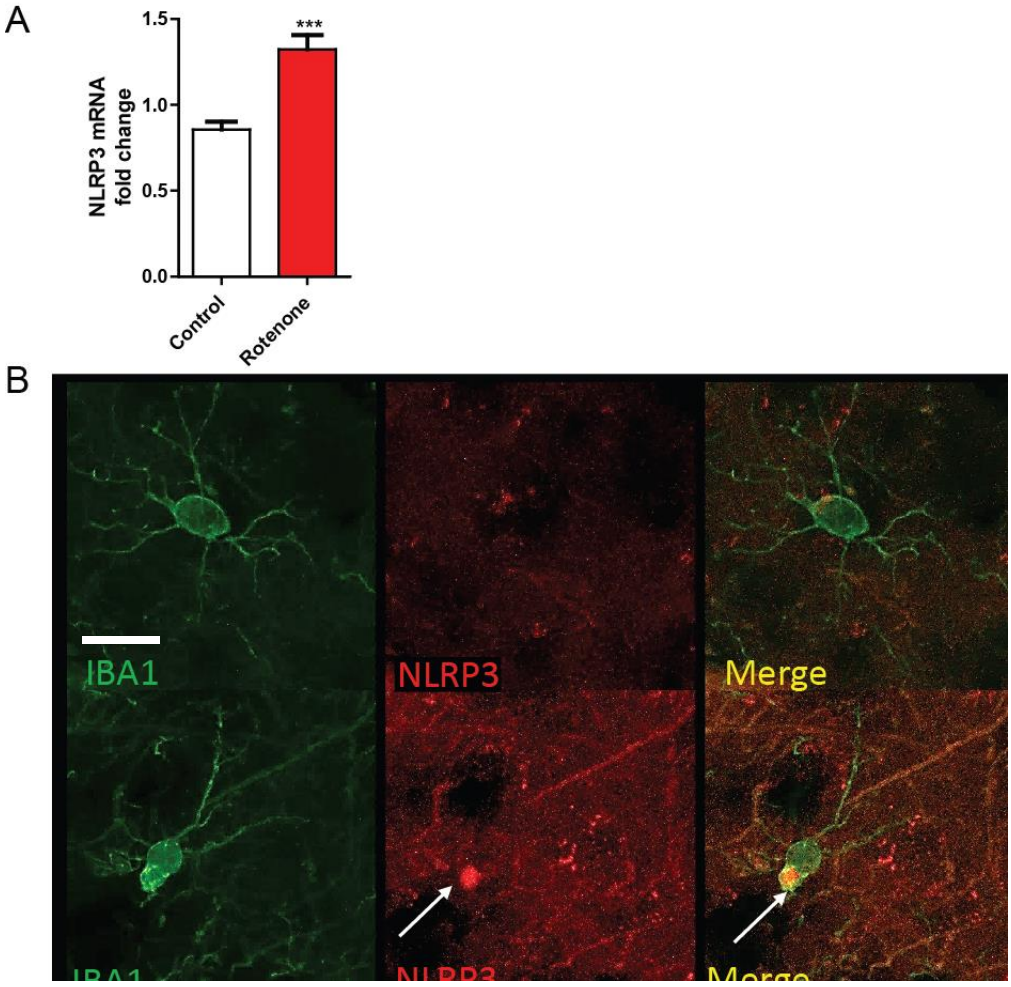

Supplementary Fig. 5: **Rotenone induced NLRP3 inflammasome activation in rat model.** (A) qRT-PCR analysis revealed NLRP3 upregulation in rotenone-treated rats. (B) IHC analysis showing increased NLRP3 in IBA1-positive cells in the striatum of rotenone treated rats. Data analyzed via Student's t-test, *p<0.05, **p<0.01, ***<0.001 and are represented as Mean±SEM with n=4. Scale bar, 15 μm.

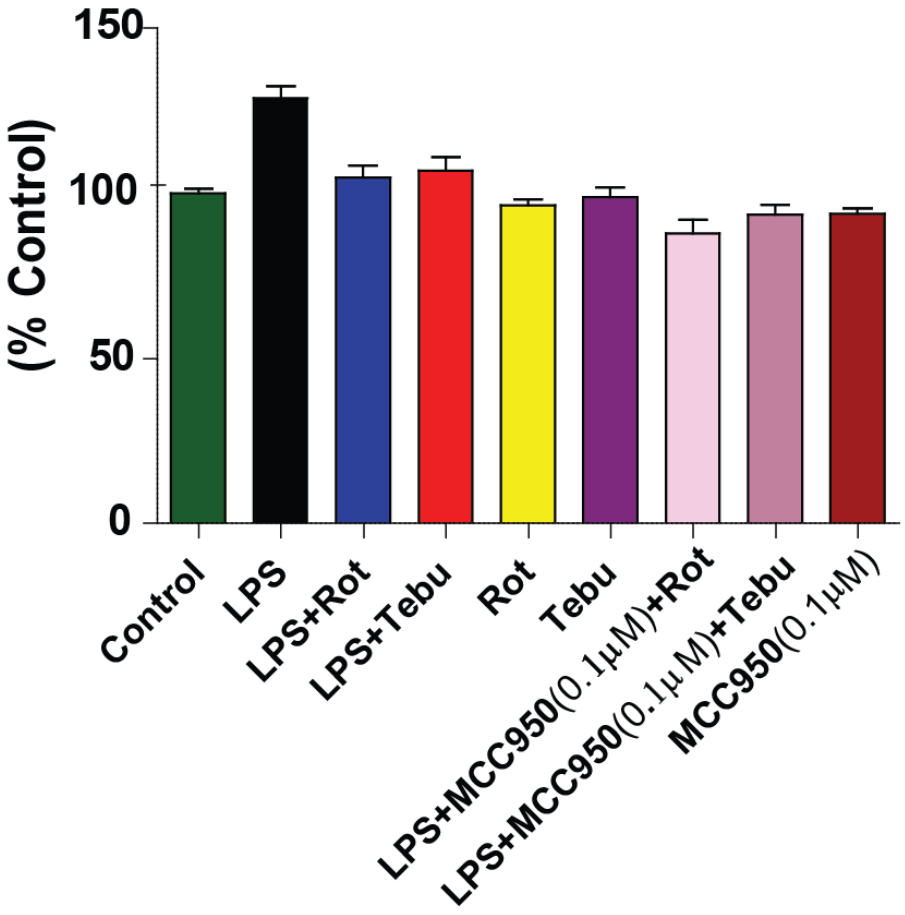

Supplementary Fig. 6: **MCC950, an NLRP3-specific inhibitor, does not affect cell viability in primary microglial culture**. MTS assay of cell viability after treatment with MCC950. Data analyzed via two-way ANOVA with Bonferroni adjustment, *p<0.05, **p<0.01, ***<0.001 and are represented as Mean±SEM with n=3-8.

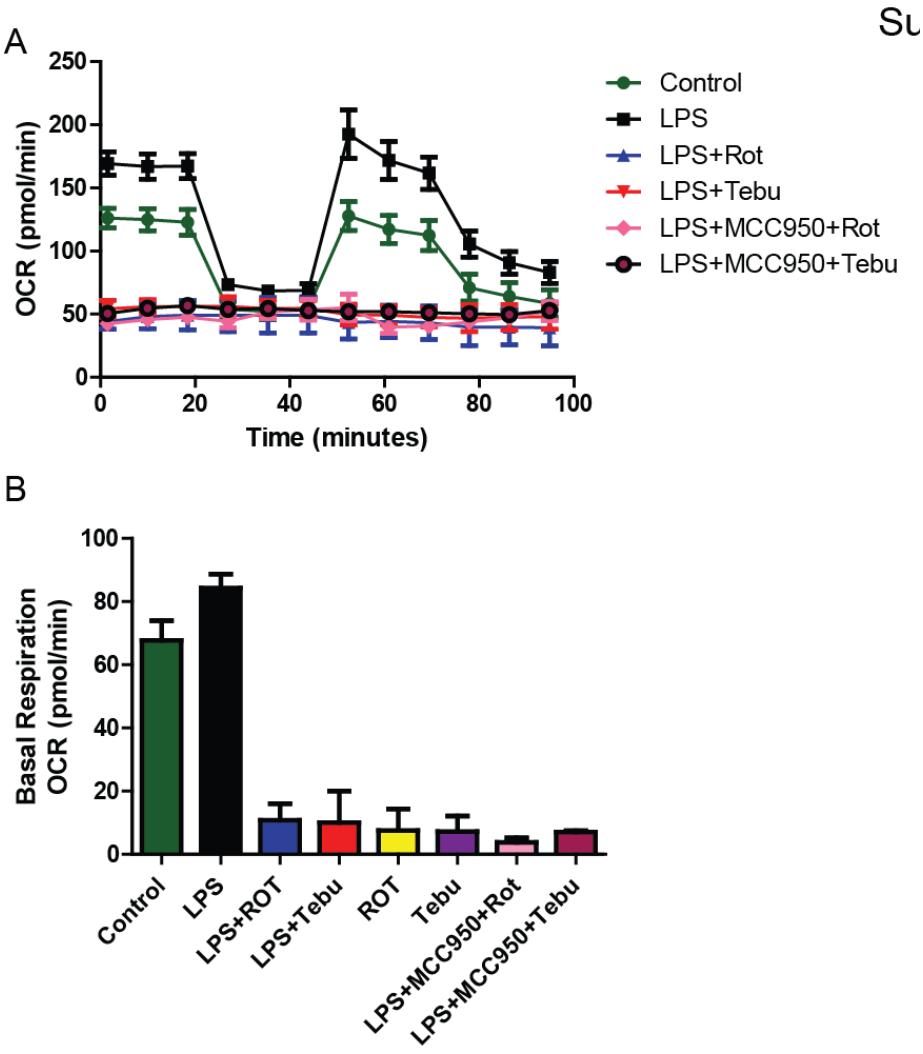

Supplementary Fig. 7: **MCC950 does not alter mitochondrial dynamics.** (A-B) Seahorse Mito Stress assays showing MCC-950 does not alter impaired mitochondrial bioenergetics in LPS-primed primary microglial cells treated with pesticides for 3 h. Data analyzed via two-way ANOVA with Bonferroni adjustment, *p<0.05, **p<0.01, ***<0.001 and are represented as Mean±SEM with n=3-8.

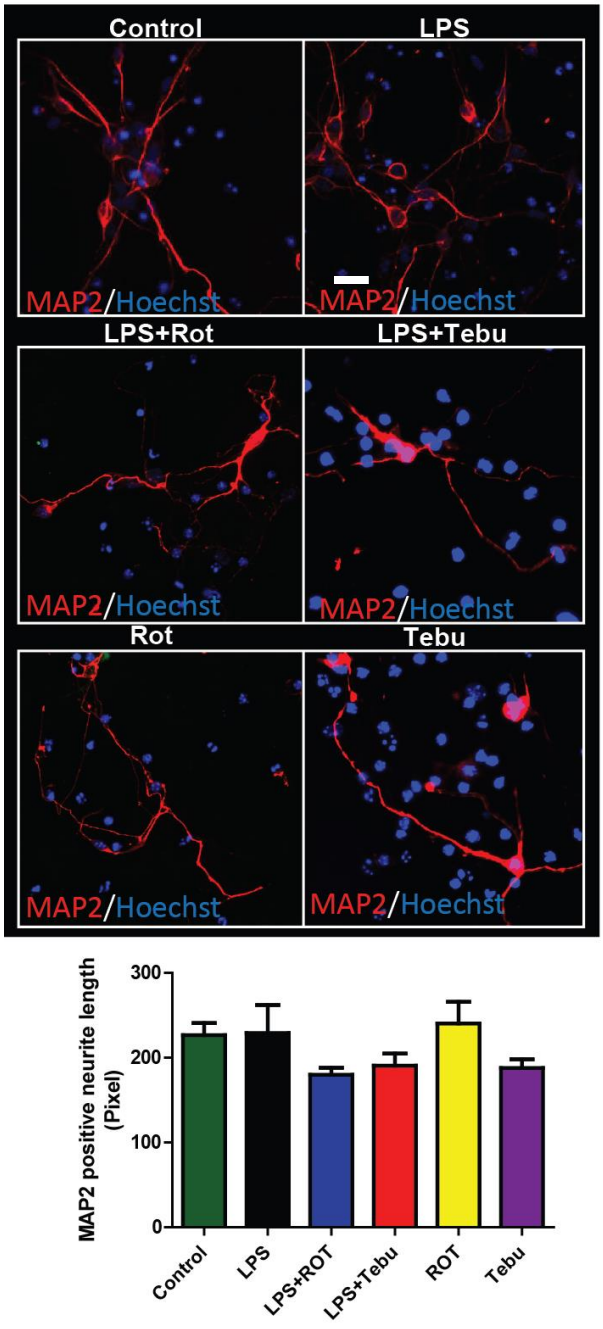

Supplementary Fig. 8: **Conditioned medium from pesticide-exposed microglial cells does not alter TH-negative neurite length.** ICC analysis showing that TH-negative neurite length is not affected on exposure to conditioned medium from primed microglial cells exposed to rotenone or pesticides. Data analyzed via two-way

ANOVA with Bonferroni adjustment, *p<0.05, **p<0.01, ***<0.001 and are represented as Mean±SEM with n=3-8. Scale bar, 100 µm.

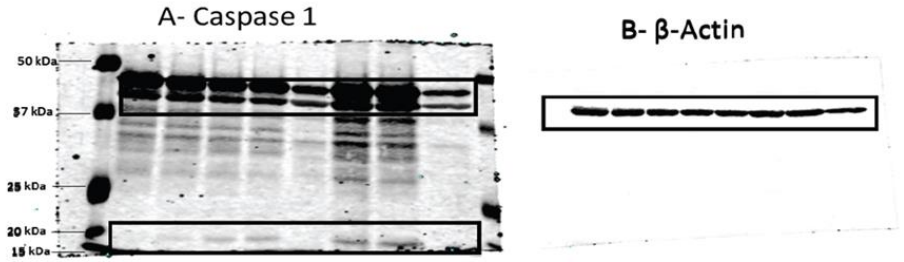

Fig A-B. Well-1 Marker, Well-2 Control, Well-3 LPS Priming, Well-4 LPS+Rot 3 h, Well-5 LPS+Rot 6 h, Well-6 Rot 6 h, Well-7 LPS+Tebu 3 h, Well-8 LPS+Tebu 6 h, Well-9 Tebu 6 h, . Well-10 Marker.

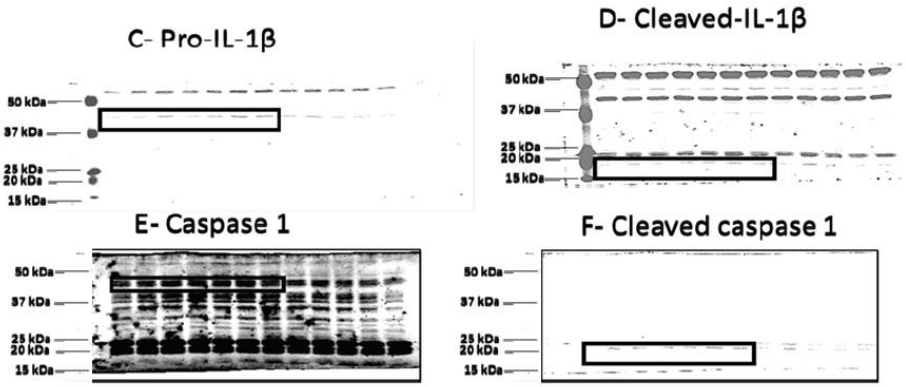

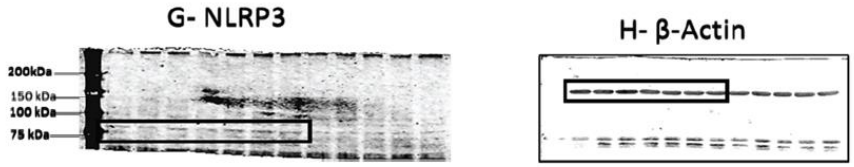

Fig C-H. Well-1 Marker, Wells 2-6 Control, Wells 7-9 Rotenone

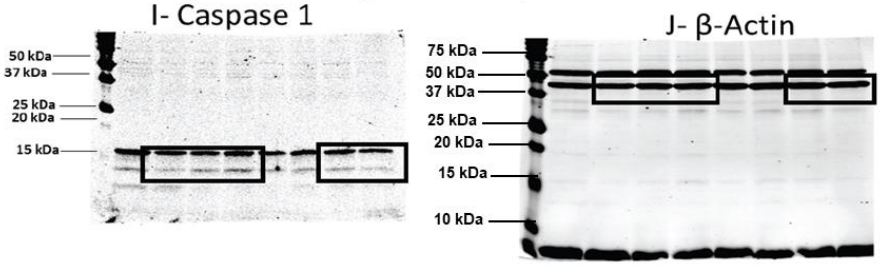

Fig I-J. Well-1 Marker, Well-3-LPS, Well-4 LPS+Rot, Well-5 LPS+Tebu, Well-8 Rot, Well-9 Tebu.

Supplementary Fig 9: **Full length Western blots shown in Fig 1.** (A-B) Full length Western blots corresponding to Fig. 1C. (C-H) Full length Western blots corresponding to Fig. 1G. (I-J) Full Western blots corresponding to Fig. 5D. Samples derive from the same experiment and gels/blots were processed in parallel.

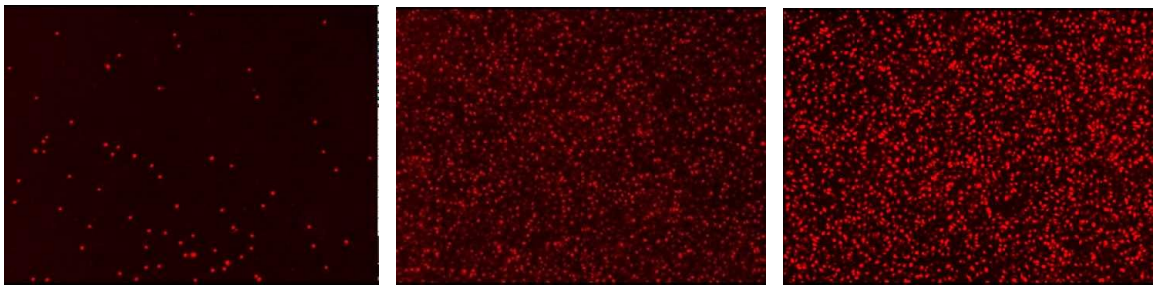

Supplementary Videos 1-3: **Time-lapse videos of mitochondrial superoxide generation in primed microglial cells treated with vehicle, rotenone, and tebufenpyrad, respectively.**

CHAPTER V

MANGANESE EXPOSURE ACTIVATES NLRP3 INFLAMMASOME SIGNALING AND PROPAGATES EXOSOMAL RELEASE OF ASC IN MICROGLIAL CELLS

Manuscript to submitted to *Science Signaling*

Souvarish Sarkar[1], Dharmin Rokad[1], Emir Malovic[1], Jie Luo[1], Dilshan Harischandra[1], Huajun Jin[1], Vellareddy Anantharam[1], Xumei Huang[2], Mechelle Lewis[2], Arthi Kanthasamy[1], Anumantha G. Kanthasamy[1*]

1-Parkinson Disorders Research Laboratory, Iowa Center for Advanced Neurotoxicology, Department of Biomedical Sciences, 2062 Veterinary Medicine Building, Iowa State University, Ames, IA 50011

2-Penn State Hershey Medical Center, Hershey, PA.

*To whom correspondence should be addressed: Anumantha Kanthasamy, Ph.D., Distinguished Professor and Chair, Department of Biomedical Sciences, Iowa State University, Ames, IA 50011. Telephone: (515) 294-2516; Fax: (515) 294-2315, Email: akanthas@iastate.edu

Abstract

Abnormal metal homeostasis is a key hallmark of multiple neurodegenerative disorders including Alzheimer's disease (AD), and Parkinson's disease (PD). Overexposure to Manganese (Mn) have been linked to PD-like symptoms. Sustained neuroinflammation is now recognized as a key pathophysiological process of neurodegenerative conditions, but the inflammatory signaling mechanism underlying

Mn neurotoxicity is equivocal. In this study, we examined whether Mn mounts its neurotoxic effect by activating NLRP3 inflammasome signaling. Exposing microglial cells, primed with LPS, to Mn significantly increased NLRP3, caspase-1 cleavage, and IL-1β maturation, indicating that Mn can induce the NLRP3 inflammasome activation cascade. Mn exposure reduced the mitochondrial dynamics of microglia cells as measured via Seahorse Mito Stress assay and downregulated mitochondrial fusion. Furthermore, Mn reduced the expression of retromer pathway protein VPS35. CRISPR KD of VPS35 further regulated mitochondrial fusion protein by increasing mitochondrial ubiquitin ligase suggesting the probable role of VPS35 in maintaining mitochondrial health. Given that the inflammasome component ASC can propagate inflammasome activation in a “prionic” manner, we explored whether Mn exposure induces cell-to-cell transfer of ASC via exosomes. Exosomes isolated from Mn-treated LPS-primed microglial cells contained higher amounts of ASC, suggesting exosomal release of ASC. Furthermore, exosomes isolated from microglial cells exposed to Mn induced pro-IL-1β, and NLRP3 expression further suggesting the role of exosomal-ASC in inflammasome propagation. Importantly, we confirmed a significantly higher ASC content in exosomes collected from welders when compared to exosomes from matched controls. Collectively, these results demonstrate that Mn neurotoxicity involves activating NLRP3 inflammasome signaling and exosomal ASC release.

Introduction

Overexposure to transition metals like manganese (Mn), iron (Fe), copper (Cu), and zinc (Zn) from occupational or environmental sources (e.g., various food products and well-water) has been linked to various neurodegenerative disorders, including Alzheimer's disease (AD) and Parkinson's disease (PD). Imbalance in metal homeostasis have been shown to modulate various cellular functions, including generation of oxidative stress, mitochondrial dysfunction, and exosome biogenesis; the processes which have been all linked to various neurodegenerative disorders (*1, 2*).

Chronic exposure to Mn in occupational settings was first noted in miners (*3, 4*), followed by welders (*5*). Recent studies of welder populations revealed that occupational exposure to Mn increases the risk of developing PD (*6*). Mn toxicity can also manifest as a disease called manganism, which shares similar symptoms as PD (*7, 8*). Mn accumulates mainly in the globus pallidus as well as in the striatum leading to the PD-like phenotype (*9*).

The etiology of PD is multifactorial. One of the major hallmarks of Parkinsonian syndromes, including manganism, is chronic and sustained inflammation (*10-15*). Inflammation in PD patients was first implicated by McGeer *et al.* (*16*). Various inflammatory factors including tumor necrosis factor-α (TNF-α) and IL-1β have been shown to be upregulated in PD patients (*17*). Microglia, the brain's frontline immune-responders, have been implicated as a key player in modulating neuroinflammation (*13, 18*). Blocking microglial activation was shown to be neuroprotective in the MPTP model of PD (*19*). Furthermore, based on recent studies from our group and others,

use of anti-inflammatory agents is protective in cell culture and animal models of PD (*20-24*). Though the effects of chronic inflammation have been well documented in neurodegenerative disorders like PD, the mechanism underlying this sustained immune response is not well understood (*25*).

The cell-derived vesicles exosomes contain diverse cargo known to induce inflammation. Aggregated α-synuclein preformed fibrils (αSyn_{PFF}) have been shown to be transmitted from cell-to-cell via exosomes, propagate inflammation, and induce cell death (*26, 27*). Exosomes from lung cancer can induce NFκB signaling (*28*). Recently, various inflammasome activations, including NLRP3 (nucleotide binding and oligomerization domain-like receptor family pyrin domain containing 3), NLRC4 (NLR family CARD domain-containing protein 4), and AIM2 (absent in melanoma 2) among others, have been implicated as mechanisms underlying inflammation in neurodegenerative disorders, like PD, AD, and traumatic brain injury (TBI) (*29*). The NLRP3 inflammasome is a multiprotein oligomeric complex comprising an adapter protein ASC (apoptosis-associated speck-like protein containing a CARD), Caspase 1, and NLRP3. Multiple external signals, including misfolded β-amyloid (*30*) and αSyn_{PFF} (*31*), have been shown to activate the NLRP3 inflammasome complex. NLRP3 inflammasome signaling requires two signals for its activation. Lipopolysaccharide (LPS), TNF-α, or any signal capable of activating NFκB can act as signal 1 (or a priming signal) to upregulate the expression of NLRP3 and pro-IL-1β. A second NLRP3-specific activation signal (signal 2, such as mitochondrial dysfunction and lysosomal damage), triggers the assembly and activation of the NLRP3 inflammasome complex. The adapter molecule ASC links the NLRP3 protein

to the recruited caspase-1, leading to caspase-1 dimerization, autocatalytic processing and the generation of active caspase-1. Active caspase-1 processes the maturation of pro-IL-1β to IL-1β, promoting inflammation (*32, 33*). Recent studies have indicated that NLRP3 inflammasome propagation is modulated by a cell-to-cell transmission of the ASC adaptor protein by an unknown mechanism (*34*). Despite these information, the exact mechanisms of inflammasome activation and propagation remain elusive.

Mn toxicity has been well documented in neurodegeneration and glial biology (*9, 35-39*). More specifically, Mn induces TNF-α and inducible nitrogen synthase (iNOS) in astrocytes (*40, 41*), causes mitochondrial dysfunction by its accumulation in mitochondria (*42*), and it was shown to induce neurotoxicity in a rat model of manganism by modulating microgliosis (*43*). Mn exposure has been shown to induce classical activation in microglial cells (*44*) as well as astrocytes(*39*) in the central nervous system, leading to production of pro-inflammatory cytokines. The plethora of pro-inflammatory factors have been shown to cause neuronal damage (*45*). Furthermore, Mn has been shown to enhance, LPS-induced production of pro-inflammatory factors in microglial cells (*37*). Recently, Mn-induced microglial activation has been shown to activate astrocytes, leading to enhanced production of pro-inflammatory factors (*46*).However, the molecular signaling mechanism of Mn-induced microglial activation is still not well understood. Microglia express multiple functional inflammasomes, including NLRP3, NLRC4 and AIM2 inflammasomes (*47*).However, the effect of Mn on microglial inflammasome activation and propagation remains equivocal.

This current study characterizes whether Mn activates inflammasome signaling in microglial cells and the mechanisms involved in activation in propagation. Furthermore, this study aims to bridge the gap between Mn-induced inflammation and mitochondrial damage in microglial cells. Moreover, there is a lack of understanding in the signaling mechanism of inflammasome propagation which we aimed to address in this study. Here, we elucidate that Mn can act as signal 2 to activate the NLRP3 inflammasome in microglial cells. In our studies reported here, we show that 1) Mn induces mitochondrial dysfunction and reduces mitochondrial fusion protein 2, or Mitofusin 2 (Mfn2); 2) Mn downregulates vacuolar protein sorting-associated protein 35 (VPS35), a retromer complex protein which regulates Mfn2 ubiquitination; 3) uptake of ASC-containing exosomes plays a role in Mn-induced inflammasome propagation; and finally, welder serum exosomes have a higher ASC load compared to age-matched controls and have higher serum pro-inflammatory cytokine levels.

Results

Mn induces NLRP3 inflammasome activation in microglial cells *in vitro* and *in vivo*

The NLRP3 inflammasome can be activated by various external signals including, ATP, pathogen-activated molecular patterns (PAMP's), and danger-associated molecular patterns (DAMP's) (*30*). However, the role of environmental PD neurotoxicants, like Mn, in inducing inflammasome activation has not been fully elucidated till date. Therefore, in the first set of experiments we investigated the ability of Mn to stimulate the processing and release of IL-1β and caspase-1 cleavage from LPS-primed microglial cells. Microglial cells were primed with 100 ng/ml of LPS for 3

h, after which the cells were treated with 100 μM Mn for 24 h. As shown in Fig. 1A, there was no detectable mature IL-1β in unstimulated or LPS priming alone cells; however, a significant amount of mature IL-1β was detected in LPS-primed, Mn-treated microglial cells (Fig. 1A and Supplementary Fig. 1A-B). Similarly, a multiplexed Luminex assay confirmed that Mn exposure induced a dramatic release of IL-1β from LPS-primed cells (Fig. 1B). Of note, Mn treatment alone had no effect on inducing IL-1β processing and release. Furthermore, Western blot analysis revealed that Mn significantly stimulated the cleavage of caspase-1 in LPS-primed cells when compared to unstimulated and LPS priming alone cells (Fig. 1A). Interestingly, we observed a slightly but not significantly increased amount of cleaved caspase-1 in Mn-treated unprimed cells (Fig. 1A and Supplementary Fig. 1C). These results suggest that Mn exposure can serve as a signal 2 to activate microglial inflammasome signaling. Recent studies have shown that ASC, a component of inflammasome activation, can form speck-like structures and helps to propagate the inflammasome from cell-to-cell (*34*). Our ICC analysis revealed that ASC was evenly distributed throughout the unstimulated and LPS priming alone cells. In contrast, the LPS-primed microglial cells exposed to Mn formed intesnse ASC specks, further indicative of inflammasome activation (Fig. 1C). Next, to identify which inflammasome was activated by Mn, we treated LPS-primed microglial cells with Mn for 6 h. Western blot analysis revealed that NLRP3 was significantly upregulated in LPS-primed cells stimulated with or without Mn (Fig. 1D), whereas NLRC4 and AIM2 proteins were not detectable (data not shown). ICC further confirmed this upregulation of NLRP3 (Fig. 1E) in both LPS priming alone and Mn-treated, LPS-primed cells. These results

provide evidence for a specific effect of Mn on NLRP3 inflammasome activation. Supporting this view, qRT-PCR analysis showed significantly increased mRNA levels of NLRP3 and pro-IL-1β (Fig. 1F). Mn-treated unprimed cells did not show any significant upregulation of pro-IL-1β and NLRP3, indicating that Mn exposure had no effect on the priming step of NLRP3 inflammsome. To further verify the specificity of Mn in metal-induced inflammasome activation, primary microglial cells were treated with Mn, copper (Cu), and zinc (Zn). Since Zn is toxic at 100 μM, a non-toxic dose of Zn (30 μM) was used. Cu was used at the same dose as Mn (100 μM). An MTS assay revealed that Mn treatment did not show obvious cytotoxicity in LPS-primed cells while Cu and Zn cause more cell death (Supplementary Fig. 2A). Regarding the capacity for inflammasome activation, again, our Luminex data revealed that Mn elicited a significant increase in IL-1β release in LPS-primed cells, whereas Cu and Zn did not (Supplementary Fig. 2B). On the other hand, LPS-treated cells stimulated with Mn, Cu or Zn released comparable amounts of TNF-α (Supplementary Fig. 2C). This data validates that inflammasome activation is not a property of all divalent transition metals. Moreover, Mn exposure potentiated LPS-induced *Nos2* mRNA (Supplementary Fig. 3A) and protein levels (Supplementary Fig. 3B and Fig. 3C) as well as nitrite release (Supplementary Fig. 3D). All these findings together show Mn can activate the NLRP3 inflammasome in primed microglial cells.

The etiology of PD is complex and multifactorial. The role of environment-gene interaction has been implicated in PD pathogenesis (*48-50*). Not only is aggregated αSyn an important component of Lewy bodies and Lewy neurites in PD, it has also been shown to induce NLRP3 inflammasome activation (*31*). We hypothesized that

Mn potentiates αSyn_{PFF}-induced microglial NRLP3 inflammasome activation. Co-treatment of Mn with αSyn_{PFF} potentiated αSyn_{PFF}-induced upregulation of NLRP3 and iNOS proteins (Fig. 1G). Luminex assay revealed that Mn further potentiated the αSyn_{PFF}-induced release of IL-1β (Fig. 1H) but not IL-6 (Supplementary Fig. 4A) or TNF-α (Supplementary Fig. 4B). These findings indicate that Mn can further potentiate αSyn_{PFF}-induced inflammasome activation in microglial cells.

To add *in vivo* relevance, we wanted to verify if Mn can induce the NLRP3 inflammasome in animals. C57BL mice were gavaged with 15 mg/kg Mn for 30 days followed by immunoblot analysis, qRT-PCR, and IHC of the striatum. Mn specifically induced NLRP3 mRNA expression, but not AIM2 and NLRC4, as revealed by qRT-PCR (Fig. 1I). IHC studies further revealed that this NLRP3 increase occurred in IBA1 (microglia marker)-positive cells (Fig. 1J). Our Western blot analysis showed that Mn significantly increased caspase-1 cleavage, and mature IL-1β (Fig. 1K and Supplementary Fig. 5A). Interestingly we did not observe an increase in pro-IL-1β level. The Mn-induced increase in cleaved caspase-1 is strongly correlated with an increase in the level of released IL-1β (Supplementary Fig. 5B). Collectively, all these findings show for the first time that Mn can activate the NLRP3 inflammasome in microglial cells both *in vitro* and *in vivo*. This NLRP3 signaling cascade could be the putative mechanism by which chronic inflammation is sustained in Mn-induced Parkinsonism.

Mn leads to mitochondrial dysfunction in primed microglial cells

The mechanism underlying inflammasome activation is currently being debated. Recent studies have attributed this activation to mitochondrial dysfunction and mitochondrial superoxide generation (*32, 33, 51-53*). Mn is known to more severely impair mitochondria under stress conditions (*54-57*). Hence, we ran the Mito Stress assay on an extracellular flux analysis system (Seahorse Bioscience, XFe24) to determine the effects of Mn on mitochondrial bioenergetics of LPS-primed microglia. Primary microglial cells were primed with LPS for 3 h followed by 24 h of treatment with Mn (100 μM). Interestingly, exposing LPS-primed microglia to Mn significantly impaired mitochondrial function (Fig. 2A) as depicted by decreased mitochondrial ATP production (Fig. 2B), basal respiration rate (Fig. 2C), maximal respiration (Fig. 2D), and spare respiratory capacity (Fig. 2E). Interestingly, Mn exposure in unprimed microglial cells showed no significant changes in mitochondrial dynamics. A previous study by Dodd *et al.* also showed that 250 μM Mn exposure in N9 microglia for 24 h caused little or no increase in ooxidative stress (*37*).Furthermore, cell phenotype analysis revealed that Mn altered the cellular metabolic phenotype in LPS-primed microglial cells. Exposure of LPS-primed primary mcirlgia to Mn significantly decreased stressed oxygen consumption rate (OCR) without significantly changing the stressed extracellular acidification rate (ECAR), as measured by the cell energy phenotype test, suggesting that Mn exposure reduced the mitochondrial metabolism rate without modulating non-mitochondrial function (Supplementary Fig. 6).

Mitochondrial dysfunction leads to superoxide generation. Thus, as expected, our MitoSox assay revealed that LPS-primed microglial cell line treated with 100 μM Mn for 24 h generated significant superoxide levels (Fig. 2F), futher confirming the effcts of Mn treatment on mitochondrial dysfunction in primed microglia. Since LPS-primed cells and unprimed microglial cells exposed to Mn both exhibited minimal or no changes in mitochondrial superoxide production (Fig. 2F), we hypothesized that LPS is modulating Mn transporters in microglia. Indeed, qRT-PCR analysis revealed that LPS significantly increased Mn importer *SLC11A2* (Supplementary Fig. 7A), while Mn exposure alone induced the expression level of Mn exporter *SLC30A10* (Supplementary Fig. 7B) without changing the importer expression.As a result, we observed an increased Mn uptake in LPS-primed, Mn-treated microglial cells compared to unprimed Mn-treated cells as revealed by ICP-MS analysis (Supplementary Fig. 7C). These data suggest that LPS priming modulates the uptake of Mn by changing Mn receptor levels.

Links to mitochondrial dysfunction were recently established for Mfn2 (*58-60*), including Mfn2 degradation by ubiquitination. Although our qRT-PCR analysis, in LPS-primed microglial cell line, showed no significant change in Mfn2 levels (Fig. 2G), our immunoblot analysis (Fig. 2H) and ICC (Fig. 2I) showed that Mfn2 decreased in primed microglial cells treated with Mn, suggesting that the Mn-induced mitochondrial dysfunction in primed microglia may be due to Mfn2 degradation. One candidate for ubiquitinating Mfn2 is mitochondrial ubiquitin ligase 1(Mul1). In fact, the mRNA level of Mul1 in Mn-treated, LPS-primed cells doubled when compared to other groups (Fig. 2J). Also, ICC analysis revealed an increase in the Mul1 protein level in Mn-treated,

LPS-primed cells (Fig. 2K). Collectively, these data suggest that Mn-induced inflammasome activation in microglia is related to mitochondrial dysfunction and that this mitochondrial dysfunction is through the degradation of Mfn2 by Mul1.

Retromer complex proteins are involved in Mn-induced mitochondrial dysfunction in LPS-primed microglia

Tang *et al*. (*61*) showed that mutating or downregulating the retromer complex protein VPS35 (Park 17) induces mitochondrial dysfunction by increasing Mul1 in dopaminergic neurons. Since we observed that Mn exposure can increase the level of Mul1 in LPS-primed microglia, we further investigated whether this increased Mul1 might be due to VPS35 downregulation. We treated LPS-primed microglial cell line with Mn for 24 h in preparation for qRT-PCR, ICC, and immunoblot analyses. Our qRT-PCR analysis revealed that Mn exposure downregulated VPS35 in LPS-primed microglial cells when compared to other groups (Fig. 3A). Another retromer complex protein, VPS29, was also downregulated in primed microglial cells treated with Mn (Fig. 3B). Further, ICC (Fig. 3C) and Western blot analyses (Fig. 3D) confirmed that VPS35 is downregulated in Mn-exposed, LPS-primed microglial cells. We further validated our cell culture findings in an animal model of Mn toxicity. Animal were similary treated with Mn as described above. Striatal VPS35 mRNA was downregulated in Mn-gavaged mice (Fig. 4E).

To further elucidate the role of VPS35 in maintaining microglial mitochondria, we developed a VPS35 stable knockdown (KD) microglial cell using the CRISPR-Cas9 system (Supplementary Fig. 8). Surprisingly, our Western blot analysis showed

VPS35 KD cells have less Mfn2 (Fig. 3F). Moreover, qRT-PCR revealed that Mul1 mRNA was significantly elevated in the VPS35 KD cells (Fig. 4G). These data collectively suggest that VPS35 is upstream of Mfn2 and the Mul1 pathway and may play a role in maintaining mitochondrial integrity.

Exosomes mediate Mn-induced cell-to-cell transmission of the inflammasome component ASC in LPS-primed microglia

Retromer deficiency can lead to an increase in the amyloid precursor protein (APP) cargo of exosomes in AD (*62*). ASC, the inflammasome adaptor component, has been recently shown to propagate inflammasomes through cell-to-cell transmission (*34*). Hence, we hypothesized that ASC migrates from one cell to another via exosomes and that Mn modulates inflammasome propagation by increasing the exosomal ASC cargo. To verify if exosomal uptake plays a role in inflammasome propagation, we knocked down two endosomal pathways, caveolin and clathrin, responsible for exosomal uptake from microglial cells using the CRISPR-Cas9 system. CRISPR control, caveolin KD, and clathrin KD microglial cells were treated with Mn for 24 h following LPS priming. Interestingly, caveolin KD significantly blocked Mn-stimulated upregulation of pro-IL-1β (Fig. 4A) and NLRP3 (Fig. 4B) mRNA levels in LPS-primed cells while clathrin KD cells no significant difference (data not shown). Both caveolin and clathrin KD cells showed reduced nos2 mRNA levels (Supplementary Fig. 9A). Furthermore, Luminex assay revealed that Mn-exposed, LPS-primed caveolin and clathrin KD cells produced significantly diminished matured IL-1β (Fig. 4C) but not TNF-α (Supplementary Fig. 9B). These data suggest that

blocking exosomal uptake reduces Mn-induced inflammasome propagation. This also indicates that exosomal cargo can be important for inflammasome activation.

To further identify the importance of exosome cargo for inflammasome propagation, exosomes were isolated from treatment media of microglial cells treated with 100 μM Mn for 24 h. Immunoblot analysis showed that Mn exposure induced exosomal release of ASC from LPS-primed microglial cells (Fig. 4D), while LPS and Mn alone had only minimal effect. Furthermore, Mn treatment significantly enhanced the number of exosomes released from primed microglial cells (Fig. 4E) without altering exosome size (Supplementary Fig. 10). ASC KO cell line exposed to Mn also induced an increase in exosome number (Fig. 4E), suggesting that increase in exosome number is independent of inflammasome activation. To further validate the cell-to-cell transmission of ASC, an ASC-CFP overexpression microglial cell line was utilized. ASC-CFP-overexpressing microglial cells were treated with 100 μM Mn for 24 h following LPS-priming, and exosomes were collected from the treatment medium and counted. An equal number of exosomes were used to treat wild-type microglial cells lacking CFP. After 24 h post-treatment, the cells were washed properly and imaged using confocal microscopy. Imaging revealed that cells treated with exosomes from Mn-treated, LPS-primed cells expressed significantly more CFP than the cells treated with exosomes collected from control medium (Fig. 4F). The exosomes used to treat wild-type cells were the only probable source of the CFP signal. Since this CFP was tagged to ASC, the CFP expression in exosome-treated cells confirms that ASC can migrate from cell-to-cell via exosomes and that Mn can upregulate the exosomal ASC content. When we treated LPS-primed microglial cells with exosomes

isolated 24 h post-Mn treatment, qRT-PCR analysis revealed significantly increased mRNA levels of NLRP3 (Fig. 4G) and pro-IL-1β (Fig. 4H) relative to control exosome-treated microglial cells. This increase in NLRP3 and pro-IL-1β level was not seen when wild-type microglial cells were treated with exosomes isolated from Mn-treated, LPS-primed ASC KO cell line (Fig. 4G-H), further validating that exosomal transfer of ASC is involved in propagation of inflammasome. Also, exosomes isolated from serum of Mn-gavaged animals significantly elevated the release of IL-1β when administered to LPS-primed primary microglial cells for 24 and 48 h (Fig. 4I); no significant change in IL-6 or TNF-α release was observed (Supplementary Fig. 11A-B). Collectively, these findings suggest that Mn induces cell-to-cell transmission of ASC through exosomes, further propagating inflammasome activation.

Serum exosomes and serum from welder population have higher load of ASC and higher pro-inflammatory cytokines, respectively, compared to age-matched controls

Welders exposed to Mn have shown a dose-dependent progression of Parkinsonian syndrome (*63*). To demonstrate the human relevance of our findings from cell culture and animal models of Mn exposure, we utilized serum exosomes collected from welders. First, the exosomes were counted and the Western blot was normalized to the number of exosomes isolated from an equal volume of serum. Our Western blot analysis (Fig. 5A) revealed that welders' serum exosomes had significantly more ASC compared to age-matched controls (Fig. 5B). This data further corroborates our *in vitro* and *in vivo* data, suggesting that Mn exposure upregulates exosomal release of ASC.

Finally, we analyzed welder serum for cytokine and chemokine profiling (Fig. 5C-F and Supplementary Fig. 12). Interestingly, we found significant upregulation of the serum pro-inflammatory cytokines TNF-α (Fig. 5C) and IL-17(Fig. 5D), and the chemokines RANTES (Fig. 5E) and MIP1b (Fig. 5F) in welders, compared to age-matched controls. The small amount of IL-1β (Supplementary Fig. 11A) detected in the serum of welders and control subjects may be attributed to the short half-life of IL-1β. The IL-17 response has been shown to be driven by inflammasome-derived IL-1β (*64*). Furthermore, MIP1b is known to be reduced in the $ASC^{-/-}$ mouse (*65*), suggesting the inflammasome plays a role in MIP1b upregulation. Together, these data suggest that exosomal ASC is upregulated in human populations occupationally exposed to Mn. Furthermore, industrial exposure to Mn may lead to systemic inflammation.

Discussion

A diverse variety of signals including ATP (*66*), various crystals (*67, 68*), mitochondrial inhibitors (*32*), and misfolded proteins (*30, 31*) have been shown to induce NLRP3 inflammasome activation. In recent years, inflammasome activation has been linked to various neurodegenerative disorders including PD, AD, and TBI (*29*). In the present study, we show for the first time that the environmental toxicant Mn can induce NLRP3 inflammasome activation in microglial cells *in vitro* and *in vivo.* Furthermore, this inflammasome activation in microglial cells is associated with mitochondrial dysfunction induced by Mfn2 degradation. We also show for the first time that Mn-stimulated exosomes contain the inflammasome component ASC and are involved in propagating the NLRP3 inflammasome. Finally, we demonstrate that

welders exposed to Mn fumes have a higher serum exosomal ASC load and more pro-inflammatory cytokines compared to age-matched controls.

The link between Mn and neurodegenerative and neuroimmune processes is becoming clearer. Chronic Mn exposure has been shown to reduce TH-positive neurons in the substantia nigra (SN) region (*69*). Furthermore, Mn induces microglial activation in the SNpc region in a primate model (*70*), while another recent study showed that microglial exposure to Mn modulates astroglial inflammation (*46*). Mn exposure also induces the pro-inflammatory cytokine profile in glial cells (*71-73*) and modulates the NFκB pro-inflammatory signaling pathway and p-38 MAPK pathway in glial cells (*45, 72*). However, the mechanism underlying sustained and chronic inflammation in Mn-induced neurotoxicity is not well understood. The inflammasome's role in modulating inflammatory responses in various disease models and in developing new therapeutics has been gaining importance in recent years (*47*). Exposure to silica and asbestos induces NLRP3 inflammasome activation in various cell types including lymphocytes and macrophages, among others (*68*). Furthermore, NLRP3 inflammasome activation has been linked to Parkinsonian syndrome (*31, 74*). Here, using cell culture and animal models of Mn toxicity, we show that Mn exposure can activate the NLRP3 inflammasome specifically in microglial cells.

Though a variety of stimuli has been shown to act as signal 2 in activating the NLRP3 inflammasome cascade, the exact mechanism underlying its assembly is not well understood. Various factors, including mitochondrial dysfunction (*32*), mitochondrial superoxide generation (*33*), and lysosomal dysfunction (*75*), have been implicated as mechanisms underlying NLRP3 inflammasome assembly. A recent

study by our group has further elucidated that mitochondrial superoxide generation plays an important role in NLRP3 inflammasome activation (*76*). Mn exposure causes mitochondrial dysfunction by accumulating in mitochondria (*9, 42, 57, 77*) in neurons and astrocytes. In this study, we show that Mn exposure leads to mitochondrial dysfunction and mitochondrial superoxide generation in microglial cells. Mfn2 plays an important role in mitochondrial fusion and is one of the targets of the PD-associated gene *PARKIN* (*78, 79*). Mfn2 overexpression and downregulation has been linked to the modulation of mitochondrial dynamics (*60, 61, 80*). Furthermore, Mfn2 has been shown to play a role in Mn-induced neurotoxicity in neuronal cells (*81*). In this study, we demonstrate that Mn exposure leads to Mfn2 downregulation in microglial cells and is accompanied by mitochondrial dysfunction and inflammasome activation.

Most studies with VPS35 have focused on neurons, while largely ignoring the role of this retromer complex protein in microglia. Recent studies have shown that VPS35 mutation or downregulation can induce mitochondrial dysfunction either by modulating Mfn2 degradation in dopaminergic neurons (*61*) or by recycling the dynamin-like protein 1 (DLP1) complex (*82*). Here we show that Mn exposure downregulates VPS35 in LPS-primed microglial cells and that VPS35 modulates Mfn2 degradation through Mul1. The exact mechanism of Mn-induced VPS35 downregulation is not clear. Previous studies reported that VPS29, another retromer complex protein, contain Mn binding sites, and that VPS35 wraps around these metal binding sites (*83, 84*). Thus Mn-induced downregulation of retromer complex proteins may be due to excessive binding of Mn to these metal binding sites, but more studies are required to confirm the exact mechanism. Still others have shown VPS35, part of

the retromer protein complex, modulates the cellular biogenesis and release of exosomes (*85, 86*). Retromer pathway dysfunction has been shown to promote amyloid precursor protein processing (*62*). Exosomes, which were presumed to be the “garbage bag” of cells, have gained importance in recent years due to their role in the progression of neurodegenerative disorders including AD and PD. Exosomes are now known to export aggregated α-Syn to other cells (*87, 88*), thereby acting as messengers. Intercellular communication via exosome cargo can also modulate neuroinflammation (*89*). NLRP3 inflammasome propagation has become an active area of research. A novel pyroptotic-phagocytic cascade has been shown to spread ASC and the NLRP3 inflammasome assembly between cells, in a “prionoid” fashion, thus propagating the inflammasome (*34*). In this study, we demonstrate for the first time that ASC can communicate cell-to-cell via exosomes. Mn exposure induced the exosomal release of ASC from LPS-primed microglial cells, whereas blocking exosomal uptake reduced IL-1β release indicating a reduction in inflammasome activation (Fig 4).

First reports of occupational exposure to Mn date back to 1837 (*90*). Due to their exposure to welding-derived nanoparticles, Swedish welders have an increased inflammatory profile (*91*). In this study, we have shown a probable mechanism for inflammation stemming from occupational exposure to Mn. Though we were not able to detect significant amounts of IL-1β in welder serum, we do show an increased ASC load in welder serum exosomes. The lack of elevated IL-1β may be attributed to its short half-life (Fig. 5).

Collectively, our study demonstrates for the first time that Mn exposure leads to NLRP3 inflammasome activation in microglial cells, thereby leading to inflammation. This inflammasome activation is accompanied by mitochondrial dysfunction that is manifested by Mfn2 degradation by Mul1. VPS35 is an upstream regulator of Mfn2 ubiquitination that is downregulated by Mn exposure. We further demonstrate for the first time that exosomes play an important role in Mn-induced NLRP3 inflammasome propagation. In this study, we show that ASC can migrate from cell-to-cell via exosomes. This finding may have broad implications for the field of immunology as exosomes can cross the blood-brain-barrier and can communicate to various organs. Our novel findings may provide some insight into the mechanism of communication between peripheral inflammation and CNS inflammation in neurodegenerative disorders, including AD and Parkinsonian syndrome. Future studies should explore the role of exosomal biogenesis during inflammation in different disease models. Overall, our novel findings suggest a probable mechanism underlying Mn-induced Parkinsonism.

Materials and Methods

Cell culture, Primary culture and Treatments

Primary microglial cells were isolated using a magnetic bead separation technique described in our previous publications (*92, 93*). Primary microglial cells were cultured in DMEM-F12, 10% FBS, 1% sodium pyruvate, 1% glutamine, 1% penicillin-streptavidin, and 1% non-essential amino acids. The wild-type microglial cell line and ASC-CFP microglial cell line were kind donations from Dr. D.T. Golenbock

(University of Massachusetts Medical School, Worcester, MA). ASC KO macrophage cell line were kind donations from Dr. K. Fitzgerald (University of Massachusetts). The wild-type microglial cell line was characterized by Halle et al. (*30*) and cultured in DMEM medium, 10% FBS, 1% glutamine, and 1% penicillin-streptavidin. Treatments were done in 2% FBS-containing medium. For LPS-priming treatments, cells were treated with LPS (100 ng/mL) for 3 h. Next, the cells were triple-washed with full serum medium to remove any excess LPS, and then treated with 100 μM Mn for 6-24 h.

CRISPR-Cas9 knockdown (KD) cell generation

CRSPR guide RNA was obtained for VPS35, clathrin, and caveolin from Sigma and transfected using protocols from our previous publications (*12, 23*). Following transfection, cells were incubated for 48 h before treatment. The lentivirus-based CRISPR/Cas9 KO plasmid against gene Vps35, with target site CAAGTCATTTCCTCAATCCAGG, in a U6gRNA-Cas9-2A-RFP vector, was purchased from Sigma-Aldrich. The lentivirus-based CRISPR/Cas9 plasmids, pLV-U6g-EPCG-Cav1 and pLV-U6g-EPCG-Cltc with the Caveolin-1 and Clathrin gRNA target sequences GTTGAGATGCTTGGGGTCGCGG and TACTGAAGCCAATGTTTGCTGG, respectively, were purchased from Sigma-Aldrich. To make the lentivirus, the lenti-CRISPR/Cas9 Vps35 KO plasmid and nontarget control plasmid were transfected into 293FT cells using the Mission Lentiviral Packaging Mix from Sigma-Aldrich according to manufacturer's instructions. The lentivirus was harvested 48 h post-transfection and added to the microglial cell line at an MOI of 100 to knockdown VPS35, Caveolin-1, and Clathrin expression.

Animal study

Eight-week-old male C57BL/6Ncrl mice, obtained from Charles River, were housed under standard conditions of constant temperature (22 ± 1°C), humidity (relative, 30%), and a 12 h light/dark cycle. After acclimating for 3 days, mice were gavaged with 15 mg/kg body weight Mn for 30 days, and then sacrificed. This Mn dose regimen was chosen based on previous studies in humans and animals (*94-96*). Use of the animals and protocol procedures were approved by the Institutional Animal Care and Use Committee (IACUC) at Iowa State University (Ames, IA, USA).

Western blot

Western Blot analyses were performed following our previous publications (*12, 97*). Briefly, cells or tissues were lysed using modified RIPA buffer. Proteins were normalized using Bradford assay before loading on SDS-acrylamide gels. For separation of proteins, 20-40 µg of protein was loaded in each well of 10-15% acrylamide gels. Acrylamide gels were run at 110 V for 2 h at 4°C. Following separation, proteins were transferred on a nitrocellulose membrane at 27 V for 18 h at 4°C. After transfer, the membranes were blocked with Li-COR blocking buffer for 45 mins and incubated in primary antibodies following manufacturer's protocol. Following primary antibody incubation, membranes were washed with PBS-TWEEN 20 (0.05%) for 1 h and incubated in Li-COR IR secondary antibodies for 1 h at room temperature, washed with PBS-TWEEN for 1 h, and imaged using an Odyssey scanner. The primary antibodies used are as follows: anti-caspase-1 (Adipogen, 1:1000) (AB_2490248), anti-NLRP3 (Adipogen, 1:1000), anti-iNOS (SantaCruz, 1:1000), anti-IL-1β (R&D systems, 1:500), anti-Mfn2 (Cell Signaling, 1:1000), anti-VPS35 (Santa Cruz, 1:500), and anti-ASC (Adipogen, 1:1000) (AB_2490440). The

secondary antibodies used are as follows: IR-800 conjugated goat anti-mouse IgG (Li-COR, 1:20000) and IR-700 conjugated goat anti-rabbit IgG (Li-COR 1:20000). For loading control, β-actin (Sigma, 1:10000) antibody was used.

qRT-PCR

RNA was isolated from tissues and cells according to a previous publication (*98*). In short, cells or tissues were lysed in 1 mL of TRIzol reagent and incubated for 5 min. After incubation, 0.2 mL of chloroform was added to each tube, incubated for 2 min and centrifuged at 12,000 g for 15 min at 4°C. After centrifugation, the top clear layer containing RNA was transferred to a fresh tube containing 0.7 mL of isopropanol, incubated for 15 min and centrifuged at 12,000 g for 10 min at 4°C to precipitate the RNA. After precipitation, the supernatant was discarded, the pellet was washed with 75% ethanol, air-dried, and dissolved in water. A NanoDrop was used to quantify the RNA and 1 µg of RNA was utilized for converting into cDNA. For cDNA synthesis, the high capacity cDNA synthesis kit from Applied Biosystems (Cat#4368814) was used according to manufacturer's protocol. Quantitative SYBR green PCR assay was performed using qRT^{2}PCR SYBR Green Mastermix (Agilent) and pre-validated primers. The following validated primers from Qiagen were used: *pro-IL-1β* (QT01048355), *NLRP3* (QT00122458), *NLRC4* (QT00264670), *AIM2* (QT00266819), *Nos2* (QT00100275), *Mfn2* (QT00134295), *Mul1* (QT00132734), *SLC30A10* (QT01199009), S*LC11A2* (QT01047368), *VPS35* (QT00160258), *VPS29* (QT00137228), and *18S* (QT02448075). The fold change in gene level was

determined by $\Delta\Delta C_t$ method where C_t is the threshold value. 18S was used as the housekeeping gene.

Immunohistochemistry and Immunocytochemistry

Immunohistochemistry (IHC) was performed on striatal sections as described in our previous publications (*20, 22*). Striatal sections (30 µm) were used for IHC. Citrate buffer was used to perform antigen retrieval (10 mM sodium citrate, pH 8.5). Following antigen retrieval, sections were washed with PBS, blocked with blocking buffer (2% BSA, 0.5% Triton 100X, and 0.05% TWEEN 20), and incubated in primary antibodies overnight at 4°C. Next, sections were washed with PBS, incubated in secondary antibodies for 1 h and stained with the nuclear dye Hoechst. Finally, sections were mounted on pre-coated slides and dried overnight before visualizing them under microscope. Confocal imaging was performed on these sections at the Iowa State University Microscopy Facility using a Leica DMEIR2 confocal microscope with 63X oil objective. For z-stacking, each section consisted of 10-15, 0.5-µm slices.

For immunocytochemical (ICC) studies on microglial cells and microglial primary culture, 4% paraformaldehyde (PFA) was used to fix the cells. Next, fixed cells were washed with PBS, blocked using blocking buffer, and incubated in primary antibodies following manufacturer's protocol. Following primary antibody incubation, cells were washed with PBS, incubated in secondary antibody and mounted on slides using Fluoromount aqueous mounting medium (Sigma). Samples were visualized using an inverted fluorescence microscope (Nikon TE-2000U). The following primary antibodies were used: IBA1 (Wako, 1:1000) (AB_2314667), IBA1 (Abcam, 1:500) (AB_870576), Mul1 (Abcam, 1:500) (AB_1860863), NLRP3 (Adipogen, 1:500)

(AB_2490202), ASC (Adipogen, 1:500), Nos2 (Santa Cruz, 1:500) (AB_2152867), VPS35 (Santa Cruz, 1:500) (AB_2215220), and Mfn2 (Cell Signaling, 1:500). Alexa dye-conjugated secondary antibodies were used for ICC and IHC experiments.

Multiplex cytokine assay

Multiple cytokine assay was performed according to our previous publication (*12*). Briefly, 40 µL of treatment media was incubated overnight with 40 µL of primary antibodies conjugated with magnetic beads. Following incubation with primary antibodies, samples were washed, incubated with a biotinylated antibody and biotin/streptavidin, and then read in a Bio-Plex plate reader. Standards were obtained from PeproTech.

For welder serum cytokine analysis, Bio-Plex Pro Human Cytokine 27-plex Assay (M500KCAF0Y, Bio-Rad) was performed according to manufacturer's protocol.

MTS mitochondrial activity assay

Cells were plated in 96-well tissue plates. Following treatment, 10 µL of MTS reagent (Promega) was added and incubated at 37°C for 1.5 h. After incubation, a plate reader was used to quantify the absorbance at 490 nm.

Griess assay

Griess assay was performed as previously described in our publication (*12*). 50,000-100,000k microglial cells were plated in 96-well plates and treated in 2% FBS containing medium. After treatment, 50 µL of medium was collected, and incubated with 50 µL of Griess reagent for 10 min. A plate reader was used to read the absorbance at 540 nm. Sodium nitrite solution was used for making standard curve.

Exosome isolation

Wild type microglial cell line-produced exosomes were isolated by filtering the cell-culture supernatant through 0.22-µm filters, followed by high-speed ultracentrifugation. Briefly, cells were grown in T-175 cell culture flasks and treated with 100 µM Mn. For each exosome sample, conditioned media from two T175 flasks were pooled with an original seeding density of $8x10^6$ cells per flask. Post treatment, the media was collected and centrifuged at 300 x g for 10 min, and 10,000 x g for 15 min successively to get rid of any cell debris before passing it through a 0.22-µm syringe filter. The filtrate was then centrifuged at 100,000 x g for 90 min using a Beckman Optima L-100 XP ultracentrifuge. The pellet containing exosomes was washed once with cold PBS and centrifuged again at 100,000 x g for 90 min using a Beckman optima MAX ultracentrifuge.

Inductively coupled plasma mass spectroscopy (ICP-MS)

Microglial cell line samples were carefully scraped and counted prior to sample preparation. Samples were analyzed for different metals including, Cd, Ca, Cr, Co, Cu, Fe, Mg, Mn, Mo, P, K, Se, Na, and Zn using ICP-MS (Analytik Jena Inc. Woburn, MA, USA) in CRI mode with hydrogen as the skimmer gas. Standards for elemental analyses were obtained from Inorganic Ventures (Christiansburg, VA) while digestion vessels; trace mineral grade nitric acid and hydrochloric acid were obtained from Fisher Scientific (Pittsburgh, PA). Briefly, samples were digested in 70 % nitric acid at 60˚C for ≥12 hours. Pre-weighed samples were transferred to 15mL tubes and 0.25 mL of 70% nitric acid was added. All samples were digested overnight at 60˚C. After

digestion, all samples were diluted to 5 mL using 1% nitric acid with 0.5% hydrochloric acid and then analyzed by ICP-MS. For quality control, Bi, Sc, In, Li, Y, and Tb were used as internal standards for the ICP-MS.

NanoSight

Ultracentrifuged exosome samples were used for nanoparticle tracking analysis (NTA), as previously described (*99*). Briefly, isolated exosomes were resuspended in 500-1000 µL of PBS, from which approximately 300 µL was loaded into the sample chamber of an LM10 unit (NanoSight, Amesbury, UK) using a disposable syringe. Sample durations of 30-60 sec per sample were analyzed with NTA 2.3 software (NanoSight). Samples containing higher numbers of exosomes were diluted before the analysis and their relative concentrations were then calculated according to the dilution factor.

Mitochondrial dynamics analysis

A Seahorse XFe24 Analyzer was used to measure mitochondrial oxygen consumption rates (OCR) and extracellular acidification rates (ECAR) using the Mito-Stress test following a previously published protocol (*100*). Primary mouse microglia were plated 90,000 cells/well of a 24-well, Seahorse plate. All treatments were done in serum-free medium. For the Mito-Stress test, 0.75 µM oligomycin, 1 µM FCCP, and 0.5 µM rotenone/antimycin were used. The Seahorse's Mito-Stress report generator and cell phenotype report generator were used for analysis.

Statistical analysis

GraphPad 5.0 was used for statistical analysis with $p \leq 0.05$ considered statistically significant. One-way ANOVA was used for comparing multiple groups with

Tukey post analysis unless otherwise mentioned. For comparing 2 groups, Student's t-test was used. "n" represents number of biological replicates unless other mentioned.

Conflict of interest

A.G.K. and V.A. are shareholders of PK Biosciences Corporation (Ames, IA) and Kinome Biosciences (Bangalore, India), which are interested in identifying novel biomarkers and potential therapeutic targets for PD and metal-induced neurotoxicity.

Acknowledgements

This work was supported by National Institutes of Health (NIH) grants ES026892 and NS088206. The authors acknowledge Gary Zenitsky for his assistance in editing this manuscript.

Author Contributions

S.S., A.K., and A.G.K. designed research; S.S., DR., E.M., J.L., D.H., J.R.K., performed research; S.S., A.G.K analyzed data; S.S., H.J., V.A., and A.G.K. wrote the paper.

Reference

1. S. A. Bellingham, B. Guo, A. F. Hill, The secret life of extracellular vesicles in metal homeostasis and neurodegeneration. *Biol Cell* **107**, 389-418 (2015).
2. K. J. Barnham, C. L. Masters, A. I. Bush, Neurodegenerative diseases and oxidative stress. *Nat Rev Drug Discov* **3**, 205-214 (2004).
3. J. Rodier, Manganese poisoning in Moroccan miners. *Br J Ind Med* **12**, 21-35 (1955).
4. F. S. Archibald, C. Tyree, Manganese poisoning and the attack of trivalent manganese upon catecholamines. *Arch Biochem Biophys* **256**, 638-650 (1987).
5. A. H. Sadek, R. Rauch, P. E. Schulz, Parkinsonism due to manganism in a welder. *Int J Toxicol* **22**, 393-401 (2003).
6. C. M. Fored, J. P. Fryzek, L. Brandt, G. Nise, B. Sjogren, J. K. McLaughlin, W. J. Blot, A. Ekbom, Parkinson's disease and other basal ganglia or movement disorders in a large nationwide cohort of Swedish welders. *Occup Environ Med* **63**, 135-140 (2006).
7. G. Kenangil, S. Ertan, I. Sayilir, S. Ozekmekci, Progressive motor syndrome in a welder with pallidal T1 hyperintensity on MRI: A two-year follow-up. *Mov Disord* **21**, 2197-2200 (2006).
8. R. M. Bowler, W. Koller, P. E. Schulz, Parkinsonism due to manganism in a welder: neurological and neuropsychological sequelae. *Neurotoxicology* **27**, 327-332 (2006).

9. D. Milatovic, Z. Yin, R. C. Gupta, M. Sidoryk, J. Albrecht, J. L. Aschner, M. Aschner, Manganese induces oxidative impairment in cultured rat astrocytes. *Toxicol Sci* **98**, 198-205 (2007).

10. L. Qin, X. Wu, M. L. Block, Y. Liu, G. R. Breese, J. S. Hong, D. J. Knapp, F. T. Crews, Systemic LPS causes chronic neuroinflammation and progressive neurodegeneration. *Glia* **55**, 453-462 (2007).

11. P. S. Whitton, Inflammation as a causative factor in the aetiology of Parkinson's disease. *Br J Pharmacol* **150**, 963-976 (2007).

12. N. Panicker, H. Saminathan, H. Jin, M. Neal, D. S. Harischandra, R. Gordon, K. Kanthasamy, V. Lawana, S. Sarkar, J. Luo, V. Anantharam, A. G. Kanthasamy, A. Kanthasamy, Fyn Kinase Regulates Microglial Neuroinflammatory Responses in Cell Culture and Animal Models of Parkinson's Disease. *J Neurosci* **35**, 10058-10077 (2015).

13. M. L. Block, L. Zecca, J. S. Hong, Microglia-mediated neurotoxicity: uncovering the molecular mechanisms. *Nat Rev Neurosci* **8**, 57-69 (2007).

14. M. G. Tansey, M. S. Goldberg, Neuroinflammation in Parkinson's disease: its role in neuronal death and implications for therapeutic intervention. *Neurobiology of disease* **37**, 510-518 (2010).

15. K. Gammon, Inflammation: A complex problem. *Nature* **502**, S86-87 (2013).

16. P. L. McGeer, S. Itagaki, B. E. Boyes, E. G. McGeer, Reactive microglia are positive for HLA-DR in the substantia nigra of Parkinson's and Alzheimer's disease brains. *Neurology* **38**, 1285-1291 (1988).

17. T. Nagatsu, M. Mogi, H. Ichinose, A. Togari, Cytokines in Parkinson's disease. *J Neural Transm Suppl*, 143-151 (2000).

18. C. K. Glass, K. Saijo, B. Winner, M. C. Marchetto, F. H. Gage, Mechanisms underlying inflammation in neurodegeneration. *Cell* **140**, 918-934 (2010).

19. D. C. Wu, V. Jackson-Lewis, M. Vila, K. Tieu, P. Teismann, C. Vadseth, D. K. Choi, H. Ischiropoulos, S. Przedborski, Blockade of microglial activation is neuroprotective in the 1-methyl-4-phenyl-1,2,3,6-tetrahydropyridine mouse model of Parkinson disease. *J Neurosci* **22**, 1763-1771 (2002).

20. A. Ghosh, M. R. Langley, D. S. Harischandra, M. L. Neal, H. Jin, V. Anantharam, J. Joseph, T. Brenza, B. Narasimhan, A. Kanthasamy, B. Kalyanaraman, A. G. Kanthasamy, Mitoapocynin Treatment Protects Against Neuroinflammation and Dopaminergic Neurodegeneration in a Preclinical Animal Model of Parkinson's Disease. *J Neuroimmune Pharmacol* **11**, 259-278 (2016).

21. A. Ghosh, T. Tyson, S. George, E. N. Hildebrandt, J. A. Steiner, Z. Madaj, E. Schulz, E. Machiela, W. G. McDonald, M. L. Escobar Galvis, J. H. Kordower, J. M. Van Raamsdonk, J. R. Colca, P. Brundin, Mitochondrial pyruvate carrier regulates autophagy, inflammation, and neurodegeneration in experimental models of Parkinson's disease. *Sci Transl Med* **8**, 368ra174 (2016).

22. A. Ghosh, A. Kanthasamy, J. Joseph, V. Anantharam, P. Srivastava, B. P. Dranka, B. Kalyanaraman, A. G. Kanthasamy, Anti-inflammatory and neuroprotective effects of an orally active apocynin derivative in pre-clinical models of Parkinson's disease. *J Neuroinflammation* **9**, 241 (2012).

23. R. Gordon, M. L. Neal, J. Luo, M. R. Langley, D. S. Harischandra, N. Panicker, A. Charli, H. Jin, V. Anantharam, T. M. Woodruff, Q. Y. Zhou, A. G. Kanthasamy, A. Kanthasamy, Prokineticin-2 upregulation during neuronal injury mediates a compensatory protective response against dopaminergic neuronal degeneration. *Nat Commun* **7**, 12932 (2016).

24. D. Milatovic, R. C. Gupta, Y. Yu, S. Zaja-Milatovic, M. Aschner, Protective effects of antioxidants and anti-inflammatory agents against manganese-induced oxidative damage and neuronal injury. *Toxicol Appl Pharmacol* **256**, 219-226 (2011).

25. M. T. Herrero, C. Estrada, L. Maatouk, S. Vyas, Inflammation in Parkinson's disease: role of glucocorticoids. *Front Neuroanat* **9**, 32 (2015).

26. K. M. Danzer, L. R. Kranich, W. P. Ruf, O. Cagsal-Getkin, A. R. Winslow, L. Zhu, C. R. Vanderburg, P. J. McLean, Exosomal cell-to-cell transmission of alpha synuclein oligomers. *Mol Neurodegener* **7**, 42 (2012).

27. L. Alvarez-Erviti, Y. Seow, A. H. Schapira, C. Gardiner, I. L. Sargent, M. J. Wood, J. M. Cooper, Lysosomal dysfunction increases exosome-mediated alpha-synuclein release and transmission. *Neurobiol Dis* **42**, 360-367 (2011).

28. X. Li, S. Wang, R. Zhu, H. Li, Q. Han, R. C. Zhao, Lung tumor exosomes induce a pro-inflammatory phenotype in mesenchymal stem cells via NFkappaB-TLR signaling pathway. *J Hematol Oncol* **9**, 42 (2016).

29. L. C. Freeman, J. P. Ting, The pathogenic role of the inflammasome in neurodegenerative diseases. *J Neurochem*, (2015).

30. A. Halle, V. Hornung, G. C. Petzold, C. R. Stewart, B. G. Monks, T. Reinheckel, K. A. Fitzgerald, E. Latz, K. J. Moore, D. T. Golenbock, The NALP3 inflammasome is involved in the innate immune response to amyloid-beta. *Nat Immunol* **9**, 857-865 (2008).

31. G. Codolo, N. Plotegher, T. Pozzobon, M. Brucale, I. Tessari, L. Bubacco, M. de Bernard, Triggering of inflammasome by aggregated alpha-synuclein, an inflammatory response in synucleinopathies. *PLoS One* **8**, e55375 (2013).

32. R. Zhou, A. S. Yazdi, P. Menu, J. Tschopp, A role for mitochondria in NLRP3 inflammasome activation. *Nature* **469**, 221-225 (2011).

33. S. Alfonso-Loeches, J. R. Urena-Peralta, M. J. Morillo-Bargues, J. Oliver-De La Cruz, C. Guerri, Role of mitochondria ROS generation in ethanol-induced NLRP3 inflammasome activation and cell death in astroglial cells. *Front Cell Neurosci* **8**, 216 (2014).

34. B. S. Franklin, L. Bossaller, D. De Nardo, J. M. Ratter, A. Stutz, G. Engels, C. Brenker, M. Nordhoff, S. R. Mirandola, A. Al-Amoudi, M. S. Mangan, S. Zimmer, B. G. Monks, M. Fricke, R. E. Schmidt, T. Espevik, B. Jones, A. G. Jarnicki, P. M. Hansbro, P. Busto, A. Marshak-Rothstein, S. Hornemann, A. Aguzzi, W. Kastenmuller, E. Latz, The adaptor ASC has extracellular and 'prionoid' activities that propagate inflammation. *Nat Immunol* **15**, 727-737 (2014).

35. M. Sidoryk-Wegrzynowicz, E. Lee, J. Albrecht, M. Aschner, Manganese disrupts astrocyte glutamine transporter expression and function. *J Neurochem* **110**, 822-830 (2009).

36. A. S. Hazell, P. Desjardins, R. F. Butterworth, Chronic exposure of rat primary astrocyte cultures to manganese results in increased binding sites for the 'peripheral-type' benzodiazepine receptor ligand 3H-PK 11195. *Neurosci Lett* **271**, 5-8 (1999).

37. C. A. Dodd, N. M. Filipov, Manganese potentiates LPS-induced heme-oxygenase 1 in microglia but not dopaminergic cells: role in controlling microglial hydrogen peroxide and inflammatory cytokine output. *Neurotoxicology* **32**, 683-692 (2011).

38. N. M. Filipov, R. F. Seegal, D. A. Lawrence, Manganese potentiates in vitro production of proinflammatory cytokines and nitric oxide by microglia through a nuclear factor kappa B-dependent mechanism. *Toxicol Sci* **84**, 139-148 (2005).

39. S. Sarkar, E. Malovic, D. S. Harischandra, H. A. Ngwa, A. Ghosh, C. Hogan, D. Rokad, G. Zenitsky, H. Jin, V. Anantharam, A. G. Kanthasamy, A. Kanthasamy, Manganese exposure induces neuroinflammation by impairing mitochondrial dynamics in astrocytes. *Neurotoxicology*, (2017).

40. J. A. Moreno, K. A. Sullivan, D. L. Carbone, W. H. Hanneman, R. B. Tjalkens, Manganese potentiates nuclear factor-kappaB-dependent expression of nitric oxide synthase 2 in astrocytes by activating soluble guanylate cyclase and extracellular responsive kinase signaling pathways. *J Neurosci Res* **86**, 2028-2038 (2008).

41. J. A. Moreno, K. M. Streifel, K. A. Sullivan, M. E. Legare, R. B. Tjalkens, Developmental exposure to manganese increases adult susceptibility to

inflammatory activation of glia and neuronal protein nitration. *Toxicol Sci* **112**, 405-415 (2009).

42. Z. Yin, J. L. Aschner, A. P. dos Santos, M. Aschner, Mitochondrial-dependent manganese neurotoxicity in rat primary astrocyte cultures. *Brain Res* **1203**, 1-11 (2008).

43. F. Zhao, T. Cai, M. Liu, G. Zheng, W. Luo, J. Chen, Manganese induces dopaminergic neurodegeneration via microglial activation in a rat model of manganism. *Toxicol Sci* **107**, 156-164 (2009).

44. J. Y. Chang, L. Z. Liu, Manganese potentiates nitric oxide production by microglia. *Brain Res Mol Brain Res* **68**, 22-28 (1999).

45. N. M. Filipov, R. F. Seegal, D. A. Lawrence, Manganese potentiates in vitro production of proinflammatory cytokines and nitric oxide by microglia through a nuclear factor kappa B-dependent mechanism. *Toxicol. Sci. Oxford University Press* **84**, (2005).

46. K. S. Kirkley, K. A. Popichak, M. F. Afzali, M. E. Legare, R. B. Tjalkens, Microglia amplify inflammatory activation of astrocytes in manganese neurotoxicity. *Journal of Neuroinflammation* **14**, 99 (2017).

47. H. Guo, J. B. Callaway, J. P. Ting, Inflammasomes: mechanism of action, role in disease, and therapeutics. *Nat Med* **21**, 677-687 (2015).

48. F. D. Dick, G. De Palma, A. Ahmadi, A. Osborne, N. W. Scott, G. J. Prescott, J. Bennett, S. Semple, S. Dick, P. Mozzoni, N. Haites, S. B. Wettinger, A. Mutti, M. Otelea, A. Seaton, P. Soderkvist, A. Felice, G. Geoparkinson Study, Gene-

environment interactions in parkinsonism and Parkinson's disease: the Geoparkinson study. *Occup Environ Med* **64**, 673-680 (2007).

49. A. A. Aboud, A. M. Tidball, K. K. Kumar, M. D. Neely, K. C. Ess, K. M. Erikson, A. B. Bowman, Genetic risk for Parkinson's disease correlates with alterations in neuronal manganese sensitivity between two human subjects. *Neurotoxicology* **33**, 1443-1449 (2012).

50. Y. H. Chuang, C. M. Lill, P. C. Lee, J. Hansen, C. F. Lassen, L. Bertram, N. Greene, J. S. Sinsheimer, B. Ritz, Gene-Environment Interaction in Parkinson's Disease: Coffee, ADORA2A, and CYP1A2. *Neuroepidemiology* **47**, 192-200 (2016).

51. E. A. Bordt, B. M. Polster, NADPH oxidase- and mitochondria-derived reactive oxygen species in proinflammatory microglial activation: a bipartisan affair? *Free Radic Biol Med* **76**, 34-46 (2014).

52. M. E. Heid, P. A. Keyel, C. Kamga, S. Shiva, S. C. Watkins, R. D. Salter, Mitochondrial reactive oxygen species induces NLRP3-dependent lysosomal damage and inflammasome activation. *J Immunol* **191**, 5230-5238 (2013).

53. M. J. Lopez-Armada, R. R. Riveiro-Naveira, C. Vaamonde-Garcia, M. N. Valcarcel-Ares, Mitochondrial dysfunction and the inflammatory response. *Mitochondrion* **13**, 106-118 (2013).

54. P. Ayotte, G. L. Plaa, Hepatic subcellular distribution of manganese in manganese and manganese-bilirubin induced cholestasis. *Biochem Pharmacol* **34**, 3857-3865 (1985).

55. J. C. Lai, M. J. Minski, A. W. Chan, T. K. Leung, L. Lim, Manganese mineral interactions in brain. *Neurotoxicology* **20**, 433-444 (1999).

56. J. J. Liccione, M. D. Maines, Selective vulnerability of glutathione metabolism and cellular defense mechanisms in rat striatum to manganese. *J Pharmacol Exp Ther* **247**, 156-161 (1988).

57. J. A. Roth, C. Horbinski, D. Higgins, P. Lein, M. D. Garrick, Mechanisms of manganese-induced rat pheochromocytoma (PC12) cell death and cell differentiation. *Neurotoxicology* **23**, 147-157 (2002).

58. W. Wang, F. Zhang, L. Li, F. Tang, S. L. Siedlak, H. Fujioka, Y. Liu, B. Su, Y. Pi, X. Wang, MFN2 couples glutamate excitotoxicity and mitochondrial dysfunction in motor neurons. *J Biol Chem* **290**, 168-182 (2015).

59. A. Martorell-Riera, M. Segarra-Mondejar, J. P. Munoz, V. Ginet, J. Olloquequi, J. Perez-Clausell, M. Palacin, M. Reina, J. Puyal, A. Zorzano, F. X. Soriano, Mfn2 downregulation in excitotoxicity causes mitochondrial dysfunction and delayed neuronal death. *EMBO J* **33**, 2388-2407 (2014).

60. N. Zhao, Y. Zhang, Q. Liu, W. Xiang, Mfn2 Affects Embryo Development via Mitochondrial Dysfunction and Apoptosis. *PLoS One* **10**, e0125680 (2015).

61. F. L. Tang, W. Liu, J. X. Hu, J. R. Erion, J. Ye, L. Mei, W. C. Xiong, VPS35 Deficiency or Mutation Causes Dopaminergic Neuronal Loss by Impairing Mitochondrial Fusion and Function. *Cell Rep* **12**, 1631-1643 (2015).

62. C. P. Sullivan, A. G. Jay, E. C. Stack, M. Pakaluk, E. Wadlinger, R. E. Fine, J. M. Wells, P. J. Morin, Retromer disruption promotes amyloidogenic APP processing. *Neurobiol Dis* **43**, 338-345 (2011).

63. B. A. Racette, S. Searles Nielsen, S. R. Criswell, L. Sheppard, N. Seixas, M. N. Warden, H. Checkoway, Dose-dependent progression of parkinsonism in manganese-exposed welders. *Neurology* **88**, 344-351 (2017).

64. K. H. Mills, L. S. Dungan, S. A. Jones, J. Harris, The role of inflammasome-derived IL-1 in driving IL-17 responses. *J Leukoc Biol* **93**, 489-497 (2013).

65. B. R. Barker, D. J. Taxman, J. P. Ting, Cross-regulation between the IL-1beta/IL-18 processing inflammasome and other inflammatory cytokines. *Curr Opin Immunol* **23**, 591-597 (2011).

66. E. K. Jo, J. K. Kim, D. M. Shin, C. Sasakawa, Molecular mechanisms regulating NLRP3 inflammasome activation. *Cell Mol Immunol* **13**, 148-159 (2016).

67. F. Martinon, V. Petrilli, A. Mayor, A. Tardivel, J. Tschopp, Gout-associated uric acid crystals activate the NALP3 inflammasome. *Nature* **440**, 237-241 (2006).

68. C. Dostert, V. Petrilli, R. Van Bruggen, C. Steele, B. T. Mossman, J. Tschopp, Innate immune activation through Nalp3 inflammasome sensing of asbestos and silica. *Science* **320**, 674-677 (2008).

69. J. L. Ordonez-Librado, V. Anaya-Martinez, A. L. Gutierrez-Valdez, L. Colin-Barenque, E. Montiel-Flores, M. R. Avila-Costa, Manganese inhalation as a Parkinson disease model. *Parkinsons Dis* **2011**, 612989 (2010).

70. T. Verina, S. F. Kiihl, J. S. Schneider, T. R. Guilarte, Manganese exposure induces microglia activation and dystrophy in the substantia nigra of non-human primates. *NeuroToxicology.* **32**, (2011).

71. C. J. Chen, Y. C. Ou, S. Y. Lin, S. L. Liao, S. Y. Chen, J. H. Chen, Manganese modulates pro-inflammatory gene expression in activated glia. *Neurochem Int* **49**, 62-71 (2006).

72. P. L. Crittenden, N. M. Filipov, Manganese-induced potentiation of in vitro proinflammatory cytokine production by activated microglial cells is associated with persistent activation of p38 MAPK. *Toxicology in Vitro.* **22**, (2008).

73. N. M. Filipov, C. A. Dodd, Role of glial cells in manganese neurotoxicity. *J. Appl. Toxicol.* **32**, (2011).

74. Z. Mao, C. Liu, S. Ji, Q. Yang, H. Ye, H. Han, Z. Xue, The NLRP3 Inflammasome is Involved in the Pathogenesis of Parkinson's Disease in Rats. *Neurochem Res* **42**, 1104-1115 (2017).

75. E. Aflaki, N. Moaven, D. K. Borger, G. Lopez, W. Westbroek, J. J. Chae, J. Marugan, S. Patnaik, E. Maniwang, A. N. Gonzalez, E. Sidransky, Lysosomal storage and impaired autophagy lead to inflammasome activation in Gaucher macrophages. *Aging Cell* **15**, 77-88 (2016).

76. S. Sarkar, E. Malovic, D. S. Harishchandra, S. Ghaisas, N. Panicker, A. Charli, B. N. Palanisamy, D. Rokad, H. Jin, V. Anantharam, A. Kanthasamy, A. G. Kanthasamy, Mitochondrial impairment in microglia amplifies NLRP3 inflammasome proinflammatory signaling in cell culture and animal models of Parkinson's disease. *NPJ Parkinsons Dis* **3**, 30 (2017).

77. K. V. Rao, M. D. Norenberg, Manganese induces the mitochondrial permeability transition in cultured astrocytes. *J Biol Chem* **279**, 32333-32338 (2004).

78. A. Rakovic, A. Grunewald, J. Kottwitz, N. Bruggemann, P. P. Pramstaller, K. Lohmann, C. Klein, Mutations in PINK1 and Parkin impair ubiquitination of Mitofusins in human fibroblasts. *PLoS One* **6**, e16746 (2011).

79. N. M. Rocha, D. A. Bulger, A. Frontini, H. Titheradge, S. B. Gribsholt, R. Knox, M. Page, J. Harris, F. Payne, C. Adams, A. Sleigh, J. Crawford, A. P. Gjesing, J. Bork-Jensen, O. Pedersen, I. Barroso, T. Hansen, H. Cox, M. Reilly, A. Rossor, R. J. Brown, S. I. Taylor, D. McHale, M. Armstrong, E. A. Oral, V. Saudek, S. I. O'Rahilly, E. R. Maher, B. Richelsen, D. B. Savage, R. K. Semple, Human biallelic MFN2 mutations induce mitochondrial dysfunction, upper body adipose hyperplasia, and suppression of leptin expression. *Elife* **6**, (2017).

80. P. Huang, T. Yu, Y. Yoon, Mitochondrial clustering induced by overexpression of the mitochondrial fusion protein Mfn2 causes mitochondrial dysfunction and cell death. *Eur J Cell Biol* **86**, 289-302 (2007).

81. X. Liu, J. Yang, C. Lu, S. Jiang, X. Nie, J. Han, L. Yin, J. Jiang, Downregulation of Mfn2 participates in manganese-induced neuronal apoptosis in rat striatum and PC12 cells. *Neurochem Int*, (2017).

82. W. Wang, X. Wang, H. Fujioka, C. Hoppel, A. L. Whone, M. A. Caldwell, P. J. Cullen, J. Liu, X. Zhu, Parkinson's disease-associated mutant VPS35 causes mitochondrial dysfunction by recycling DLP1 complexes. *Nat Med* **22**, 54-63 (2016).

83. V. J. Mecozzi, D. E. Berman, S. Simoes, C. Vetanovetz, M. R. Awal, V. M. Patel, R. T. Schneider, G. A. Petsko, D. Ringe, S. A. Small, Pharmacological

chaperones stabilize retromer to limit APP processing. *Nat Chem Biol* **10**, 443-449 (2014).

84. J. D. Swarbrick, D. J. Shaw, S. Chhabra, R. Ghai, E. Valkov, S. J. Norwood, M. N. Seaman, B. M. Collins, VPS29 is not an active metallo-phosphatase but is a rigid scaffold required for retromer interaction with accessory proteins. *PLoS One* **6**, e20420 (2011).

85. J. Follett, S. J. Norwood, N. A. Hamilton, M. Mohan, O. Kovtun, S. Tay, Y. Zhe, S. A. Wood, G. D. Mellick, P. A. Silburn, B. M. Collins, A. Bugarcic, R. D. Teasdale, The Vps35 D620N mutation linked to Parkinson's disease disrupts the cargo sorting function of retromer. *Traffic* **15**, 230-244 (2014).

86. L. J. Vella, A. F. Hill, L. Cheng, Focus on Extracellular Vesicles: Exosomes and Their Role in Protein Trafficking and Biomarker Potential in Alzheimer's and Parkinson's Disease. *Int J Mol Sci* **17**, 173 (2016).

87. I. Russo, L. Bubacco, E. Greggio, Exosomes-associated neurodegeneration and progression of Parkinson's disease. *Am J Neurodegener Dis* **1**, 217-225 (2012).

88. K. C. Luk, V. Kehm, J. Carroll, B. Zhang, P. O'Brien, J. Q. Trojanowski, V. M. Lee, Pathological alpha-synuclein transmission initiates Parkinson-like neurodegeneration in nontransgenic mice. *Science* **338**, 949-953 (2012).

89. A. Gupta, L. Pulliam, Exosomes as mediators of neuroinflammation. *J Neuroinflammation* **11**, 68 (2014).

90. M. Aschner, K. M. Erikson, E. Herrero Hernandez, R. Tjalkens, Manganese and its role in Parkinson's disease: from transport to neuropathology. *Neuromolecular Med* **11**, 252-266 (2009).

91. K. Dierschke, C. Isaxon, U. B. Andersson, E. Assarsson, A. Axmon, L. Stockfelt, A. Gudmundsson, B. A. Jonsson, M. Karedal, J. Londahl, J. Pagels, A. Wierzbicka, M. Bohgard, J. Nielsen, Acute respiratory effects and biomarkers of inflammation due to welding-derived nanoparticle aggregates. *Int Arch Occup Environ Health*, (2017).

92. R. Gordon, C. E. Hogan, M. L. Neal, V. Anantharam, A. G. Kanthasamy, A. Kanthasamy, A simple magnetic separation method for high-yield isolation of pure primary microglia. *J Neurosci Methods* **194**, 287-296 (2011).

93. S. Sarkar, E. Malovic, B. Plante, G. Zenitsky, H. Jin, V. Anantharam, A. Kanthasamy, A. G. Kanthasamy, Rapid and Refined CD11b Magnetic Isolation of Primary Microglia with Enhanced Purity and Versatility. *J Vis Exp*, (2017).

94. J. Crossgrove, W. Zheng, Manganese toxicity upon overexposure. *NMR Biomed* **17**, 544-553 (2004).

95. G. J. Li, B. S. Choi, X. Wang, J. Liu, M. P. Waalkes, W. Zheng, Molecular mechanism of distorted iron regulation in the blood-CSF barrier and regional blood-brain barrier following in vivo subchronic manganese exposure. *Neurotoxicology* **27**, 737-744 (2006).

96. W. Zheng, H. Kim, Q. Zhao, Comparative toxicokinetics of manganese chloride and methylcyclopentadienyl manganese tricarbonyl (MMT) in Sprague-Dawley

rats. *Toxicological sciences : an official journal of the Society of Toxicology* **54**, 295-301 (2000).

97. R. Gordon, N. Singh, V. Lawana, A. Ghosh, D. S. Harischandra, H. Jin, C. Hogan, S. Sarkar, D. Rokad, N. Panicker, V. Anantharam, A. G. Kanthasamy, A. Kanthasamy, Protein kinase Cdelta upregulation in microglia drives neuroinflammatory responses and dopaminergic neurodegeneration in experimental models of Parkinson's disease. *Neurobiol Dis* **93**, 96-114 (2016).

98. J. Seo, E. W. Ottesen, R. N. Singh, Antisense methods to modulate pre-mRNA splicing. *Methods Mol Biol* **1126**, 271-283 (2014).

99. D. S. Harischandra, S. Ghaisas, D. Rokad, M. Zamanian, H. Jin, V. Anantharam, M. Kimber, A. Kanthasamy, A. G. Kanthasamy, Environmental neurotoxicant manganese regulates exosome-mediated extracellular miRNAs in cell culture model of Parkinson's disease: Relevance to alpha-synuclein misfolding in metal neurotoxicity. *Neurotoxicology*, (2017).

100. A. Charli, H. Jin, V. Anantharam, A. Kanthasamy, A. G. Kanthasamy, Alterations in mitochondrial dynamics induced by tebufenpyrad and pyridaben in a dopaminergic neuronal cell culture model. *NeuroToxicology* **53**, 302-313 (2016).

Figure Legends

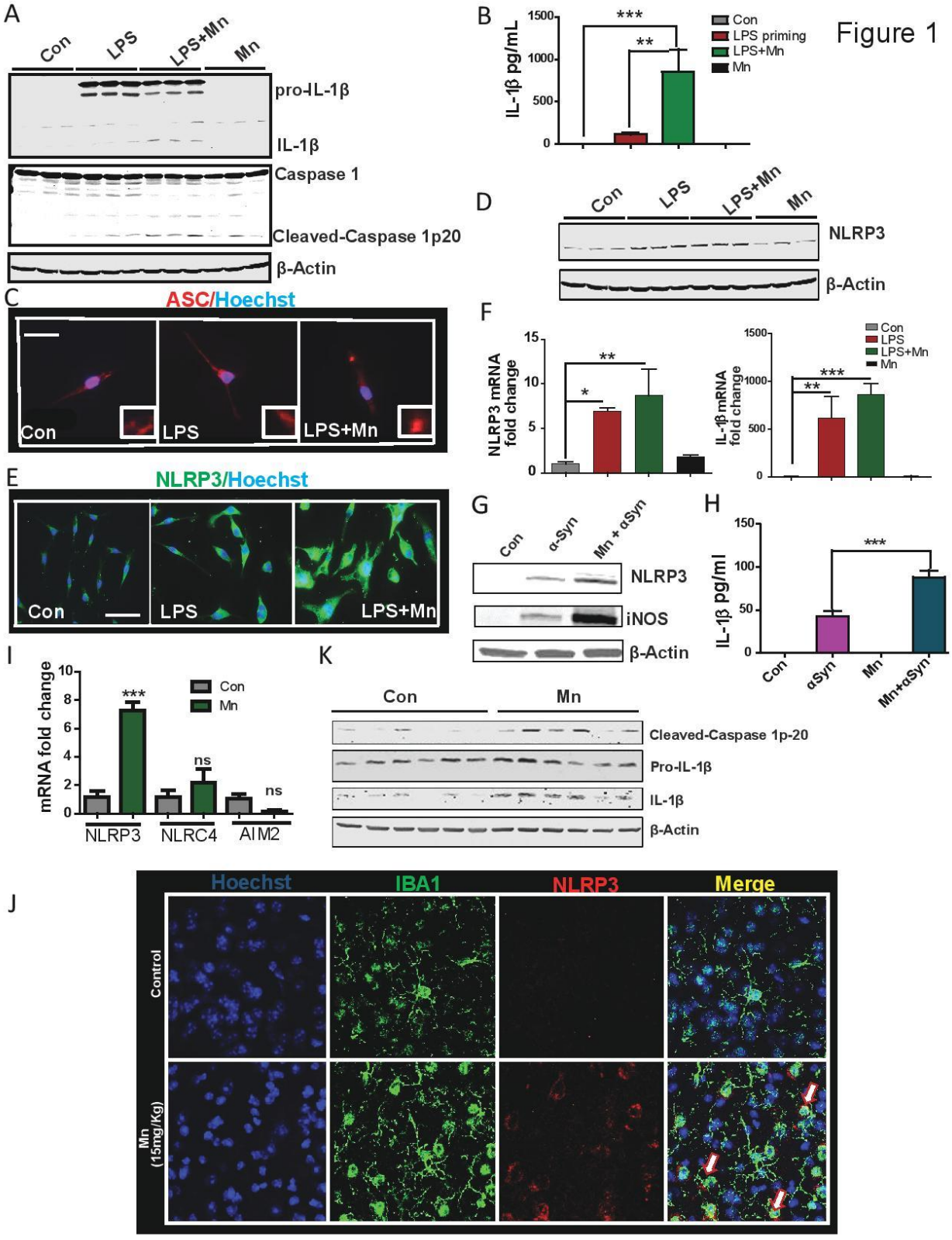

Fig. 1: Manganese induced NLRP3 inflammasome activation in microglial cells *in vivo* and *in vitro*. Microglial cell line was primed with LPS for 3 h and exposed to 100 µM Mn for 6-24 h. A) Western blot analysis showing Mn exposure led to Caspase 1 cleavage and cleavage of IL-1β in an LPS-primed microglial cell line. n=4 B) Luminex analysis revealing Mn (24 h) exposure led to IL-1β release in primed microglial cells, n=8. C) ICC analysis reveals that 100 µM Mn exposure led to formation of ASC specs in microglial cells. D-E) Western blot (D) and ICC (E) analyses showing LPS-priming induced NLRP3 protein expression, n=3. F) qRT-PCR analysis shows increased NLRP3 and pro-IL-1β mRNA expression following LPS priming, n=3. G) Wild-type microglial cells were cotreated with 100 µM Mn and 1 µM αSyn_{Agg}. Western Blot analysis reveals that Mn exposure potentiated αSyn_{Agg}-induced NLRP3 expression. H) Luminex analysis demonstrates that Mn potentiated IL-1β release induced by αSyn_{Agg}, n=4. I) Mn exposure induced mRNA expression of NLRP3, but not NLRC4 or AIM2, in the striata of C57BL mice gavaged with 15 mg/Kg Mn for 30 days as revealed by qRT-PCR, n=5. J) IHC analysis revealing increased level of NLRP3 in IBA1-positive microglial cells in striatal region of Mn-exposed mice compared to controls, n=3. K) Western blot analysis demonstrating that Mn exposure leads to increased matured IL-1β and cleaved caspase-1p20 in striatum, n=6. Data analyzed via ANOVA with Tukey post analysis, *$p<0.05$, **$p<0.01$, ***$p<0.001$. Data represented as mean±SEM.

Figure 2

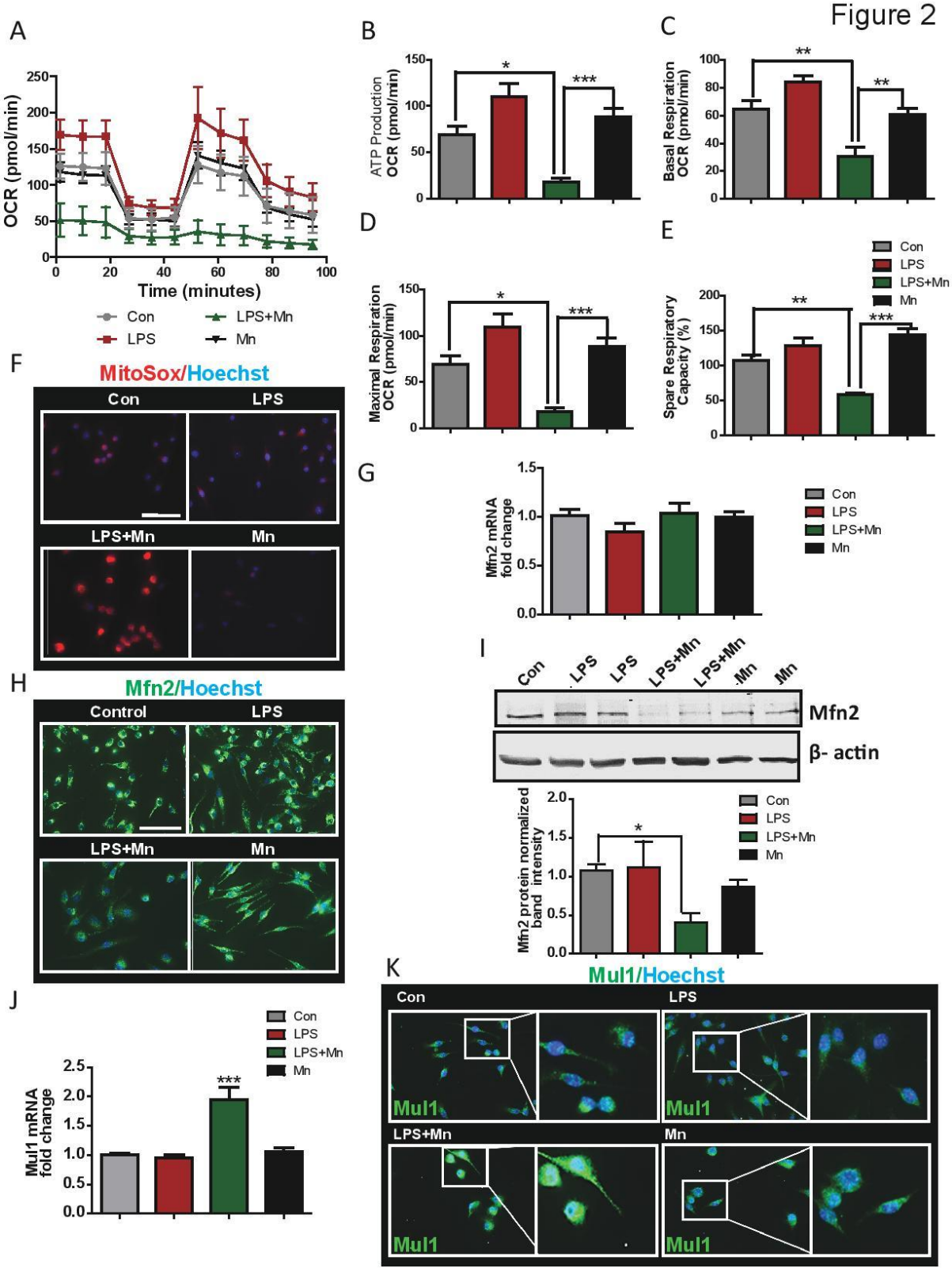
A
OCR (pmol/min)
Time (minutes)
Con
LPS
LPS+Mn
Mn
B
ATP Production OCR (pmol/min)
C
Basal Respiration OCR (pmol/min)
D
Maximal Respiration OCR (pmol/min)
E
Spare Respiratory Capacity (%)
F
MitoSox/Hoechst
Con
LPS
LPS+Mn
Mn
G
Mfn2 mRNA fold change
H
Mfn2/Hoechst
Control
LPS
LPS+Mn
Mn
I
Mfn2
β- actin
Mfn2 protein normalized band intensity
J
Mul1 mRNA fold change
K
Mul1/Hoechst
Mul1

Fig. 2: Mn induced mitochondrial damage by modulating Mfn2 and Mul1 expression in microglial cells. Primary microglial culture and microglial cell line was primed with LPS for 3 h and exposed to 100 µM Mn for 6-24 h. A) Seahorse Mito Stress showing change in mitochondrial dynamics in Mn-exposed LPS-primed primary microglial cells. Mn exposure lead to diminished B) mitochondrial ATP production, C) basal respiration rate, D) maximal respiration, and E) spare respiratory capacity. n=5 F) Mn exposure increased mitochondrial superoxide generation as demonstrated by MitoSOX dye. G) qRT-PCR analysis demonstrates no change in Mfn2 mRNA level on Mn exposure in microglial cells. n=3 H) ICC and I) Western blot analyses revealing that Mn exposure reduced Mfn2 protein level in microglial cells. n=4 J) qRT-PCR analysis reveals that Mul1, the protein which ubiquitinates Mfn2, was upregulated on Mn exposure in microglial cells. n=3 K) ICC analysis revealing increased Mul1 protein on Mn exposure. Data analyzed via ANOVA with Tukey post analysis, *$p<0.05$, **$p<0.01$, ***$p<0.001$. Data represented as mean±SEM.

Figure 3

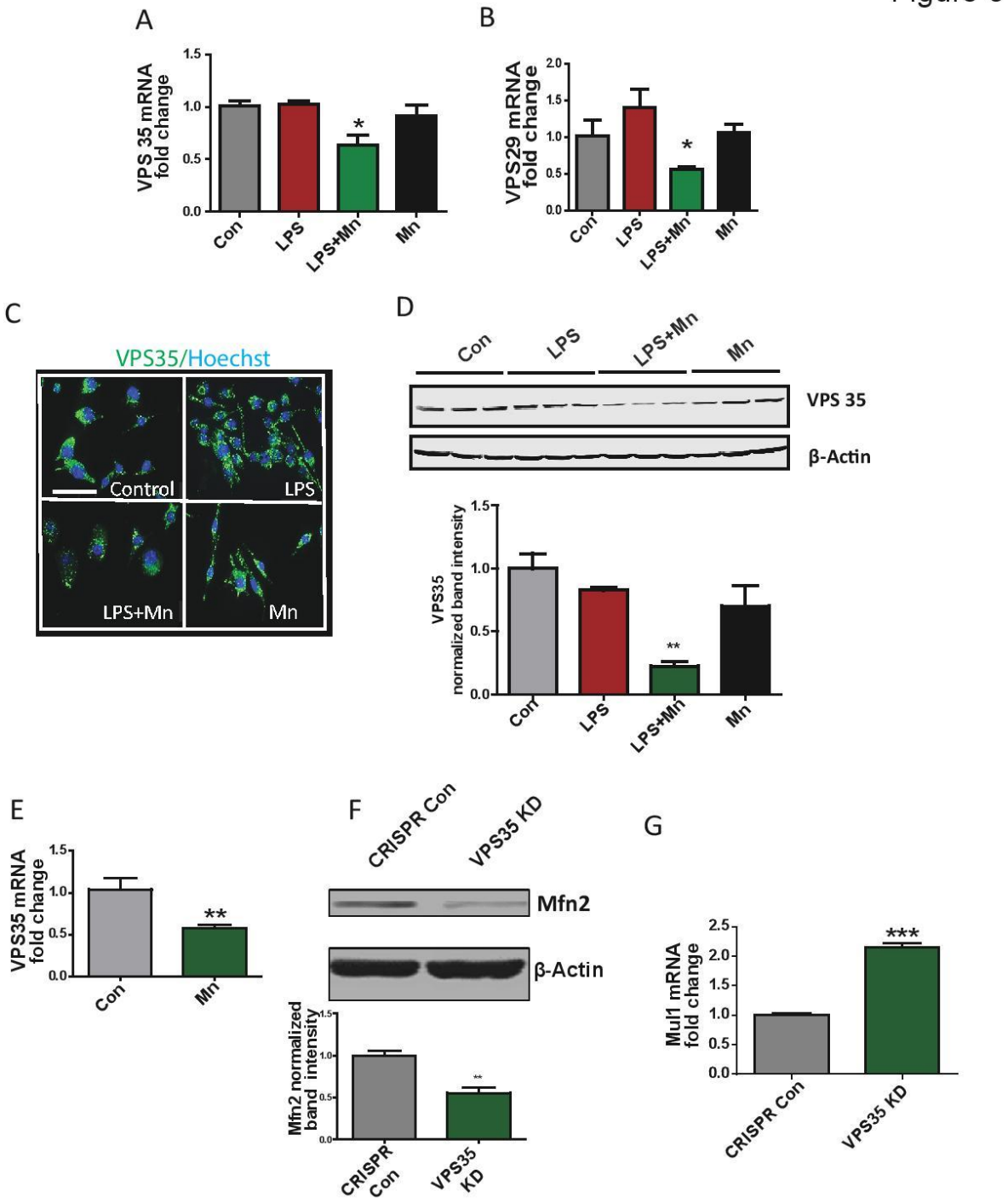
A
VPS 35 mRNA fold change
1.5
1.0
0.5
0.0
*
Con
LPS
LPS+Mn
Mn
B
VPS29 mRNA fold change
2.0
1.5
1.0
0.5
0.0
*
Con
LPS
LPS+Mn
Mn
C
VPS35/Hoechst
Control
LPS
LPS+Mn
Mn
D
Con
LPS
LPS+Mn
Mn
VPS 35
β-Actin
VPS35 normalized band intensity
1.5
1.0
0.5
0.0
**
Con
LPS
LPS+Mn
Mn
E
VPS35 mRNA fold change
1.5
1.0
0.5
0.0
**
Con
Mn
F
CRISPR Con
VPS35 KD
Mfn2
β-Actin
Mfn2 normalized band intensity
1.5
1.0
0.5
0.0
**
CRISPR Con
VPS35 KD
G
Mul1 mRNA fold change
2.5
2.0
1.5
1.0
0.5
0.0
***
CRISPR Con
VPS35 KD

Fig. 3: VPS35, a retromer complex protein, can modulate Mfn2 degradation during Mn-induced inflammasome activation. Microglial cell line was primed with LPS for 3 h and exposed to 100 µM Mn for 24 h. A-B) qRT-PCR analysis reveals that Mn exposure led to downregulation of the retromer complex components VPS35 and VPS29. n=3 C) ICC analysis and D) Western blot analysis revealing that Mn exposure downregulates VPS35 protein level in microglial cell line. n=3 E) C57BL mice were gavaged with 15 mg/Kg Mn for 30 days. qRT-PCR reveals that Mn exposure reduced VPS35 mRNA expression in striatum. n=6 F) Western blot analysis from VPS35 CRISPR-cas9 KD cells demonstrates lower Mfn2 protein level compared to wild-type microglial cells. G) qRT-PCR analysis reveals increased Mul1 mRNA level in VPS35 KD microglial cells compared to wild-type cells. n=3 Data analyzed via ANOVA with Tukey post analysis, *$p<0.05$, **$p<0.01$, ***$p<0.001$. Data represented as mean±SEM.

Figure 4

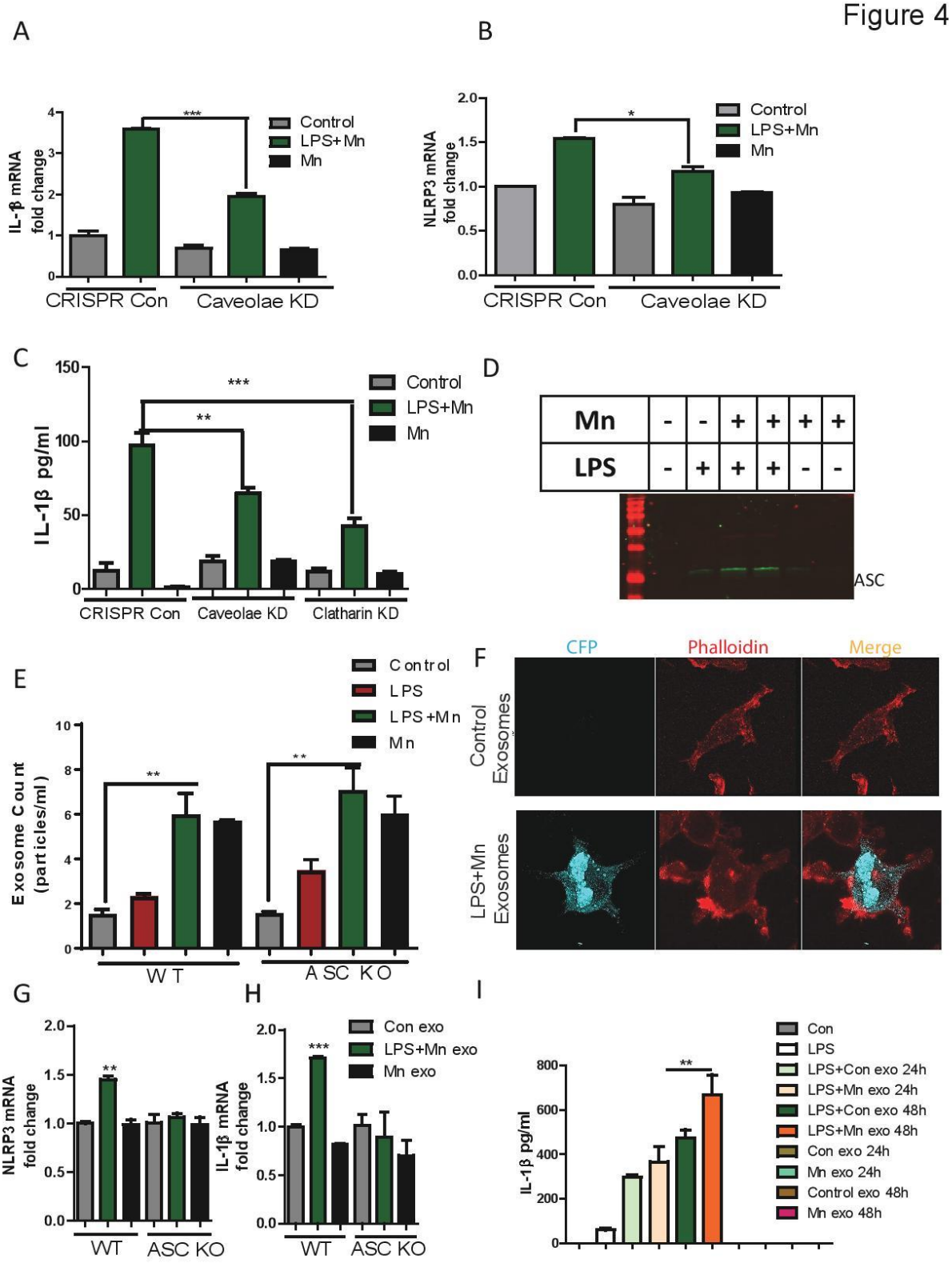
A
IL-1β mRNA fold change
Control
LPS+Mn
Mn
CRISPR Con
Caveolae KD
B
NLRP3 mRNA fold change
Control
LPS+Mn
Mn
CRISPR Con
Caveolae KD
C
IL-1β pg/ml
Control
LPS+Mn
Mn
CRISPR Con
Caveolae KD
Clatharin KD
D
Mn
LPS
ASC
E
Exosome Count (particles/ml)
Control
LPS
LPS+Mn
Mn
WT
ASC KO
F
CFP
Phalloidin
Merge
Control Exosomes
LPS+Mn Exosomes
G
NLRP3 mRNA fold change
WT
ASC KO
H
IL-1β mRNA fold change
Con exo
LPS+Mn exo
Mn exo
WT
ASC KO
I
IL-1β pg/ml
Con
LPS
LPS+Con exo 24h
LPS+Mn exo 24h
LPS+Con exo 48h
LPS+Mn exo 48h
Con exo 24h
Mn exo 24h
Control exo 48h
Mn exo 48h

Fig. 4: Exosomal release of the inflammasome component ASC propagates Mn-induced inflammasome activation. Caveolae and clathrin KD cells were treated with 100 μM Mn for 24 h. A) qRT-PCR analysis demonstrating that Mn exposure led to diminished mRNA production of NLRP3 and B) pro-IL-1β in caveolae KD cells compared to wild-type microglial cells. n=3 C) Luminex analysis demonstrates both caveolae and clathrin KD microglial cells attenuated release of IL-1β on Mn exposure. n=8 D) Western blot analysis of exosomes isolated from Mn-treated microglial cells reveals increased exosomal release of ASC. E) NanoSight analysis reveals that Mn increased the number of exosomes released from wild-type and ASC KO microglial cells. n=3 F) Exosomes were collected from ASC-CFP-overexpressing microglial cells treated with 100 μM Mn. Wild-type cells were treated with these isolated exosomes. ICC analysis demonstrates that Mn exposure led to cell-to-cell transmission of ASC. G) Exosomes isolated from Mn-exposed wild type and ASC KO cells were used to treat wild-type microglial cells. qRT-PCR analysis reveals that exosomes isolated from wild-type cells treated with Mn induced NLRP3, and H) pro-IL-1β expression compared to exosomes isolated from control cells, while exosomes isolated from ASC KO cells failed to elicit this response. n=3 I) Exosomes were isolated from serum of Mn-gavaged animals and used to treat primary microglial cells. Luminex multiplex assay reveals that exosomes isolated from Mn-gavaged animals elicited significantly higher IL-1β production than did exosomes isolated from control animals. n=8. Data analyzed via ANOVA with Tukey post analysis, *$p<0.05$, **$p<0.01$, ***$p<0.001$. Data represented as mean±SEM.

Figure 5

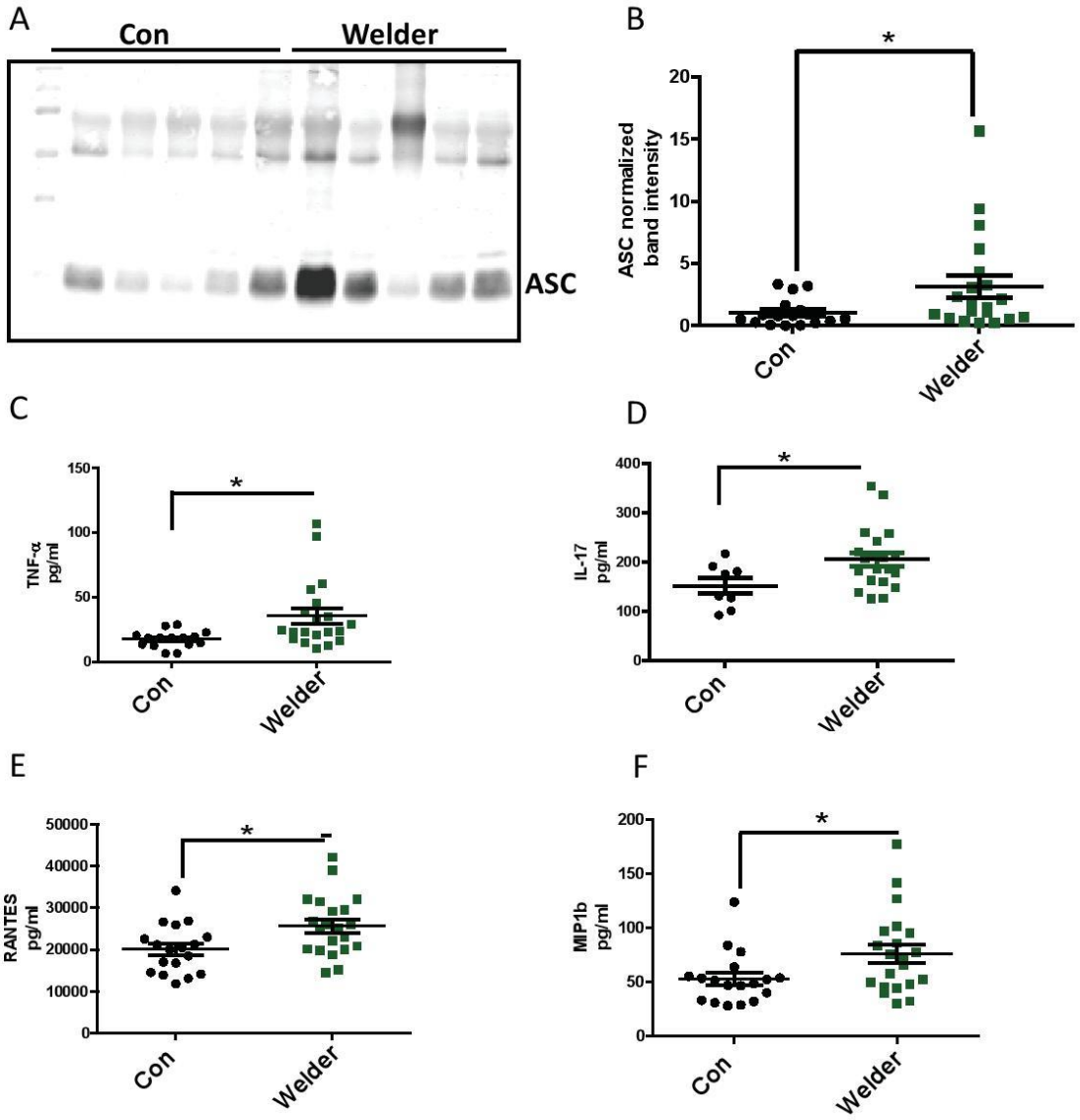

Fig. 5: Serum exosomes and serum from welder population have higher load of ASC and higher pro-inflammatory cytokines, respectively, when compared to age-matched controls. A) Western blot analysis and B) densitometric analysis of Western blot show increased level of exosomal ASC load in welder population. C-F) Multiplex assay revealing increased level of pro-inflammatory cytokines and chemokines. C) TNF-α, D) IL-17, E) Rantes, and F) MIP-1b in welder serum

population. Data analyzed via Student-t test, *p<0.05, **p <0.01, ***p<0.001. Data represented as mean±SEM.

Figure 6

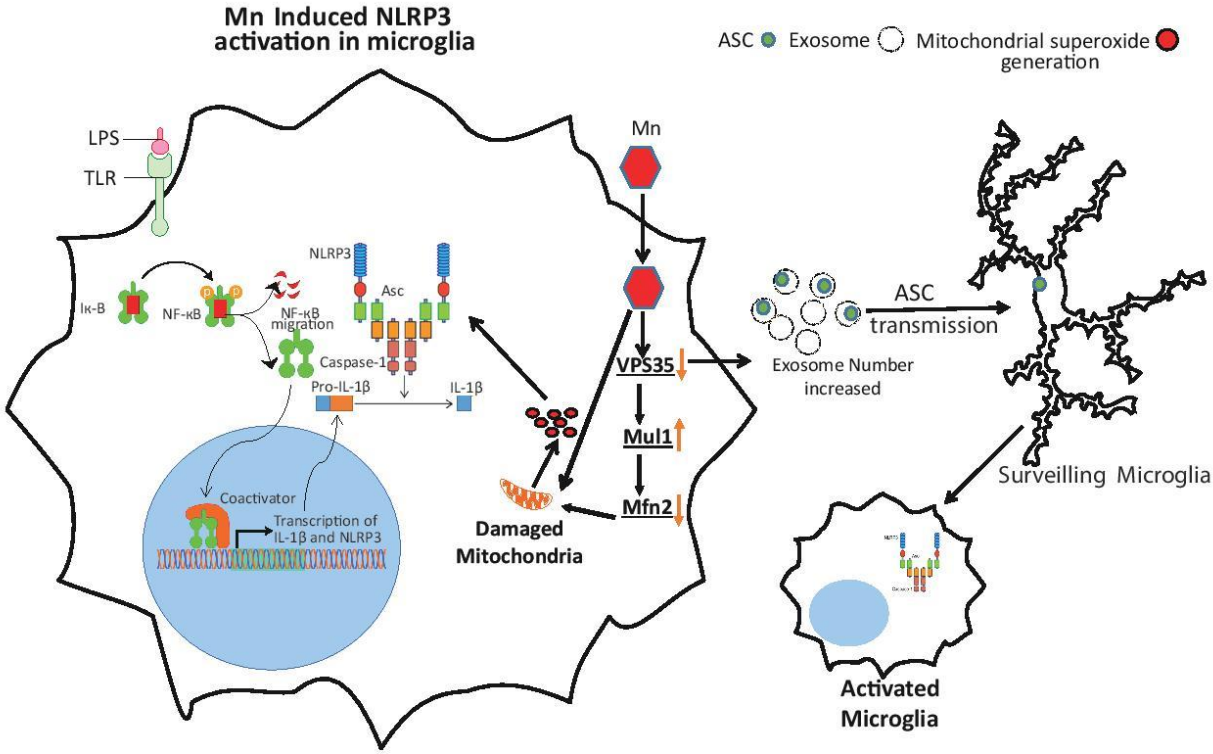

Fig. 6. Working Hypothesis. Mn induces mitochondrial dysfunction leading to inflammasome activation by degradation of Mfn2. Mn also induces the release of exosomal ASC, thereby leading to NLRP3 inflammasome propagation.

Supplementary Figure 1

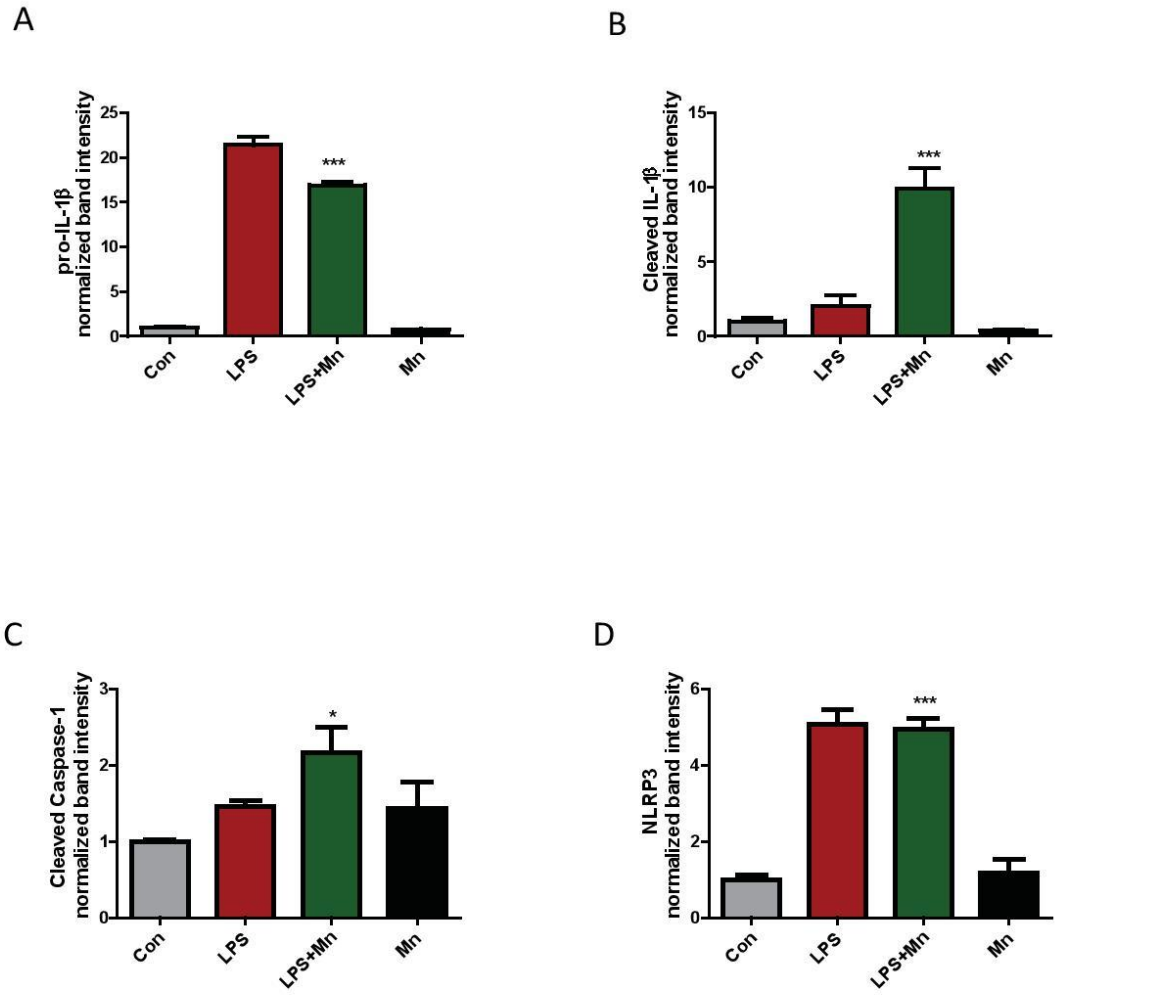

Supplementary Fig. 1: Mn leads to NLRP3 inflammasome activation in LPS-primed microglial cells: A-D) Densitometric analysis of western blots from Fig.1 A and Fig. 1D. Data analyzed via ANOVA with Tukey post analysis, *p<0.05, **p <0.01, ***p<0.001. Data represented as mean±SEM.

Supplementary Figure 2

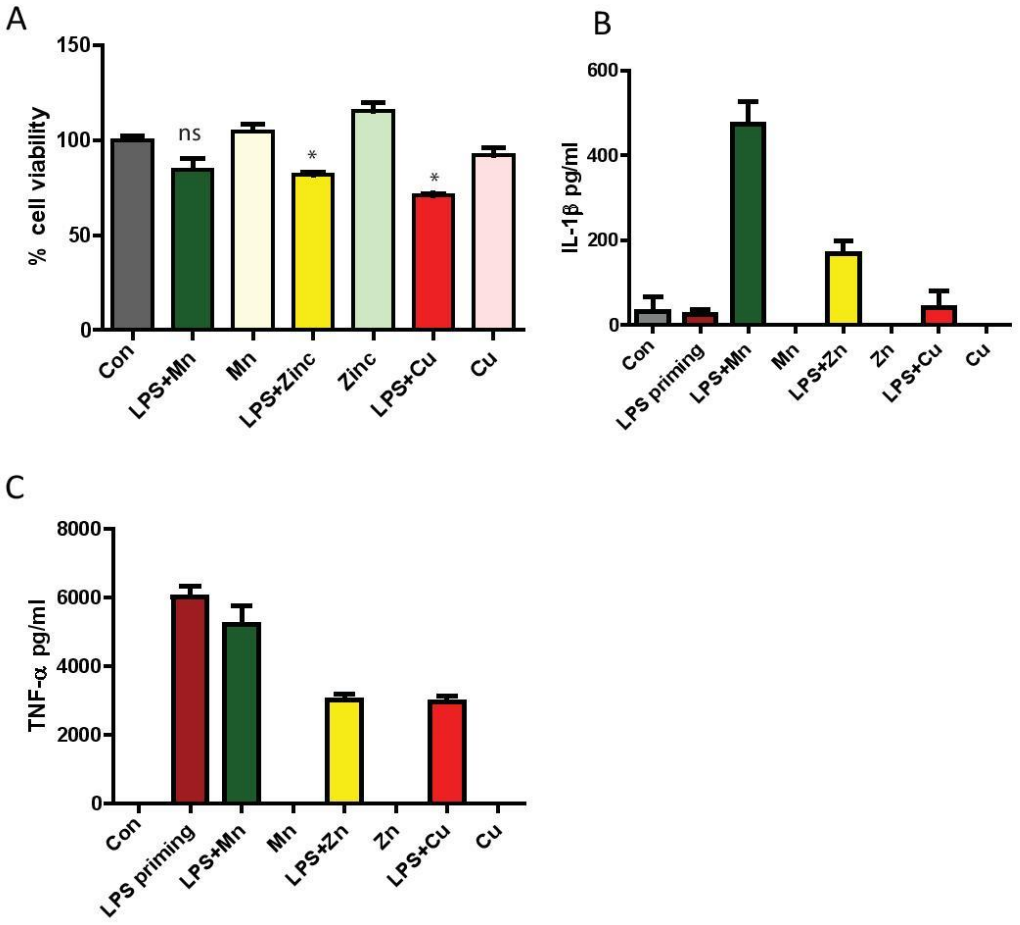

Supplementary Fig. 2: Mn specifically induced inflammasome activation in primary microglial culture. A) MTS assay shows that divalent metal exposure did not lead to significant cell death. B) Luminex assay reveals that Mn exposure significantly induced IL-1β release over Cu, or Zn, but C) TNF-α secretion was not altered. Data analyzed via ANOVA with Tukey post analysis, *p<0.05, **p <0.01, ***p<0.001. Data represented as mean±SEM.

Supplementary Figure 3

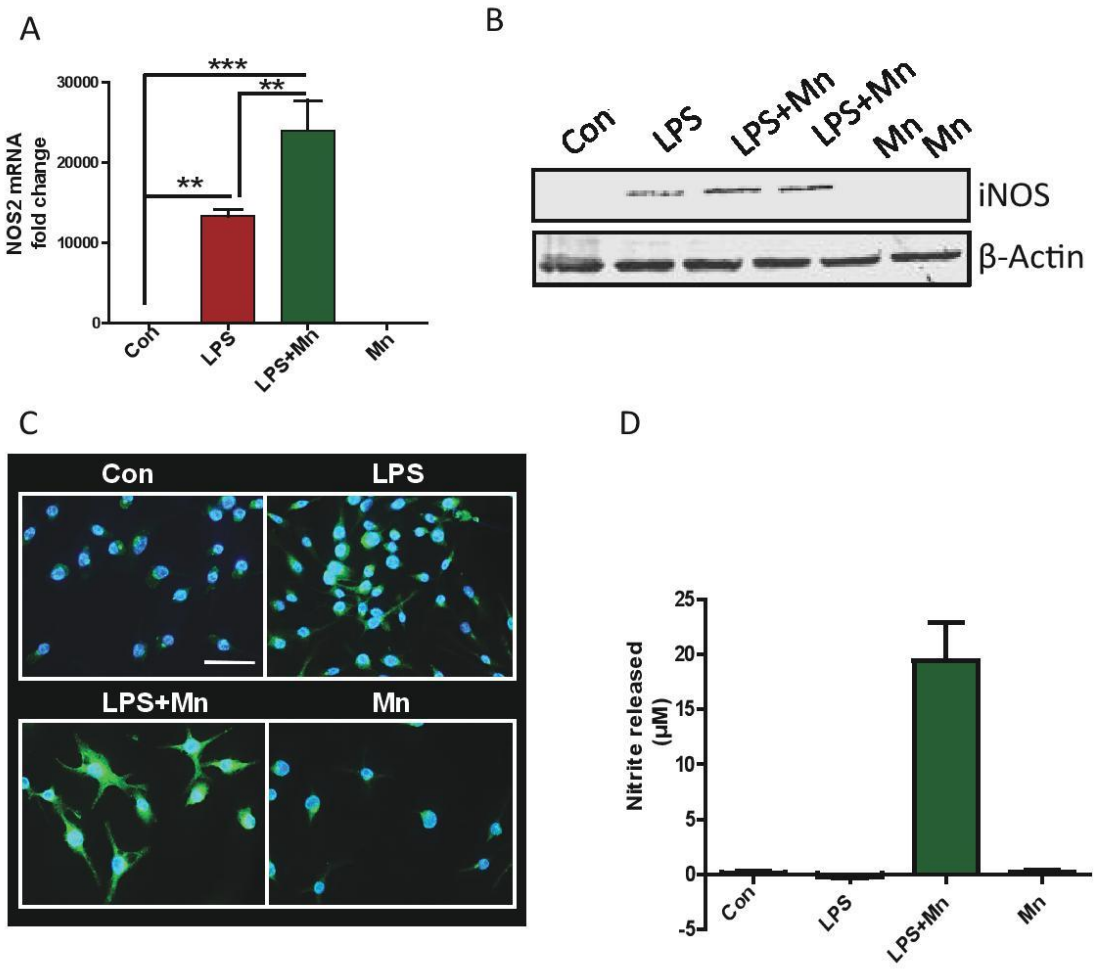

Supplementary Fig. 3: Mn potentiated LPS-induced nitrite generation. A) qRT-PCR analysis reveals that Mn exposure potentiated Nos2 mRNA level in LPS-primed microglial cells. B) Western blot and C) ICC analyses show upregulation of Nos2 in microglial cells on Mn exposure. D) Griess assay reveals that Mn potentiated Nitrite release in primed microglial cells. Data analyzed via ANOVA with Tukey post analysis, *p<0.05, **p <0.01, ***p<0.001. Data represented as mean±SEM.

Supplementary Figure 4

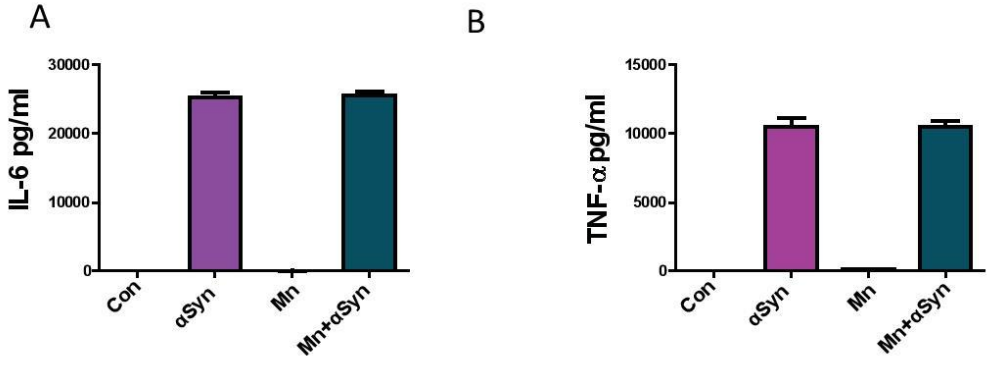

Supplementary Fig. 4: Mn exposure failed to potentiate αSyn_{Agg}-induced release of the pro-inflammatory factors TNF-α and IL-6. Luminex assay reveals that Mn failed to potentiate A) TNF-α, or B) IL-6 secretion induced by αSyn_{Agg}. Data analyzed via ANOVA with Tukey post analysis, *p<0.05, **p <0.01, ***p<0.001. Data represented as mean±SEM.

Supplementary Figure 5

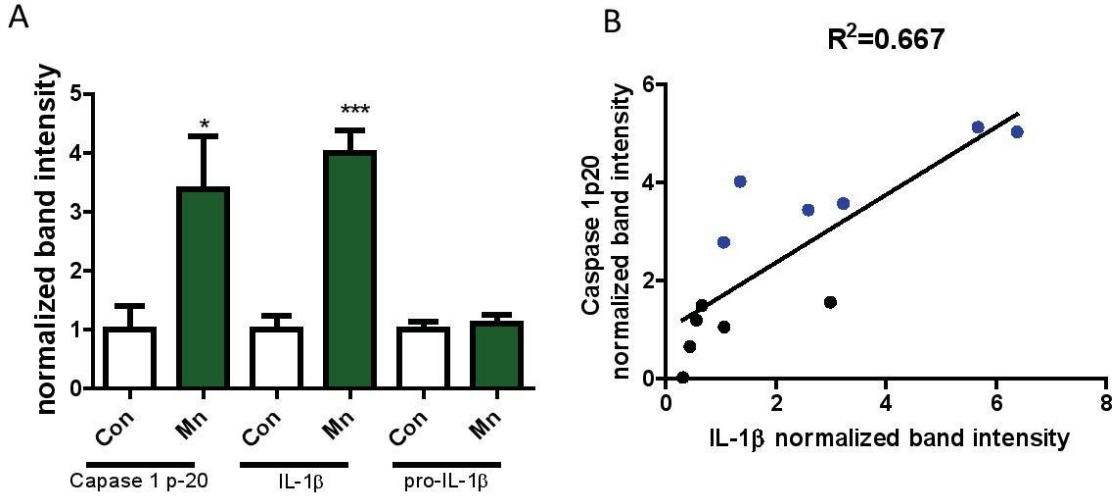

Supplementary Fig. 5: Caspase-1p20 induced cleavage of pro-IL-1β. A) Densitometric analysis of Western blot represented in Fig. 1J. B) Correlation plot showing the relation between cleaved caspase-1p20 and cleaved IL-1β. Data analyzed via ANOVA with Tukey post analysis, *p<0.05, **p <0.01, ***p<0.001. Data represented as mean±SEM.

Supplementary Figure 6

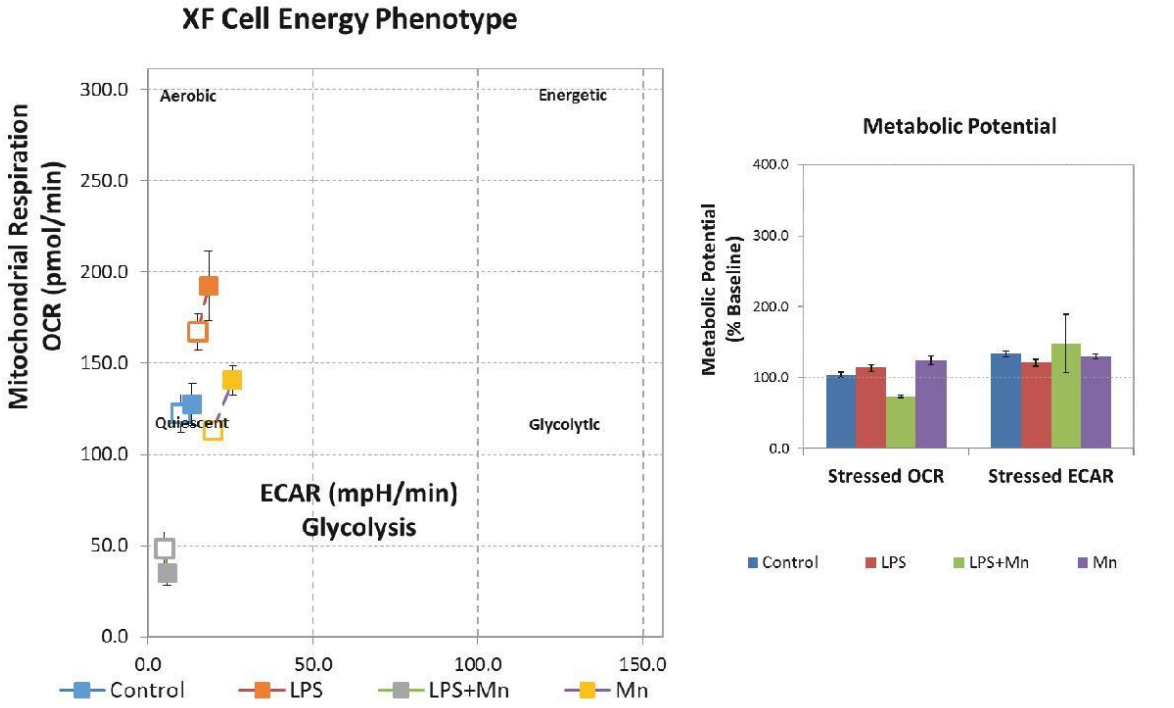

Supplementary Fig. 6: Mn exposure modulated metabolic cellular phenotype in primary microglial cells. A**)** Mn exposure changed metabolic phenotype in LPS-primed microglial cells. B) Mn changed the metabolic potential with respect to OCR but it did not alter stressed ECAR. C) Mn altered stressed OCAR and D) ECAR in

primed microglial cells. Data analyzed via ANOVA with Tukey post analysis, *p<0.05, **p <0.01, ***p<0.001. Data represented as mean±SEM.

Supplementary Figure 7

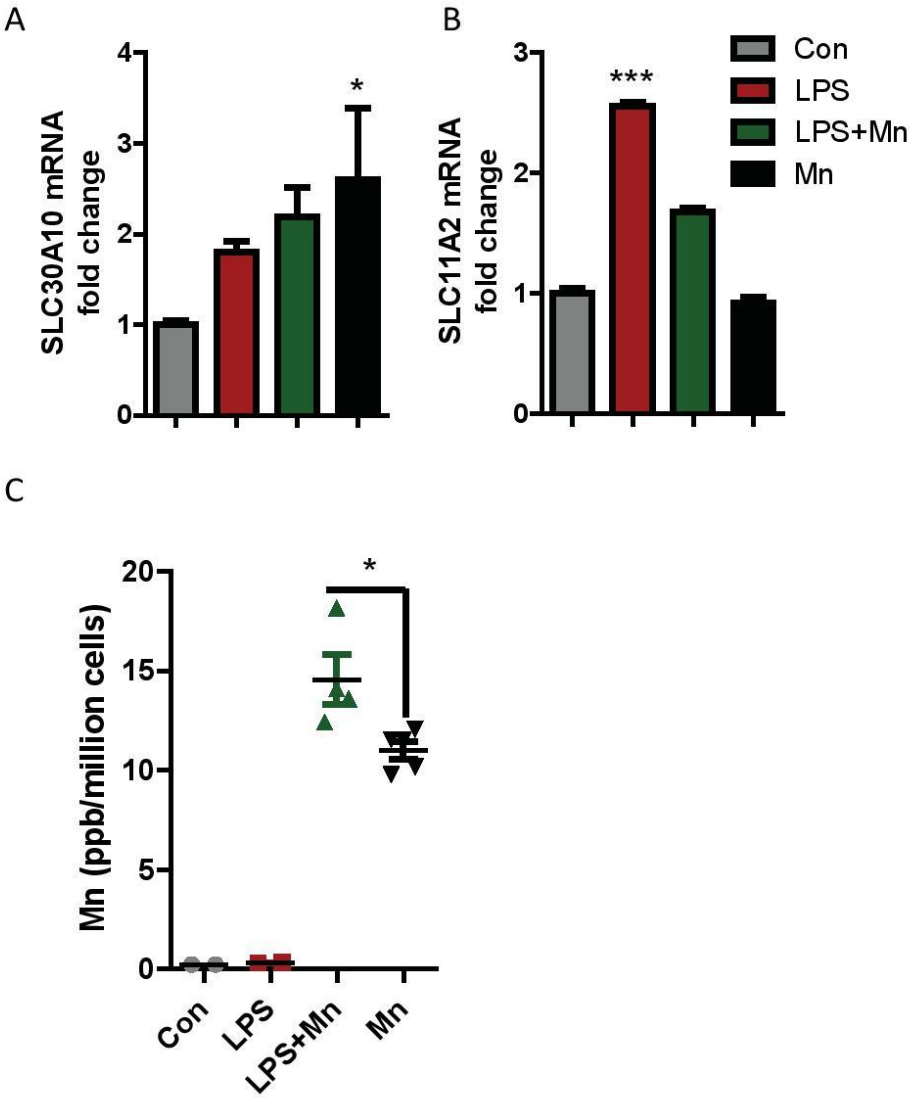

Supplementary Fig. 7: LPS modulated Mn transporters and Mn uptake in microglial cells. A) qRT-PCR analysis reveals that Mn increased the divalent metal exporter SLC30A10 level, while B) LPS priming led to an increased level of the Mn

importer in microglial cells. Data analyzed via ANOVA with Tukey post analysis, *p<0.05, **p <0.01, ***p<0.001. Data represented as mean±SEM.

Supplementary Figure 8

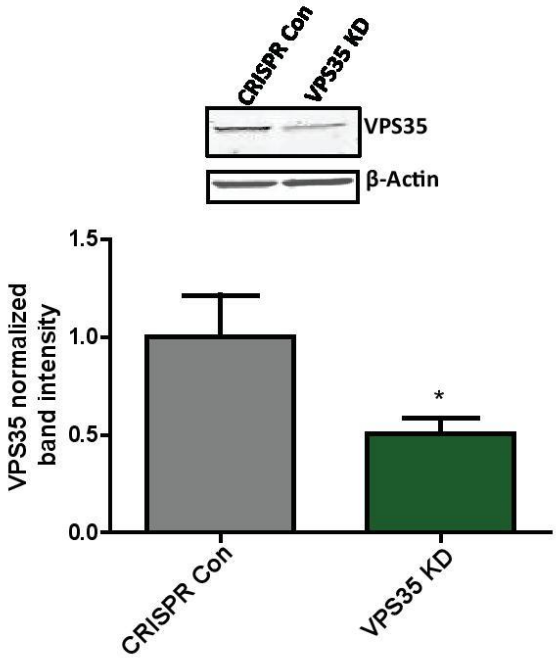

Supplementary Fig. 8: Generation of CRISPR-Cas9 VPS35 KD cells. Western blot analysis showing VPS35 KD using **CRISPR**-cas9 system. Data analyzed via Student-t test, *p<0.05, **p <0.01, ***p<0.001. Data represented as mean±SEM.

Supplementary Figure 9

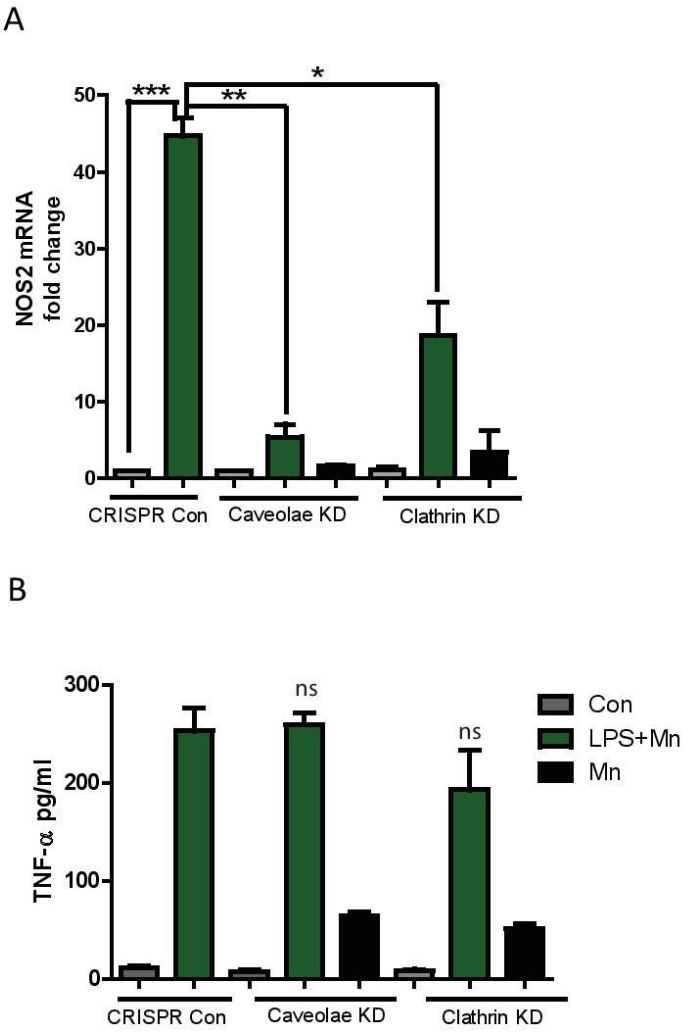

Supplementary Fig. 9: Caveolae and clathrin KD cells modulated Mn-induced Nos2 but not the pro-inflammatory factor TNF-α. A) qRT-PCR analysis reveals that Mn-induced Nos2 upregulation was attenuated in caveolae and clathrin KD cells. B) Luminex analysis reveals that clathrin or caveolae KD did not alter TNF-α secretion induced by Mn in a primed microglial cell line. Data analyzed via ANOVA with Tukey post analysis, *p<0.05, **p <0.01, ***p<0.001. Data represented as mean±SEM.

Supplementary Figure 10

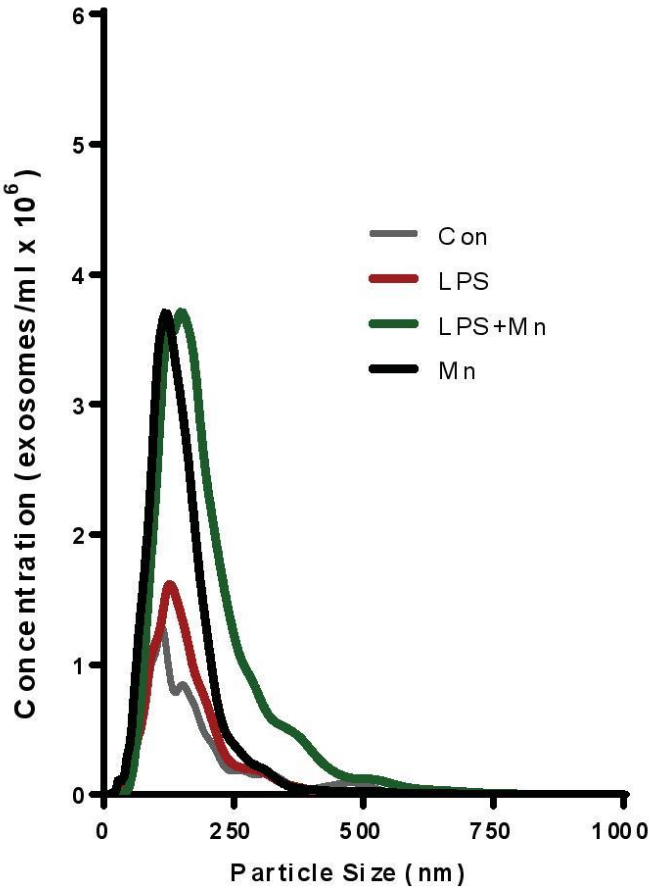

Supplementary Fig. 10: Mn exposure did not change the size distribution of the exosomes secreted by microglial cells. Size distribution of exosomes exposed to Mn.

Supplementary Figure 11

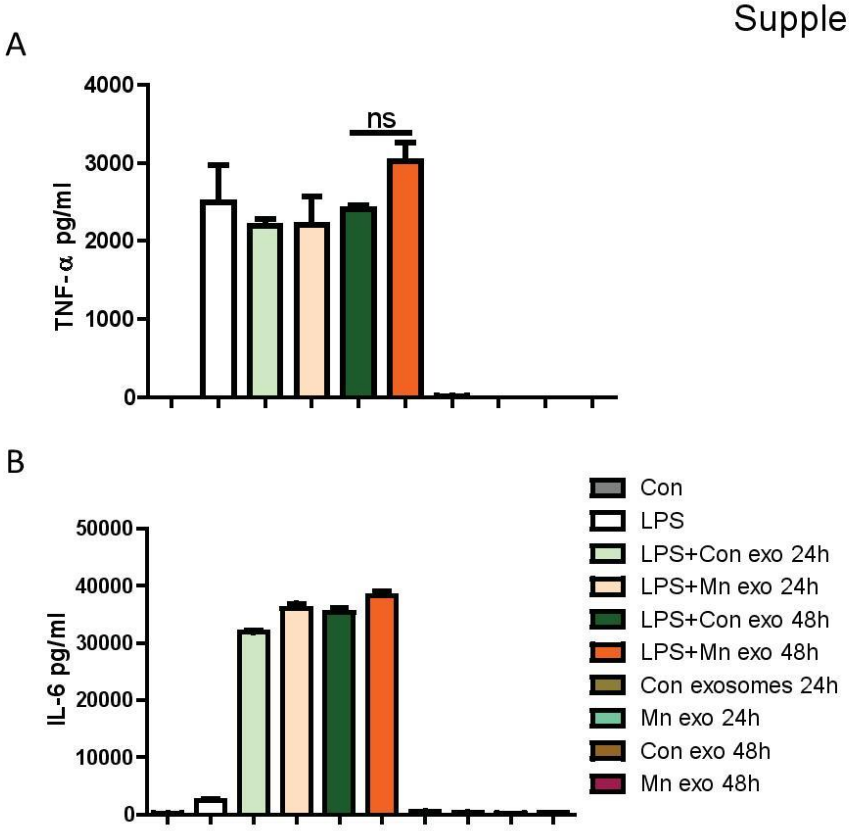

Supplementary Fig. 11: Exposure to exosomes isolated from Mn-gavaged animals did not alter release of the pro-inflammatory factors IL-6 and TNF-α. Luminex assay reveals that exosomes isolated from Mn-gavaged animals failed to potentiate A) TNF-α, or B) IL-6 secretion when compared to exosomes isolated from control animals.

Supplementary Figure 12

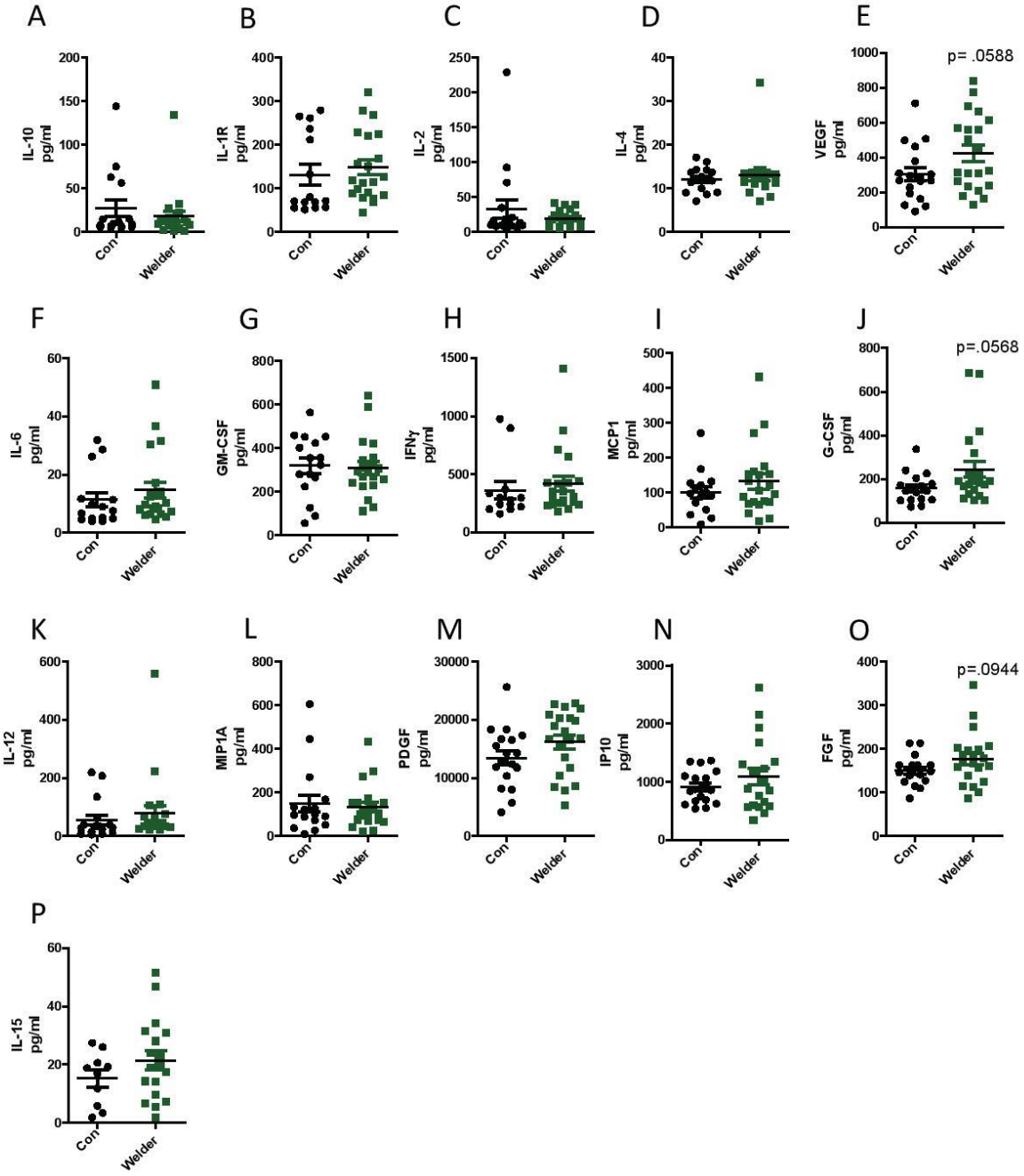

Supplementary Fig. 12: Pro-inflammatory cytokine profile of welder and age-matched control population. A-P) Pro-inflammatory serum cytokine profile of welders compared to age-matched controls. Data analyzed via Student-t test, *p<0.05, **p <0.01, ***p<0.001. Data represented as mean±SEM.

CHAPTER VI

KV1.3 MODULATES NEUROINFLAMMATION AND NEURODEGENERATION IN PARKINSON'S DISEASE MODELS

Manuscript to be submitted to *Nature Medicine*

Souvarish Sarkar[1], Hai M. Nguyen[2*], Emir Malovic[1*], Jie Luo[1#], Monica Langley[1#], Bharathi N Palanisamy[1], Neeraj Singh[1], Matthew Neal[1], Michelle Gabrielle[3], Ahmed Abdalla[1], Poojya Anantharam[4], Nikhil Panicker[1], Vikram Singh[2], Dharmin Rokad[1], Huajun Jin[1], Vellareddy Anantharam[1], Arthi Kanthasamy[1], Heike Wulff[2], Anumantha G. Kanthasamy[1$]

1- Parkinson Disorders Research Laboratory, Iowa Center for Advanced Neurotoxicology, Department of Biomedical Sciences, 2062 Veterinary Medicine Building, Iowa State University, Ames, IA 50011

2- Department of Pharmacology, School of Medicine, University of California, Davis

3- University of Western Ontario

4- Department of Veterinary Diagnostic and Production Animal Medicine, Veterinary Medicine Building, Iowa State University, Ames, IA 50011

[*]These authors made equal contributions

[#] These authors made equal contributions

[$]To whom correspondence should be addressed: Anumantha Kanthasamy, Ph.D. Distinguished Professor and Chair, Department of Biomedical Sciences, Iowa State University, Ames, IA 50011, Telephone: (515) 294-2516; Fax: (515) 294-2315, Email: akanthas@iastate.edu

Abstract

Chronic neuroinflammation mediated by persistent microglia activation has been well recognized as a major pathophysiological contributor to the progression of neurodegenerative processes in Parkinson's disease (PD). Identification of key targets contributing to sustained microglia activation and the regulation of these targets could provide potential treatments to halt disease progression. In this study, we show that microglial Kv1.3, a voltage-gated potassium channel, was highly upregulated in aggregated α-synuclein (αSyn)-stimulated primary microglia cultures, animal models of PD, as well as in human PD postmortem samples. Importantly, patch-clamp electrophysiological studies confirm that the observed Kv1.3 upregulation translates to increased Kv1.3 channel activity. We further demonstrate that Fyn, a non-receptor tyrosine kinase, modulated the transcriptional upregulation of microglial Kv1.3. Using multiple state-of-the-art techniques, including DuoLink PLA technology, we show that Fyn directly binds to Kv1.3 and post-translationally modified its channel activity. Furthermore, we demonstrate the functional relevance of Kv1.3 with respect to neuroinflammation by using Kv1.3 knockout (KO) microglia and the Kv1.3-specific small molecule inhibitor PAP-1. Kv1.3 KO microglial cells treated with aggregated αSyn produced fewer pro-inflammatory cytokines. PAP-1 significantly attenuated aggregated αSyn-induced inflammation in both a microglial cell line and primary microglia, thus highlighting Kv1.3's importance in inflammation. Administration of PAP-1 significantly inhibited MPTP-induced neurodegeneration and inflammation *in vivo*. PAP-1 also significantly reversed behavioral deficits and

dopamine loss in MitoPark mice, a progressive model of PD. Our results collectively show that the Fyn-dependent Kv1.3 channel plays an important role in inflammation in PD and has potential therapeutic significance.

Introduction

Parkinson's disease (PD) is a neurodegenerative motor disorder that is characterized by the slow and progressive loss of dopaminergic neurons in the substantia nigra pars compacta (SNpc) region of the brain. This progressive loss of neurons is characterized by the release of a misfolded and aggregated protein, α-synuclein (αSyn), which is predominantly expressed in neurons throughout the brain. Recent studies have also shown the loss of extra-striatal neurons and the presence of non-motor deficits in PD (*1, 2*). Though the underlying cause of this neuronal loss is not completely clear, recent post-mortem studies have implicated nigral inflammation characterized by persistent and excessive microgliosis and astrogliosis. Various lines of evidence, including cell culture, animal models, and post-mortem tissue analysis, have implicated sustained neuroinflammation as being critical to PD progression (*3-6*). Currently, there are no treatments for preventing the progression of PD and the only available therapies are directed towards mitigating the symptoms of the disorder.

Gene mutations (e.g., *PARK1/4*) can lead to misfolding and aggregation of αSyn, whose accumulation into Lewy bodies and neurites is the hallmark of both sporadic and genetically inherited PD. Interaction between aggregated αSyn

(αSyn_{Agg}) and microglial immune receptors, such as the pattern recognition receptors TLR2 and CD36, on microglial plasma membranes can lead to microglial activation (*7*). Furthermore, αSyn has been demonstrated to induce IL-1β production in monocytes (*8, 9*) and in microglia (*10*). However, much remains unknown regarding the key signaling pathways involved in either αSyn_{Agg}-mediated neuroinflammation in the nigral dopaminergic system (*11, 12*) or the chronic inflammation in microglia.

The voltage-gated potassium channel Kv1.3 was first identified in T cells (*13-15*), but has since been identified in other lymphocytes such as B cells and macrophages, retinal ganglion cells, microglia, and various other cell types. Similar to the other 40 Kv channels found in humans, Kv1.3 is a tetrameric protein consisting of α-subunits, each with six six transmembrane segments (S1-S6) and a voltage sensor in the S4 segment that is responsible for opening the channel in response to membrane depolarization. Kv1.3 knockout (KO) mice are resistant to diet-induced obesity (*16, 17*), immune to experimental autoimmune encephalomyelitis (EAE)(*18*), and also exhibit enhance olfaction (*19*). These findings reveal the diverse functions of this voltage-gated channel, though its investigation has mostly been limited to autoimmune disease, ischemia, and the development of retinal ganglion cells. Kv1.3 also reportedly plays an important role in microglia mediated neuronal killing(*20*). Recently, Kv1.3 was shown to be upregulated in the post-mortem brains of Alzheimer's disease (AD) patients (*21*). Interestingly, Kv1.3 contains multiple proline-rich sequences to which Src homology (SH) domains can bind, and recently, our lab showed that Fyn, a src family kinase, is upregulated in PD models and plays an important role in microglial inflammation (*22*). Furthermore, Fyn inhibition has been

shown to reduce inflammation in AD (*23*). Clearly, the potential role of Kv1.3 in neuroinflammatory and neurodegenerative processes needs to be elucidated.

In this study, we have aimed to show the importance of microglial Kv1.3 in PD, and to further demonstrate the transcriptional and post-translational modification of this channel in PD models. Our *in vitro* studies show that Kv1.3 is highly upregulated in microglial cells treated with αSyn_{Agg}. Kv1.3 is also upregulated in multiple animal models of PD, and in post-mortem human PD brains. Kv1.3 upregulation was not confined to the brain, as monocytes isolated from PD patients contain higher levels of Kv1.3, making it a potential biomarker. Furthermore, we report that Fyn can regulate Kv1.3 both transcriptionally and post-translationally, thereby modulating channel activity. Lastly, PAP-1, a small molecule inhibitor of Kv1.3 that can cross the blood brain barrier, was able to reduce neuroinflammation and neurodegeneration in cell culture and animal models of PD. Our findings have significant pre-clinical potential and therapeutic implications for the treatment of PD.

Materials and Methods

Cell Culture, Primary Culture and Treatments

Primary microglial cells were isolated from mixed glial culture using a magnetic bead separation protocol published by our lab (*24, 25*). Primary cells were maintained in Dulbecco's modified Eagle's medium (DMEM)-F12, 10% fetal bovine serum (FBS), 1% sodium pyruvate, 1% glutamine, 1% penicillin-streptavidin, and 1% non-essential amino acids. A Mouse microglial cell (MMC) line was donated by Dr. D.T. Golenbock (University of Massachusetts Medical School, Worcester, MA). The MMC line was characterized by our group (*26*) and Halle *et al.* (*27*) and cultured in DMEM medium,

10% FBS, 1% glutamine, and 1% penicillin-streptavidin. Treatments were performed in 2% FBS-containing medium. Green fluorescent protein (GFP) and human αSyn overexpressing adeno-associated viruses (AAV-GFP, 0.95 X 10^{13} viral particles per mL and AAV-SYN, 1 X 10^{13} viral particles per mL) were obtained from The University of North Carolina Viral Vector Core. Both viral vectors were of the AAV-5 serotype and coded for GFP and human αSyn, respectively, under a chicken β-actin promoter.

Animal Studies

All animals were housed under standard conditions of constant temperature (22 ± 1°C), humidity (relative, 30%), and a 12 h light/dark cycle. Use of the animals and protocol procedures were approved by the Institutional Animal Care and Use Committee (IACUC) at Iowa State University (ISU), Ames, IA, USA.

αSyn-AAV Study

8-week old, male C57BL/6Ncrl mice were anesthetized with a xylazine/ketamine cocktail. Toe pinch was used to gauge a surgical depth of anesthesia. An incision was made at the back of the head and the area was disinfected using povidone-iodine. Mice were mounted on the Angle 2 stereotaxic apparatus (Leica Biosystems, St. Louis, MO). The bregma was found and the injection into the SN subsequently performed. The coordinates indicating distance (mm) from bregma were: anteroposterior (AP) -3.1, mediolateral (ML) -1.2, and dorsoventral (DV) -4.0. The injection rate for GFP-AAV or αSyn-AAV solution was 0.2 µL/min. The needle was left in for 5 min post-injection to maximize forward tissue diffusion and to minimize

backflow up needle track. The needle was retracted at the rate of 1 mm/min. Lactated Ringer's solution was subcutaneously injected post-surgery to assist recovery.

MitoPark Animal Study

MitoPark mice were originally generated and provided by Dr. Nils-Goran Larson at the Karolinska Institute in Stockholm (*28*). All mice for this study were bred, maintained, genotyped, and further characterized at ISU. MitoPark mice ($DAT^{+/Cre}$, $TFAM^{LoxP/LoxP}$) and their littermate controls ($DAT^{+/+}$, $TFAM^{+/LoxP}$) were fed *ad libitum* and housed under standard conditions approved and supervised by IACUC at ISU. Mice were weighed weekly and subjected to behavior tests every two weeks. Neurochemical, biochemical, and histological studies were performed following sacrifice at 24 weeks.

MPTP Animal Study

8 weeks old male C57BL/6NCrl mice were injected intraperitoneally (i.p.) with either 20 mg/kg MPTP or equal volumes of saline (vehicle) once daily for four consecutive days and sacrificed 24 h after the last MPTP injection (*29*).

αSyn_{Agg} Injection in $Fyn^{+/+}$ and $Fyn^{-/-}$ Mice

8-10 weeks old male $Fyn^{+/+}$ and $Fyn^{-/-}$ mice used in these studies were bred in our animal facility. $Fyn^{-/-}$ mice were originally obtained from Dr. Dorit Ron's laboratory at the University of California, San Francisco, and are available from Jackson Laboratory (stock number 002271). Mice were anesthetized as previously described and then injected with 4 µL of αSyn_{Agg} or vehicle. The coordinates indicating distance (mm) from bregma were: AP 0.7, ML 2 and DV 2.4.

MitoPark Animal Study with Saracatinib

8-week-old MitoPark mice were gavaged with saracatinib (25 mg/kg) or vehicle (0.5% HPMC in 0.1% Polysorbate 80) every alternate day for 8 weeks. Mice were weighed weekly. Neurochemical, biochemical, and histological studies were performed following sacrifice at 20 weeks**.**

MitoPark Animal Study with PAP-1

All mice for this study were bred, maintained, genotyped, and further characterized at Iowa State University. C57BL/6J and MitoPark mice were fed *ad libitum* and housed under standard conditions approved and supervised by IACUC at ISU. Fourteen-week-old mice (n=7-10/group) received either vehicle or 40 mg/kg/day PAP-1 for 30 days by i.p injection. Mice were weighed weekly and subjected to behavior tests biweekly. Neurochemical, biochemical, and histological studies were performed following sacrifice at 20 weeks.

MPTP Animal Study with PAP-1

Eight-week-old male C57BL/6NCrl mice (7 animals per group) were obtained from Charles River. From the *in vitro data,* we estimated 3-4 animals per group as sufficient to detect significant biochemical changes. All mice were pre-screened for normal baseline performance during behavioral assessments conducted before randomly assigning animals to experimental groups. All treatments were blinded and randomized. After acclimating for 3 days, mice were injected with 20 mg/kg daily for 5 days. After 2 h post-MPTP injections, mice were injected daily with either PAP-1 (i.p) at 40 mg/kg or vehicle (Miglyol-812) with these treatments continuing for 1 week after the last MPTP injection, after which the mice were sacrificed. This paradigm of MPTP exposure has been widely used in PD-related models of neurodegeneration (*29*).

Western Blot

Immunoblot analyses were performed following our previously published studies (*22, 30*). Briefly, cells or tissues were homogenized and lysed using modified RIPA buffer. Proteins were normalized using Bradford assay before loading on an SDS-acrylamide gel. Ten to 40 µg of protein was loaded in each well of 10-18% acrylamide gels, which were ran at 110 V for 2-3 h at 4°C. Following separation, proteins were transferred on a nitrocellulose membrane at 27 V for 18 h at 4°C. After transfer, the membranes were blocked with LI-COR (Lincoln, NE) blocking buffer for 45 min and incubated in primary antibodies and secondary antibodies following manufacturer's protocol. The primary antibodies included: anti-Kv1.3 (Alomone Labs, 1:1000) (AB_2040151), Kv1.3 (Sigma 1:1000) (AB_2265087) phospho-p38 (Cell Signaling Technologies, 1:1000) (AB_331641), p38 (Cell Signaling Technologies, 1:1000) (AB_330713), phospho-Kv1.3 (Sigma, 1:1000) (SAB4504254), and PKCδ (Santa Cruz, 1:500) (AB_628145) . The secondary antibodies included: IR-800 conjugated goat anti-mouse IgG (LI-COR, 1:20000), IR-700 conjugated goat anti-rabbit IgG (LI-COR 1:20000).

qRT-PCR

For RNA isolation, we followed previously published protocols (*26, 31*). Briefly, TriZol reagent was used to isolate total RNA from cells or tissues. NanoDrop was used to quantify RNA and 1 µg of RNA was converted to cDNA using the high capacity cDNA synthesis kit from Applied Biosystems (# 4368814, Foster City, CA). Quantitative SYBR green PCR assay was performed using qRT^{2}PCR SYBR Green Master Mix (Agilent Technologies, Santa Clara, CA) using pre-validated primers. The

following validated primers from Qiagen (Germantown, MD) were used: *pro-IL-1β* (QT01048355), *Nos2* (QT00100275), *Mfn2* (QT00134295), *CSF2* (QT00251286), *IL-6* (QT00098875), *TNFα* (QT00104006), mouse *Kv1.3* (QT00257467), human *Kv1.3* (QT00211197), *Kv1.1* (QT01537263), *Kv1.5* (QT00268387), *KCa3.1* (QT00105672), *Fyn* (QT00176666), and *18S* (QT02448075). The primers for *MRC1* and *IRF4* were synthesized at ISU's DNA facility. The fold change in gene expression was determined by $\Delta\Delta C_t$ method where C_t is the threshold value. 18S was used as the housekeeping gene.

Immunohistochemistry and Immunocytochemistry

Immunohistochemistry (IHC) was performed on 30-μm mouse striatal and nigral sections as well as human nigral sections as described in our previous publications (*32, 33*). For antigen retrieval, 10 mM citrate buffer at pH 7.4 was used for animal samples, whereas citraconic anhydride was used for human samples. Following antigen retrieval, sections were washed with PBS, blocked with blocking buffer (2% BSA, 0.5% Triton-X100, and 0.05% Tween 20) and incubated in primary antibodies overnight at 4°C. Next, sections were washed with PBS, incubated in secondary antibodies for 1 h and stained with Hoechst nuclear dye. Finally, sections were mounted on pre-coated slides and dried overnight before visualizing them under microscope. Confocal imaging was performed on these sections at ISU's Microscope Facility using a Leica DMEIR2 confocal microscope with 63X oil objective. For z-stacking, each optical section consisted of 10-15, 0.5-μm thick slices.

For immunocytochemistry (ICC) on immortalized and primary microglia, 4% PFA was used to fix the cells. Next, fixed cells were washed with PBS, blocked using blocking buffer and incubated in primary antibodies following manufacturer's protocol. Following overnight primary antibody incubation, cells were washed with PBS, incubated in secondary antibody for 75 min, and mounted on slides using Fluoromount aqueous mounting medium (Sigma, St. Louis, MO). Samples were visualized using an inverted fluorescence microscope (TE-2000U, Nikon, Tokyo, Japan). For DAB staining, we followed previously published protocols from our lab (*22, 30, 34*). The following primary antibodies were used: Iba1 (Wako, 1:1000) (AB_2314667), Iba1 (abcam, 1:500) (AB_870576), Kv1.3 (Alomone Labs, 1:500) (AB_2040151), Kv1.3 (Millipore, 1:500)(AB_11212692), phospho-Kv1.3 (Sigma 1:500) (SAB4504254), p38 (Cell Signaling Technology, 1:500) (AB_330713), and tyrosine hydroxylase (TH) (Millipore, 1:1000) (AB_2201526). Alexa dye-conjugated secondary antibodies were used for both ICC and IHC.

Flow Cytometry

We plated 50,000 MMCs per well in 12-well cell culture plates. Cells were treated with 1 μg/mL LPS or 1 μM αSyn_{Agg} for 24 h. Following treatment, cells were doubled washed with HBSS, and blocked with 2% BSA in HBSS for 30 min at 37° C. After blocking, cells were incubated in the Kv1.3 antibody conjugated to FITC (1:1000, in 1% BSA in HBSS) (AB_2040147) for 1 h at 37° C. Following incubation, any unbound antibody was double washed with HBSS and the cells were scraped from the plate and suspended in 500 μL HBSS. A FACSCanto cell analyzer (BD

Biosciences, San Jose, CA) was used for flow cytometry analysis at ISU's flow cytometry facility.

DuoLink Proximal Ligation Assay (PLA)

DuoLink PLA was performed according to previously published methods (*35*). Briefly, 10,000 primary microglial cells/well were plated on coverslips in 96-well cell culture plates. Cells were treated with 1 μM αSyn_{Agg} for 24 h, after which the cells were fixed with 4% PFA, blocked (2% BSA, 0.5% Triton-X100, 0.05% Tween20 in PBS), and incubated overnight in primary antibody. Following primary antibody incubation, Duolink In Situ Red Starter Kit (#DUO92101) was used according to manufacturer's protocol. Mouse Fyn monoclonal antibody (Thermo-Fisher, 1:500) (AB_1074491) and rabbit Kv1.3 antibody (Alomone Labs, 1:500) (AB_2040151) were used as primary antibodies. Slides were imaged using a Leica DMEIR2 confocal microscope with 63X oil objective. For z-stacking, each optical section consisted of 10-15, 0.5-μm thick slices.

Immunoprecipitation

Immunoprecipitation was performed following our lab's previously published protocol (*22*). Briefly, $5x10^6$ microglial cells were homogenized using NP40 lysis buffer. Lysates were incubated overnight with Fyn antibody (Thermo-Fisher) (AB_1074491) and Kv1.3 antibody Kv1.3 (Alomone Labs) (AB_2040151) separately. Protein G-sepharose beads were used for pull down. The lysates were incubated with the protein G-sepharose beads and then washed 4 times before loading.

Multiple Sequence Alignment

Kv1.3 sequences were downloaded from NCBI. T-Coffee was used for multiple sequence alignment of Kv1.3.

Whole-cell Patch Clamp

Primary microglia cultures were prepared as mixed glia cultures derived from P0 to P1 postnatal C57BL/6J wild-type, Fyn kinase KO, and PKCδ KO mice, as described in (*35*), and maintained in DMEM and 25 mM glucose supplemented with 10% FBS, 1 mM Na^+ pyruvate, 100 units/mL penicillin, and 100 µg/mL streptomycin. Cultures were maintained in a humidified, 5% CO_2 incubator at 37° C. Microglia were gently shaken off from their feeding astrocyte layer and harvested between 14 and 21 days in culture and plated at 100,000 – 150,000 cells per well in 24-well plates for 8 to 12 h before stimulation with either 300 ng/mL LPS or 1 µM αSyn_{Agg} in the presence or absence of 10 µM saracatinib. After 40-48 h post-stimulation, microglial cells were detached by trypsinization, washed, attached to poly-L-lysine-coated glass coverslips, and then studied within 20 to 90 min after plating in the whole-cell mode of the patch-clamp technique with an EPC-10 HEKA amplifier. B lymphocytes were thawed, plated, and maintained in a tissue culture incubator for 30 to 60 min before recording. All currents were recorded in normal Ringer's solution containing (in mM): 160 NaCl, 4.5 KCl, 2 $CaCl_2$, 1 $MgCl_2$, 10 HEPES (adjusted to pH 7.4 and 290–310 mOsm). Patch pipettes were pulled from soda lime glass (micro-hematocrit tubes, Kimble Chase, Rochester, NY) to resistances of 2-3 MΩ when submerged in the bath solution and filled with a KF-based Ca^{2+}-free internal pipette solution containing (in mM): 145 KF, 2 $MgCl_2$, 10 HEPES, 10 EGTA (pH 7.2, 290–310 mOsm). K^+ currents were elicited with voltage ramps from −120 to 40 mV of 200 ms duration applied every 10 s and

Kv1.3 current was identified as an outward rectifying current component at depolarized membrane potentials positive to -20 mV and sensitive to the selective inhibitor PAP-1. Additionally, Kv1.3 currents were identified by their distinct use-dependent C-type current inactivation induced by repeated stimulation to +40 mV at a frequency of 1 Hz. Cell capacitance, a direct measurement of cell surface area, and access resistance were continuously monitored during recordings. Kv1.3 current density is calculated as current amplitude divided by the cell capacitance measured for individual cells.

LC/MS for PAP-1 detection

Stock and working standard solutions of PAP-1 were prepared in acetonitrile.. Spiked serum samples for a calibration curve were obtained by spiking 180 µL of drug-free serum with PAP-1 solutions (final volume 200 µL) to yield a final concentration range of 5 nM to 5 µM and were used immediately. Commercial SPE cartridges (Hypersep C18, 100 mg, 1 mL) were purchased from Thermo Scientific (Houston, TX, U.S.A). Before the extraction, cartridges were conditioned with acetonitrile (2 × 1 mL), followed by water (2 × 1 mL). After loading the SPE cartridges with serum samples, they were washed successively with 1 mL each of 20% and 40% acetonitrile in water followed by elution with 2 mL of acetonitrile. Eluted fractions were collected and evaporated to dryness. The residues were reconstituted to solution with 200 µL acetonitrile and were used for LC-MS analysis.

Brain samples were treated as follows: 4.0 mL of acetonitrile was added to 200 mg of brain sample, which was homogenized thoroughly using a T25 digital ULTRA-TURRAX homogenizer (IKA Works Inc., NC, USA). The homogenized samples were

centrifuged for 10 min at 4000 rpm, and then the supernatant was separated and evaporated under a constant air flow as described above. The residues were reconstituted in 200 µL acetonitrile. The reconstituted material was loaded onto the preconditioned SPE cartridges and then eluted with 2 mL of acetonitrile. Load and eluted fractions were collected and evaporated to dryness. The residues were reconstituted in solution with 200 µL acetonitrile and were used for LC/MS analysis. LC/MS analysis was performed with a Waters Acquity UPLC (Waters, NY, USA) equipped with an Acquity UPLC BEH 1.7µM C-18 column (Waters, New York, NY) interfaced to a TSQ Quantum Access Max mass spectrometer (MS) (Thermo Fisher Scientific, Waltham, MA, USA). The isocratic mobile phase consisted of 80% acetonitrile and 20% water, both containing 0.1% formic acid with a flow rate of 0.25 mL/min. Under these conditions, PAP-1 had a retention time of 1.05 minute.

Using heated electrospray ionization source (HESI II) in positive ion mode, capillary temperature 270° C, vaporizer temperature 350° C, spray voltage 3000 V, sheath gas pressure (N2) 30 units, PAP-1 was analyzed by the selective reaction monitoring (SRM) transition of its molecular ion peak 351.16 (M+1) into 107.19 m/z. A 10-point calibration curve ranging from 5 nM to 10 µM was developed for quantification.

HPLC

HPLC for neurotransmitters was performed following previously published methods (*26*). Briefly, the left striatum was weighed and lysed using an extraction solution (0.1 M perchloric acid containing 0.05% Na_2EDTA and 0.1% $Na_2S_2O_5$) and isoproterenol (internal standard). A C-18 reversed phase column isocratically separated dopamine, 3,4-dihydroxyphenylacetic acid (DOPAC), homovanillic acid

(HVA) and norepinephrine (NE) using a Dionex Ultimate 3000 HPLC system (pump ISO-3100SD, Thermo Scientific, Bannockburn, IL), and a detector equipped with a CoulArray model 5600A coupled with an analytical cell (microdialysis cell 5014B) and a guard cell (model 5020) with potentials set at 350, 0, -150, and 220 mV. Chromeleon 7 and ESA CoulArray 3.10 HPLC software were used for data acquisition and analysis.

Multiplex cytokine assays

Multiple cytokine assay was performed according to our previous publication (*22*). Briefly, 40 µL of treatment media was incubated overnight with 40 µL of primary antibodies conjugated with magnetic beads. Following incubation with primary antibodies, samples were washed, incubated with biotinylated antibody and with biotin/streptavidin, and then assayed on a Bio-Plex plate reader. Standards were obtained from Peprotech.

Griess Assay

Griess assay was performed as previously described in our publication (*22*). Briefly, after treatment, 50 µL of medium was incubated with 50 µL of Griess reagent for 10 min and a plate reader was used to read the absorbance at 540 nm.

Statistical Analysis

GraphPad 5.0 was used for statistical analysis with $p \leq 0.05$ considered statistically significant. One-way ANOVA was used for comparing multiple groups. In

most cases, Tukey post analysis was applied. Student's t-test was used for comparing 2 groups.

Results

Upregulation of Kv1.3 potassium channel expression upon αSyn_{Agg} stimulation in microglial cells *in vitro*

Since αSyn_{Agg} contributes to chronic neuroinflammation by activating microglia (*36*), and since microglial $K_v1.3$ plays an important role in neuronal death and damage (*20*) and is also upregulated in AD brains (*21*), we characterized changes in Kv1.3 levels in primary microglia treated with αSyn_{Agg} for 24 h. Whole-cell patch clamping revealed that the αSyn_{Agg} treatment increased functional Kv1.3 channel activity (Fig. 1A). Our qRT-PCR analysis showed that αSyn_{Agg} specifically induced Kv1.3 mRNA expression without inducing other potassium channels such as KCa3.1, Kv1.1, or Kv1.5 (Fig. 1B). Likewise, $K_v1.3$ protein level also increased as revealed by Western blot analysis (Fig. 1C) and ICC (Fig. 1D). Next, we corroborated each of our primary microglia findings using MMCs by both qRT-PCR analysis (Supplementary Fig. 1A), ICC (Supplementary Fig. 1B) and Western blot analysis (Supplementary Fig. 1C). Moreover, whole-cell patch clamping revealed that LPS-induced Kv1.3 channel activity (Supplementary Fig. 1D) in primary microglial cells. Furthermore, flow cytometry analysis using a FITC-labelled Kv1.3 antibody against an extracellular epitope revealed that αSyn_{Agg} (Fig. 1E) induced surface expression of Kv1.3. After treating the MMCs with LPS (1 µg/mL) and IL-4 (20 ng/mL) for 6 h to induce classical and alternative activation, respectively, we observed LPS-induced $K_v1.3$ mRNA expression, while IL-4 did not alter $K_v1.3$ expression (Supplementary Fig. 1F), further

validating that this voltage-gated potassium channel is related to the classical, pro-inflammatory activation of microglia which also corroborates previously published data (*10*). Flow cytometry also confirmed that LPS induces surface Kv1.3 expression in MMCs (Supplementary Fig. 1E). Following our *in vitro* studies of microglia cultures, we next adopted an *ex vivo* organotypic midbrain slice culture model, wherein qRT-PCR found that a 24-h exposure to 1 μM of αSyn_{Agg} significantly induced expression of Kv1.3 mRNA (Fig. 1F) and the pro-inflammatory genes *Nos2, CSF2, IL-6, IL-1β* and *TNFα* (Supplementary Fig. 1G). The αSyn_{Agg}-induced Kv1.3 expression in the midbrain slice culture was also revealed by immunoblot analysis (Fig. 1G). Our series of *in vitro* models of synucleinopathy also included experiments on human-derived lymphocytes obtained from PD patients, which showed higher expression of $K_v1.3$ when compared to lymphocytes from age-matched controls (Fig. 1H). Lastly, whole-cell patch clamping revealed that lymphocytes from PD patients had higher Kv1.3 channel activity than did lymphocytes from age-matched controls (Fig. 1I). Collectively, these findings demonstrate that inflammatory stimuli, such as LPS or αSyn_{Agg}, induce functionally relevant increases in microglial $K_v1.3$ protein and mRNA levels as indicated by enhanced channel activity in microglial cells. Taken together, these data suggest a possible role of $K_v1.3$ in PD pathogenesis and progression.

Kv1.3 channel expression is highly induced in microglial cells in experimental *in vivo* models of PD and in postmortem human PD brains

PD is a multifactorial disease and to date no *in vivo* model can reproduce all the symptoms of PD. Hence, to better understand the potential role of Kv1.3, we utilized multiple animal models of PD to recapitulate various clinical and pathological

aspects of the disease. One of the major pathological hallmarks in PD is protein aggregation, which can be recapitulated in the αSyn-AAV mouse model (*37*), wherein αSyn-AAV was stereotaxically injected into the striatum and the mice were sacrificed 6 mo later (Supplementary Fig. 2A). Western blot analysis revealed a rapid induction of K_V1.3 in this animal model of PD (Fig. 2A).

To verify whether Kv1.3 channel expression is induced in a more gradually progressive PD model, we utilized the recently developed MitoPark transgenic mouse model. MitoPark mice were developed by inactivating the mitochondrial transcription factor A (TFAM) in dopaminergic neurons (*28*) to model the mitochondrial dysfunction exhibited by the progressively neurodegenerative Parkinsonian syndrome with its diverse spectrum of motor and nonmotor symptoms. In this model, progressive dopaminergic degeneration and PD-like motor deficits begin at around 12 weeks of age, and these motor deficits are accompanied by a progressive loss of striatal dopamine beginning at 20 weeks (*28, 34, 38, 39*). Herein, we show that Kv1.3 gene expression was highly induced in the SN of 16- and 24-week old MitoParks as compared to age-matched littermate controls (Fig. 2B). Our Western blot analysis further revealed that Kv1.3 was upregulated in 24-week-old MitoPark mice (Fig. 2C), and we confirm that this upregulation was localized to Iba-1-positive SN microglia (Fig. 2D).

Next, we adopted the well-characterized subacute MPTP paradigm where mice received 20 mg/kg MPTP daily for 4 consecutive days and were sacrificed on the 5th day (Supplementary Fig 2B). This subacute MPTP paradigm has been associated with significant CNS neuroinflammation and dopaminergic degeneration (*33, 40-42*).

In line with our *in vitro* results, MPTP significantly increased mRNA and protein expression of nigral Kv1.3 (Fig. 2E-2F).

To further establish Kv1.3's clinical relevance in the Parkinsonian syndrome, we assessed Kv1.3 channel expression in postmortem human brains from patients with PD and dementia with Lewy bodies. When comparing striatal brain sections, we observed Kv1.3 mRNA levels that were higher in postmortem human PD than in control brains (Fig. 2G). Western blot analysis of PD and age-matched controls further showed increased Kv1.3 levels in the substantia nigra (Fig. 2H). Immunostaining for Kv1.3 and Iba-1 further showed upregulated Kv1.3 immunoreactivity in the SN of PD brain sections that was localized to Iba-1-positive microglia (Fig. 2I). Histochemical analysis of DLB postmortem brains revealed significantly increased Kv1.3 expression in HLA-DR-positive microglial cells (Fig. 2J). Together, these findings demonstrate that microglial Kv1.3 is highly induced in both animal models and PD patients.

Fyn modulates transcriptional regulation of Kv1.3 in microglial cells through the Fyn-PKCδ kinase signaling cascade

After confirming the expression of Kv1.3 in various animal models and cell culture models of PD, we investigated the molecular mechanism behind the transcriptional upregulation of the Kv1.3 gene. Though a recent study demonstrated the epigenetic regulation of Kv1.3 (*43*), its transcriptional regulation is not well understood. Our *in silico* analysis of the Kv1.3 promoter revealed multiple NFκB and SP1 binding sites (Fig. 3A), and D'Addario *et al.* (*44*) showed that SP1 phosphorylation is dependent on the p38 MAPK pathway. Hence, we used the cell-permeable NFκB

inhibitor SN50 and the p38 MAPK inhibitor SB203580. Both inhibitors independently attenuated αSyn_{Agg}-induced Kv1.3 upregulation in the microglial cell line (Fig. 3B).

We previously demonstrated that Fyn acts as a regulator of the NFκB transcription factor by regulating the nuclear translocation of p-65 (*22*). Fyn has also been shown to modulate LPS-induced activation of the p38 MAPK pathway. Our Western blot analysis of primary microglial cultures revealed that Fyn KO attenuated αSyn_{Agg}-induced p38 phosphorylation (Fig. 3C), further demonstrating the probable role of Fyn upstream of the p38 MAPK pathway. Fyn KO in primary microglial cultures also attenuated αSyn_{Agg}-induced Kv1.3 expression as revealed by qRT-PCR (Fig 3D) and ICC (Fig. 3F) analyses. Our whole-cell patch clamp study on LPS-treated microglial cells revealed that Fyn KO microglia have lower Kv1.3 current density compared to wild-type (Fig. 3E). Next, we pharmacologically inhibited Fyn in αSyn_{Agg}-microglial cells by co-treating them with Saracatinib (1 μM) for 6 h. Electrophysiological analysis revealed that Saracatinib reduced both LPS and αSyn_{Agg}-induced Kv1.3 channel activity, suggesting the probable role of Fyn in modulating Kv1.3 activity (Supplementary Fig. 3A). Western blot and qRT-PCR analyses revealed that Saracatinib reduced αSyn_{Agg}-induced p38 activation (Supplementary Fig. 3B), Kv1.3 expression (Supplementary Fig. 3E), as well as the pro-inflammatory gene *Nos2* (Supplementary Fig. 3D) and the cytokines TNF-α and IL-1β (Supplementary Fig. 3F-G), without altering the mRNA expression of Fyn itself (Supplementary Fig. 3C). When we injected αSyn_{Agg} in Fyn WT and KO animals, IHC analysis revealed 6 mo post-injection that Fyn KO had attenuated αSyn_{Agg}-induced

Kv1.3 protein expression in the SN (Fig. 3G), further suggesting a probable role of Fyn kinase in modulating Kv1.3 upregulation.

Our group recently showed that PKCδ, a serine/threonine kinase involved in microglial inflammation (*30*), is modulated by Fyn (*22*). In this study, we demonstrate that PKCδ is significantly induced in primary microglial culture (Supplementary Fig. 4A), as well as in the previously described αSyn-AAV (Supplementary Fig. 4B) and MPTP (Supplementary Fig. 4C) mouse models of PD. In microglial cells, PKCδ KO attenuated the αSyn_{Agg}-induced production of the pro-inflammatory cytokines IL-1β, TNF-α, and IL-6 (Supplementary Fig. 4D-F), solidifying the role of this novel PKC kinase in inflammation. To further validate the role of the Fyn-PKCδ proinflammatory cascade in mediating p38 MAPK pathway activation, we treated WT and PKC KO primary microglial cells with 1 μM αSyn_{Agg} for 5-30 min. PKCδ KO in primary microglial culture attenuated αSyn_{Agg}-induced p38 phosphorylation as revealed by Western blot (Fig. 3H), while ICC revealed reduced nuclear translocation of p65 (Supplementary Fig. 4G). Next, primary microglial cells were treated with 1 μM αSyn_{Agg} for 1 h, after which qRT-PCR (Fig 3I) and ICC (Supplementary Fig. 4H) revealed that PKCδ KO attenuated αSyn_{Agg}-induced Kv1.3 mRNA and protein expression. Moreover, whole-cell patch clamp revealed that PKCδ KO reduced Kv1.3 current density in microglia treated with either αSyn_{Agg} (1μM) for 24 h or LPS (300 ng/mL) for 48 h (Fig. 3J). These findings collectively suggest that the Fyn-PKCδ kinase signaling cascade plays a crucial role in Kv1.3 upregulation in response to inflammatory stimuli.

Fyn modulates post-translational modification of Kv1.3

Post-translational modification of Kv1.3 activities and other cellular functions have been attributed to phosphorylation of serine/threonine residues or tyrosine residues by various kinases, and de-phosphorylation by phosphatases (*45-48*). As part of its N-terminal and C terminal end, Kv1.3 has a proline-rich region, which can bind to the src-homology domain 3 (SH3) of src kinases. Our group has recently linked Fyn to the regulation of microglial inflammation (*22*), which prompted us to hypothesize that Fyn plays an important role in regulating the phosphorylation profile of Kv1.3 (*49*). Our multiple sequence alignment using T-Coffee (*50*) to align N-terminal of Kv1.3 sequences from seven different organisms demonstrated that Kv1.3 is highly conserved and that the tyrosine residue at 139 is conserved in all species (Supplementary Fig. 5A). Our *in silico* docking analysis revealed a probable interaction between Fyn and Kv1.3 (Fig. 4A).

To further verify if Fyn directly interacts with Kv1.3, we performed co-immunoprecipitation (IP). Primary microglial cells were treated with αSyn_{Agg} for 24 h following which Fyn and Kv1.3 were pulled down and probed for Kv1.3 and Fyn, respectively. Our immunoblot analysis revealed that following αSyn_{Agg} exposure Fyn interacted with Kv1.3 (Fig. 4B). We performed a proximal ligation assay using DuoLink, which further verified the interaction of Fyn with Kv1.3 (Fig. 4C). We also treated primary microglial from $Fyn^{+/+}$ and $Fyn^{-/-}$ mice with αSyn_{Agg} and both our Western blot (Fig. 4D) and ICC (Supplementary Fig. 6A) analyses revealed that the αSyn_{Agg}-induced upregulation of phosphorylation of Kv1.3 at 139-residue is diminished in $Fyn^{-/-}$ microglia. Whole-cell patch clamp revealed that αSyn_{Agg} and LPS-

treated $Fyn^{-/-}$ primary microglial cells exhibited reduced current amplitudes compared to $Fyn^{+/+}$ (Fig. 4E). To confirm that these *in vitro* Fyn-Kv1.3 interactions also apply *in vivo,* we gavaged MitoPark mice with the Fyn inhibitor saracatinib daily from 8 to 16 weeks of age. IHC analysis revealed that Fyn inhibition had increased pKv1.3 in the SN region of 16-week-old MitoPark mice, specifically by reducing the induction of pY139Kv1.3 (Fig. 4F). These data collectively suggest that Fyn modulates the phosphorylation of Kv1.3 at tyrosine residue 139 in PD models.

To further evaluate the role of this phosphorylation at residue 139, we utilized site-directed mutagenesis. MMCs were transfected with a Kv1.3 plasmid where the tyrosine residue at 139 was mutated to alanine. Following transfection, cells were treated with 1 μM αSyn_{Agg} for 24 h. Western blot analysis revealed that the mutation attenuated the αSyn_{Agg}-induced upregulation of Kv1.3 phosphorylation (Supplementary Fig. 6B), while qPCR, Griess assay and Luminex analyses further revealed reduced αSyn_{Agg}-induced upregulation of *Nos2* mRNA (Fig. 4G), nitrite release (Fig. 4H) and the pro-inflammatory cytokine IL-1β (Fig. 4I-J). Together, these results suggest that Fyn phosphorylates Kv1.3 at residue 139 and that Fyn-induced tyrosine phosphorylation plays a role in Kv1.3-mediated inflammation in PD models.

Kv1.3 modulates neuroinflammation in a cell culture model of PD

Given the potential role of Kv1.3 in modulating inflammation in various disease models including MS and AD (*21, 51*), we performed a series of Kv1.3 knockout and overexpression studies to demonstrate the role of Kv1.3 in αSyn_{Agg}-induced microglial activation. Primary microglial cells were isolated from Kv1.3 WT and KO animals, and treated with αSyn_{Agg} for 24 h. Luminex assays of the αSyn_{Agg}-treated WT and KO

media revealed that primary microglial cells from Kv1.3 KO mice secreted significantly less TNF-α (Fig. 5A), IL-12 (Fig. 5B) and IL-1β (Fig. 5C) compared to WT microglial cells. Next, we overexpressed K_v1.3 in MMCs, and treated with αSyn_{Agg} for 24 h. Our qRT-PCR analys s revealed that K_v1.3 overexpression (Supplementary Fig. 7) significantly increased αSyn_{Agg}-induced mRNA levels of Nos2 (Fig. 5D, pro-IL-1β (Fig. 5E), and TNF-α (Fig. 5F). Multiplex assays further revealed that K_v1.3 overexpression significantly induced the secretion of IL-6 (Fig. 5G) and IL-12 (Fig. 5H). These data collectively suggest that K_v1.3 plays an important role in αSyn_{Agg}-induced microglial inflammation.

The small molecule PAP-1 is a pharmacological inhibitor that specifically blocks K_v1.3 activity (*52*), and is known to reduce inflammation in various model systems (*53, 54*). We co-treated primary murine microglia with αSyn_{Agg}. Patch clamping showed that PAP-1 blocked Kv1.3 currents in αSyn_{Agg}-stimulated microglia (Fig. 5I). An LDH assay revealed that PAP-1 blocked the αSyn_{Agg}-induced increased release of LDH into the extracellular space (Fig. 5J). PAP-1 also significantly reduced the αSyn_{Agg}-induced pro-inflammatory cytokines IL-12 (Fig. 5K), TNF-α (Fig. 5L), and IL-6 (Fig. 5M) as revealed by Luminex multiplex cytokine analysis. To further demonstrate the efficacy of PAP-1 in reducing microglial inflammation, MMCs were co-treated with PAP-1 (1 μM) and αSyn_{Agg}. The Griess assay showed that PAP-1 reduced αSyn_{Agg}-induced nitrite release in these immortalized microglial cells (Supplementary Fig. 8A), while our qRT-PCR analysis revealed that PAP-1 reduced expression of the αSyn_{Agg}-induced inflammatory genes *Nos2* (Supplementary Fig. 8B), *IL-6* (Supplementary Fig. 8C), *TNF-α* (Supplementary Fig. 8D) and *IL-1β* (Supplementary Fig. 8E). However,

PAP-1 treatment did not induce the markers for alternative activation of microglia, IRF4 (Supplementary Fig. 8F) and MRC1 (Supplementary Fig. 8G). Luminex assays further demonstrated that PAP-1 can significantly attenuate αSyn_{Agg}-induced release of the pro-inflammatory cytokines IL-1β (Supplementary Fig. 8H), TNF-α (Supplementary Fig. 8I) and IL-6 (Supplementary Fig. 8J). Together, these findings suggest that the microglial channel Kv1.3 contributes to classical microglial activation, which can be attenuated by PAP-1, but Kv1.3 inhibition does not promote the alternative activation.

PAP-1 reduced inflammation and neurodegeneration in mouse models of PD

PAP-1 has been widely used in animal models of various diseases including psoriasis, obesity, and ischemic stroke (*53*) and its chronic administration is well tolerated in mice, rats, adn primates (*17*). To validate the therapeutic potential of PAP-1 in Parkinsonian syndrome, we utilized the transgenic MitoPark and the toxin-based MPTP mouse models of PD.

MitoPark mice were injected daily with 40 mg/kg PAP-1 from 14 to 20 weeks of age (Supplementary Fig. 9A). During treatment, no significant weight loss was observed (Supplementary Fig. 9B). Furthermore, blood chemistry revealed no significant changes between PAP-1- and vehicle-treated MitoPark groups or between MitoPark and littermate control groups (Supplementary Fig. 9C). To verify the bioavailability and brain penetrance of PAP-1, LC-MS analysiss was performed on serum and brain samples taken at the end of the study, revealing that treated animals had average total plasma concentrations of 322±122 and brain concentrations of 848±295 at 24 hours after the last administration (Fig. 6A). No PAP-1 was detectable

in the plasma and brain of vehicle treated animals. Behavioral tests revealed that PAP-1 significantly reduced motor deficits in MitoPark mice. As evident from the VersaPlot (Fig. 6B), PAP-1 treatment significantly increased horizontal activity in the open-field test (Fig. 6C). PAP-1 also significantly increased the time spent on the rotarod by MitoPark mice (Fig. 6D). Biochemical analysis of the striatum revealed that PAP-1 reduced the loss of the neurotransmitter dopamine (Fig. 6E) and its derivatives DOPAC (Fig. 6F) and homovanillic acid (HVA) (Fig. 6G) in MitoPark mice, however, no significant changes in norepinephrine (Fig. 6H) were observed.

Next, we evaluated the efficacy of PAP-1 in protecting against MPTP-induced neuronal loss and inflammation (Supplementary Fig. 10A). IHC analysis further demonstrated that PAP-1 reduced MPTP-induced microgliosis in both the striatum and SN (Fig. 6I). Skeletonization analysis revealed that PAP-1 reduced microglial soma size and increased the number of branches compared to MPTP alone (Fig. 6J). Increased microglial soma size and decreased branch number are indicative of classical activation of microglia. Moreover, qRT-PCR analysis revealed that Kv1.3 inhibition reduced the MPTP-induced expression of the pro-inflammatory cytokines TNF-α and pro-IL-1β (Fig. 6K). Biochemical analysis revealed that PAP-1 significantly increased the amount of dopamine (Supplementary Fig. 10E) and its metabolites DOPAC (Supplementary Fig. 10C) and HVA (Supplementary Fig. 10D) as compared to MPTP alone. TH neuronal staining further demonstrated that PAP-1 protected against MPTP-induced TH loss in the SN (Fig. 6L). Stereology analysis revealed that pharmacological inhibition of Kv1.3 protected against the MPTP-induced loss of TH-positive neurons (Fig. 6M). Collectively, these pre-clinical studies suggest that PAP-1

can reduce microgliosis, inflammation, and neuronal loss in PD models and that inhibition of Kv1.3 by a brain penetrant small molecule has clinical potential for PD treatment.

Discussion

Although neuroinflammation is one of the key pathophysiological hallmarks of neurodegenerative disorders, including PD, the molecular mechanisms and the key regulators of this chronic, sustained inflammation are not well understood (*4*). Recently, various anti-inflammatory drugs targeting cellular pathways modulating inflammation have gained importance in clinical and preclinical trials in AD and PD (*23, 55*). In the present study, we demonstrate for the first time that the microglial voltage-gated potassium channel $K_V1.3$ is upregulated in Parkinsonian syndrome. We showed previously that exposure to an inflammagen activates the SFK kinase Fyn, which regulates the p38 MAPK and the NFκB pathways in microglial cells (*22*) and that Fyn phosphorylates PKCδ, a novel PKC isoform that also regulates the microglial NfκB pathway (*30*). In this study, we reveal that both the p38 MAPK and the classical NfκB pathways mediate the transcriptional regulation of Kv1.3. Furthermore, we identify the Fyn-PKCδ inflammatory pathway as one of the key regulators of Kv1.3 transcription. We demonstrate that the phosphorylation profile of Kv1.3 can be modulated by αSyn_{Agg} and that Fyn kinase plays an important role in this αSyn_{Agg}-induced Kv1.3 phosphorylation. Finally, we show that PAP-1, a brain penetrant small molecule Kv1.3 inhibitor, can reduce neuroinflammation and neurodegeneration in multiple animal models of PD.

The role of microglia in mediating neurodegeneration in PD was first identified in 1988 (*56*), and neuroinflammation has since then been an active area of PD research. Although the exact molecular mechanism of this sustained inflammation remains equivocal, meta-analyses have revealed that non-steroidal anti-inflammatory drugs (NSAIDs) can protecting against neurodegenerative disorders (*57*). Recent studies have shown that αSyn_{Agg}, a major component of Lewy bodies and neurites, can be transferred from cell-to-cell in a prion-like manner, leading to the spread of disease pathology (*58*). Although αSyn_{Agg} can induce inflammation in cell culture and animal models of PD, the downstream signaling mechanism is not well understood (*30*). In this study, we show that microglial Kv1.3 is upregulated in response to αSyn_{Agg}. This induction of Kv1.3 is seen in multiple *in vivo* models of PD, recapitulating various key hallmarks of PD. Moreover, Kv1.3 is also upregulated in Parkinsonian syndrome patients (PD and DLB).

Ion channels play an important role in the immune system by regulating membrane potential and calcium signaling. The potassium channels Kv1.3 in particular is widely regarded as promising target for immunosuppression (*59*) and has been demonstrated to constitute a valid target for treating T cell mediated autoimmune diseases in animal models of multiple sclerosis, autoimmune diabetes, rheumatoid arthritis, and psoriasis (*54*). Kv1.3 blockers have also been shown rescue neurogenesis by inhibiting gramizydine granzyme B releasing CD8+ T cells (*60*). In microglial cells, the resident immune cells of the brain, Fordyce *et al.* (*20*) demonstrated in 2005 that Kv1.3 is involved in microglia mediated neuronal killing, while others (*61*) have implicated Kv1.3 in HIV-induced microglial neurotoxicity. More

recently, two studies, including us, have shown that increased Kv1.3 expression in microglia is associated with classical “M1-like” activation (*10*) and that Kv1.3 is involved in modulating microglia-induced inflammation, phagocytosis and antigen presentation (*62*). In humans, increased microglial Kv1.3 expression has further been demonstrated in postmortem AD and stroke brains, while the Kv1.3 blocker PAP-1 has been found to reduce neuroinflammation and improve cognition or neurological deficit in rodent models of Alzheimers disease and ischemic stroke (*63*). Interestingly, Kv1.3-mediated current has been reported to be reduced in striatal cholinergic neurons (*64*) in PD mouse model, similar to the finding that ion channel activity decreases in dopaminergic neurons in PD animal models (*65*). However, it is not clear how this observation relates to our proof-of-concept animal studies reported here that demonstrate that Kv1.3 inhibition with PAP-1 protects from neuronal loss and inflammation in PD models and which further support an important role for Kv1.3 in neuroinflammation.

Research on the transcriptional regulation of Kv1.3 has been limited. Recent Kv1.3 studies have implicated the enzyme cereblon in its epigenetic regulation (*43*), its age-dependent methylation in colorectal cancer patients (*66*), and DNA methylation of its promoter in breast cancer (*67*). Also, p38 MAPK in microglia has been shown to modulate Kv1.3 expression in HIV-glycoprotein 120-induced neurotoxicity (*61*). In this study, we identified the NfκB and p38 MAPK pathways as contributing to the αSyn_{Agg}-induced transcriptional upregulation of Kv1.3. Our group showed previously that Fyn is induced in cell culture and animal models of PD, and is important in modulating microglial inflammation by mediating the NfκB and p38 MAPK pathways (*22*). We also

showed that Fyn is upstream of the pro-apoptotic and pro-inflammatory kinase PKCδ (*22, 30*). Fyn also has a role in regulating inflammation in AD, wherein inhibiting Fyn kinase with saracatinib protects against neurodegeneration in rodent models of AD (*23*). We report here that Fyn and PKCδ regulate Kv1.3 transcription by regulating NfκB and p38 MAPK signaling. We significantly reduced Kv1.3 expression as well as its transcriptional upregulation by pharmacologically inhibiting Fyn. Our results collectively show that the Fyn-PKCδ inflammatory signaling cascade modulates Kv1.3 transcriptional upregulation.

Post-translational modification of potassium channels, leading to modulation of channel activity, has been actively researched. Kv1.3 has multiple phosphorylation sites, including both tyrosine and serine/threonine (*45, 46*). Jimenez-Perez *et al.* (*68*) implicated Kv1.3's tyrosine phosphorylation sites in modulating proliferation. Holmes et al. (*45*) demonstrated that endogenous kinases and phosphates continuously phosphorylate and dephosphorylate Kv1.3 and any change in this dynamic phosphorylation/ dephosphorylation can drastically alter Kv1.3 activity. Various tyrosine kinase proteins, including v-Src, are known to phosphorylate Kv1.3, and different adaptor proteins, including Grb10, modulate this phosphorylation of Kv1.3, thereby differentially regulating its activity (*19, 48*). We show here that Fyn, a non-receptor tyrosine kinase, can phosphorylate Kv1.3, thereby modulating its function.

Collectively, we demonstrate that Kv1.3 is upregulated in Parkinsonian syndrome models. This upregulation is controlled by the Fyn-PKCδ kinase signaling cascade through the NFκB and p38 MAPK pathways. Fyn can further phosphorylate Kv1.3, which modulates Kv1.3 channel activity. Kv1.3 upregulation in PD models plays

a major role in neuroinflammation-mediated neurodegeneration. These findings further demonstrate a probable Kv1.3-mediated signaling cascade (Supplementary Fig. 11) that can modulate microglial inflammation in a Parkinsonian syndrome. The diverse roles of Kv1.3 emerging from our findings together with other studies have potential therapeutic implications.

Conflict of interest

AGK and VA are shareholders of PK Biosciences Corporation (Ames, IA), which is interested in identifying novel biomarkers and potential therapeutic targets for PD. AGK and VA do not have any commercial interests in the work presented herein. HW is an inventor on University of California patent claiming PAP-1 as an immunosuppressant. This patent has recently been abandoned because of its short remaining patent life.

Acknowledgements

This study was supported by NIH grants NS088206 and NS100090. Special thanks to Dr. Golenbock of U. Mass Med School for providing the MMC cell line. The W. Eugene and Linda Lloyd Endowed Chair and Eminent Scholar to AGK and the Salisbury Endowed Chair to AK are also acknowledged. We also thank Mr. Gary Zenitsky for assistance in preparing this manuscript and the Alzheimer's Disease Center at UC Davis for supplying AD and DLB samples.

Reference

1. K. J. Doorn *et al.*, Emerging roles of microglial activation and non-motor symptoms in Parkinson's disease. *Prog Neurobiol* **98**, 222-238 (2012).
2. E. Wolters, Non-motor extranigral signs and symptoms in Parkinson's disease. *Parkinsonism Relat Disord* **15 Suppl 3**, S6-12 (2009).
3. M. G. Tansey, M. S. Goldberg, Neuroinflammation in Parkinson's disease: its role in neuronal death and implications for therapeutic intervention. *Neurobiology of disease* **37**, 510-518 (2010).
4. M. L. Block, L. Zecca, J. S. Hong, Microglia-mediated neurotoxicity: uncovering the molecular mechanisms. *Nat Rev Neurosci* **8**, 57-69 (2007).
5. C. K. Glass, K. Saijo, B. Winner, M. C. Marchetto, F. H. Gage, Mechanisms underlying inflammation in neurodegeneration. *Cell* **140**, 918-934 (2010).
6. K. Imamura *et al.*, Distribution of major histocompatibility complex class II-positive microglia and cytokine profile of Parkinson's disease brains. *Acta Neuropathol* **106**, 518-526 (2003).
7. C. Kim *et al.*, Neuron-released oligomeric alpha-synuclein is an endogenous agonist of TLR2 for paracrine activation of microglia. *Nature communications* **4**, 1562 (2013).
8. A. Gustot *et al.*, Amyloid fibrils are the molecular trigger of inflammation in Parkinson's disease. *Biochem J* **471**, 323-333 (2015).
9. G. Codolo *et al.*, Triggering of inflammasome by aggregated alpha-synuclein, an inflammatory response in synucleinopathies. *PLoS One* **8**, e55375 (2013).

10. H. M. Nguyen *et al.*, Differential Kv1.3, KCa3.1, and Kir2.1 expression in "classically" and "alternatively" activated microglia. *Glia* **65**, 106-121 (2017).

11. S. G. Daniele *et al.*, Activation of MyD88-dependent TLR1/2 signaling by misfolded alpha-synuclein, a protein linked to neurodegenerative disorders. *Sci Signal* **8**, ra45 (2015).

12. E. J. Lee *et al.*, Alpha-synuclein activates microglia by inducing the expressions of matrix metalloproteinases and the subsequent activation of protease-activated receptor-1. *J Immunol* **185**, 615-623 (2010).

13. T. E. DeCoursey, K. G. Chandy, S. Gupta, M. D. Cahalan, Voltage-dependent ion channels in T-lymphocytes. *J Neuroimmunol* **10**, 71-95 (1985).

14. D. R. Matteson, C. Deutsch, K channels in T lymphocytes: a patch clamp study using monoclonal antibody adhesion. *Nature* **307**, 468-471 (1984).

15. S. Grissmer *et al.*, Expression and chromosomal localization of a lymphocyte K+ channel gene. *Proc Natl Acad Sci U S A* **87**, 9411-9415 (1990).

16. J. Xu *et al.*, The voltage-gated potassium channel Kv1.3 regulates peripheral insulin sensitivity. *Proc Natl Acad Sci U S A* **101**, 3112-3117 (2004).

17. S. K. Upadhyay *et al.*, Selective Kv1.3 channel blocker as therapeutic for obesity and insulin resistance. *Proceedings of the National Academy of Sciences of the United States of America* **110**, E2239-2248 (2013).

18. A. R. Gocke *et al.*, Kv1.3 deletion biases T cells toward an immunoregulatory phenotype and renders mice resistant to autoimmune encephalomyelitis. *J Immunol* **188**, 5877-5886 (2012).

19. D. A. Fadool *et al.*, Kv1.3 channel gene-targeted deletion produces "Super-Smeller Mice" with altered glomeruli, interacting scaffolding proteins, and biophysics. *Neuron* **41**, 389-404 (2004).

20. C. B. Fordyce, R. Jagasia, X. Zhu, L. C. Schlichter, Microglia Kv1.3 channels contribute to their ability to kill neurons. *J Neurosci* **25**, 7139-7149 (2005).

21. S. Rangaraju, M. Gearing, L. W. Jin, A. Levey, Potassium channel Kv1.3 is highly expressed by microglia in human Alzheimer's disease. *J Alzheimers Dis* **44**, 797-808 (2015).

22. N. Panicker *et al.*, Fyn Kinase Regulates Microglial Neuroinflammatory Responses in Cell Culture and Animal Models of Parkinson's Disease. *J Neurosci* **35**, 10058-10077 (2015).

23. H. B. Nygaard, C. H. van Dyck, S. M. Strittmatter, Fyn kinase inhibition as a novel therapy for Alzheimer's disease. *Alzheimers Res Ther* **6**, 8 (2014).

24. R. Gordon *et al.*, A simple magnetic separation method for high-yield isolation of pure primary microglia. *J Neurosci Methods* **194**, 287-296 (2011).

25. S. Sarkar *et al.*, Rapid and Refined CD11b Magnetic Isolation of Primary Microglia with Enhanced Purity and Versatility. *J Vis Exp*, (2017).

26. S. Sarkar *et al.*, Manganese exposure induces neuroinflammation by impairing mitochondrial dynamics in astrocytes. *Neurotoxicology*, (2017).

27. A. Halle *et al.*, The NALP3 inflammasome is involved in the innate immune response to amyloid-beta. *Nat Immunol* **9**, 857-865 (2008).

28. M. I. Ekstrand *et al.*, Progressive parkinsonism in mice with respiratory-chain-deficient dopamine neurons. *Proceedings of the National Academy of Sciences of the United States of America* **104**, 1325-1330 (2007).

29. R. Gordon *et al.*, Prokineticin-2 upregulation during neuronal injury mediates a compensatory protective response against dopaminergic neuronal degeneration. *Nat Commun* **7**, 12932 (2016).

30. R. Gordon *et al.*, Protein kinase Cdelta upregulation in microglia drives neuroinflammatory responses and dopaminergic neurodegeneration in experimental models of Parkinson's disease. *Neurobiol Dis* **93**, 96-114 (2016).

31. J. Seo, E. W. Ottesen, R. N. Singh, Antisense methods to modulate pre-mRNA splicing. *Methods Mol Biol* **1126**, 271-283 (2014).

32. A. Ghosh *et al.*, Mitoapocynin Treatment Protects Against Neuroinflammation and Dopaminergic Neurodegeneration in a Preclinical Animal Model of Parkinson's Disease. *J Neuroimmune Pharmacol* **11**, 259-278 (2016).

33. A. Ghosh *et al.*, Anti-inflammatory and neuroprotective effects of an orally active apocynin derivative in pre-clinical models of Parkinson's disease. *J Neuroinflammation* **9**, 241 (2012).

34. M. Langley *et al.*, Mito-Apocynin Prevents Mitochondrial Dysfunction, Microglial Activation, Oxidative Damage, and Progressive Neurodegeneration in MitoPark Transgenic Mice. *Antioxid Redox Signal*, (2017).

35. S. Sarkar *et al.*, Mitochondrial impairment in microglia amplifies NLRP3 inflammasome proinflammatory signaling in cell culture and animal models of Parkinson's disease. *NPJ Parkinsons Dis* **3**, 30 (2017).

36. L. Alvarez-Erviti, Y. Couch, J. Richardson, J. M. Cooper, M. J. Wood, Alpha-synuclein release by neurons activates the inflammatory response in a microglial cell line. *Neurosci Res* **69**, 337-342 (2011).

37. C. E. Khodr *et al.*, An alpha-synuclein AAV gene silencing vector ameliorates a behavioral deficit in a rat model of Parkinson's disease, but displays toxicity in dopamine neurons. *Brain Res* **1395**, 94-107 (2011).

38. M. F. Chesselet *et al.*, A progressive mouse model of Parkinson's disease: the Thy1-aSyn ("Line 61") mice. *Neurotherapeutics : the journal of the American Society for Experimental NeuroTherapeutics* **9**, 297-314 (2012).

39. X. Li *et al.*, Cognitive dysfunction precedes the onset of motor symptoms in the MitoPark mouse model of Parkinson's disease. *PloS one* **8**, e71341 (2013).

40. V. Jackson-Lewis, S. Przedborski, Protocol for the MPTP mouse model of Parkinson's disease. *Nat Protoc* **2**, 141-151 (2007).

41. G. E. Meredith, D. J. Rademacher, MPTP mouse models of Parkinson's disease: an update. *J Parkinsons Dis* **1**, 19-33 (2011).

42. S. P. Patil, P. D. Jain, P. J. Ghumatkar, R. Tambe, S. Sathaye, Neuroprotective effect of metformin in MPTP-induced Parkinson's disease in mice. *Neuroscience* **277**, 747-754 (2014).

43. J. A. Kang *et al.*, Epigenetic regulation of Kcna3-encoding Kv1.3 potassium channel by cereblon contributes to regulation of CD4+ T-cell activation. *Proc Natl Acad Sci U S A* **113**, 8771-8776 (2016).

44. M. D'Addario, P. D. Arora, C. A. McCulloch, Role of p38 in stress activation of Sp1. *Gene* **379**, 51-61 (2006).

45. T. C. Holmes, D. A. Fadool, I. B. Levitan, Tyrosine phosphorylation of the Kv1.3 potassium channel. *J Neurosci* **16**, 1581-1590 (1996).

46. M. R. Bowlby, D. A. Fadool, T. C. Holmes, I. B. Levitan, Modulation of the Kv1.3 potassium channel by receptor tyrosine kinases. *J Gen Physiol* **110**, 601-610 (1997).

47. I. Chung, L. C. Schlichter, Regulation of native Kv1.3 channels by cAMP-dependent protein phosphorylation. *Am J Physiol* **273**, C622-633 (1997).

48. K. K. Cook, D. A. Fadool, Two adaptor proteins differentially modulate the phosphorylation and biophysics of Kv1.3 ion channel by SRC kinase. *J Biol Chem* **277**, 13268-13280 (2002).

49. E. Yamada, C. C. Bastie, Disruption of Fyn SH3 domain interaction with a proline-rich motif in liver kinase B1 results in activation of AMP-activated protein kinase. *PLoS One* **9**, e89604 (2014).

50. C. Notredame, D. G. Higgins, J. Heringa, T-coffee: a novel method for fast and accurate multiple sequence alignment11Edited by J. Thornton. *Journal of Molecular Biology* **302**, 205-217 (2000).

51. H. Rus *et al.*, The voltage-gated potassium channel Kv1.3 is highly expressed on inflammatory infiltrates in multiple sclerosis brain. *Proc Natl Acad Sci U S A* **102**, 11094-11099 (2005).

52. A. Schmitz *et al.*, Design of PAP-1, a selective small molecule Kv1.3 blocker, for the suppression of effector memory T cells in autoimmune diseases. *Mol Pharmacol* **68**, 1254-1270 (2005).

53. S. Kundu-Raychaudhuri, Y. J. Chen, H. Wulff, S. P. Raychaudhuri, Kv1.3 in psoriatic disease: PAP-1, a small molecule inhibitor of Kv1.3 is effective in the SCID mouse psoriasis--xenograft model. *Journal of autoimmunity* **55**, 63-72 (2014).

54. C. Beeton *et al.*, Kv1.3 channels are a therapeutic target for T cell-mediated autoimmune diseases. *Proc Natl Acad Sci U S A* **103**, 17414-17419 (2006).

55. S. S. Karuppagounder *et al.*, The c-Abl inhibitor, nilotinib, protects dopaminergic neurons in a preclinical animal model of Parkinson's disease. *Sci Rep* **4**, 4874 (2014).

56. P. L. McGeer, S. Itagaki, B. E. Boyes, E. G. McGeer, Reactive microglia are positive for HLA-DR in the substantia nigra of Parkinson's and Alzheimer's disease brains. *Neurology* **38**, 1285-1291 (1988).

57. V. H. Perry, Innate inflammation in Parkinson's disease. *Cold Spring Harb Perspect Med* **2**, a009373 (2012).

58. X. Mao *et al.*, Pathological alpha-synuclein transmission initiated by binding lymphocyte-activation gene 3. *Science* **353**, (2016).

59. M. D. Cahalan, K. G. Chandy, The functional network of ion channels in T lymphocytes. *Immunol Rev* **231**, 59-87 (2009).

60. T. Wang *et al.*, Activated T-cells inhibit neurogenesis by releasing granzyme B: rescue by Kv1.3 blockers. *J Neurosci* **30**, 5020-5027 (2010).

61. J. Liu, C. Xu, L. Chen, P. Xu, H. Xiong, Involvement of Kv1.3 and p38 MAPK signaling in HIV-1 glycoprotein 120-induced microglia neurotoxicity. *Cell Death Dis* **3**, e254 (2012).

62. S. Rangaraju *et al.*, A systems pharmacology-based approach to identify novel Kv1.3 channel-dependent mechanisms in microglial activation. *J Neuroinflammation* **14**, 128 (2017).

63. I. Maezawa *et al.*, Kv1.3 inhibition as a potential microglia-targeted therapy for Alzheimer's disease: preclinical proof of concept. *Brain*, (2017).

64. C. Tubert *et al.*, Decrease of a Current Mediated by Kv1.3 Channels Causes Striatal Cholinergic Interneuron Hyperexcitability in Experimental Parkinsonism. *Cell Rep* **16**, 2749-2762 (2016).

65. S. Y. Branch *et al.*, Dopaminergic Neurons Exhibit an Age-Dependent Decline in Electrophysiological Parameters in the MitoPark Mouse Model of Parkinson's Disease. *J Neurosci* **36**, 4026-4037 (2016).

66. T. He *et al.*, Epigenetic regulation of voltage-gated potassium ion channel molecule Kv1.3 in mechanisms of colorectal cancer. *Discov Med* **23**, 155-162 (2017).

67. M. Brevet, N. Haren, H. Sevestre, P. Merviel, H. Ouadid-Ahidouch, DNA methylation of K(v)1.3 potassium channel gene promoter is associated with poorly differentiated breast adenocarcinoma. *Cell Physiol Biochem* **24**, 25-32 (2009).

68. L. Jimenez-Perez *et al.*, Molecular Determinants of Kv1.3 Potassium Channels-induced Proliferation. *J Biol Chem* **291**, 3569-3580 (2016).

Fig. 1

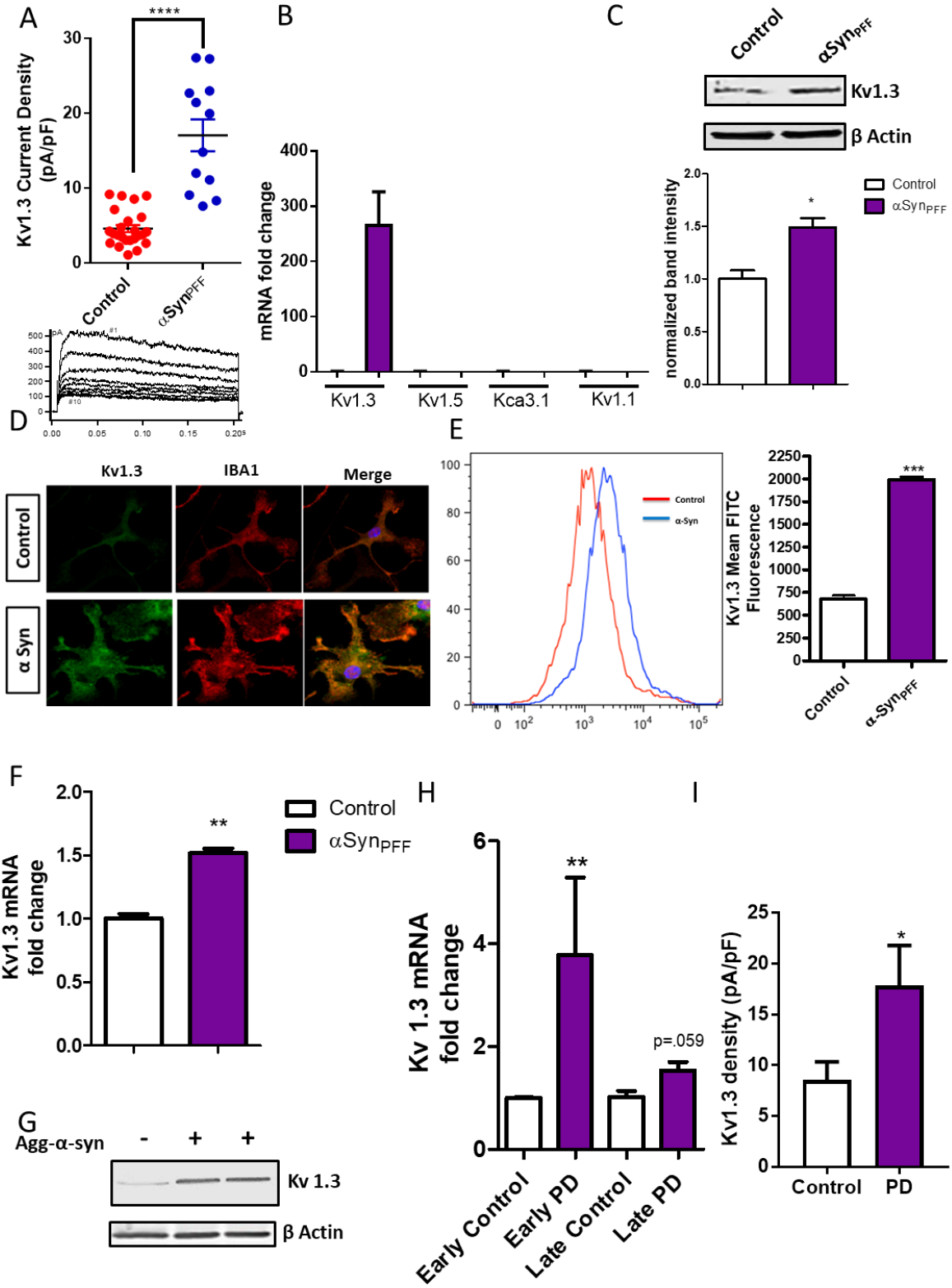
A
Kv1.3 Current Density (pA/pF)
****
Control
αSynPFF
B
mRNA fold change
Kv1.3
Kv1.5
Kca3.1
Kv1.1
C
Control
αSynPFF
Kv1.3
β Actin
normalized band intensity
Control
αSynPFF
D
Kv1.3
IBA1
Merge
Control
α Syn
E
Control
α-Syn
Kv1.3 Mean FITC Fluorescence
Control
α-SynPFF
F
Kv1.3 mRNA fold change
Control
αSynPFF
G
Agg-α-syn
Kv 1.3
β Actin
H
Kv 1.3 mRNA fold change
p=.059
Early Control
Early PD
Late Control
Late PD
I
Kv1.3 density (pA/pF)
Control
PD

Fig. 1: Upregulated expression of the potassium channel Kv1.3 upon aggregated αSyn stimulation in microglial cells *in vitro*. A) Whole-cell patch clamping of primary microglial cells treated with 1 µM $αSyn_{Agg}$ for 24-48 h showing $αSyn_{Agg}$-induced increased Kv1.3 activity. Voltage-ramp from -120 mV to 40 mV elicited characteristic outward rectifying current in $αSyn_{Agg}$-treated microglia. B) qRT-PCR showing that $αSyn_{Agg}$ induced Kv1.3 mRNA expression without significantly altering other potassium channels. C) Western blot of $αSyn_{Agg}$-induced Kv1.3 protein expression in primary microglial cells. D) ICC of $αSyn_{Agg}$-induced Kv1.3 protein expression in primary microglial cells. E) Flow cytometry of MMC treated with 1 µM $αSyn_{Agg}$ for 24 h showing $αSyn_{Agg}$-induced Kv1.3 surface expression. F-G) Midbrain slice cultures were treated with 1 µM $αSyn_{Agg}$ for 24 h. F) qRT-PCR showing upregulated Kv1.3 mRNA. G) Western blot showing upregulated Kv1.3 protein. H) qRT-PCR showing increased Kv1.3 mRNA expression in B cell lymphocytes isolated from PD patients compared to age-matched controls. I) Whole-cell patch clamping of B cell lymphocytes isolated from PD patients showing higher Kv1.3 channel activity compared to age-matched control. Data represented as mean±SEM with 3-4 biological replicates from 2-3 independent experiments. *$p \leq 0.05$, **$p < 0.01$, ***$p < 0.001$.

Fig. 2

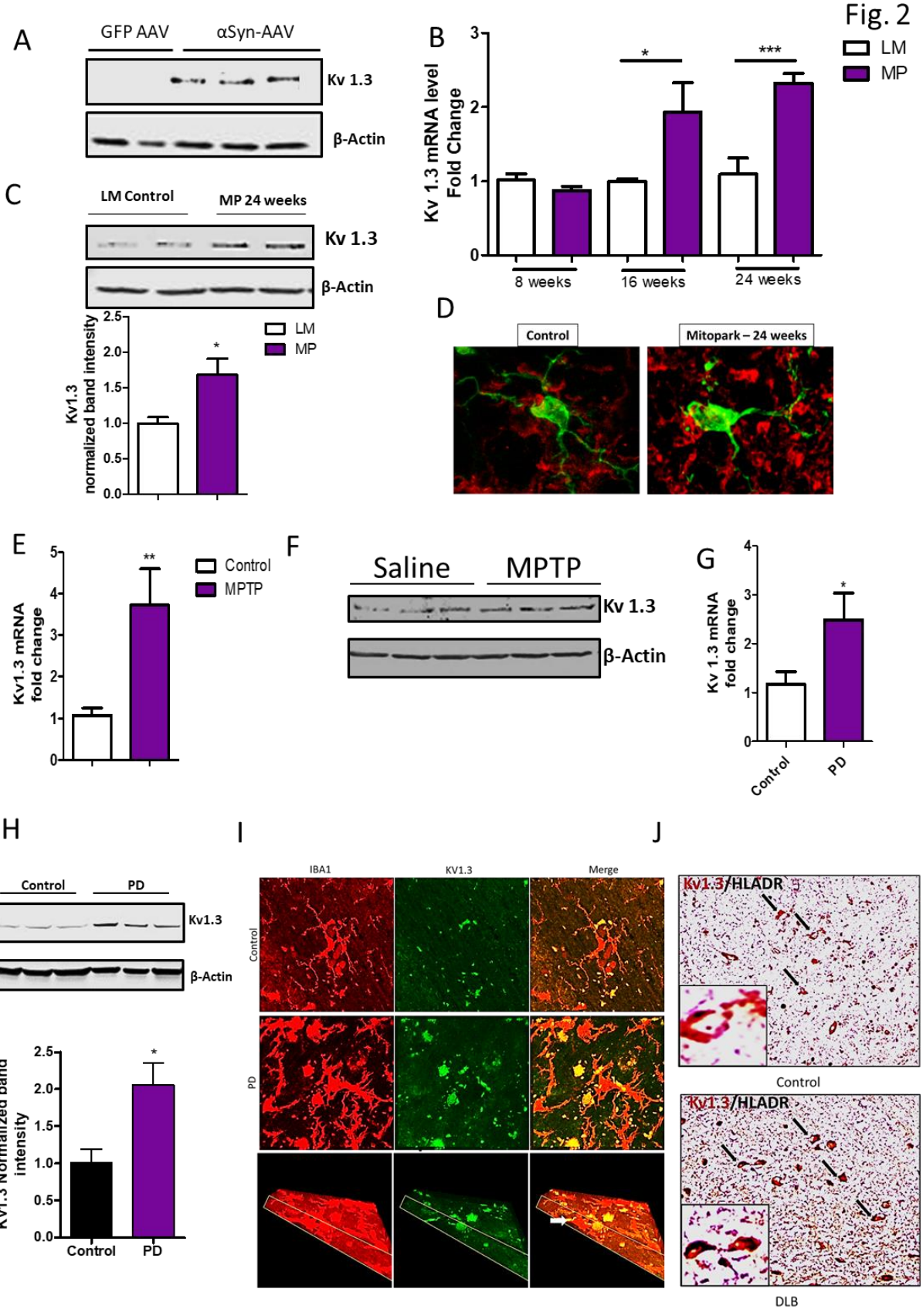
A
GFP AAV
αSyn-AAV
Kv 1.3
β-Actin
B
Kv 1.3 mRNA level Fold Change
LM
MP
8 weeks
16 weeks
24 weeks
C
LM Control
MP 24 weeks
Kv 1.3
β-Actin
Kv1.3 normalized band intensity
D
Control
Mitopark – 24 weeks
E
Kv1.3 mRNA fold change
Control
MPTP
F
Saline
MPTP
Kv 1.3
β-Actin
G
Kv 1.3 mRNA fold change
Control
PD
H
Control
PD
Kv1.3
β-Actin
Kv1.3 Normalized band intensity
I
IBA1
KV1.3
Merge
Control
PD
J
Kv1.3/HLADR
Control
Kv1.3/HLADR
DLB

Fig. 2: Kv1.3 expression is highly induced in microglial cells in experimental models of PD and postmortem PD brains. A) Western blot showing increased Kv1.3 protein level in substantia nigra of Syn-AAV mouse model of PD. B) qRT-PCR of 8- to 24-week-old nigral tissues from MitoPark mouse model of PD showing Kv1.3 induction. C) Western blot of 24-week-old nigral tissues from MitoPark mouse model of PD showing induction of Kv1.3 protein expression compared to age-matched controls. D) IHC of 24-week-old nigral tissues from MitoPark mouse model of PD showing higher Kv1.3 protein level in IBA1-positive microglial cells compared to age-matched controls. E) qRT-PCR of nigral tissues from MPTP mouse model revealing induction of Kv1.3 mRNA expression. F) Western blot showing increased Kv1.3 protein level in substantia nigra of MPTP mouse model of PD. G) qRT-PCR of post-mortem PD brains showing elevated Kv1.3 mRNA. H) Western blot of post-mortem PD patients showing induction of Kv1.3 protein expression compared to age-matched controls. n=6-8. I) Dual immunostaining revealing higher Kv1.3 level in microglial cells in post-mortem PD brains compared to age matched controls. J) Dual DAB-staining showing induction of Kv1.3 expression in HLA-DR-positive microglial cells in DLB patients compared to age-matched controls. Data represented as mean±SEM with 3-4 biological replicates from 2-3 independent experiments. *p≤0.05, **p<0.01, ***p<0.001.

Fig. 3

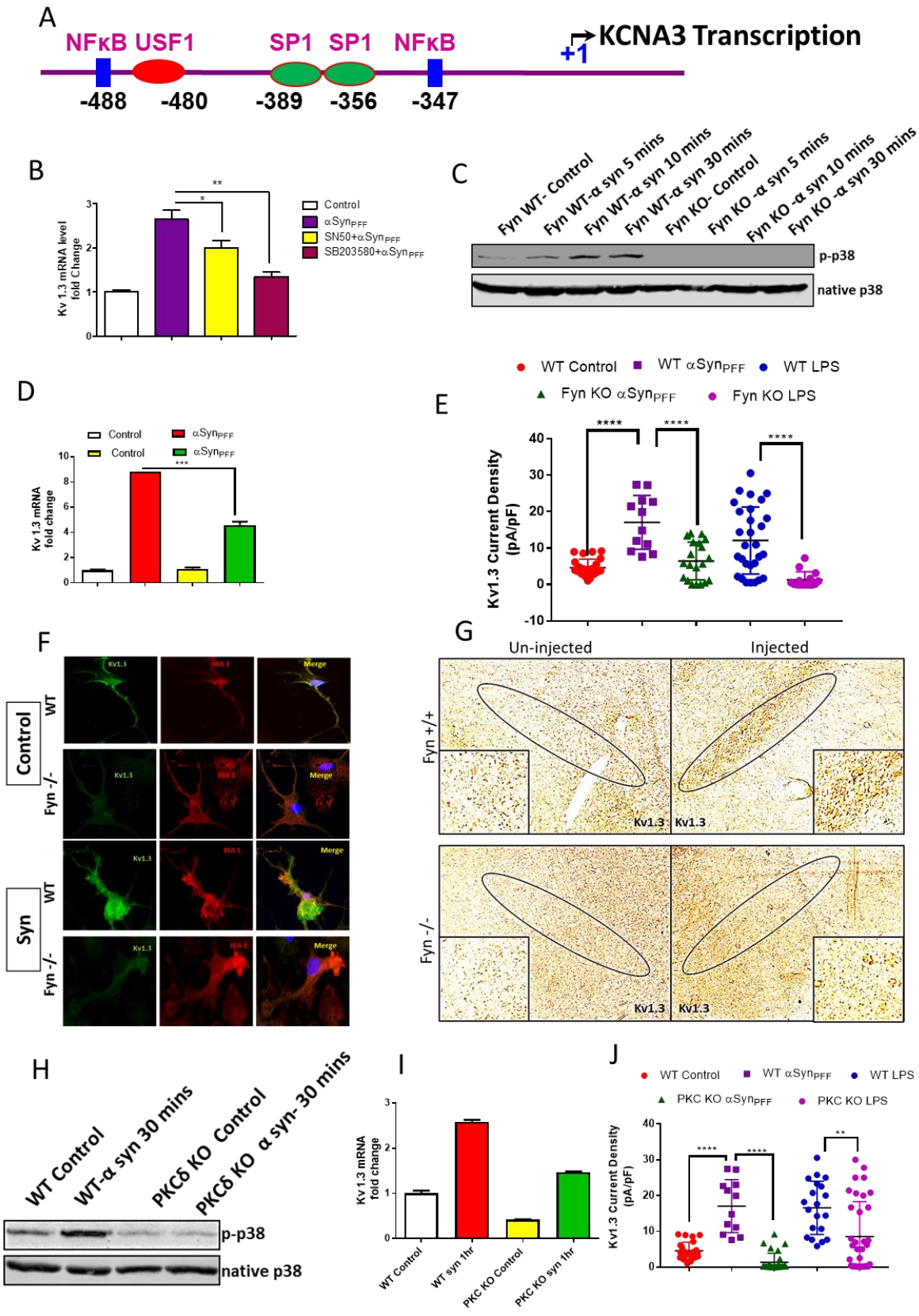
A
NFκB USF1
SP1 SP1 NFκB
+1
KCNA3 Transcription
-488 -480 -389 -356 -347
B
Kv 1.3 mRNA level fold Change
Control
αSynPFF
SN50+αSynPFF
SB203580+αSynPFF
C
Fyn WT- Control
Fyn WT-α syn 5 mins
Fyn WT-α syn 10 mins
Fyn WT-α syn 30 mins
Fyn KO- Control
Fyn KO -α syn 5 mins
Fyn KO -α syn 10 mins
Fyn KO -α syn 30 mins
p-p38
native p38
D
Kv 1.3 mRNA fold change
E
WT Control
WT αSynPFF
WT LPS
Fyn KO αSynPFF
Fyn KO LPS
Kv1.3 Current Density (pA/pF)
F
Control
Syn
WT
Fyn -/-
Kv1.3
IBA 1
Merge
G
Un-injected
Injected
Fyn +/+
Fyn -/-
Kv1.3
H
WT Control
WT-α syn 30 mins
PKCδ KO Control
PKCδ KO α syn- 30 mins
p-p38
native p38
I
Kv 1.3 mRNA fold change
WT Control
WT syn 1hr
PKC KO Control
PKC KO syn 1hr
J
WT Control
WT αSynPFF
WT LPS
PKC KO αSynPFF
PKC KO LPS
Kv1.3 Current Density (pA/pF)

Fig. 3: Fyn modulates transcriptional regulation of Kv1.3 in microglial cells through the Fyn-PKCδ kinase signaling cascade. A) *In-silico* analysis of promoter sequence of Kv1.3 revealing probable site of NfκB and SP1 binding sites. B) qRT-PCR of MMC co-treated with αSyn_{Agg} and either SN50 or SB203580 showing that both SN50 and SB203580 attenuated αSyn_{Agg}-induced Kv1.3 expression. C) Western blot of Fyn WT and KO primary microglial cells treated with αSyn_{Agg} showing that Fyn KO reduced induction of the p38 MAPK pathway. D) qRT-PCR revealing that Fyn KO reduced αSyn_{Agg}-induced Kv1.3 mRNA level. E) Whole-cell patch-clamp showing that Fyn KO attenuated αSyn_{Agg}- and LPS-induced Kv1.3 activity compared to Fyn WT microglial cells. F) ICC showing Fyn KO reduced αSyn_{Agg}-induced Kv1.3 protein levels in primary microglial cells. G) IHC of substantia nigra 6 mo post-αSyn_{PFF} injection showing Fyn KO mice with reduced induction of Kv1.3 protein. H) Western blot of primary microglial cells treated with αSyn_{Agg} showing that PKC KO reduced induction of the p38 MAPK pathway. I) qRT-PCR of microglial cells showing that PKC KO reduced expression of αSyn_{Agg}-induced Kv1.3 mRNA. J) Whole-cell patch-clamping of microglial cells showing that PKC KO attenuated αSyn_{Agg}- and LPS-induced Kv1.3 activity compared to PKC WT microglial cells. Data represented as mean±SEM with 3-4 biological replicates from 2-3 independent experiments. *$p \leq 0.05$, **$p < 0.01$, ***$p < 0.001$.

Fig. 4

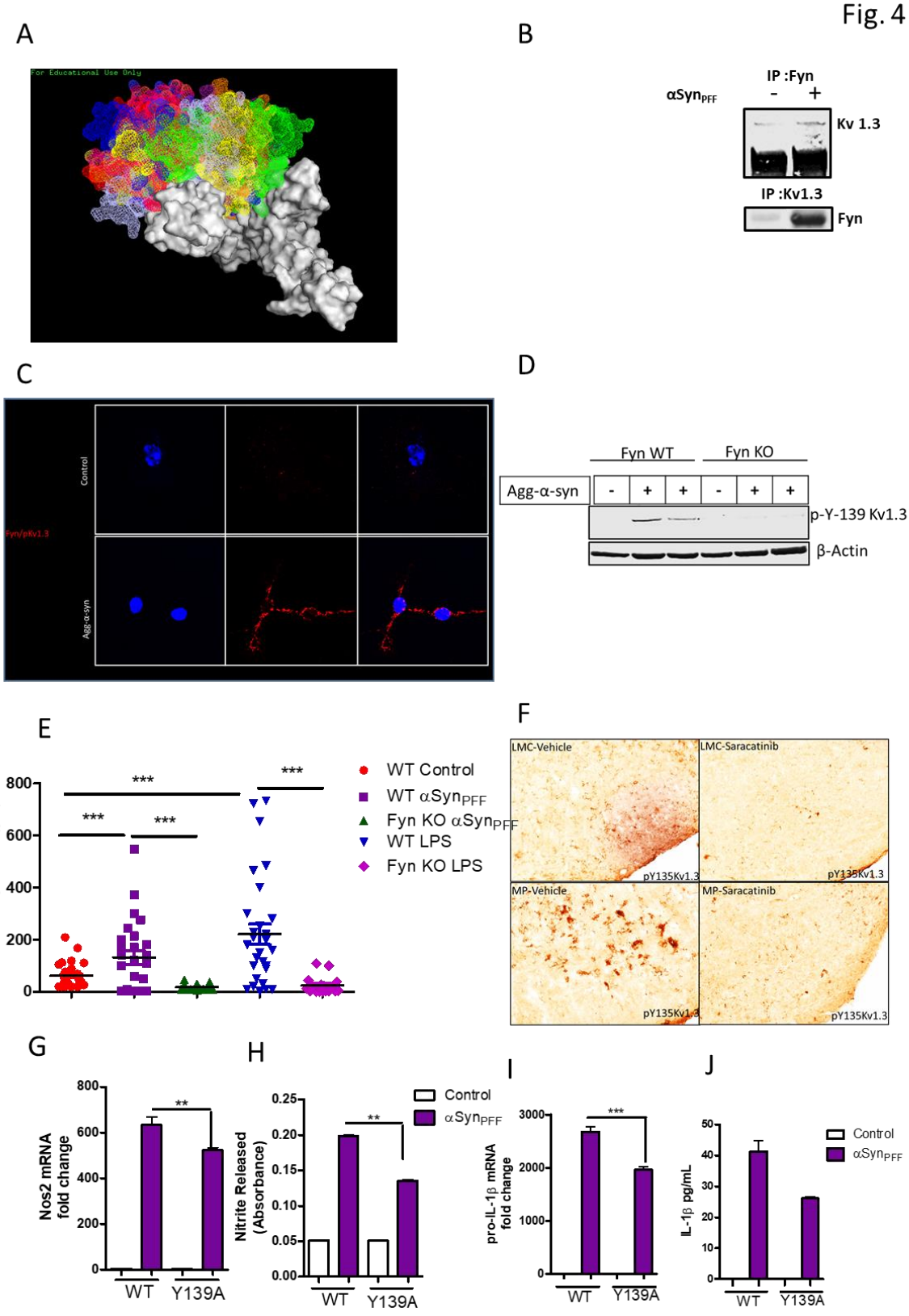
A
B
αSynPFF
IP :Fyn
-
+
Kv 1.3
IP :Kv1.3
Fyn
C
Control
Agg-α-syn
D
Fyn WT
Fyn KO
Agg-α-syn
p-Y-139 Kv1.3
β-Actin
E
Kv1.3 Amplitude (pA)
WT Control
WT αSynPFF
Fyn KO αSynPFF
WT LPS
Fyn KO LPS
F
LMC-Vehicle
LMC-Saracatinib
MP-Vehicle
MP-Saracatinib
pY135Kv1.3
G
Nos2 mRNA fold change
H
Nitrite Released (Absorbance)
Control
αSynPFF
I
pro-IL-1β mRNA fold change
J
IL-1β pg/mL
WT
Y139A

Fig. 4: Fyn modulates post translational modification of Kv1.3. A) *In silico* docking analysis of Kv1.3 and SH domain of Fyn. B) Immunoprecipitation of Fyn and Kv1.3 showing direct Fyn-Kv1.3 interaction post-αSyn_{Agg} treatment. C) Duolink proximal ligation assay showing αSyn_{Agg}-induced interaction between Kv1.3 and Fyn. D) Western blot of Fyn WT and KO primary microglia reveals that Kv1.3 phosphorylation at residue 139 is Fyn-dependent. E) Whole-cell patch clamping of LPS- or Syn_{Agg}-treated microglia showing that Fyn KO lowered the amplitude of Kv1.3 currents compared to Fyn WT microglial cells. F) IHC of substantia nigra from MitoPark mice and their littermate controls showing that pharmacological inhibition of Fyn by saracatinib reduced Kv1.3 phosphorylation. G-J) MMC were either transfected with WT or Y130A Kv1.3 plasmid. G) qRT-PCR and H) Griess assay showing reduced levels of iNOS and Nitrite release, respectively, in Y139A Kv1.3 transfected cells compared to WT. I) qRT-PCR showing reduced IL-1β production in Y139A Kv1.3-transfected versus WT Kv1.3-transfected MMCs. J) Luminex assay showing reduced IL-1β secretion in Y139A Kv1.3-transfected compared to WT Kv1.3-transfected MMCs. Data represented as mean±SEM with 3-4 biological replicates from 2-3 independent experiments. $^{**}p<0.01$, $^{***}p<0.001$.

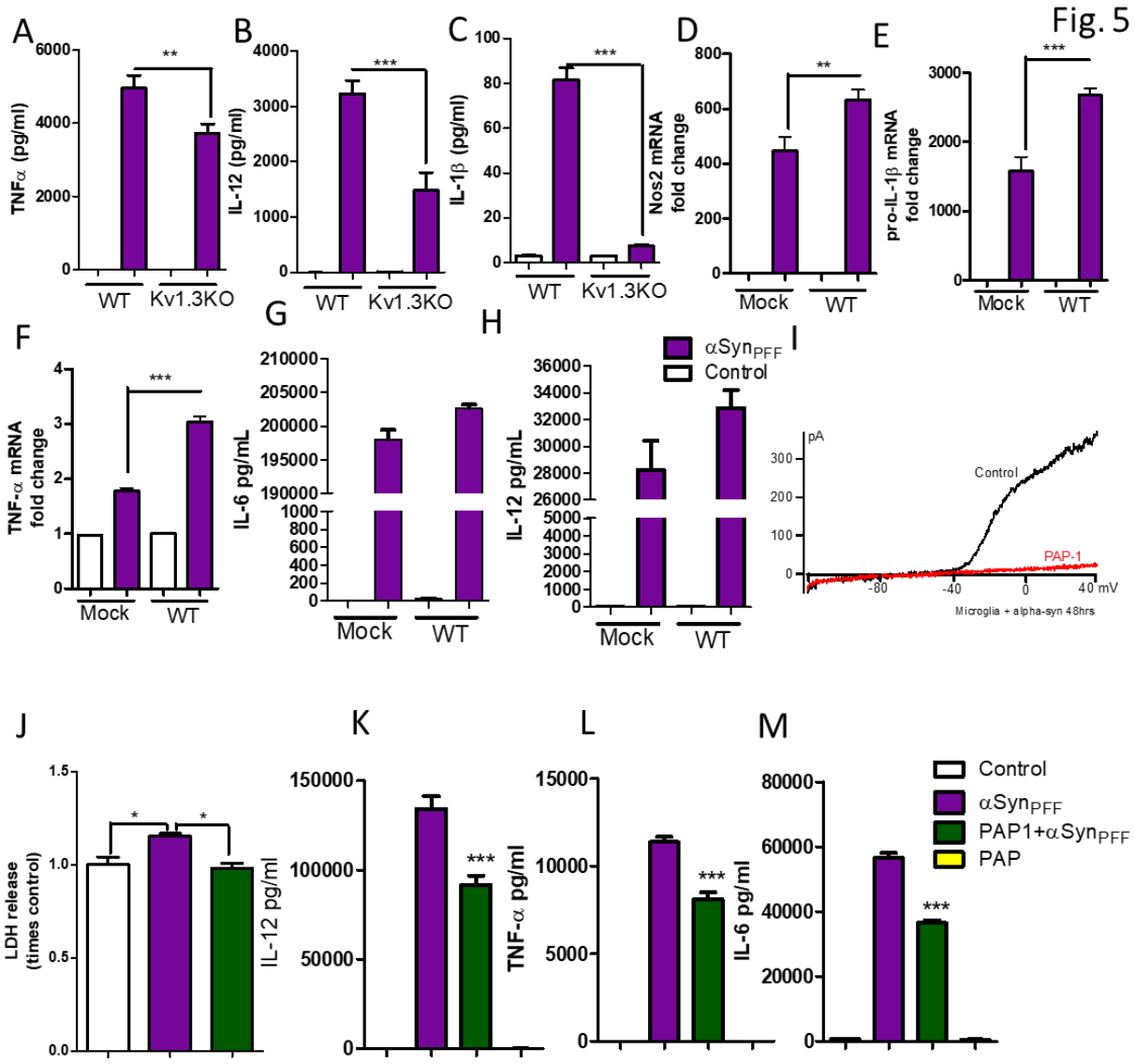

Fig. 5: Kv1.3 modulates neuroinflammation in cell culture model of PD. A-C) Kv1.3 WT and KO primary microglial cells were treated with 1 μM αSyn_{Agg} for 24 h. Luminex analysis showing that Kv1.3 KO reduced release of the αSyn_{Agg}-induced pro-inflammatory factors A) TNFα, B) IL-12, and C) IL-1β. D-H) MMCs were transfected with WT Kv1.3 plasmid, and then 48-h post-transfection, cells were treated with 1 μM αSyn_{Agg} for 24 h. D-F) qRT-PCR showing that Kv1.3 overexpression aggravated αSyn_{Agg}-induced production of the pro-inflammatory factors D) Nos2, E) pro-IL-1β, and

F) TNFα. G-H) Luminex analysis showing Kv1.3 overexpression potentiated release of the pro-inflammatory factors G) IL-6, and H) IL-12. I) Voltage-ramp from -120 mV to 40 mV elicited characteristic outward rectifying current in αSyn_{Agg}-treated microglia that was sensitive to the Kv1.3-selective inhibitor PAP-1 and displayed voltage-dependent activation by voltage-steps from -80 mV to 60 mV. J) LDH assay showing PAP-1 reduced αSyn_{Agg}-induced LDH release from microglial cells. K-M) Luminex assay revealing that PAP-1 attenuated the αSyn_{Agg}-induced proinflammatory factors K) IL-6, L) TNFα, and M) IL-12. Data represented as mean±SEM with 3-4 biological replicates from 2-3 independent experiments. *$p \leq 0.05$, **$p < 0.01$, ***$p < 0.001$.

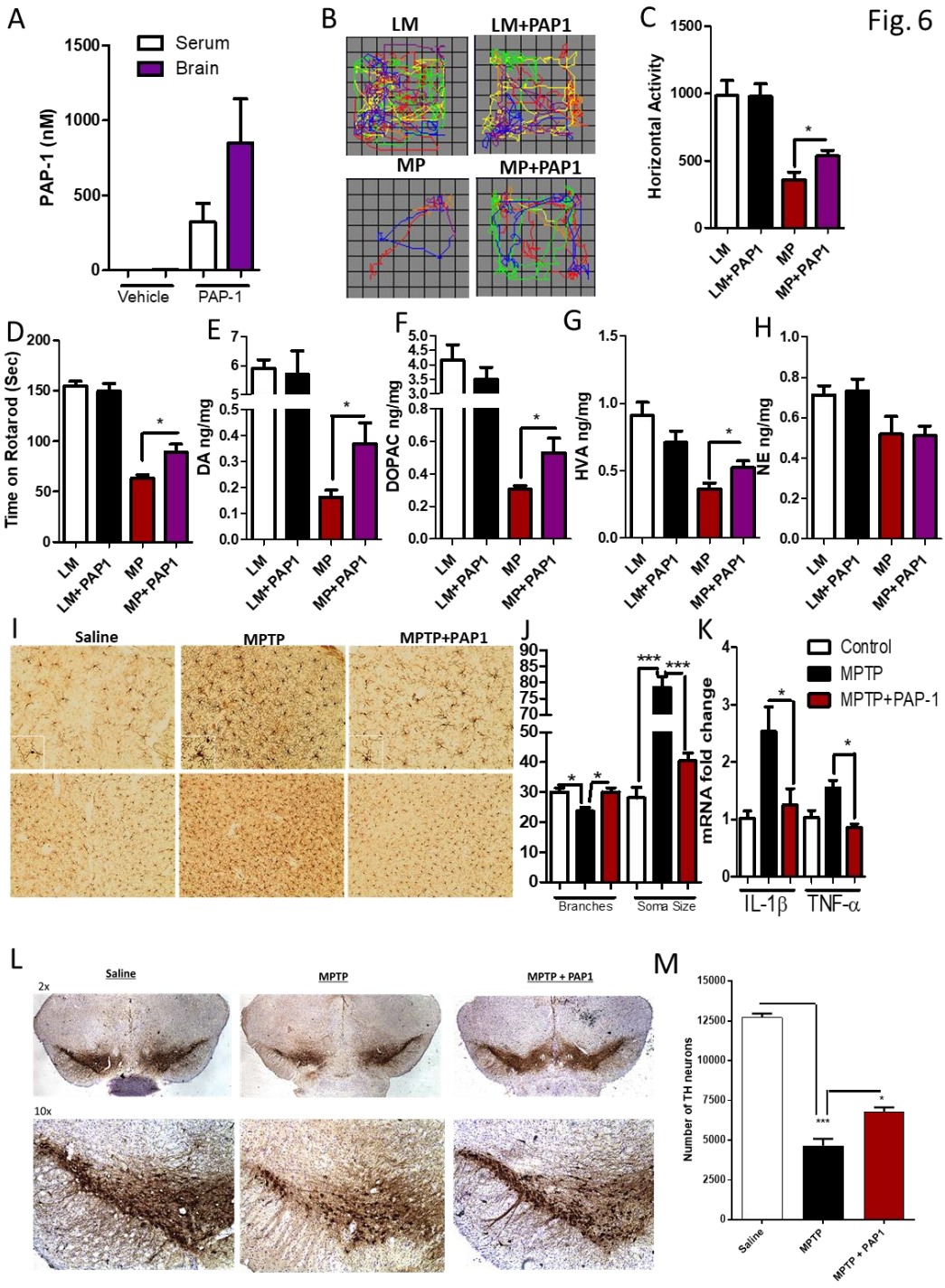

Fig. 6: PAP-1 reduced inflammation and neurodegeneration in mouse models of PD. A-H) MitoPark Mouse Model. A) LC-MS of Serum and Brian concentration of PAP-1 in MitoPark mice 6 weeks post-injection. B) Representative VersaPlots showing

PAP-1 rescued movement deficits of MitoPark mice at 20 weeks. C) VersaMax open-field test showing increased horizontal activity of MitoParks treated with PAP-1 compared to vehicle group. D) Rotarod behavior test revealing increased time spent on the rotarod by MitoParks treated with PAP-1 compared to vehicle group. E-H) HPLC showing that PAP-1 treatment protected MitoPark mice from loss of E) Dopamine, F) DOPAC, and G) HVA, but did not alter H) Norepinephrine levels. I-M) MPTP mouse model. I) IHC of MPTP-exposed substantia nigra and striatum showing that PAP-1 altered microgliosis. J) ImageJ analysis of MPTP-exposed substantia nigra showing PAP-1 reduced soma size and increased the number of microglial branches. K) qRT-PCR of striatum post-MPTP showing reduced proinflammatory factors IL-1β and TNFα. L) IHC of SNpc showing that PAP-1 protected against MPTP-induced loss of TH-positive neurons. M) Stereology analysis of the SNpc showing that PAP-1 decreased the loss of TH-positive neurons post-MPTP treatment. Data represented as mean±SEM with 3-4 biological replicates from 2-3 independent experiments. *p≤0.05, ***p<0.001.

Supplementary Fig 1

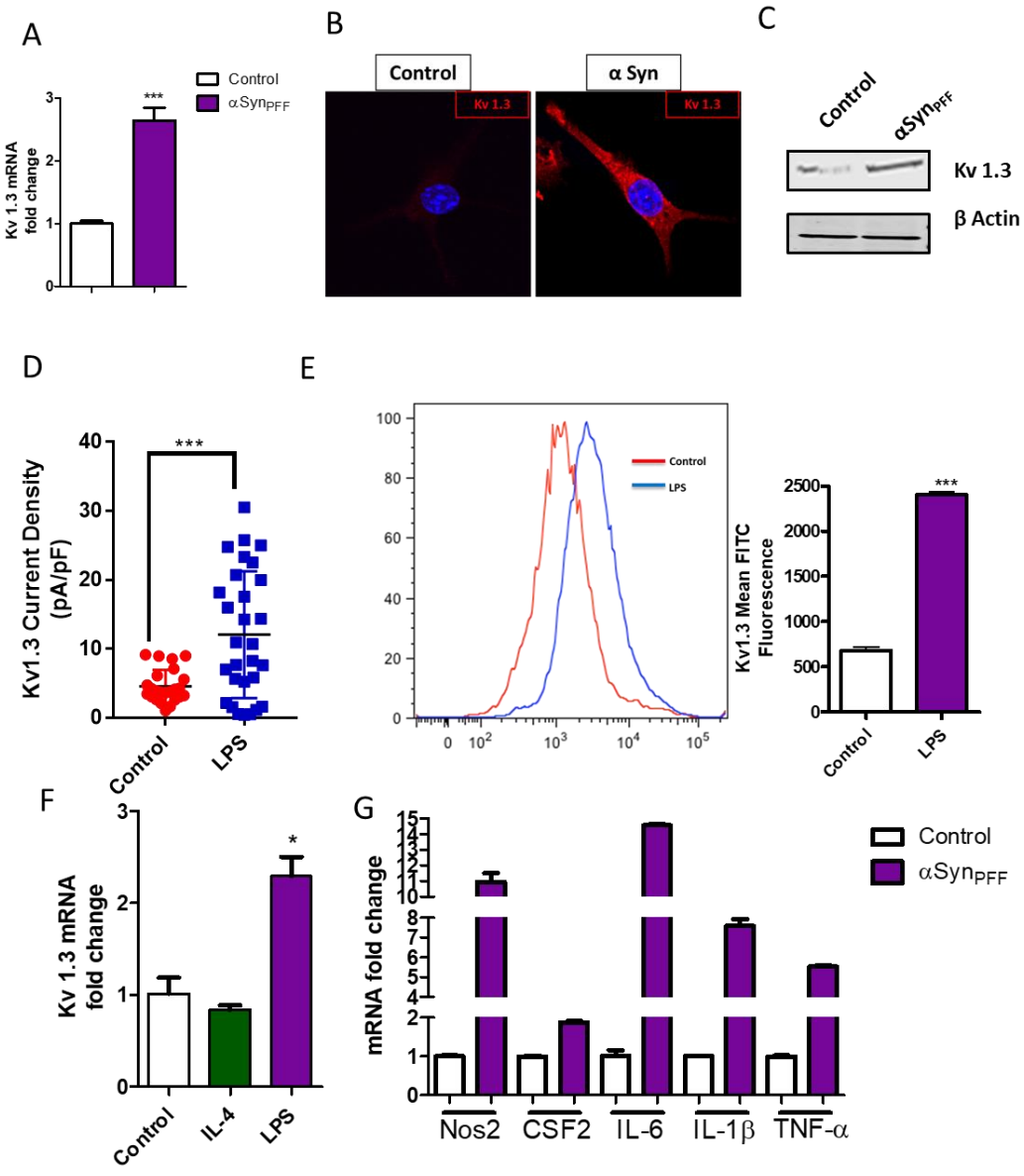

Supplementary Fig. 1: Kv1.3 is upregulated in microglia inflammatory models. MMCs were treated with 1 μM αSyn_{Agg} for 24-48 h. A) qRT-PCR revealing αSyn_{Agg}-induced Kv1.3 mRNA expression. B) ICC of primary microglial cells revealing αSyn_{Agg}-induced Kv1.3 protein expression. C) Western blot of primary microglial cells showing αSyn_{Agg}-induced Kv1.3 protein expression. D) Whole-cell patch clamping of primary

microglial cells showing LPS-induced Kv1.3 activity. E) Flow cytometry of MMCs treated with 1 µg/mL LPS for 24 h revealing LPS-induced surface expression of Kv1.3 protein. F) qRT PCR of MMCs treated with LPS (1 µg/mL) and IL-4 (20 ng/mL) for 6 h showing LPS-induced Kv1.3 expression. G) qRT-PCR of midbrain slice culture treated with 1 µM αSyn_{Agg} for 24 h revealing upregulation of the pro-inflammatory factors Nos2, CSF-2, IL-6, IL-1β and TNFα. Data represented as mean±SEM with 3-4 biological replicates from 2-3 independent experiments. *p≤0.05, ***p<0.001.

Supplementary Fig. 2

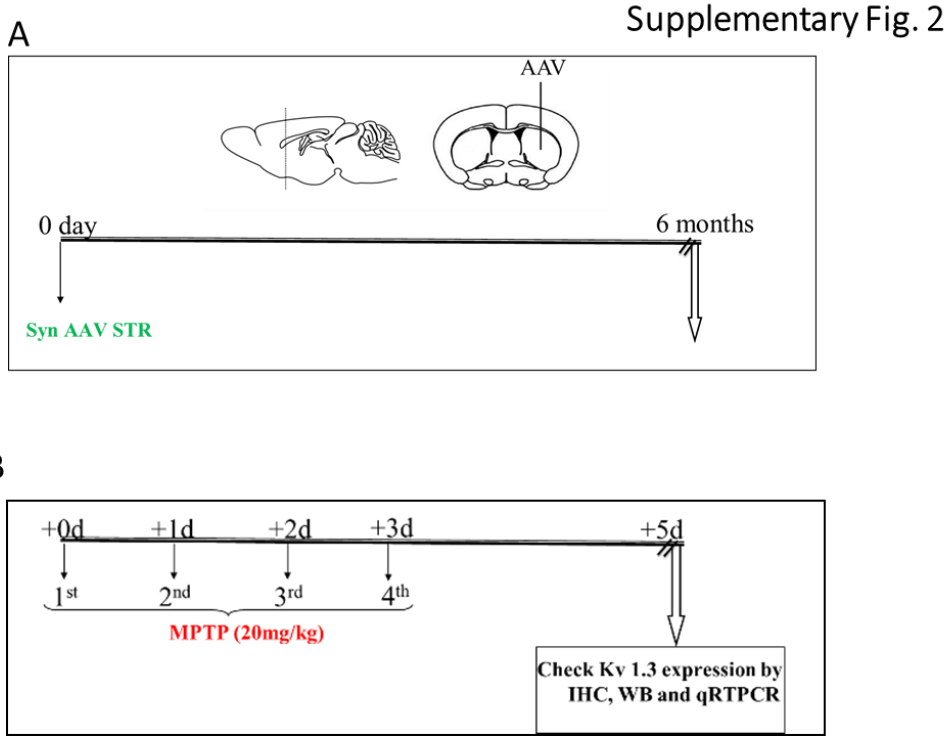

Supplementary Fig. 2: Animal treatment paradigm corresponding to Fig. 2. A) Treatment paradigm corresponding to Syn-AAV mouse model of PD in Fig. 2A. B) Treatment paradigm corresponding to MPTP mouse model of PD in Fig. 2E-F.

Supplementary Fig. 3

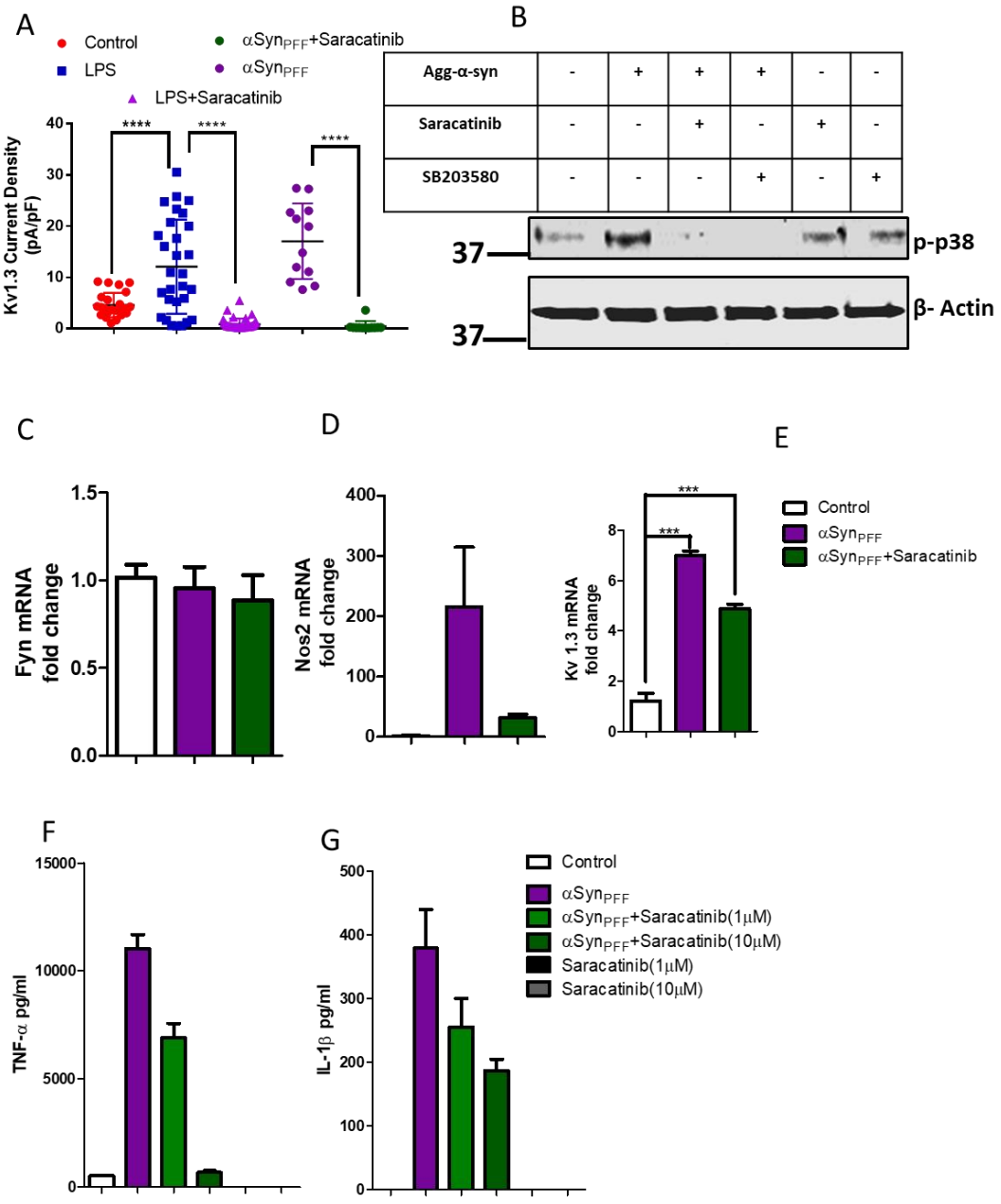

Supplementary Fig. 3: Pharmacological inhibition of Fyn reduces αSyn$_{Agg}$-induced Kv1.3 expression. A) Whole cell patch clamping of primary microglial cells showing that saracatinib attenuated the αSyn$_{Agg}$- and LPS-induced Kv1.3 activity. B) Western blot showing saracatinib-reduced induction of the p38 MAPK pathway post-αSyn$_{Agg}$ treatment. C-E) qRT-PCR showing that saracatinib did not alter C) Fyn mRNA but attenuated the αSyn$_{Agg}$-induced pro-inflammatory factor D) Nos2 and E) Kv1.3 expression. F-G) Luminex analysis showing that saracatinib treatment attenuated production of the pro-inflammatory factors F) TNFα and G) IL-1β post-αSyn$_{Agg}$ treatment. Data represented as mean±SEM with 3-4 biological replicates from 2-3 independent experiments. ***$p<0.001$.

Supplementary Fig. 4

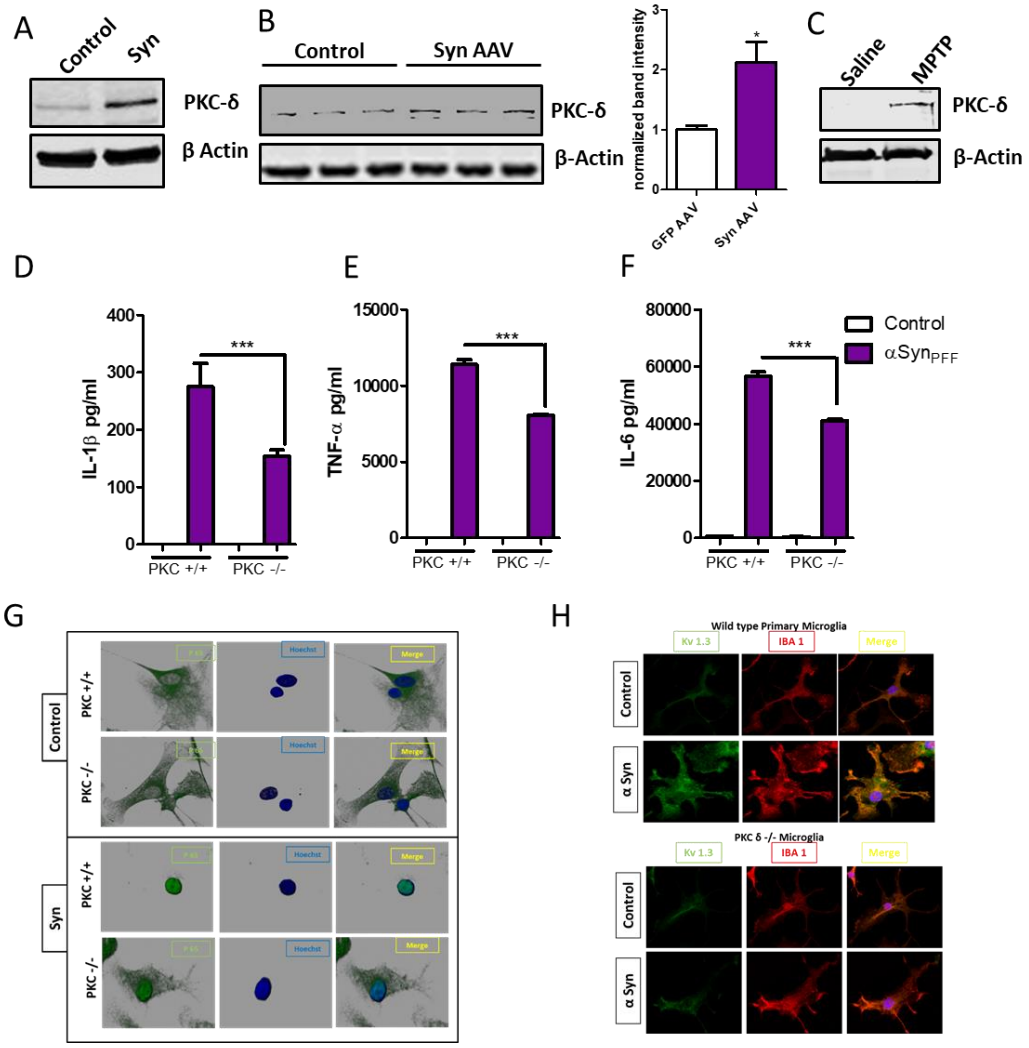

Supplementary Fig. 4: PKCδ is upregulated in cell culture and animal models of PD and regulates inflammation. A) Western blot showing increased PKC-δ protein expression 24 h post-αSyn_{Agg} treatment in primary mouse microglial cells. B) Western blot showing increased PKCδ protein level in striatum of αSyn AAV-injected mice. C) Western blot showing increased PKCδ protein level in MPTP mouse model of PD. D-F) Luminex analysis of αSyn_{Agg}-treated primary microglial cells showing that PKCδ KO attenuated production of the pro-inflammatory factors D) IL-1β, E) TNFα, and F)

IL-6. G) ICC of primary microglial cells revealing that αSyn_{Agg}-induced p65 nuclear translocation is reduced by PKCδ KO. H) ICC of primary microglial cells revealing that αSyn_{Agg}-induced Kv1.3 protein expression is reduced by PKCδ KO. Data represented as mean±SEM with 3-4 biological replicates from 2-3 independent experiments. *p≤0.05, ***p<0.001.

Supplementary Fig. 5

Supplementary Fig. 5: Multiple Sequence Alignment of Kv1.3. Multiple sequence alignment of N-terminal of Kv1.3 protein sequence from multiple organisms using T-Coffee, showing the conserved tyrosine residue.

Supplementary Fig. 6

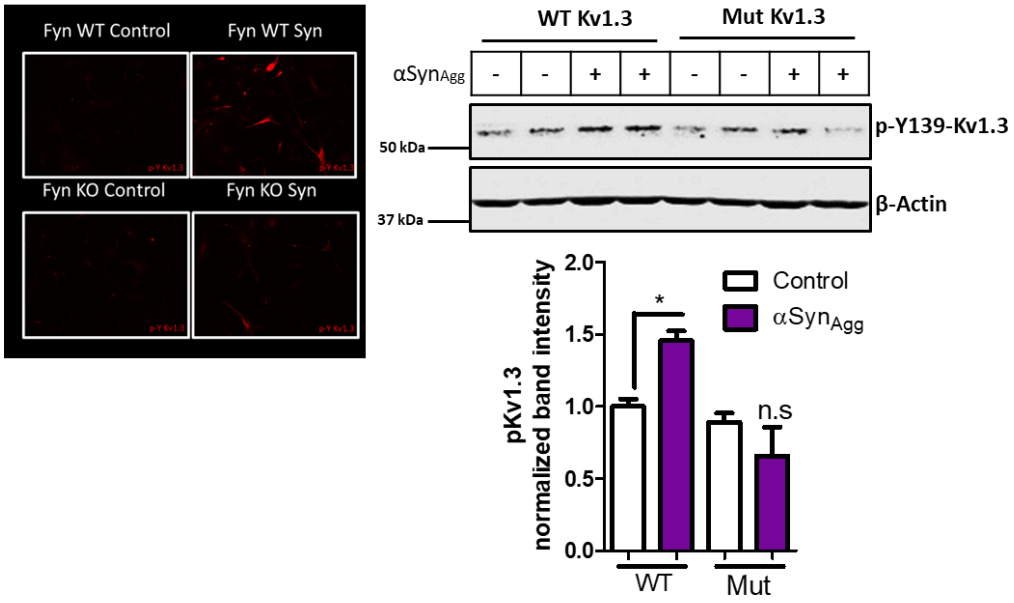

Supplementary Fig. 6: Fyn modifies Kv1.3 post-translationally. A) ICC of αSyn_{Agg}-treated Fyn WT and KO microglia showing that Fyn KO reduced Kv1.3 phosphorylation. B) Western blot revealing that αSyn_{Agg} induced Kv1.3 phosphorylation in MMCs transfected with WT Kv1.3 but not in MMCs transfected with Y139A Kv1.3.

Supplementary Fig. 7

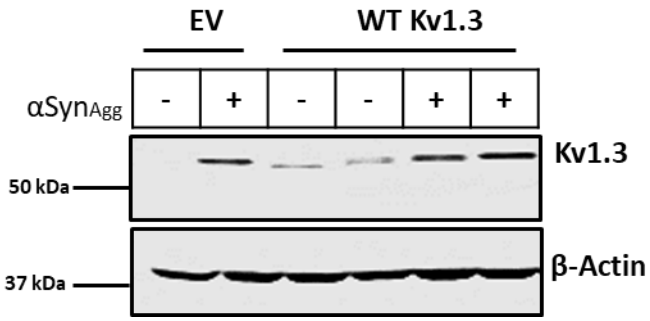

Supplementary Fig. 7: Overexpression of Kv1.3 in MMC. Western Blot showing that MMCs transfected with Kv1.3 plasmids had higher basal level of Kv1.3.

Supplementary Fig. 8

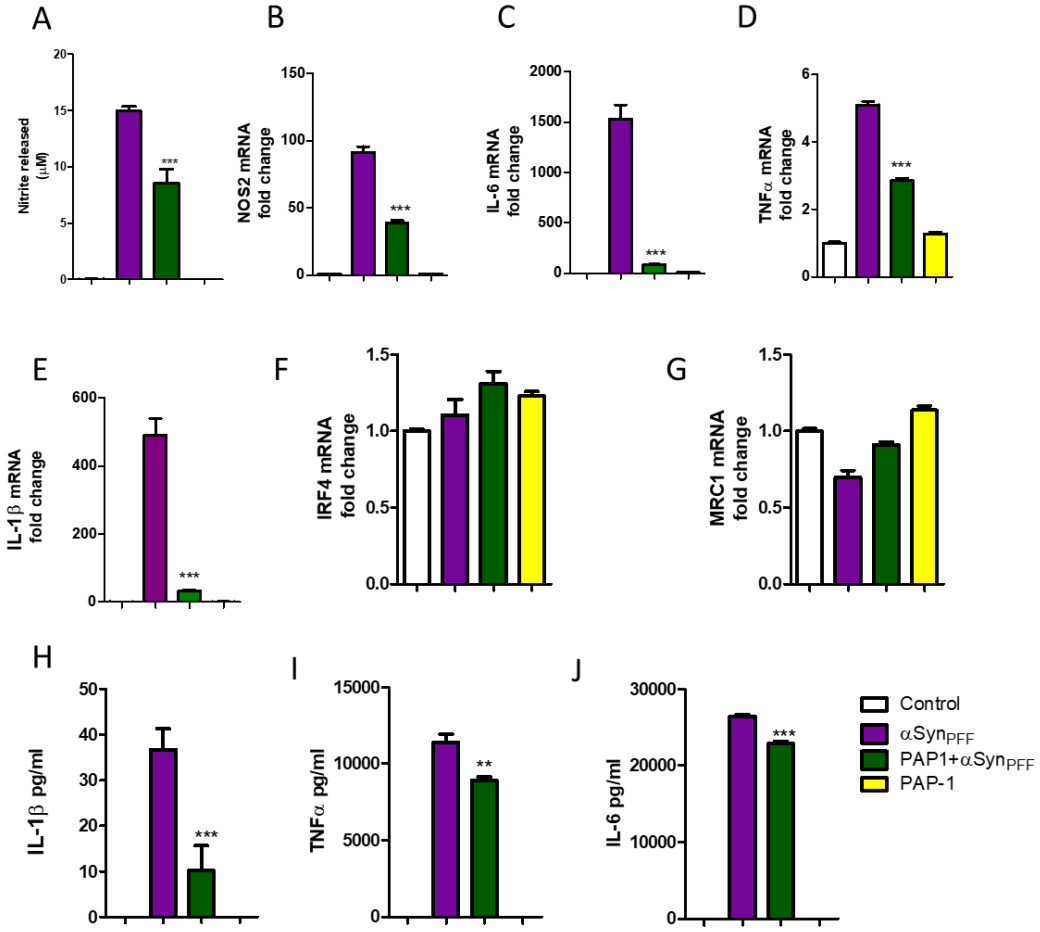

Supplementary Fig. 8: PAP-1 reduces inflammation in MMC. A) Griess assay showing PAP-1 reduced αSyn_{Agg}-induced release of nitrites from MMC. B-G) qRT-PCR revealing PAP-1 reduced the αSyn_{Agg}-induced proinflammatory factors B) Nos2, C) IL-6, D) TNFα, and E) IL-1β, but did not significantly alter the markers of alternative microglial activation of F) IRF4, and G) MRC1. H-J) Luminex assay revealing that PAP-1 attenuated the αSyn_{Agg}-induced proinflammatory factors H) IL-1β, I) TNFα, and J) IL-6. Data represented as mean±SEM with 3-4 biological replicates from 2-3 independent experiments. **p<0.01, ***p<0.001.

Supplementary Fig. 9

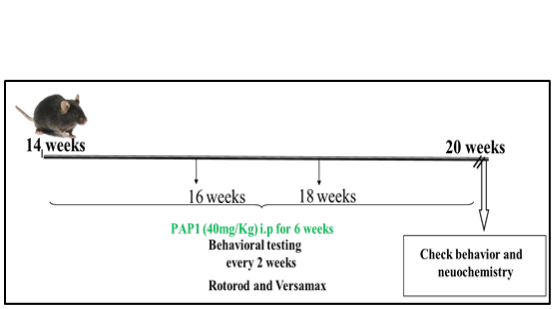

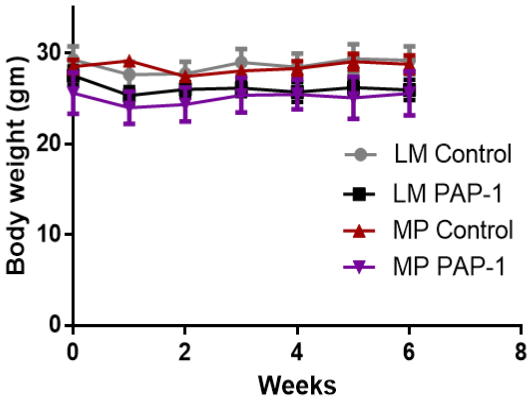

	MP		LM	
	Mean	SEM	Mean	SEM
Albumin (Abaxis)	3.966667	0.176383	4.025	0.127825
Alk Phos (Abaxis)	53.33333	4.096069	52	5.599745
ALT (Abaxis)	41.66667	2.403701	36.875	4.763843
Amylase	928.6667	7.055337	1005.625	38.55837
T. Bilirubin (Abaxis)	0.233333	0.033333	0.2375	0.018298
BUN (Abaxis)	13	0.57735	13.375	0.843833
Calcium (Abaxis)	10.76667	0.176383	11.1375	0.179222
Phosphorus (Abaxis)	11	0.3	10.525	0.393587
Creatinine (Abaxis)	0.233333	0.033333	0.325	0.017678
Glucose (Abaxis)	200.3333	29.06506	248	14.7624
Sodium (Abaxis)	153	0.57735	153	0.566947
Potassium - Abaxis	8.5	0	8.35	0.075593
T. Protein (Abaxis)	5.566667	0.133333	5.5875	0.078916

	Vehicle		PAP-1	
	Mean	SEM	Mean	SEM
Albumin (Abaxis)	4.06	0.186011	3.966667	0.114504
Alk Phos (Abaxis)	52.6	7.460563	52.16667	4.989433
ALT (Abaxis)	36.6	5.878775	39.5	4.624212
Amylase	981.6	33.821	987.1667	49.50314
T. Bilirubin (Abaxis)	0.24	0.024495	0.233333	0.021082
BUN (Abaxis)	13.2	1.019804	13.33333	0.843274
Calcium (Abaxis)	11.36	0.242074	10.76667	0.071492
Phosphorus (Abaxis)	11.08	0.502394	10.3	0.316228
Creatinine (Abaxis)	0.266667	0.02582	0.3	0.033333
Glucose (Abaxis)	266	14.67992	209.1667	17.42683
Sodium (Abaxis)	153.2	0.583095	152.8333	0.654047
Potassium - Abaxis	8.5	0	8.2	0.088192
T. Protein (Abaxis)	5.62	0.115758	5.55	0.076376

Supplementary Fig. 9: PAP-1 does not alter blood chemistry in MitoPark mouse model of PD. A) Treatment paradigm corresponding to MitoPark mouse model of PD in Fig. 6A-H. B) Stable body weight throughout the course of treatment. C-D) Whole blood analysis showing unchanging blood chemistry between C) littermate control and MitoPark mice or between D) vehicle and PAP-1 treatment group n=3.

Supplementary Fig. 10

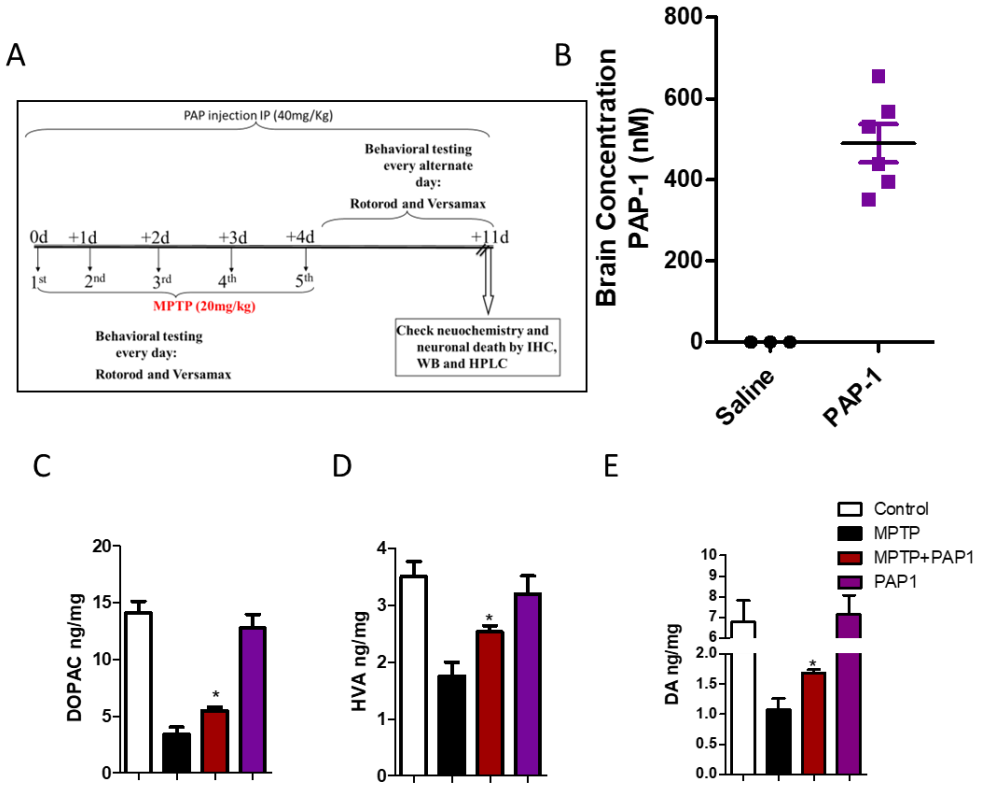

Supplementary Fig. 10: PAP-1 reduces neurotransmitter loss in MPTP model of PD. A) Treatment paradigm corresponding to MPTP mouse model of PD in Fig. 6I-M. B) LC-MS of amount of PAP-1 detected in brains post-sacrifice. C-E) HPLC of striatum showing that PAP-1 reduced the MPTP-induced loss of C) DOPAC, D) HVA, and E) dopamine. Data represented as mean±SEM with 4-6 animals/group. *p≤0.05.

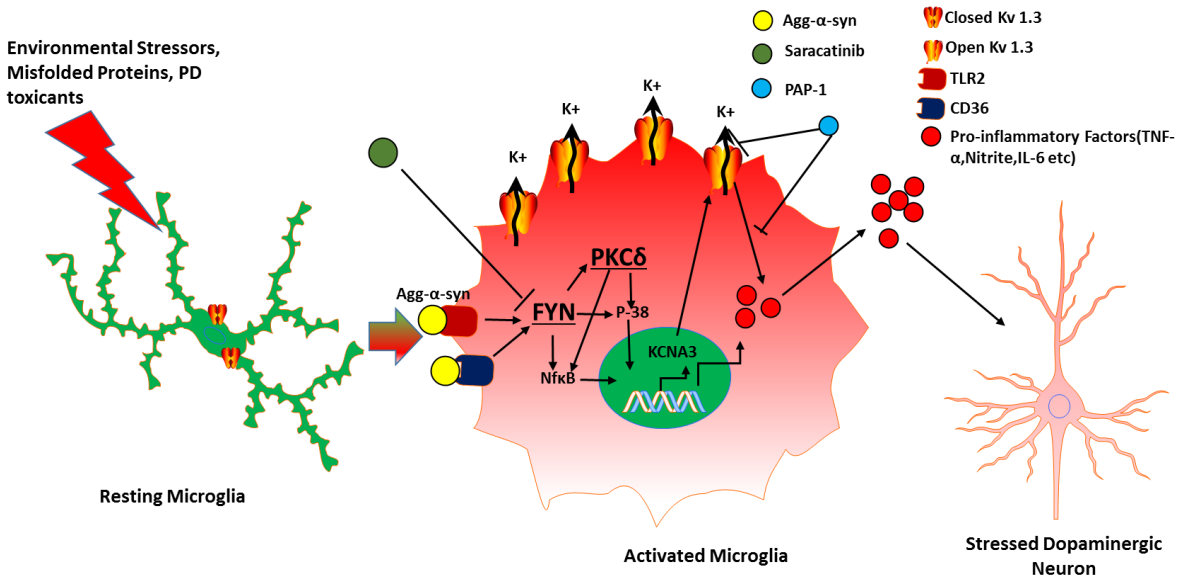

Scheme 1:Kv 1.3 dependent synuclein induced neuroinflammation in microglial cells

Supplementary Fig. 11: Working Hypothesis. Kv1.3 modulates microglial inflammation, leading to neurodegeneration in PD models, and is regulated by Fyn both transcriptionally and post-translationally.

CHAPTER V

GENERAL CONCLUSION AND FUTURE DIRECTIONS

This section presents a general overview of the results and findings described in the thesis, with a special emphasis on future directions and overall implications of these findings for the pathogenesis and progression of Parkinson's disease. The major findings pertaining to each research manuscript and their specific implications are covered in the 'results and discussion' sections of the relevant chapter.

Pesticide exposure leads to NLRP3 inflammasome activation in microglial cells *in vitro* and *in vivo.*

The primary finding from Chapter 2 of the thesis is that rotenone and tebufenpyrad, pesticides inhibiting mitochondrial complex 1, exposure leads to activation of NLRP3 inflammasome pathway in microglial cells. Further we showed, that NLRP3 activation is related to mitochondrial superoxide generation and lysosomal dysfunction. NLRP3 is recruited to the mitochondria post activation. Moreover, conditioned medium from glial cells post NLRP3 activation induced TH neuronal loss and inhibition of NLRP3 inflammasome reduced the neuronal loss in culture (Sarkar et al., 2017). Although we have demonstrated conclusively that mitochondrial dysfunction is important for NLRP3 inflammasome activation in glial cells future studies will identify key molecular pathways which are involved in the glial mitochondrial dynamics. Mitochondrial fusion and fission play an important role in regulating mitochondrial dynamics. Recent studies, have shown that Mfn2 degradation may lead to mitochondrial dysfunction (Tang et al., 2015). Moreover,

mitochondria associated adaptor molecule MAVS, have been implicated in recruitment of NLRP3 to the mitochondria during activation (Subramanian et al., 2013). We will generate CRISPR- Cas9 KD cells for these targets and study the role of these molecules in the recruitment of NLRP3 to mitochondria, and NLRP3 activation in glia.

Manganese leads to NLRP3 inflammasome activation in glial cells

In Chapter 3, we also showed that manganese induces mitochondrial dysfunction leading to NLRP3 inflammasome activation. We further show that manganese leads to downregulation of retromer protein VPS35 which leads to mitochondrial dysfunction by regulation of Mfn2. But it was not clear how manganese reduced the expression of VPS35 or other retromer complex protein VPS29. It is known that manganese can bind VPS29 (Swarbrick et al., 2011). Further, in retromer complex VPS35 wraps around the metal binding site of VPS29 (Hierro et al., 2007). We intend to build upon these studies. We will use recombinant proteins and *in vitro* cell free studies to show that excessive metal binding to VPS29 may lead to collapse of the retromer complex hence leading to downregulation of the retromer proteins. We will also study the promoter sequence of VPS35 to understand the probable role of metals in regulating the transcription of VPS35

Manganese plays a role in exosomal release ASC and propagation of NLRP3 inflammasome

Chapter 3 further demonstrates that manganese not only contributes to the activation of inflammasome but also propagates inflammasome by exosomal release

of ASC from microglia. Though we conclusively showed that manganese promotes exosomal release of ASC, we have not yet studied the mechanism of exosome release from glial cells. Various Rab proteins including Rab27 and Rab11 have been implicated in various steps of exosome biogenesis (Chen et al., 2017; Ostrowski et al., 2010). We will conduct studies looking into the probable role of Rab proteins in regulating manganese induced exosomal release of ASC.

Together, the first two research chapter demonstrated the role of environmental factors regulating inflammasome activation and regulating neuroinflammation in PD models (Refer to Fig 3 Page 51).

Kv1.3 plays a role in regulating neuroinflammation and neurodegeneration in PD

In Chapter 4, we utilized various *in vivo* and *in vitro* models of PD, as well as post mortem PD brains to conclusively show that Kv1.3, a voltage gated potassium channel is upregulated in microglial cells. Further, we showed in multiple animal models as well as cell culture models of PD that PAP-1, a small molecule inhibitor of Kv1.3, reduced neuroinflammation and neurodegeneration. Though we conclusively showed that Kv1.3 inhibition reduced neuroinflammation, the mechanism is still not clearly understood. We will perform whole cell and post translational proteome analysis to identify key Kv1.3 dependent microglial functions and validate them. Kv1.3 have been implicated in clearing of amyloid β plaques (Maezawa et al., 2017). Hence, to verify the role of Kv1.3 in synuclein uptake and clearance by glial cells we will perform RT-QUIC assay from Kv1.3 WT and KO microglia treated with αSyn_{Agg}. Further, to verify the role of Kv1.3 in aggregation of synuclein *in vivo,* we will generate

double transgenic mice by crossing A53T mouse with Kv1.3 KO mice to generate A53T Kv1.3 KO mice and characterize the mouse model.

Fyn, a src family kinase, transcriptionally and post-translationally modulated Kv1.3

In Chapter 4, we further showed that Kv1.3 is regulated transcriptionally by Fyn-PKCδ signaling pathway by regulating p38 and NFκb. Further, we have demonstrated that Fyn directly phosphorylate Kv1.3 modulating its channel activity. To further understand other key players in regulating Kv1.3 activity, we will perform immunoprecipitation studies and then perform mass spectrometry analysis to identify novel Kv1.3 binding partners. We will also mutate other probable phosphorylation sites on Kv1.3 to further understand the mechanism of channel regulation.

REFERENCES

Chen, Y.D., Fang, Y.T., Cheng, Y.L., Lin, C.F., Hsu, L.J., Wang, S.Y., Anderson, R., Chang, C.P., Lin, Y.S., 2017. Exophagy of annexin A2 via RAB11, RAB8A and RAB27A in IFN-gamma-stimulated lung epithelial cells. Sci Rep 7(1), 5676.

Dodd, C.A., Filipov, N.M., 2011. Manganese potentiates LPS-induced heme-oxygenase 1 in microglia but not dopaminergic cells: role in controlling microglial hydrogen peroxide and inflammatory cytokine output. Neurotoxicology 32(6), 683-692.

Filipov, N.M., Seegal, R.F., Lawrence, D.A., 2005. Manganese potentiates in vitro production of proinflammatory cytokines and nitric oxide by microglia through a nuclear factor kappa B-dependent mechanism. Toxicol Sci 84(1), 139-148.

Gammon, K., 2013. Inflammation: A complex problem. Nature 502(7473), S86-87.

Gerhard, A., 2016. TSPO imaging in parkinsonian disorders. Clin Transl Imaging 4, 183-190.

Ghosh, A., Langley, M.R., Harischandra, D.S., Neal, M.L., Jin, H., Anantharam, V., Joseph, J., Brenza, T., Narasimhan, B., Kanthasamy, A., Kalyanaraman, B., Kanthasamy, A.G., 2016. Mitoapocynin Treatment Protects Against Neuroinflammation and Dopaminergic Neurodegeneration in a Preclinical Animal Model of Parkinson's Disease. J Neuroimmune Pharmacol 11(2), 259-278.

Goldman, S.M., 2014. Environmental toxins and Parkinson's disease. Annu Rev Pharmacol Toxicol 54, 141-164.

Grozdanov, V., Bliederhaeuser, C., Ruf, W.P., Roth, V., Fundel-Clemens, K., Zondler, L., Brenner, D., Martin-Villalba, A., Hengerer, B., Kassubek, J., Ludolph, A.C.,

Weishaupt, J.H., Danzer, K.M., 2014. Inflammatory dysregulation of blood monocytes in Parkinson's disease patients. Acta Neuropathol 128(5), 651-663.

Hierro, A., Rojas, A.L., Rojas, R., Murthy, N., Effantin, G., Kajava, A.V., Steven, A.C., Bonifacino, J.S., Hurley, J.H., 2007. Functional architecture of the retromer cargo-recognition complex. Nature 449(7165), 1063-1067.

Kim, C., Ho, D.H., Suk, J.E., You, S., Michael, S., Kang, J., Joong Lee, S., Masliah, E., Hwang, D., Lee, H.J., Lee, S.J., 2013. Neuron-released oligomeric alpha-synuclein is an endogenous agonist of TLR2 for paracrine activation of microglia. Nature communications 4, 1562.

Kim, J., Byun, J.W., Choi, I., Kim, B., Jeong, H.K., Jou, I., Joe, E., 2013. PINK1 Deficiency Enhances Inflammatory Cytokine Release from Acutely Prepared Brain Slices. Experimental neurobiology 22(1), 38-44.

Kim, J.H., Choi, D.J., Jeong, H.K., Kim, J., Kim, D.W., Choi, S.Y., Park, S.M., Suh, Y.H., Jou, I., Joe, E.H., 2013. DJ-1 facilitates the interaction between STAT1 and its phosphatase, SHP-1, in brain microglia and astrocytes: A novel anti-inflammatory function of DJ-1. Neurobiology of disease 60, 1-10.

Kirkley, K.S., Popichak, K.A., Afzali, M.F., Legare, M.E., Tjalkens, R.B., 2017. Microglia amplify inflammatory activation of astrocytes in manganese neurotoxicity. Journal of Neuroinflammation 14(1), 99.

Kosloski, L.M., Kosmacek, E.A., Olson, K.E., Mosley, R.L., Gendelman, H.E., 2013. GM-CSF induces neuroprotective and anti-inflammatory responses in 1-methyl-4-phenyl-1,2,3,6-tetrahydropyridine intoxicated mice. J Neuroimmunol 265(1-2), 1-10.

Lee, E.J., Woo, M.S., Moon, P.G., Baek, M.C., Choi, I.Y., Kim, W.K., Junn, E., Kim, H.S., 2010. Alpha-synuclein activates microglia by inducing the expressions of matrix metalloproteinases and the subsequent activation of protease-activated receptor-1. J Immunol 185(1), 615-623.

Levesque, S., Taetzsch, T., Lull, M.E., Johnson, J.A., McGraw, C., Block, M.L., 2013. The role of MAC1 in diesel exhaust particle-induced microglial activation and loss of dopaminergic neuron function. J Neurochem 125(5), 756-765.

Liu, B., Hong, J.S., 2003. Role of microglia in inflammation-mediated neurodegenerative diseases: mechanisms and strategies for therapeutic intervention. J Pharmacol Exp Ther 304(1), 1-7.

Lotharius, J., Brundin, P., 2002. Pathogenesis of Parkinson's disease: dopamine, vesicles and alpha-synuclein. Nat Rev Neurosci 3(12), 932-942.

Maezawa, I., Nguyen, H.M., Di Lucente, J., Jenkins, D.P., Singh, V., Hilt, S., Kim, K., Rangaraju, S., Levey, A.I., Wulff, H., Jin, L.W., 2017. Kv1.3 inhibition as a potential microglia-targeted therapy for Alzheimer's disease: preclinical proof of concept. Brain.

Manyam, B.V., 1990. Paralysis agitans and levodopa in "Ayurveda": ancient Indian medical treatise. Mov Disord 5(1), 47-48.

McGeer, P.L., Itagaki, S., Boyes, B.E., McGeer, E.G., 1988. Reactive microglia are positive for HLA-DR in the substantia nigra of Parkinson's and Alzheimer's disease brains. Neurology 38(8), 1285-1291.

Moehle, M.S., Webber, P.J., Tse, T., Sukar, N., Standaert, D.G., DeSilva, T.M., Cowell, R.M., West, A.B., 2012. LRRK2 inhibition attenuates microglial inflammatory

responses. The Journal of neuroscience : the official journal of the Society for Neuroscience 32(5), 1602-1611.

Mogi, M., Harada, M., Riederer, P., Narabayashi, H., Fujita, K., Nagatsu, T., 1994. Tumor necrosis factor-alpha (TNF-alpha) increases both in the brain and in the cerebrospinal fluid from parkinsonian patients. Neurosci Lett 165(1-2), 208-210.

Mosley, R.L., Hutter-Saunders, J.A., Stone, D.K., Gendelman, H.E., 2012. Inflammation and adaptive immunity in Parkinson's disease. Cold Spring Harb Perspect Med 2(1), a009381.

Mullin, S., Schapira, A.H., 2015. Pathogenic mechanisms of neurodegeneration in Parkinson disease. Neurol Clin 33(1), 1-17.

Nagatsu, T., Mogi, M., Ichinose, H., Togari, A., 2000. Cytokines in Parkinson's disease. J Neural Transm Suppl(58), 143-151.

Ostrowski, M., Carmo, N.B., Krumeich, S., Fanget, I., Raposo, G., Savina, A., Moita, C.F., Schauer, K., Hume, A.N., Freitas, R.P., Goud, B., Benaroch, P., Hacohen, N., Fukuda, M., Desnos, C., Seabra, M.C., Darchen, F., Amigorena, S., Moita, L.F., Thery, C., 2010. Rab27a and Rab27b control different steps of the exosome secretion pathway. Nat Cell Biol 12(1), 19-30; sup pp 11-13.

Panicker, N., Saminathan, H., Jin, H., Neal, M., Harischandra, D.S., Gordon, R., Kanthasamy, K., Lawana, V., Sarkar, S., Luo, J., Anantharam, V., Kanthasamy, A.G., Kanthasamy, A., 2015. Fyn Kinase Regulates Microglial Neuroinflammatory Responses in Cell Culture and Animal Models of Parkinson's Disease. J Neurosci 35(27), 10058-10077.

Rees, K., Stowe, R., Patel, S., Ives, N., Breen, K., Clarke, C.E., Ben-Shlomo, Y., 2011. Non-steroidal anti-inflammatory drugs as disease-modifying agents for Parkinson's disease: evidence from observational studies. Cochrane Database Syst Rev(11), CD008454.

Sarkar, S., Malovic, E., Harishchandra, D.S., Ghaisas, S., Panicker, N., Charli, A., Palanisamy, B.N., Rokad, D., Jin, H., Anantharam, V., Kanthasamy, A., Kanthasamy, A.G., 2017. Mitochondrial impairment in microglia amplifies NLRP3 inflammasome proinflammatory signaling in cell culture and animal models of Parkinson's disease. NPJ Parkinsons Dis 3, 30.

Su, X., Maguire-Zeiss, K.A., Giuliano, R., Prifti, L., Venkatesh, K., Federoff, H.J., 2008. Synuclein activates microglia in a model of Parkinson's disease. Neurobiol Aging 29(11), 1690-1701.

Subramanian, N., Natarajan, K., Clatworthy, M.R., Wang, Z., Germain, R.N., 2013. The adaptor MAVS promotes NLRP3 mitochondrial localization and inflammasome activation. Cell 153(2), 348-361.

Swarbrick, J.D., Shaw, D.J., Chhabra, S., Ghai, R., Valkov, E., Norwood, S.J., Seaman, M.N., Collins, B.M., 2011. VPS29 is not an active metallo-phosphatase but is a rigid scaffold required for retromer interaction with accessory proteins. PLoS One 6(5), e20420.

Tang, F.L., Liu, W., Hu, J.X., Erion, J.R., Ye, J., Mei, L., Xiong, W.C., 2015. VPS35 Deficiency or Mutation Causes Dopaminergic Neuronal Loss by Impairing Mitochondrial Fusion and Function. Cell Rep 12(10), 1631-1643.

Whitton, P.S., 2007. Inflammation as a causative factor in the aetiology of Parkinson's disease. Br J Pharmacol 150(8), 963-976.

Wolters, E., 2009. Non-motor extranigral signs and symptoms in Parkinson's disease. Parkinsonism Relat Disord 15 Suppl 3, S6-12.

ACKNOWLEDGEMENTS

I would like to thank Dr. Anumantha Kanthasamy for giving me the opportunity to perform research in his laboratory. I would also like to thank Dr. Vellareddy Anantharam, Dr. Huajun Jin, and Gary Zenitsky for all their suggestions, guidelines, and research ideas that I have benefited from immensely. I also thank my committee for sitting through my POS meeting and prelims, and for providing constructive advice. I am also indebted to the past and present members of my lab, particularly Emir, Matthew, Nikhil, Dilshan, Dharmin, Muhammet, Monica, Dan, and Poojya. Finally, I would like to thank my fiancée, Tulip, for her constant support, love and motivation, and my parents for for their unending support.

APPENDIX I

RAPID AND REFINED CD11B MAGNETIC ISOLATION OF PRIMARY MICROGLIA WITH ENHANCED PURITY AND VERSATILITY

Manuscript published in *Journal of Visualized Experiment*

AUTHOR:

Souvarish Sarkar[*1], Emir Malovic[*1], Brandon Plante[1], Gary Zenitsky[1], Huajun Jin[1], Vellareddy Anantharam[1], Arthi Kanthasamy[1], Anumantha G. Kanthasamy[1]

[1] Biomedical Sciences & Iowa Center for Advanced Neurotoxicology, Iowa State University, Ames, IA, USA

Sarkar,Souvarish

rakras26@iastate.edu

Malovic,Emir

emalovic@iastate.edu

Plante, Brandon

bplante69@gmail.com

Zenitsky, Gary

zenitsky@iastate.edu

Jin, Huajun

egb761@iastate.edu

Anantharam, Vellareddy

anantram@iastate.edu

Kanthasamy, Arthi

arthik@iastate.edu

Kanthasamy, Anumantha

akanthas@iastate.edu

***These authors have made equal contribution to this study**

CORRESPONDING AUTHOR:

Anumantha G. Kanthasamy

akanthas@iastate.edu

Phone: 515-294-2516

KEYWORDS

CD11b, microglia, primary culture, magnetic isolation, brain, aging, neurodegeneration, neuroinflammation, neurodegenerative disorders

SHORT ABSTRACT

Here, we present a protocol to isolate microglia from postnatal mouse pups (day 1) for *in vitro* experimentation. This improvised method of isolation generates both high yield and purity, a significant advantage over alternate methods that allows broad range experimentation for the purposes of elucidating microglial biology.

LONG ABSTRACT

Microglia are the primary responders to central nervous system insults; however, much remains unknown about their role in regulating neuroinflammation. Microglia are mesodermal cells that function similarly to macrophages in surveying inflammatory stress. The classical (M1-type) and alternative (M2-type) activations of macrophages have also been extended to microglia in an effort to better understand the underlying interplay these phenotypes have in neuroinflammatory conditions such as Parkinson's, Alzheimer's, and Huntington's diseases. *In vitro* experimentation utilizing primary microglia offers rapid and reliable results that may be extended to the *in vivo* environment. Although this is a clear advantage over *in vivo* experimentation, isolating microglia while achieving adequate yields of optimal purity has been a challenge. Common methods currently in use either suffer from low recovery, low purity, or both. Herein, we demonstrate a refinement of the column-free CD11b magnetic separation method that achieves a high cell recovery and enhanced purity in half the amount of time. We propose this optimized method as a highly useful model

of primary microglial isolation for the purposes of studying neuroinflammation and neurodegeneration.

INTRODUCTION

Microglia are Myb-independent resident macrophages of mesodermal origin, which differentiate from c-kit+/CD45- erythromyeloid progenitors in the blood islands of the yolk sac[1,2]. Once embryological microglia have colonized the central nervous system (CNS), they transition from an amoeboid to a ramified form[3]. These adult microglia are classified as surveillant since their dynamic ramifications probe the healthy brain parenchyma for potential insults[4]. Although microglia only contribute to approximately 10% of the CNS cell population, their ability to tile amongst each other ensures maximal scanning of the parenchyma[4,5]. Danger-associated molecular patterns (DAMPs), such as α-synuclein[6,7] and amyloid-β[8], or pathogen-associated molecular patterns (PAMPs) such as lipopolysaccharide (LPS)[9], classically activate microglia to promote an inflammatory response characterized by reversion to the amoeboid active state and the production of nitric oxide, tumor necrosis factor-α (TNFα), interleukin 1β (IL-1β), IL-6, IL-12, and the chemokine C-C motif ligand 2[9-11]. In neuroinflammatory conditions such as Parkinson's disease, in which pathogenic α-synuclein has accumulated, a neurodegenerative cycle is created from the death of dopaminergic neurons, which release more aggregated α-synuclein, further promoting classical activation of microglia[7]. Similar to peripheral macrophages, microglia may also have the ability to alternatively activate in the presence of the anti-inflammatory

cytokines IL-4 and IL-10, giving them the potential of promoting neural repair and attenuating inflammation[2,11]. Aside from their immunological roles in the CNS, microglia have been described as vital regulators of neuronal circuitry by pruning synapses during development. For example, *Cx3cr1*-KO mice have less dense microglia and reduced synaptic pruning, which leads to an overabundance of dendritic spines, immature synapses, and the electrophysiological patterns of an underdeveloped CNS[12]. Understanding these physiological complexities and the diverse functional roles of microglia in the homeostasis of the CNS are critical to the search for therapeutics targeting neurodegenerative disorders.

In the area of neuroimmunology, *in vitro* experiments are highly desirable because of greater feasibility for mechanistic studies, lower maintenance costs, and for being less time- and labor-intensive. Furthermore, the ability to isolate cell populations is critical to delineating the functionality of those target cells under prescribed conditions. Numerous microglial isolation methods exist, but they are limited by their ability to obtain relatively high numbers and purity for broad experimentation[13-15]. For example, cluster of differentiation 11b (CD11b) is a common surface marker of monocytes, macrophages, and microglia[16]. By exploiting CD11b, a method of magnetic separation was first described as a column-based approach that yielded ~99.5% purity and ~1.6 x 10^6 microglia per neonatal brain[17]. Our laboratory recently developed a column-free CD11b magnetic separation method[15], which we performed in a polystyrene tube by tagging CD11b with a monoclonal antibody conjugated to phycoerythrin (PE). A bispecific secondary antibody to PE and dextran

complexes with the PE. Once bound, dextran-coated magnetic particles are introduced, which bind to the dextran end of the antibody complex. Lastly, the polystyrene tube is placed in a magnet for microglial isolation. This approach doubled the yield to ~3.2 x 10^6 microglia per neonatal brain but at the cost of reducing purity to ~97%.

Herein, we demonstrate a rapid and refined column-free CD11b magnetic separation protocol (Figure 1). This improved method remains as feasible as our original column-free method since the price of the CD11b magnetic separation kit is the same. The completion time is reduced by half, which can be crucial to maximizing cell survival and yield. Notably, the purity achieved from this optimized method is ~>99%, a marked improvement over the purity achieved from the original column-free method developed by our laboratory[15]. Most importantly, CD11b-PE is not utilized, eliminating the need to incubate away from light and allowing use of the red channel for fluorescence microscopy. Lastly, as in the original CD11b method, an astrocytic fraction of high yield and purity is obtained with this improved method. Astrocytes are the most numerous glial cells in the CNS, leading to the idea that their homeostatic functions are indispensable in relation to pathophysiology[18]. These glial cells play a role in diverse physiological functions such as forming the blood-brain barrier, providing nutrient support, maintaining neurotransmitter homeostasis, forming glial scars in response to injury, neuroprotection, learning and memory, and neuroinflammation, exemplifying their investigatory potential in glial biology[19]. Morphology and functionality of microglia and astrocytes have been ascertained via confocal microscopy, Western blotting, quantitative real-time polymerase chain

reaction (qRT-PCR), Griess nitrite assay, and the Luminex multiplex cytokine assay. The refinement provided by this protocol offers increased confidence pertaining to microglial or astrocytic purity, broader application of fluorescence microscopy with the availability of the red channel, and saves time, all of which are important for *in vitro* experimentation.

PROTOCOL

Use of the animals and protocol procedures were approved and supervised by the Institutional Animal Care and Use Committee (IACUC) at Iowa State University (Ames, IA, USA)

1. Growing of mixed glial cultures.

1.1 Decapitate one-to-two-day old pups quickly with 5.5 inch operating scissors, and place the heads immediately in a 50 mL Corning Centristar tube on ice. Note, this decapitation is the mode of euthanasia.

1.2 In a laminar airflow hood, make a small incision in the skull and meninges using 4.5 inch straight micro-dissecting scissors. Begin cutting from the caudal end to the rostral end (nose). Get underneath the skin by using the opening formed by the decapitation.

1.2.1 After the incision, peel one of the hemispheres to the side.

1.2.2 Then use a pair of curved or hooked tweezers to remove the entire brain.

1.3 Immerse the brain(s) in a new 50 mL tube containing trypsin-ethylenedinitrilotetraacetic acid (EDTA) for 15 min in a 37 °C water bath. Use **2 mL** of trypsin-EDTA per brain.

1.4 Wash the brain(s) with fresh **Growth Media** (10% FBS, DMEM/F12, 1% penicillin/streptomycin, 1% L-glutamine, 1% sodium pyruvate, and 1% non-essential amino acids) by adding and aspirating or discarding the fresh media 4 different times.

1.5 For each brain, **two** T-75 flasks containing growth media will be plated. Therefore, add **2 mL** of growth media per brain to the tube. Thus, it will be an equivalent of **1 mL** of homogenized brain with **8-9 mL** of growth media per T-75 flask.

1.6 Homogenize by triturating the brain(s) with pipettes of differing aperture size, in order from largest to smallest. When it is visible that the brain tissue is not getting smaller, transition to the next pipette. At the end of the trituration, the suspension should be clear, with no visible chunks.

1.6.1 Use a 25 mL pipette, 5 mL pipette, and then a 10 mL pipette sequentially.

1.7 Pass each homogenous brain suspension through a 70 µm cell strainer to make it into a single cell culture.

1.8 For each homogenized brain, plate **two** T-75 flasks containing growth media, as described in step 1.5 (**1 mL** of homogenized brain with **8-9 mL** of growth media per T-75 flask).

1.9 Change growth media after 6 days and grow until isolation on the 16th day.

2. Isolation of microglial cells.

2.1 After 16 days, remove the growth media from the flask and place it in a fresh 50mL tube.

2.1.1 Next, add 3 mL trypsin-EDTA to each T-75 flask.

2.1.2 Shake the flasks for 5 min at room temperature on an orbital shaker such as a belly dancer.

2.1.3 The removed growth media may be centrifuged at 0.4 x g for 5min and used to stop the trypsin-EDTA reaction in the subsequent step.

2.2 After shaking for 5 min, add a minimum of 4 mL of growth media (fresh or the used media) to stop the trypsin-EDTA reaction.

2.3 Triturate to ensure that all the cells have been detached.

2.4 After trituration, pass the cells through a 70 µm cell strainer to make it into a single cell culture and spin down the cells at 0.4 x g for 5 min.

2.5 For every 100 million cells (roughly 15 T-75 flasks) use **1 mL** of **Recommended Media** (2% FBS, DPBS (Calicum and Magnesium Chloride free), 1 mM EDTA) to re-suspend the cell pellet.

2.6 **All following steps are tailored for a 1mL separation.** Take a 5 mL polystyrene tube, add 1 mL of recommended media, and mark the meniscus.

2.6.1 Next, add recommended media up to 2.5 mL and mark it as well.

2.6.2 Finally, discard the recommended media and transfer the re-suspended cells to the 5 mL polystyrene tube.

2.7 Add 50 µL of rat serum for every 1 mL of suspended cells.

2.7.1 Incubate for 5 min at room temperature.

2.8 Prepare selection cocktail by mixing 25 µL of component A and 25 µL of component B. These components are proprietary.

2.9 Add 50 µL of the selection cocktail to the cells.

2.10 Incubate for 5 min at room temperature.

2.10.1 For purer cultures, repeat steps 2.9 and 2.10 (recommended but not mandatory).

2.12 Vortex microspheres for 45 s. Add 75 µL of microspheres per 1 mL of sample.

2.13 Incubate for 3 min at room temperature.

2.14 Bring the volume to 2.5 mL in polystyrene tube by adding recommended medium.

2.15 Put the tube in the magnet for 3 min at room temperature. Incubation may be adjusted for the purposes of increasing purity.

2.16 Slowly pour out the recommended medium into a 15 mL tube with the polystyrene tube still in magnet.

2.17 Repeat steps 15-17 **three** more times. Additional magnetic incubations may be performed for the purposes of increasing purity.

2.18 Add 3 mL of growth media and count the number of cells using cell counter.

2.19 Plate cells accordingly in poly-D-lysine-coated plates for treatments. Begin treating the cells 48 h after seeding in poly-D-lysine-coated plates. This allows the cells to recover from the stress of separation.

2.20 Check the purity of the culture using immunocytochemistry as described previously[15].

2.21 Plate the negative fraction (collected in a 15 mL tube), which mostly contains astrocytes, in T-75 flasks in the growth medium.

2.22 After at least 6 h of incubation in 37 °C incubator, change the medium and let it grow overnight.

2.23 Split the astrocytes the next day for treatments.

REPRESENTATIVE RESULTS

Microglia isolated using CD11b Positive Selection kit II have high purity

Primary mouse microglia were isolated using the above mentioned protocol and plated on poly-D-lysine-coated coverslips to check the purity of isolation. Ten thousand cells were plated per well and immunocytochemical analysis was performed using ionized calcium-binding adaptor molecule 1 (Iba1) as a marker of microglia and glial fibrillary acidic protein (GFAP) as a marker of astrocytes to check for the purity of the isolated microglia. The isolated culture only expressed Iba1 without GFAP expression (Figure 2A), suggesting that the culture isolated was pure microglia. Unlike other previously published methods for primary microglial separation, which achieve ~97% purity, using this method we obtained ~>99% purity in half the time. To further validate the purity of this culture, we ran a Western blot [20] for Iba1 and GFAP. Immunoblot analysis further revealed that this isolation from the mixed glial cultures was a nearly pure microglial culture (Figure 2B).

The modified isolation procedure does not have any auto-fluorescence from magnetic beads

The red channel cannot be used for immunocytochemistry (ICC) when using the previous CD11b isolation kit for microglial separation as mentioned by Gordon et al. (2011)[15] because of the use of PE labeling during separation. Using this new PE-free isolation kit, we can use the red channel for immunocytochemical analysis (Figure 3). From this ICC, it is evident that this new method enables us to use all the channels for flow cytometry or other fluorescent imaging studies.

Isolated microglial cultures functionally respond to LPS stimulus

To verify that the isolated microglia are functionally active, we treated the cells with LPS, a widely used stimulant[9] to activate microglia, for 24 h before probing for various pro-inflammatory factors. Classical microglial activation is accompanied by the release of nitrite and various pro-inflammatory cytokines into the media. Hence, we used multiple complementary assays to confirm the functional activity of our isolated microglia. First, we used the Griess assay to show that LPS dramatically induced nitrite secretion from the isolated microglia (Figure 4A). To further validate the activity of isolated microglia, we used qRT-PCR to show (messenger ribonucleic acid) mRNA levels of *NOS2*, another hallmark of microglial inflammation, significantly enhanced with LPS treatment (Figure 4B). Next, we used a bead-based multiplex assay, Luminex[21], to verify that LPS significantly stimulated the secretion of pro-inflammatory cytokines from the microglial culture (Figure 5A). Furthermore, we verified via qRT-

PCR analysis that LPS treatment enhanced the gene expression levels of several pro-inflammatory cytokines including *IL-1β* and *TNFα* (Figure 5B). All these data together suggest that primary microglia isolated using this newly refined method are functionally active and show a similar activation profile as primary microglia isolated using previously published methods.

Isolated microglia can be used for signaling studies

Using the previous methods of microglial isolation, running Western blot for signaling studies was difficult and infeasible due to low yield and purity. Previously, we have shown that Fyn, a Src family kinase, is involved in a pro-inflammatory signaling cascade in microglial cells[9]. Here we plated one million microglial cells in a 12-well plate and after 48 h collected the cells to run Western blots for native Fyn and Src kinases phosphorylated at tyrosine residue 416 (p-Src-Y416). We were able to detect both Fyn and p-Src-Y416 levels in our isolated microglial cells (Figure 6), showing that this method is applicable to Western blotting techniques for signaling studies.

The negative fraction from the microglial separation contains astrocytes that can be used for signaling studies

Astrocytes are key players in neuroinflammation, and understanding the signaling mechanisms behind astrocytic inflammation and neuron-astrocyte cross-talk is important[19]. Here, we show that the negative fraction from the microglial separation contains GFAP-positive astrocytic cells (Figure 7A). Also, our Western blot analysis

for Fyn and p-Src-Y416 (Figure 7B) showed that both of these proteins can be detected in the negative fraction as well. These results together show that the negative fraction is an ideal preparation for astrocytic studies aimed at identifying proteins important for inflammatory signaling cascades.

DISCUSSION

Older microglial isolation methods have limited recoveries that are not appropriate for various protein analyses by Western blot and RNA analyses by qRT-PCR. The differential adherence and mild trypsinization methods are two common approaches with low microglial yields [13-15]. The column-based CD11b approach also has low recovery, but achieves greater purity than differential adherence and mild trypsinization [13-15,17]. Our original column-free CD11b approach greatly improved the isolated yields, making it suitable for protein and RNA analyses such as Western blotting and qRT-PCR, but at the cost of decreased purity [15].

Our newly modified method retains the yields of the original method and increases the purity slightly from ~95-97% to ~>99%, but in half the completion time, which is critical for cell survival. Crucial steps within the protocol can assure optimal microglial isolation. While decapitating the pups, care should be taken to keep the heads on ice and then dissected in a laminar airflow chamber within 5-10 mins. Prolonged brain excision times will make it difficult to obtain the full of brain because it begins to lose its solidity at ambient temperatures, compromising the microglial yields. Notably, if steps 2.9 and 2.10 are repeated at least once, there is an observable increase in the purity and the viability. If the yield from the separation is

low, the separation can be repeated using fewer flasks per mL of recommended media, or by increasing the volume of separation (>1mL). Decreasing cell crowding generally will improve purity, viability, and yield. The magnetic incubation time may be extended in step 2.15 for the purposes of increasing purity. This can assure proper magnetic binding of the microspheres that are attached to the microglia. Furthermore, additional magnetic incubations may be performed in step 2.17 for the sake of increasing purity and yield.

The feasibility of the protocol is equivalent to or better than the original CD11b method, however, the new method is refined and shorter. Another significant advantage gained from this refined method is the option of utilizing the red channel for fluorescence microscopy, which is occupied by PE in the original method (Table 1) [15]. Though we get high yield and purity of microglia with the method, the astrocytic yield obtained from this separation is less pure since it retains some fibroblasts. As described in step 2.22, after plating the astrocytes and incubating for 6 h, the growth media should be replaced with fresh media. Astrocytes are the first to attach to the flask, while much of the fibroblasts remain in suspension. The replacement of the media generally will remove the majority of contaminating fibroblasts. Although this technique assures a high purity of astrocytes, a secondary purification method to achieve purer cultures of is warranted.

Overall, this modified CD11b isolation method generates highly pure primary microglial cells and astrocytes in a short amount of time. The shorter isolation time generally improves cell survival rates. It provides a useful model system for elucidating the signaling mechanisms underlying both microglial and astroglial biology.

ACKNOWLEDGEMENTS:

This work was supported by National Institutes of Health (NIH) Grants: NS088206 and ES026892. The W. Eugene and Linda Lloyd Endowed Chair to AGK and Deans Professorship to AK are also acknowledged.

DISCLOSURES:

The authors declare that they have no competing financial interests.

REFERENCES

1 Schulz, C. *et al.* A lineage of myeloid cells independent of Myb and hematopoietic stem cells. *Science.* **336** (6077), 86-90, doi:10.1126/science.1219179, (2012).

2 Prinz, M. & Priller, J. Microglia and brain macrophages in the molecular age: from origin to neuropsychiatric disease. *Nat Rev Neurosci.* **15** (5), 300-312, doi:10.1038/nrn3722, (2014).

3 Alliot, F., Godin, I. & Pessac, B. Microglia derive from progenitors, originating from the yolk sac, and which proliferate in the brain. *Brain Res Dev Brain Res.* **117** (2), 145-152 (1999).

4 Ransohoff, R. M. & Cardona, A. E. The myeloid cells of the central nervous system parenchyma. *Nature.* **468** (7321), 253-262, doi:10.1038/nature09615, (2010).

5 Kettenmann, H., Kirchhoff, F. & Verkhratsky, A. Microglia: new roles for the synaptic stripper. *Neuron.* **77** (1), 10-18, doi:10.1016/j.neuron.2012.12.023, (2013).

6 Su, X. *et al.* Synuclein activates microglia in a model of Parkinson's disease. *Neurobiol Aging.* **29** (11), 1690-1701, doi:10.1016/j.neurobiolaging.2007.04.006, (2008).

7 Dzamko, N., Geczy, C. L. & Halliday, G. M. Inflammation is genetically implicated in Parkinson's disease. *Neuroscience.* **302** 89-102, doi:10.1016/j.neuroscience.2014.10.028, (2015).

8 Xing, B., Bachstetter, A. D. & Van Eldik, L. J. Microglial p38alpha MAPK is critical for LPS-induced neuron degeneration, through a mechanism involving TNFalpha. *Mol Neurodegener.* **6** 84, doi:10.1186/1750-1326-6-84, (2011).

9 Panicker, N. *et al.* Fyn Kinase Regulates Microglial Neuroinflammatory Responses in Cell Culture and Animal Models of Parkinson's Disease. *J Neurosci.* **35** (27), 10058-10077, doi:10.1523/JNEUROSCI.0302-15.2015, (2015).

10 Moehle, M. S. & West, A. B. M1 and M2 immune activation in Parkinson's Disease: Foe and ally? *Neuroscience.* **302** 59-73, doi:10.1016/j.neuroscience.2014.11.018, (2015).

11 Saijo, K. & Glass, C. K. Microglial cell origin and phenotypes in health and disease. *Nat Rev Immunol.* **11** (11), 775-787, doi:10.1038/nri3086, (2011).

12 Paolicelli, R. C. *et al.* Synaptic pruning by microglia is necessary for normal brain development. *Science.* **333** (6048), 1456-1458, doi:10.1126/science.1202529, (2011).

13 Floden, A. M. & Combs, C. K. Microglia repetitively isolated from in vitro mixed glial cultures retain their initial phenotype. *J Neurosci Methods.* **164** (2), 218-224, doi:10.1016/j.jneumeth.2007.04.018, (2007).

14 Saura, J., Tusell, J. M. & Serratosa, J. High-yield isolation of murine microglia by mild trypsinization. *Glia.* **44** (3), 183-189, doi:10.1002/glia.10274, (2003).

15 Gordon, R. *et al.* A simple magnetic separation method for high-yield isolation of pure primary microglia. *J Neurosci Methods.* **194** (2), 287-296, doi:10.1016/j.jneumeth.2010.11.001, (2011).

16 Prinz, M., Priller, J., Sisodia, S. S. & Ransohoff, R. M. Heterogeneity of CNS myeloid cells and their roles in neurodegeneration. *Nat Neurosci.* **14** (10), 1227-1235, doi:10.1038/nn.2923, (2011).

17 Marek, R., Caruso, M., Rostami, A., Grinspan, J. B. & Das Sarma, J. Magnetic cell sorting: a fast and effective method of concurrent isolation of high purity viable astrocytes and microglia from neonatal mouse brain tissue. *J Neurosci Methods.* **175** (1), 108-118, doi:10.1016/j.jneumeth.2008.08.016, (2008).

18 Hasko, G., Pacher, P., Vizi, E. S. & Illes, P. Adenosine receptor signaling in the brain immune system. *Trends Pharmacol Sci.* **26** (10), 511-516, doi:10.1016/j.tips.2005.08.004, (2005).

19 Radulovic, M., Yoon, H., Wu, J., Mustafa, K. & Scarisbrick, I. A. Targeting the thrombin receptor modulates inflammation and astrogliosis to improve recovery

after spinal cord injury. *Neurobiol Dis.* **93** 226-242, doi:10.1016/j.nbd.2016.04.010, (2016).

20 Ay, M. *et al.* Molecular cloning, epigenetic regulation, and functional characterization of Prkd1 gene promoter in dopaminergic cell culture models of Parkinson's disease. *J Neurochem.* **135** (2), 402-415, doi:10.1111/jnc.13261, (2015).

21 Gordon, R. *et al.* Protein kinase Cdelta upregulation in microglia drives neuroinflammatory responses and dopaminergic neurodegeneration in experimental models of Parkinson's disease. *Neurobiol Dis.* **93** 96-114, doi:10.1016/j.nbd.2016.04.008, (2016).

Scheme 1

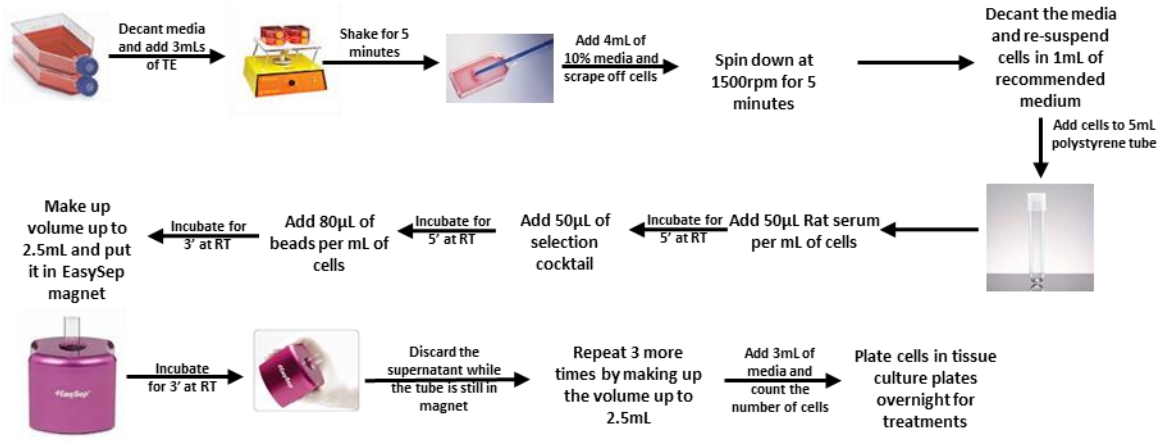

Figure 1: Schematic of isolation of microglial cells from 1-2 day post-natal pups.

Figure 2

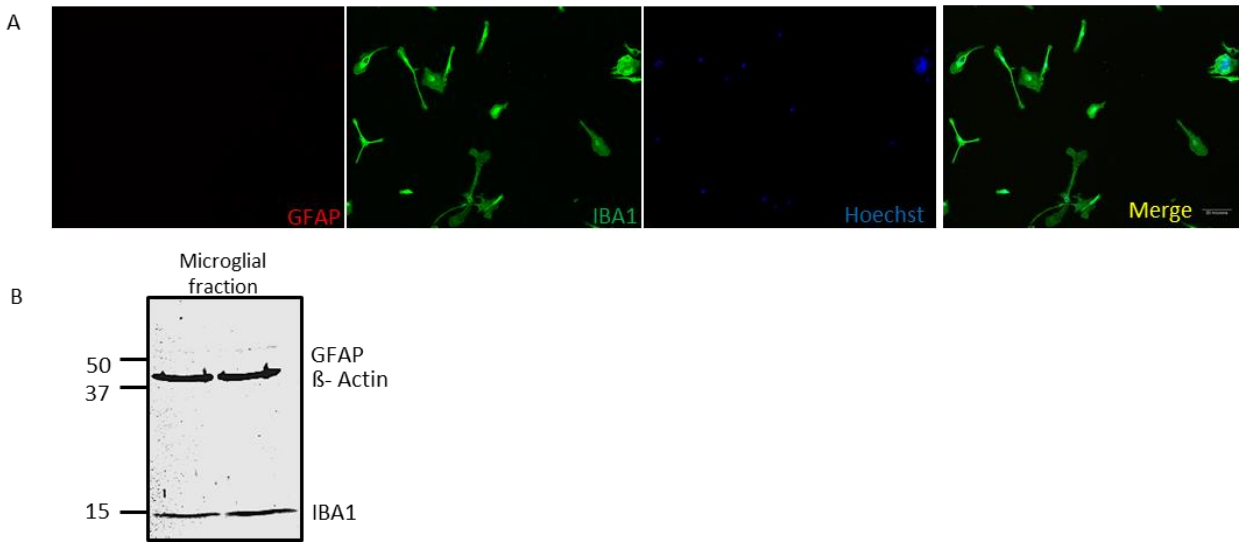

Figure 2: Microglia isolated using CD11b positive selection kit II have high purity.

a) Immunocytochemistry of isolated microglial culture probing for GFAP in red channel and IBA1 in green channel. b) Immunoblot of isolated microglial culture probing for GFAP (~ 51 kDa), IBA1 (~15 kDa) and β-Actin (~42 kDa).

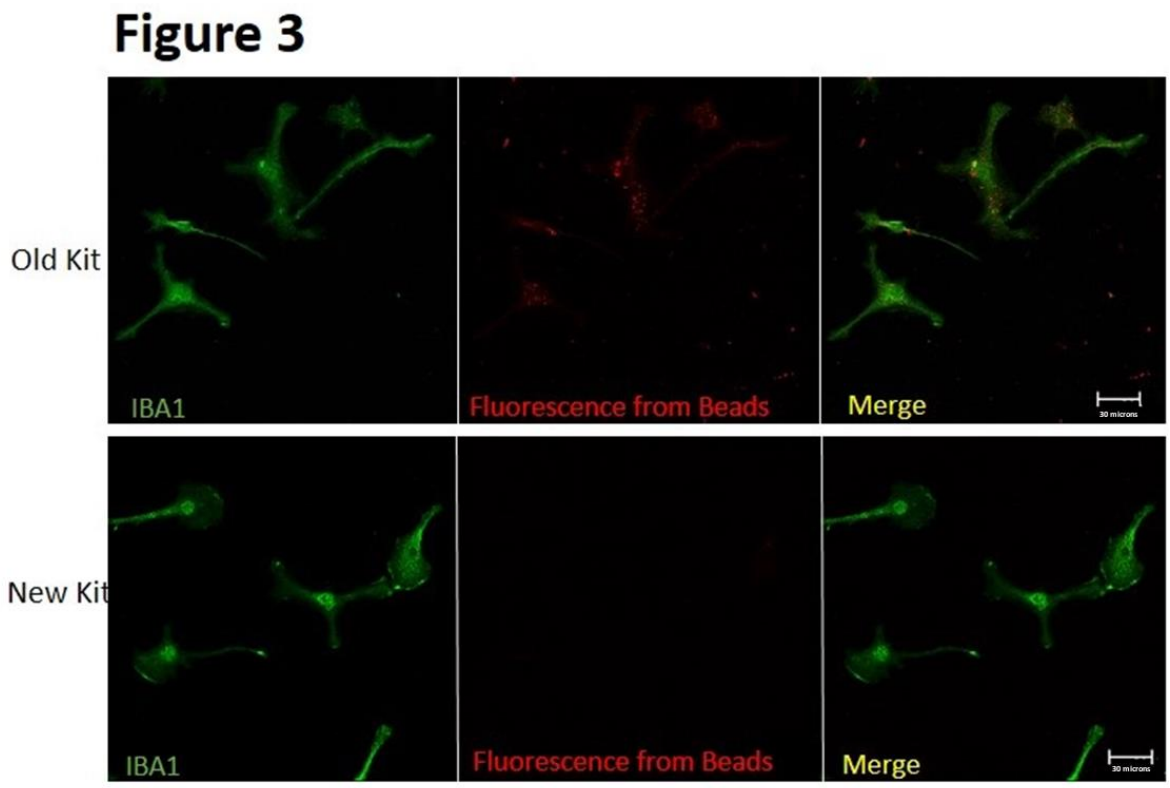

Figure 3: The modified isolation procedure does not have any auto-fluorescence from magnetic beads.

Immunocytochemistry of isolated microglial culture using the new isolation method and old (original) method probing for IBA1 in green channel and PE fluorescence in red channel.

Figure 4

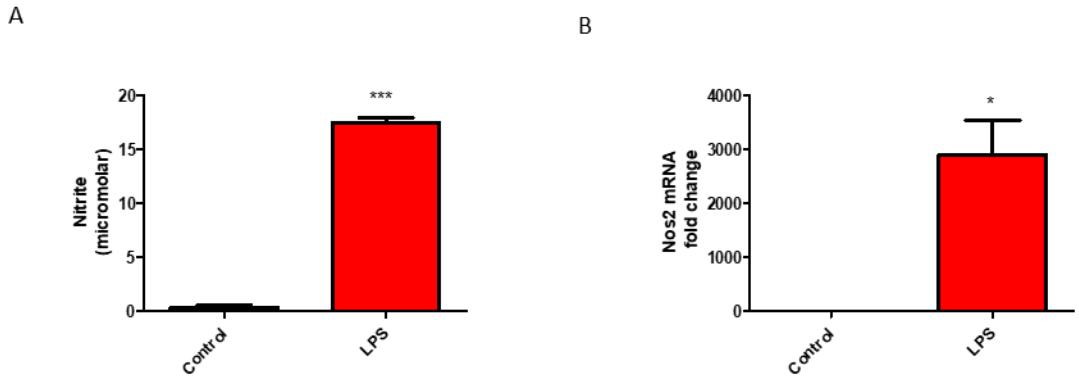

Figure 4: LPS stimulation increased nitrite production in microglial culture.

a) Isolated microglial cells treated with 1 µg/mL LPS for 24 h and treatment medium were collected to determine nitrite release by Griess assay. b) q-RT-PCR for Nos2 from isolated microglia treated with LPS for 24 h. The figures represent mean ± SE from 2 or more independent experiments. Data analyzed using Student's t test (*p<0.05, **p<0.01, ***p<0.001)

Figure 5

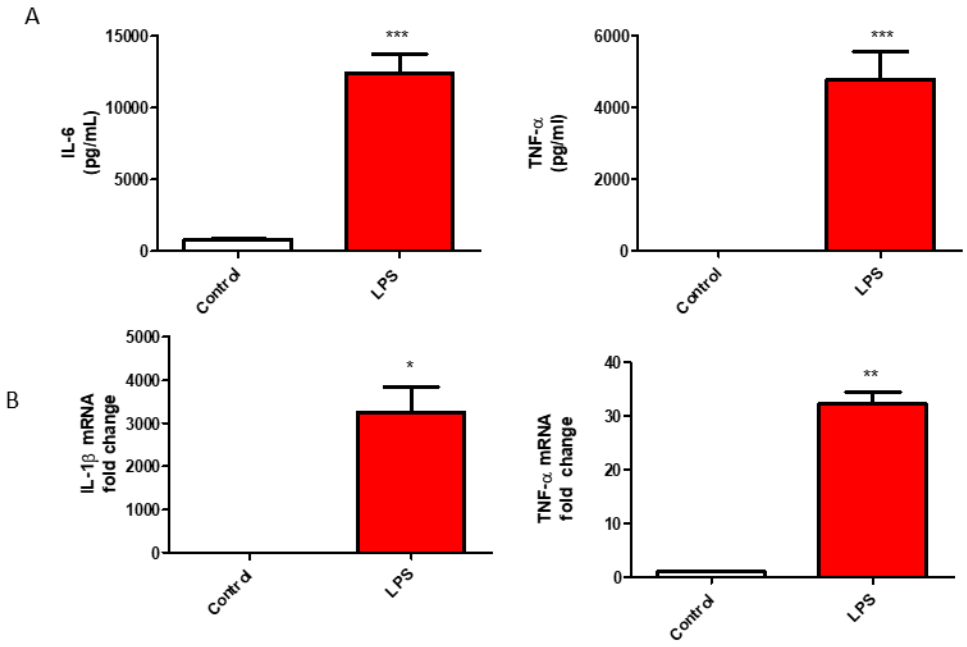

Figure 5: LPS induced pro-inflammatory cytokine release from microglial cells. a) Luminex multiplex assay was performed on treatment medium collected from isolated microglial cells treated with 1 µg/mL LPS for 24 h. b) q-RT-PCR for IL-1βand TNFα from isolated microglia treated with LPS for 24 h. The figures represent mean ± SE from 2 or more independent experiments. Data analyzed using Student's t test (*p<0.05, **p<0.01, ***p<0.001)

Figure 6

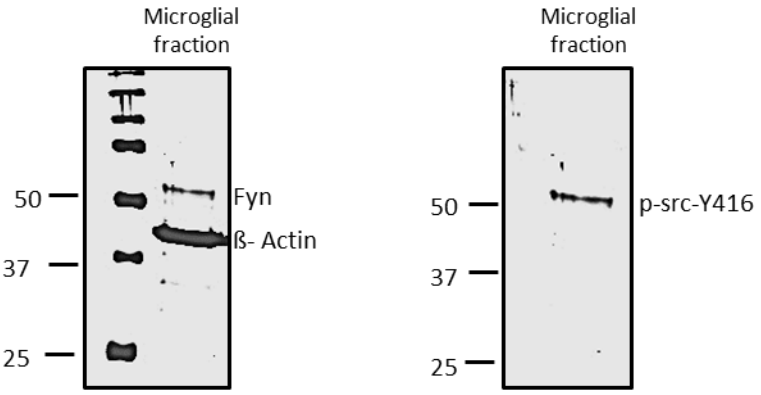

Figure 6: Isolated microglia can be used for signaling studies.

Western blot analysis showing that Fyn and p-Src-Y416 can be detected from microglia isolated with our newly refined method.

Figure 7

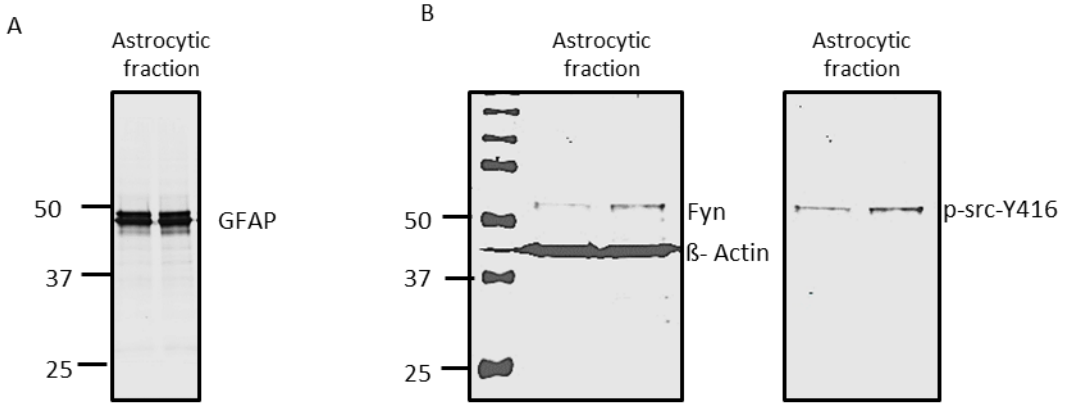

Figure 7: The negative fraction from the microglial separation contains astrocytes that can be used for signaling studies.

a) Western blotting shows that the negative fraction contains GFAP-positive cells. b) Western blot analysis showing that Fyn and p-Src-Y416 can be detected from the GFAP-positive cells.

Parameters	**Current method**	**Modified method**
Cost	$620	$620
Time	55 min	25 min
Fluorescence	Yes (red channel)	No
Purity	~97%	~99%

Table 1: Comparative analysis between the refined microglial isolation method and the original method of isolation.

APPENDIX II

CHARACTERIZATION AND COMPARATIVE ANALYSIS OF A NEW MOUSE MICROGLIAL CELL MODEL FOR STUDYING NEUROINFLAMMATORY MECHANISMS DURING NEUROTOXIC INSULTS.

A manuscript under revision in *Neurotoxicology*

Souvarish Sarkar[#], Emir Malovic[#], Deeksha Sarda, Vivek Lawana, Dharmin Rokad, Huajun Jin, Vellareddy Anantharam, Arthi Kanthasamy, Anumantha G. Kanthasamy*

Parkinson Disorders Research Laboratory, Iowa Center for Advanced Neurotoxicology, Department of Biomedical Sciences, 2062 Veterinary Medicine Building, Iowa State University, Ames, IA 50011.

#These authors made equal contributions

*To whom correspondence should be addressed: Anumantha Kanthasamy, Ph.D. Distinguished Professor and Chair, Lloyd Endowed Chair and Eminent Scholar, Department of Biomedical Sciences, Iowa State University, Ames, IA 50011, Telephone: (515) 294-2516; Fax: (515) 294-2315, Email: akanthas@iastate.edu

Abstract

Microglia are the first responders of the central nervous system, acting as the key modulators of neuroinflammation observed during neurotoxic insults as well as in the pathophysiology of several neurodegenerative disorders including Alzheimer's, Parkinson's, and Huntington's diseases. The number of publications on microglia has increased steadily throughout the past decade because of immense interests in the neuroinflammation that precedes the neurodegenerative process. To study microglial biology and its role in modulating neuroinflammation, immortalized microglial cell lines representing mouse, rat, and human have been developed. Among these, the BV2 mouse microglial cell line is the most well characterized and widely used cell culture model. However, even unstimulated BV2 cells exhibit an amoeboid morphology, indicating a highly activated and inflammatory state compared to primary microglia, thus making them less than ideal for studying low-dose effects of toxicants on microglial activation. Therefore, we performed an in-depth characterization of a recently developed mouse microglial cell (MMC) line, which we compared with primary microglia (PMG) and BV2s to determine the ideal cell line for studying neurotoxicant effects on microglial function. Comparative analyses reveal that MMCs are strikingly similar to PMG in basal activity, morphology, and sensitivity, characteristics that BV2s lack. Basal nitrite and inflammatory cytokine levels are significantly higher in BV2s compared to MMCs. Furthermore, BV2 cells are less reactive to the inflammagen LPS compared to MMCs, due to their higher basal activation state. Collectively, we demonstrate, based on in-depth analyses of morphology, basal activity, and responsivity to three different stimuli (LPS, aggregated α-synuclein, and neurotoxic

manganese), that MMCs mimic neonatal PMG, and are discernibly more suitable than BV2s for studying neuroinflammatory mechanisms of neurotoxicants.

Introduction

Microglia are the first immune responders in the brain. Persistently active and unregulated microglia are key modulators of chronic neuroinflammation observed in several neurodegenerative disorders. Activated microglia are distinct from resting microglia both morphologically as well as functionally with respect to the production and secretion of proinflammatory factors (Glass et al., 2010; Panicker et al., 2015). Several lines of evidence, from cell culture to animal models to postmortem tissue analyses to genetic linkage analyses, conclusively demonstrate that sustained neuroinflammation negatively affects neuron health, and in fact, contributes to neuronal death (Block et al., 2007; Gordon et al., 2016; Kirkley et al., 2017; Panicker et al., 2015; Sarkar et al., 2017b). Lipopolysaccharide (LPS)-activated microglia undergo morphological changes from ramified (surveillant) type to amoeboid type, releasing ROS, nitrite, and various other pro-inflammatory mediators and cytokines that can be toxic over time. Like macrophages, microglia can also undergo an alternative activation, which leads to production of anti-inflammatory factors. For example, IL-4 can induce this alternative anti-inflammatory phenotype in microglial cells (Nakagawa and Chiba, 2014). Walker and Lue (2015) suggested the probable existence of another microglial phenotype, known as M3. Thus, microglial activation is complex, and the molecular footprints underlying the various phenotypes are the focus of much research.

Microglial activation leading to neurodegeneration has been well documented in AD, PD, and other neurodegenerative disease (Block et al., 2007; Glass et al., 2010; Solito and Sastre, 2012). Misfolded proteins, including aggregated α-synuclein

(αSyn_{Agg}) and amyloid-β, that are pathological hallmarks of PD and AD, can hyperactivate microglia, leading to chronic inflammation and loss of neurons (Halle et al., 2008; Heneka et al., 2013).

Various xenobiotics, including manganese (Mn) (Aschner et al., 2009a; Aschner et al., 2009b; Filipov et al., 2005a; Guilarte, 2010; Moreno et al., 2009a; Moreno et al., 2008; Moreno et al., 2009b; Neal and Guilarte, 2012; Streifel et al., 2012; Verina et al., 2011), copper (Cu) (Choo et al., 2013; Zhang et al., 2011), and zinc (Zn) (Kauppinen et al., 2008), are also known to activate microglial cells. Exposure to such environmental neurotoxicants has been linked to an increased risk of Parkinsonian syndrome. Importantly, Mn-induced microglial activation leads to the production of pro-inflammatory factors that have been shown to cause neuronal damage (Burton and Guilarte, 2009; Filipov et al., 2005b). Mn also enhances the LPS-induced production of pro-inflammatory factors in microglial cells (Dodd and Filipov, 2011). Mn-induced microglial activation can also subsequently activate astrocytes, leading to an exacerbation of the pro-inflammatory condition (Kirkley et al., 2017); however, many of the molecular signaling mechanisms of metal-induced microglial activation remain unknown.

Microglia are not only involved in disease pathogenesis, but also play an important role in nervous system development. Microglia have been shown to play an important role in shaping the neuronal circuit during development (Wu et al., 2013) by modulating the axon processes via synaptic pruning. The number of publications on microglial cells in the last decade have increased steadily with every passing year (Fig. 1A), especially the importance of microglia in AD, PD, multiple sclerosis (MS),

and other neurodegenerative disorders. To study microglial biology and its role in modulating neuroinflammation, several immortalized microglial cell lines have been developed (Fig. 1B), including BV2, N9, and EOC (mouse microglial cell lines); HAPI (rat microglial cell line); and the HMC3 and HMO6 (human microglial cell lines). Among the six prevalent cell lines, BV2 cell lines have been used in ~75% of the publications (Fig. 1B). Since 2010, the number of publications on BV2 has substantially increased (Fig. 1C). Though BV2 microglial cell lines are not identical to primary microglia in morphology or activation state, the prevalent use of BV2 may be attributed to the following: i) lack of good, easily obtainable cell lines; ii) cost of primary culture; iii) low yield of primary microglial cells; and iv) difficulty in isolating primary cells.

In this study, we performed a more in-depth characterization of a newly developed microglial cell line which was immortalized from primary mouse microglia. We compared this new mouse microglial cell line (MMC) with the predominantly used BV2 microglia, demonstrating that the basal level of BV2 microglia is higher than that of MMCs. We also demonstrate that the MMC responded to a variety of stimuli, including LPS, misfolded αSyn_{Agg}, and the environmental neurotoxicant Mn.

Material and Methods

Chemicals and Reagents

Dulbecco's modified Eagle's medium (DMEM), DMEM-F12, fetal bovine serum (FBS), L-glutamine (Q), penicillin/streptomycin (P/S), Sodium Pyruvate (SP), and Non-Essential Amino Acids (NEAA) were obtained from Invitrogen (Carlsbad, CA). CellTiter Glo Luminescent Cell Viability Assay kit was obtained from Promega (Madison, WI). The CD11b magnetic separation kit was purchased from Stem Cell

Technologies (Vancouver, Canada). All standards used for the Luminex multiplex cytokine assay were purchased from PeproTech Inc (Rocky Hill, NJ). Streptavidin-Biotin and biotinylated antibodies used for Luminex were purchased from eBioSciences (San Diego, CA). Phagocytosis assay kit was purchased from Cayman Chemicals (Ann Arbor, MI).

Literature Review

To assess the use of microglial cell lines in peer-reviewed studies, the following terms were searched in PubMed: microglia, BV2 microglia, HAPI microglia, N9 microglia, HMO6 microglia, HMC3 microglia, EOC microglia.

Cell culture and Treatments

Primary Microglia: Primary microglia were obtained from 1- to 3-day postnatal mouse pups, as described in our published protocol (Sarkar et al., 2017c). The brains were excised, immersed in 0.25% trypsin-EDTA (TE), and incubated for 15 min in a 37° C water bath with occasional mixing. The TE was neutralized with growth medium (10% FBS with 1% P/S, Q, SP, NEAA in DMEM-F12), and the brains were washed 4 times by adding and removing fresh growth medium. The brains were then homogenized via trituration, filtered through a 70-µm filter, and then the cell suspension was plated in T75 flasks (2 T75 flasks per brain). After 6 days, the growth medium was decanted and replaced with fresh growth medium. On the 16th day, the cells were collected, subjected to an antibody CD11b positive selection, and isolated using a magnetic column that binds magnetic spheres complexed onto the CD11b surface marker. Once the cells are seeded appropriately, they are ready for treatments

after 48 h. All experiments were performed in treatment medium (2% FBS with 1% P/S, Q, SP, NEAA in DMEM-F12).

BV2: BV2 microglia were maintained in 10% FBS with 1% P/S and Q in DMEM. All experiments were performed in treatment medium (2% FBS with 1% P/S and Q in DMEM).

Wild-type mouse microglial cell (MMC) line: MMCs were derived by viral-transduced immortalization of primary microglia, which were a kind gift from Dr. D. Golenbock (University of Massachusetts). These cells have similar morphology and surface markers as primary microglial cells (Halle et al., 2008). MMCs were maintained in 10% FBS with 1% P/S, Q, and SP in DMEM-F12. All experiments were performed in treatment medium (2% FBS with 1% P/S, Q, and SP in DMEM-F12) (Sarkar et al., 2017b).

Immunocytochemistry (ICC)

For ICC, coverslips were placed in 24-well plates, immersed in poly-D-Lysine, and then washed with phosphate-buffered saline (PBS). Next, cells were seeded with their respective growth medium. After the experiment, the treatment medium was decanted and the cells on the coverslips were fixed by incubating at RT with 4% paraformaldehyde for 25 min. The cells were then washed with PBS 4 times. Next, the cells were blocked with blocking buffer (2% BSA with 0.05% Triton-X100 and 0.005% Tween-20 in PBS) for 45 min to 1 h. Primary antibodies were made with 1% BSA in PBS, incubated overnight at 4° C, and then washed for 30 min with PBS. All secondary antibodies were made with 1% BSA in PBS, incubated at RT for 90 min, and then washed for 30 min with PBS. Finally, Hoechst nuclear stain was made in

PBS at 1:5000 and added for 5 min. After washing, the coverslips were mounted on pre-coated slides using Fluoromount (Sigma-Aldrich). The following antibodies were used: IBA1 (AB_2314667, 1:1000), iNos (AB_2152867, 1:500). Alexa dye-conjugated secondary antibodies were used for ICC experiments.

Recombinant human α-synuclein purification and aggregation

Recombinant human α-synuclein was purified following our previous publication (Sarkar et al., 2017a). Briefly, *E. coli* cells were transformed with human α-synuclein plasmid and grown on an agar plate with ampicillin (Amp). Pre-culture was prepared by inoculation of a single bacterial colony from the agar plate into a tube containing 10 mL of LB broth with Amp and incubated overnight at 37 °C. Next, the pre-culture was inoculated into 1 L of LB medium containing Amp, and every hour the OD_{600} was taken until the culture reached an OD of 0.5. The α-synuclein expression was induced by adding 1 mM isopropyl β-D-1-thiogalactopyranoside (Invitrogen), and the cells were further incubated at 37 °C for 8 h before harvesting. Cells were lysed and recombinant α-synuclein was purified and aggregated as previously described (Sarkar et al., 2017a).

qRT-PCR

RNA extraction and qRT-PCR were performed as described previously (Sarkar et al., 2017b; Seo et al., 2014). Briefly, cells were plated in 6-well plates and treated. Following treatment, TRIzol reagent was used to isolate total RNA from the cells and the concentration was measured using NanoDrop. Affinity Script qPCR cDNA synthesis system (Agilent Technologies) was used to convert RNA to cDNA. Real-time PCR was performed with the RT^2 SYBR Green master mix (Thermo Fisher

#K0172). The following genes from QuantiTect Primer Assay (Qiagen) were used for qRT-PCR: *pro-IL-1β, pro-IL-18, IL-12b, TNF-α, IL-6*, and *NOS2*. The housekeeping gene *18S* rRNA (Qiagen #PPM57735E) was used as the reference for all qRT-PCR experiments. The results are reported as fold change in gene expression, which was determined via the ΔΔCt method using the threshold cycle (Ct) value for the housekeeping gene and for the respective gene of interest in each sample (Lawana et al., 2017).

Western Blotting

Western blot analysis was performed according to previous published protocols (Langley et al., 2017). Briefly, cell samples were lysed using modified RIPA buffer and sonicated using a refrigerated cup-sonicator. Bradford assay was performed for protein estimation. Next, 25 µg of protein was loaded in each well of 10% SDS-acrylamide gel and ran for 2-2.5 h at 110 V. Proteins were transferred to a nitrocellulose membrane at 27 V for 18 h at 4° C. The nitrocellulose membranes were blocked using LI-COR blocking buffer for 1 h. The blocked nitrocellulose membranes were incubated in the primary antibody for gp91-phox (BD Biosciences) for 3 to 18 h, washed with PBS-Tween (0.01%), incubated in infrared LI-COR secondary antibodies for 1 h, washed again with PBS-Tween, and imaged using a LI-COR scanner. Secondary antibodies were used according to manufacturer's instructions. β-actin was used as the loading control.

Phagocytic Assay

Phagocytic assay was performed according to manufacturer's protocol. Briefly, 40,000 MMCs were plated on PDL-coated coverslips in 24-well cell culture plates.

Cells were treated with 1 μM αSyn_{Agg} for 24 h. FITC-labeled IgG beads were added along with the treatment at a dilution of 1:300. Following treatment, excess FITC-labelled beads were washed away with Hanks' balanced salt solution (HBSS). Cells were fixed using 4% PFA and imaged using a fluorescent microscope.

Luminex Multiplex Cytokine Assay

Luminex cytokine assay was performed according to our previous publications (Panicker et al., 2015; Sarkar et al., 2017a). Briefly, PMG and MMCs (100,000 cells/well) were treated in 96-well plates. After treatment, 40 μL of the medium was collected and added to 40 μL of primary antibody conjugated to magnetic microspheres and incubated overnight at 4°C in a clear-bottomed, black 96-well plate. Following incubation in primary antibodies, each well was triple-washed using a magnetic washer, incubated for 1 h with biotin-conjugated secondary antibodies, triple-washed again, incubated with streptavidin/phycoerythrin for 30 min and washed two more times. A Bio-Plex reader was used to read the 96-well plates.

MTS Assay

MTS assay was performed according to our previous publication (Sarkar et al., 2017a). Briefly, 100,000 cells/well were plated in a 96-well tissue culture plate and treated with 1–3000 ng/mL of LPS for 24 h. After treatment, 10 μL of MTS dye was added to each well and incubated for 60 min at 37° C. Absorbance readings were measured using a plate reader at 490 nm, and a 640-nm readout was used for background subtraction.

Griess Assay

Griess assay was performed according to our previous publication (Langley et al., 2017). Briefly, 100,000 cells/well were plated in 96-well plates. Cells were treated with 1–3000 ng/mL of LPS. Following treatment, 50 µL of media was mixed with an equal volume of Griess reagent and incubated for 10 min. The plate was read using a plate reader at 540 nM. Sodium nitrite was used to make the standard curve.

Data Analysis

Prism 7.0 (GraphPad) was used for statistical analysis with $p \leq 0.05$ considered statistically significant. One-way ANOVA was used for comparison among multiple groups. In most cases, Tukey post-hoc analysis was applied. For comparing 2 groups, Student's t-test was performed.

Results

LPS effects on the morphology of BV2s, MMCs, and PMG

Classical activation of microglia leads to an amoeboid morphology with enlarged soma and fewer processes. In this experiment, we determined the morphological changes associated with LPS treatment in BV2s, MMCs, and PMG. Cell lines were treated with 1 µg/mL of LPS for 6 h, fixed and subjected to ICC. Microscopic analysis demonstrates a change in morphology of MMCs and PMG upon LPS exposure from a ramified to a more amoeboid shape that includes drastic hypertrophy. On the contrary, the widely used microglial cell line BV2 exhibits an amoeboid shape prior to treatment suggesting that they are already activated and LPS treatment does not induce further change in morphology (Figs. 1D-E). These results suggest that LPS-induced morphological changes in MMCs are more similar to the

morphological changes seen in PMG. Therefore, the hypertrophic morphological changes observed in MMCs and PMG could be used as a measure of microglial activation, which is lacking in BV2s.

Comparison of LPS-induced iNOS expression and nitrite production in microglial cell lines

Hallmarks of microglial inflammation include iNOS induction and subsequent nitrite production (Gordon et al., 2016; Panicker et al., 2015). Nitrite released from activated glial cells is neurotoxic and contributes to the neurodegenerative process (Mander and Brown, 2005). Probing for basal iNOS expression revealed that BV2 microglial cells exhibited higher iNOS levels when compared to both MMCs and PMG (Fig. 2A). Upon LPS treatment (1 µg/mL) for 6 h, iNOS expression was rapidly induced in MMCs and PMG relative to controls, whereas iNOS induction in BV2 cells was not strikingly different from controls.

Since increased iNOS expression will result in increased nitrite production, we quantified basal, extracellularly released nitrite levels by Griess assay. BV2 cells released significantly higher nitrite than did MMCs or PMG (Fig. 2B). Extracellularly released nitrite levels did not differ significantly between PMG and MMCs (Fig. 2B). Together, these findings show that BV2 cells are already in an activated state under basal conditions compared to MMCs and PMG.

LPS increases the expression and production of pro-inflammatory factors significantly more in MMCs than in BV2s

Similar to nitrite production, the production and secretion of pro-inflammatory cytokines are also major hallmarks of microglial inflammation (Gordon et al., 2016;

Panicker et al., 2015). Pro-inflammatory cytokines released from activated glial cells are neurotoxic and contribute to the neurodegenerative process. We performed qRT-PCR to compare the basal expression levels of pro-inflammatory cytokines and *NOS2* (Fig. 3). The qRT-PCR analysis revealed that BV2s have significantly higher basal gene expression of the pro-inflammatory factors *pro-IL-1β* (Fig. 3A), *IL-6* (Fig. 3B), *IL-12b* (Fig. 3C), *TNF-α* (Fig. 3D) and *NOS2* (Fig. 3E), with one exception being *pro-IL-18* (Fig. 3F). These data suggest significantly higher mRNA expression levels of pro-inflammatory factors in BV2s compared to MMCs. However, when these cell lines are exposed to LPS for 6 h, pro-inflammatory cytokines and iNOS mRNA levels were significantly higher only in MMCs, not BV2 cells, when compared to their respective untreated controls. When compared to LPS-stimulated BV2 cells, *pro-IL-1β* (Fig. 4A), *IL-6* (Fig. 4B), *IL-12b* (Fig. 4C), *pro-IL-18* (Fig. 4D), *TNF-α* (Fig. 4E) and *NOS2* (Fig. 4F) were rapidly upregulated in MMCs. These data collectively suggest that MMCs are a good model system for understanding the mechanism of microglial inflammation.

LPS induces gp-91phox in the MMCs

Gp91-phox is a key component of NADPH oxidase (Nox-2) complex and has been identified as one of the major downstream effectors of LPS-induced inflammation. LPS-induced free-radical formation is diminished in Nox2/gp91-phox deficient mice (Clement et al., 2010), and gp91-phox plays a role in neuroinflammation in PD (Langley et al., 2017). To further verify the downstream effector of LPS-induced inflammation in the MMCs, cells were treated with LPS for 1 h. Western blot analysis revealed that LPS induced gp91-phox in the MMCs (Fig. 5A), which was corroborated by ICC analysis (Fig. 5B). These data support previous findings in glial cells, further

showing that this cell line can be used for studying Nox-2 signaling mechanisms underlying microglial activation.

LPS induces proinflammatory response in MMC cells in a dose-dependent manner

To further characterize the response of the MMCs upon exposure to an inflammatory stimulus, we performed a dose-response analysis of various LPS-induced inflammatory parameters. Given that LPS treatment can induce mitochondrial dysfunction (Kuwabara and Imajoh-Ohmi, 2004), we treated the MMCs with different doses of LPS (1-3000 ng/mL) for 24 h. An MTS assay revealed that LPS reduced metabolic activity in a dose-dependent manner (Fig. 6A). The 24 h IC_{50} concentration was calculated to be 8.6 ng/mL LPS. Moreover, a Griess assay revealed that LPS induced a dose-dependent increase in nitrite release (Fig. 6B). Our Luminex assay demonstrated that low-dose LPS exposure (1 ng/mL) produced pro-inflammatory factors including IL-6 (Fig. 6C), IL-12 (Fig. 6D), TNF-α (Fig. 6E), and IL-1β (Fig. 6F). Together, these data suggest that LPS stimulation can induce a broad dose-dependent inflammatory response in MMCs.

αSyn_{Agg} induces comparable pro-inflammatory responses in MMCs and PMG

Misfolded αSyn and its aggregates are major pathological features of PD. We have previously shown that αSyn_{Agg} classically activates microglial cells, producing pro-inflammatory cytokines and nitrite in BV2 cells and primary microglia (Gordon et al., 2016). To determine if MMCs can be activated by αSyn_{Agg}, we treated MMC cells with 1 μM αSyn_{Agg} for 24 h and compared them with PMG. The αSyn_{Agg} treatment

elicited an inflammatory response in MMCs that was comparable to the response in PMG, as revealed by Luminex analysis of IL-1β (Fig. 7A), TNF-α (Fig. 7B), and IL-6 (Fig. 7C). Although IL-6 production was lower in the MMCs than in PMG, production of the other pro-inflammatory factors was consistent between the two cell lines. In addition, a phagocytic assay revealed that the MMCs were able to engulf FITC-labeled IgG beads (Fig. 7D), thus demonstrating phagocytic activity, which was increased by exposing these cells to αSyn_{Agg}. These data further demonstrate that the MMCs may be used as a microglial model for neuroinflammation in diseases associated with protein misfolding.

Manganese activates the MMCs producing inflammatory factors

We have recently demonstrated that the environmental toxicant Mn also induces microglial inflammation in primary microglia and in animal models of Parkinsonism (Dodd and Filipov, 2011; Sarkar et al., 2017b)**.** To verify if MMCs can be used to model metal-induced inflammation, cells were treated with 100 μM Mn for 24 h. Mn significantly induced *NOS2* mRNA levels in the MMCs, as revealed by qRT-PCR analysis (Fig. 8A). Furthermore, a Luminex assay revealed that Mn significantly upregulated release of the pro-inflammatory factors TNF-α (Fig. 8B) and IL-6 (Fig. 8C). These data suggest that these cells can be used to study neurotoxic metal-induced inflammation in microglia.

Discussion

Notably, in the past two decades, chronic neuroinflammation has been the subject of intense research (Fig. 1A). Elucidating the role of microglia in CNS pathophysiology is now regarded as fundamental in therapeutically targeting

neurodegenerative disorders such as Parkinson's, Alzheimer's, and Huntington's (Schapansky et al., 2015). Optimal *in vitro* models are thus indispensable for delineating cellular pathways and identifying molecular targets that could be exploited for such therapeutics. Herein, we provide an in-depth comparative analysis of the inflammatory states of the most widely used cell line, BV2 (Fig. 1C) and a novel, immortalized wild-type mouse microglial cell line (MMC). We argue that the MMCs are more advantageous for studies of neuroinflammation because of their inherent tendency to remain basally surveillant, yet more sensitive and comparable to neonatal mouse primary microglia than the widely used BV2 cell line.

As evidenced in knockout animals, iNOS is a critical intracellular mediator of inflammation, conferring resistance against MPTP-induced loss of substantia nigral neurons (Liberatore et al., 1999). Furthermore, iNOS converts arginine to citrulline while also forming the byproduct nitric oxide (NO), a powerful signaling molecule (Hallemeesch et al., 2003; Moehle and West, 2015). However, in highly oxygenated conditions, NO can react with superoxide to form peroxynitrite, which can exert cytotoxic effects. Levels of its breakdown product, nitrite, correlate with the degree of inflammation (Hunter et al., 2013; Pacher et al., 2007). In this study, basal or unstimulated BV2s exhibited higher levels of iNOS compared to MMCs and PMG, which was corroborated by measuring nitrite levels in Griess assays (Fig. 2A-B). Significantly lower levels of basal iNOS and nitrite in MMCs make them far more suitable for signaling studies involving iNOS, NO, and potentially other unrelated oxidative stress mechanisms. Since oxidative stressors are prime factors that contribute to the neuroinflammatory and degenerative processes (Sarkar et al.,

2017b), MMCs appear to be the more appropriate immortalized cell culture model for studying microglial activation.

Both the BV2s and the MMCs were immortalized from C57BL/6 mice utilizing the J2 retrovirus carrying the v-myc/v-raf genes (Blasi et al., 1990; Halle et al., 2008). However, basal gene expression for various cytokines, as well as *NOS2*, were all significantly higher in BV2s except for *pro-IL-18* (Fig. 3). Upon stimulation with LPS, MMCs demonstrated significantly greater sensitivity by exerting a more robust transcriptional burst of inflammatory genes (Fig. 4). This sensitivity and robustness may be crucial to more effectively defining signaling mechanisms of inflammation spurred by microglia, especially at earlier time points and in low-dose neurotoxicant exposure studies.

Although MMCs were initially generated by Golenbock and colleagues, the cell model was not well characterized for neurotoxicity studies (Halle et al., 2008). Here, we provide a more comprehensive analysis of their fundamental responsivity to stimulants such as LPS, Mn, and αSyn_{Agg}. LPS is known to dysregulate the mitochondrial membrane potential (Kuwabara and Imajoh-Ohmi, 2004) and to modulate mitochondrial bioenergetics at early time points (Sarkar et al., 2017b). As such, we employed the MTS assay to assess LPS's effects on mitochondrially related metabolic activity of MMCs. At the traditional 24-h time point, an effective dose of 8.6 ng/mL of LPS inhibited metabolic activity (Fig. 6A). This was further supported by the dose-dependent release of nitrite, in which 10 ng/mL LPS was sufficient to produce ~15 μM of nitrite (Fig. 6B). Similarly, inflammatory cytokine analysis revealed that LPS treatment increased IL-1β levels in a dose-dependent manner. Although a dose

response for IL-6, IL-12, or TNFα was lacking, 10 ng/mL was sufficient to elicit a substantial quantity of cytokines. Interestingly, IL-6 appears to function as the primary cytokine effector since a major release was observed even at 1 ng/mL. Based on this analysis, low-dose LPS for time points of 24 h or longer should be appropriate without significant cytotoxicity. On the other hand, higher doses should be effective at earlier time points. This is apparent from the significant increase in gp91-phox protein, a key generator of superoxide that reacts with NO to produce peroxynitrite (Fig. 5) (Pacher et al., 2007).

Others have shown that αSyn_{Agg} induces microgliosis (Sanchez-Guajardo et al., 2013; Wang et al., 2015), which promotes inflammatory signaling through critical kinases such as protein kinase Cδ (Gordon et al., 2016). Comparatively the MMCs are not drastically different from PMG in releasing the major cytokines IL-1β, IL-6, and TNFα after being exposed to αSyn_{Agg} (Fig. 7). Similar results were obtained for IL-1β by stimulating the MMCs and PMG with fibrillar amyloid-β (Halle et al., 2008). These results further highlight the flexibility of MMCs, making them ideally suited for various *in vitro* paradigms. The metal Mn is known to be neurotoxic (Harischandra et al., 2015), but it also can be a potent inducer and exacerbator of inflammation (Sarkar et al., 2017a; Tjalkens et al., 2017). Here, we corroborate the existing data by demonstrating elevated levels of *NOS2* and the cytokines TNFα and IL-6 after Mn treatment (Fig. 8). Collectively, these results support adopting MMCs to supplant BV2s as the model system of choice.

In conclusion, we demonstrate that the newly available MMC line is an excellent *in vitro* cell culture model that can appropriately supplant the widely used BV2 cell line

for the purposes of testing neurotoxic chemicals for inducing neuroinflammatory responses. MMCs mirror primary microglia exceptionally well when compared to BV2s. While unstimulated, they resemble a surveillant state of primary microglia, but under stimulation, their responsivity is remarkably similar to activated primary microglia. Their inherent sensitivity enables them to generate similar inflammatory mediators under various inflammatory stimuli that encompass classical, chronic, and environmental paradigms. Thus, MMCs are a better alternative to BV2s for studying the cellular and molecular mechanisms underlying microglial activation during neurotoxic insults.

Conflict of interest

A.G.K. and V.A. are shareholders of PK Biosciences Corporation (Ames, IA), which is interested in identifying novel biomarkers and potential therapeutic targets for PD. A.G.K and V.A. do not have any commercial interests in the work presented in here.

Acknowledgements

This study was supported by NIH grants NS088206, ES026892, and ES027245. Special thanks to Dr. Golenbock of U. Mass Med School for providing the MMC cell line. The W. Eugene and Linda Lloyd Endowed Chair and Eminent Scholar to AGK and the Salisbury Endowed Chair to AK are also acknowledged. We also thank Mr. Gary Zenitsky for assistance in preparing this manuscript.

References

Aschner, M., Erikson, K.M., Hernández, E.H., Tjalkens, R., 2009a. Manganese and its role in Parkinson’s disease: from transport to neuropathology. Neuromol Med. Humana Press Inc 11.

Aschner, M., Erikson, K.M., Herrero Hernandez, E., Tjalkens, R., 2009b. Manganese and its role in Parkinson's disease: from transport to neuropathology. Neuromolecular Med 11(4), 252-266.

Blasi, E., Barluzzi, R., Bocchini, V., Mazzolla, R., Bistoni, F., 1990. Immortalization of murine microglial cells by a v-raf/v-myc carrying retrovirus. J Neuroimmunol 27(2-3), 229-237.

Block, M.L., Zecca, L., Hong, J.S., 2007. Microglia-mediated neurotoxicity: uncovering the molecular mechanisms. Nat Rev Neurosci 8(1), 57-69.

Burton, N.C., Guilarte, T.R., 2009. Manganese neurotoxicity: lessons learned from longitudinal studies in nonhuman primates. Environ Health Perspect 117(3), 325-332.

Choo, X.Y., Alukaidey, L., White, A.R., Grubman, A., 2013. Neuroinflammation and copper in Alzheimer's disease. Int J Alzheimers Dis 2013, 145345.

Clement, H.W., Vazquez, J.F., Sommer, O., Heiser, P., Morawietz, H., Hopt, U., Schulz, E., von Dobschutz, E., 2010. Lipopolysaccharide-induced radical formation in the striatum is abolished in Nox2 gp91phox-deficient mice. J Neural Transm (Vienna) 117(1), 13-22.

Dodd, C.A., Filipov, N.M., 2011. Manganese potentiates LPS-induced heme-oxygenase 1 in microglia but not dopaminergic cells: role in controlling microglial

hydrogen peroxide and inflammatory cytokine output. Neurotoxicology 32(6), 683-692.

Filipov, N.M., Seegal, R.F., Lawrence, D.A., 2005a. Manganese potentiates in vitro production of proinflammatory cytokines and nitric oxide by microglia through a nuclear factor kappa B-dependent mechanism. Toxicol Sci 84(1), 139-148.

Filipov, N.M., Seegal, R.F., Lawrence, D.A., 2005b. Manganese potentiates in vitro production of proinflammatory cytokines and nitric oxide by microglia through a nuclear factor kappa B-dependent mechanism. Toxicol. Sci. Oxford University Press 84.

Glass, C.K., Saijo, K., Winner, B., Marchetto, M.C., Gage, F.H., 2010. Mechanisms underlying inflammation in neurodegeneration. Cell. 140.

Gordon, R., Singh, N., Lawana, V., Ghosh, A., Harischandra, D.S., Jin, H., Hogan, C., Sarkar, S., Rokad, D., Panicker, N., Anantharam, V., Kanthasamy, A.G., Kanthasamy, A., 2016. Protein kinase Cdelta upregulation in microglia drives neuroinflammatory responses and dopaminergic neurodegeneration in experimental models of Parkinson's disease. Neurobiol Dis 93, 96-114.

Guilarte, T.R., 2010. Manganese and Parkinson’s disease: a critical review and new findings. Environ Health Perspect. 118.

Halle, A., Hornung, V., Petzold, G.C., Stewart, C.R., Monks, B.G., Reinheckel, T., Fitzgerald, K.A., Latz, E., Moore, K.J., Golenbock, D.T., 2008. The NALP3 inflammasome is involved in the innate immune response to amyloid-beta. Nat Immunol 9(8), 857-865.

Hallemeesch, M.M., Janssen, B.J., de Jonge, W.J., Soeters, P.B., Lamers, W.H., Deutz, N.E., 2003. NO production by cNOS and iNOS reflects blood pressure changes in LPS-challenged mice. Am J Physiol Endocrinol Metab 285(4), E871-875.

Harischandra, D.S., Jin, H., Anantharam, V., Kanthasamy, A., Kanthasamy, A.G., 2015. alpha-Synuclein protects against manganese neurotoxic insult during the early stages of exposure in a dopaminergic cell model of Parkinson's disease. Toxicol Sci 143(2), 454-468.

Heneka, M.T., Kummer, M.P., Stutz, A., Delekate, A., Schwartz, S., Vieira-Saecker, A., Griep, A., Axt, D., Remus, A., Tzeng, T.C., Gelpi, E., Halle, A., Korte, M., Latz, E., Golenbock, D.T., 2013. NLRP3 is activated in Alzheimer's disease and contributes to pathology in APP/PS1 mice. Nature 493(7434), 674-678.

Hunter, R.A., Storm, W.L., Coneski, P.N., Schoenfisch, M.H., 2013. Inaccuracies of nitric oxide measurement methods in biological media. Anal Chem 85(3), 1957-1963.

Kauppinen, T.M., Higashi, Y., Suh, S.W., Escartin, C., Nagasawa, K., Swanson, R.A., 2008. Zinc triggers microglial activation. J Neurosci 28(22), 5827-5835.

Kirkley, K.S., Popichak, K.A., Afzali, M.F., Legare, M.E., Tjalkens, R.B., 2017. Microglia amplify inflammatory activation of astrocytes in manganese neurotoxicity. Journal of Neuroinflammation 14(1), 99.

Kuwabara, T., Imajoh-Ohmi, S., 2004. LPS-induced apoptosis is dependent upon mitochondrial dysfunction. Apoptosis 9(4), 467-474.

Langley, M., Ghosh, A., Charli, A., Sarkar, S., Ay, M., Luo, J., Zielonka, J., Brenza, T., Bennett, B., Jin, H., Ghaisas, S., Schlichtmann, B., Kim, D., Anantharam, V., Kanthasamy, A., Narasimhan, B., Kalyanaraman, B., Kanthasamy, A.G., 2017. Mito-

Apocynin Prevents Mitochondrial Dysfunction, Microglial Activation, Oxidative Damage, and Progressive Neurodegeneration in MitoPark Transgenic Mice. Antioxid Redox Signal.

Lawana, V., Singh, N., Sarkar, S., Charli, A., Jin, H., Anantharam, V., Kanthasamy, A.G., Kanthasamy, A., 2017. Involvement of c-Abl Kinase in Microglial Activation of NLRP3 Inflammasome and Impairment in Autolysosomal System. J Neuroimmune Pharmacol.

Liberatore, G.T., Jackson-Lewis, V., Vukosavic, S., Mandir, A.S., Vila, M., McAuliffe, W.G., Dawson, V.L., Dawson, T.M., Przedborski, S., 1999. Inducible nitric oxide synthase stimulates dopaminergic neurodegeneration in the MPTP model of Parkinson disease. Nat Med 5(12), 1403-1409.

Mander, P., Brown, G.C., 2005. Activation of microglial NADPH oxidase is synergistic with glial iNOS expression in inducing neuronal death: a dual-key mechanism of inflammatory neurodegeneration. J Neuroinflammation 2, 20.

Moehle, M.S., West, A.B., 2015. M1 and M2 immune activation in Parkinson's Disease: Foe and ally? Neuroscience 302, 59-73.

Moreno, J.A., Streifel, K.M., Sullivan, K.A., Legare, M.E., Tjalkens, R.B., 2009a. Developmental exposure to manganese increases adult susceptibility to inflammatory activation of glia and neuronal protein nitration. Toxicol Sci 112(2), 405-415.

Moreno, J.A., Sullivan, K.A., Carbone, D.L., Hanneman, W.H., Tjalkens, R.B., 2008. Manganese potentiates nuclear factor-kappaB-dependent expression of nitric oxide synthase 2 in astrocytes by activating soluble guanylate cyclase and extracellular responsive kinase signaling pathways. J Neurosci Res 86(9), 2028-2038.

Moreno, J.A., Yeomans, E.C., Streifel, K.M., Brattin, B.L., Taylor, R.J., Tjalkens, R.B., 2009b. Age-dependent susceptibility to manganese-induced neurological dysfunction. Toxicological Sciences. 112.

Nakagawa, Y., Chiba, K., 2014. Role of microglial m1/m2 polarization in relapse and remission of psychiatric disorders and diseases. Pharmaceuticals (Basel) 7(12), 1028-1048.

Neal, A.P., Guilarte, T.R., 2012. Mechanisms of heavy metal neurotoxicity: lead and manganese. J Drug Metab Toxicol S. 5.

Pacher, P., Beckman, J.S., Liaudet, L., 2007. Nitric oxide and peroxynitrite in health and disease. Physiol Rev 87(1), 315-424.

Panicker, N., Saminathan, H., Jin, H., Neal, M., Harischandra, D.S., Gordon, R., Kanthasamy, K., Lawana, V., Sarkar, S., Luo, J., Anantharam, V., Kanthasamy, A.G., Kanthasamy, A., 2015. Fyn Kinase Regulates Microglial Neuroinflammatory Responses in Cell Culture and Animal Models of Parkinson's Disease. J Neurosci 35(27), 10058-10077.

Sanchez-Guajardo, V., Barnum, C.J., Tansey, M.G., Romero-Ramos, M., 2013. Neuroimmunological processes in Parkinson's disease and their relation to alpha-synuclein: microglia as the referee between neuronal processes and peripheral immunity. ASN Neuro 5(2), 113-139.

Sarkar, S., Malovic, E., Harischandra, D.S., Ngwa, H.A., Ghosh, A., Hogan, C., Rokad, D., Zenitsky, G., Jin, H., Anantharam, V., Kanthasamy, A.G., Kanthasamy, A., 2017a. Manganese exposure induces neuroinflammation by impairing mitochondrial dynamics in astrocytes. Neurotoxicology.

Sarkar, S., Malovic, E., Harishchandra, D.S., Ghaisas, S., Panicker, N., Charli, A., Palanisamy, B.N., Rokad, D., Jin, H., Anantharam, V., Kanthasamy, A., Kanthasamy, A.G., 2017b. Mitochondrial impairment in microglia amplifies NLRP3 inflammasome proinflammatory signaling in cell culture and animal models of Parkinson's disease. NPJ Parkinsons Dis 3, 30.

Sarkar, S., Malovic, E., Plante, B., Zenitsky, G., Jin, H., Anantharam, V., Kanthasamy, A., Kanthasamy, A.G., 2017c. Rapid and Refined CD11b Magnetic Isolation of Primary Microglia with Enhanced Purity and Versatility. J Vis Exp(122).

Schapansky, J., Nardozzi, J.D., LaVoie, M.J., 2015. The complex relationships between microglia, alpha-synuclein, and LRRK2 in Parkinson's disease. Neuroscience 302, 74-88.

Seo, J., Ottesen, E.W., Singh, R.N., 2014. Antisense methods to modulate pre-mRNA splicing. Methods Mol Biol 1126, 271-283.

Solito, E., Sastre, M., 2012. Microglia function in Alzheimer's disease. Front Pharmacol 3, 14.

Streifel, K.M., Moreno, J.A., Hanneman, W.H., Legare, M.E., Tjalkens, R.B., 2012. Gene deletion of nos2 protects against manganese-induced neurological dysfunction in juvenile mice. Toxicological Sciences. 126.

Tjalkens, R.B., Popichak, K.A., Kirkley, K.A., 2017. Inflammatory Activation of Microglia and Astrocytes in Manganese Neurotoxicity. Adv Neurobiol 18, 159-181.

Verina, T., Kiihl, S.F., Schneider, J.S., Guilarte, T.R., 2011. Manganese exposure induces microglia activation and dystrophy in the substantia nigra of non-human primates. NeuroToxicology. 32.

Walker, D.G., Lue, L.F., 2015. Immune phenotypes of microglia in human neurodegenerative disease: challenges to detecting microglial polarization in human brains. Alzheimers Res Ther 7(1), 56.

Wang, S., Chu, C.H., Stewart, T., Ginghina, C., Wang, Y., Nie, H., Guo, M., Wilson, B., Hong, J.S., Zhang, J., 2015. alpha-Synuclein, a chemoattractant, directs microglial migration via H2O2-dependent Lyn phosphorylation. Proc Natl Acad Sci U S A 112(15), E1926-1935.

Wu, L.J., Stevens, B., Duan, S., MacVicar, B.A., 2013. Microglia in neuronal circuits. Neural Plast 2013, 586426.

Zhang, W., Phillips, K., Wielgus, A.R., Liu, J., Albertini, A., Zucca, F.A., Faust, R., Qian, S.Y., Miller, D.S., Chignell, C.F., Wilson, B., Jackson-Lewis, V., Przedborski, S., Joset, D., Loike, J., Hong, J.S., Sulzer, D., Zecca, L., 2011. Neuromelanin activates microglia and induces degeneration of dopaminergic neurons: implications for progression of Parkinson's disease. Neurotox Res 19(1), 63-72.

Figures.

Figure. 1

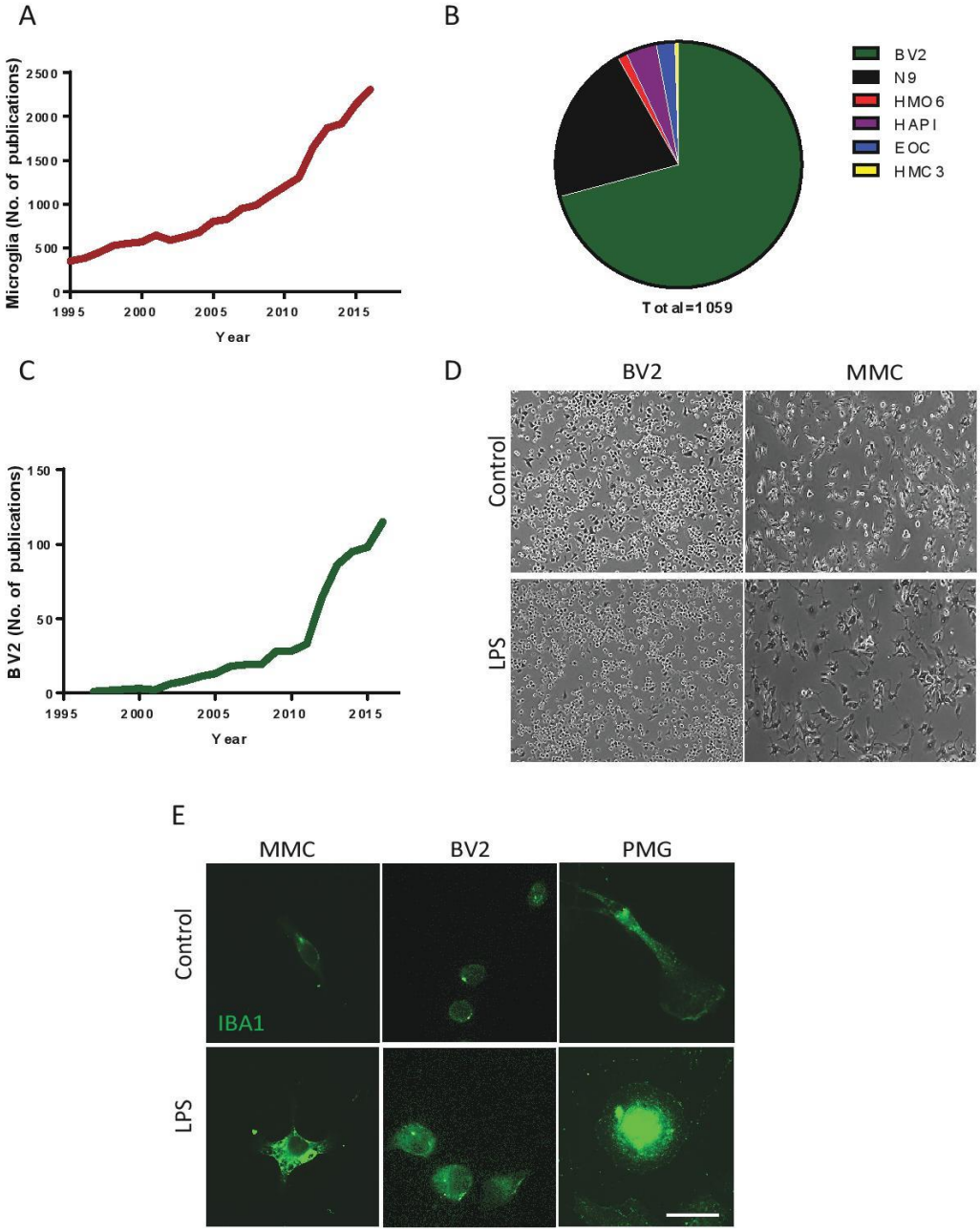

Figure 1: Morphological comparison between the mouse microglial cell (MMC) line, the BV2 cell line, and primary microglia (PMG). A) Number of yearly

publications on microglia in PubMed. B) Distribution of the number of PubMed-indexed publications on various microglial cell lines. C) Number of yearly publications on BV2 microglia in PubMed. D) Phase contrast microscopy of BV2 and MMC after LPS treatment. E) Immunostaining for IBA1 on BV2, MMC, and PMG cells after a 6-h LPS exposure.

Figure. 2

A

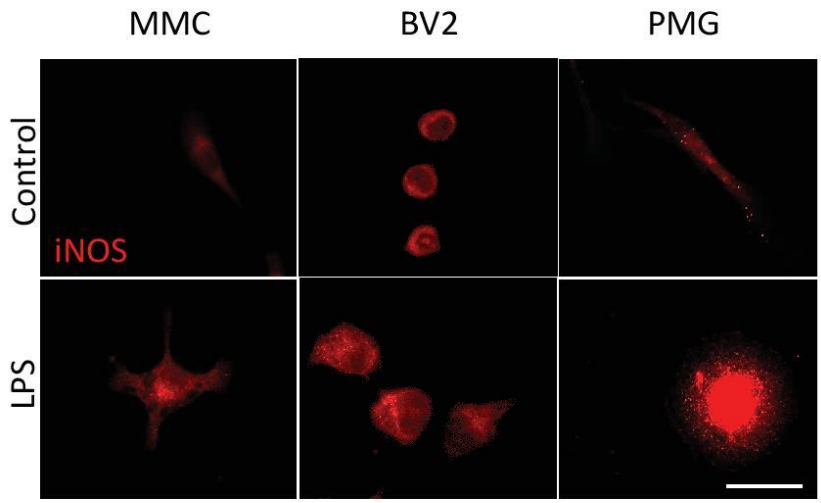

B

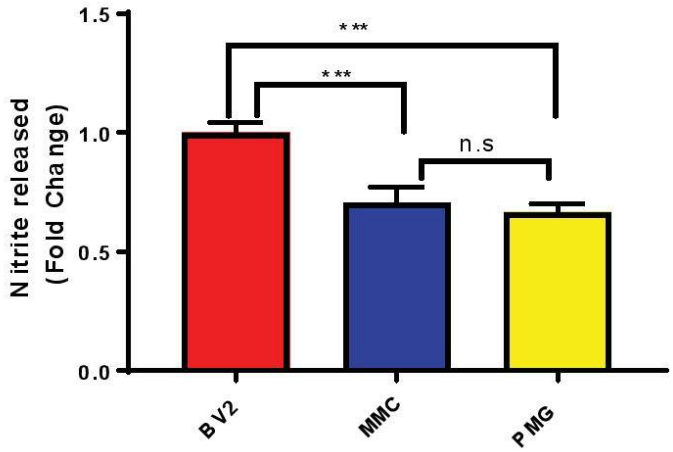

Figure 2: BV2s have higher basal nitrite levels compared to MMCs and PMG. A) ICC analysis showing BV2 cells have higher iNOS level compared to MMC and PMG. B) Griess assay showing BV2 cells produce higher nitrite compared to MMC and PMG. Data analyzed via ANOVA with Tukey post-hoc analysis, ***$p<0.001$. Data represented as mean±SEM with 3-4 biological replicates from 2-3 independent experiments.

Figure. 3

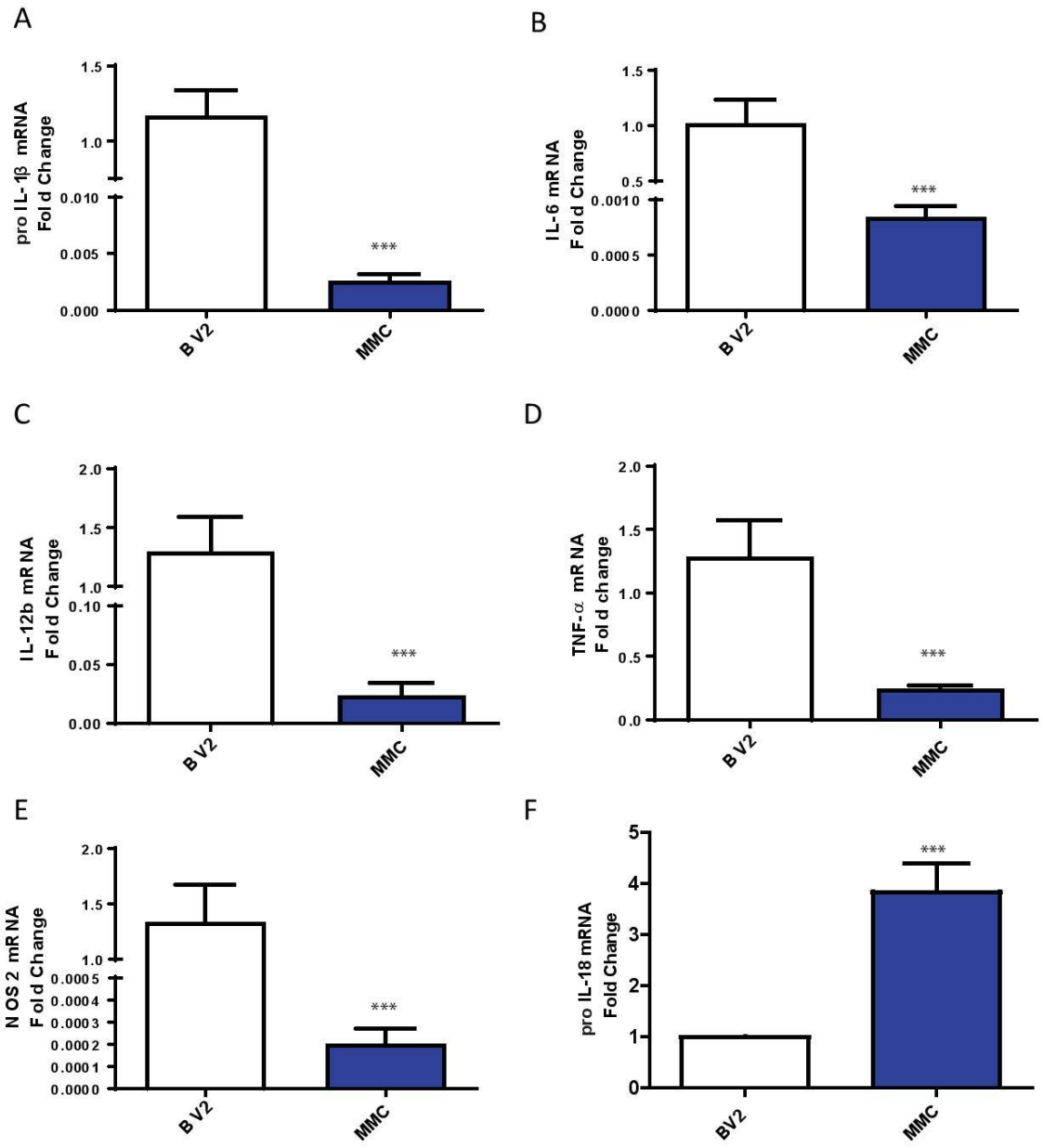

Figure 3: BV2s have higher basal pro-inflammatory factors compared to MMCs. A-F) qRT-PCR analyses of basal levels of A) *pro-IL-1β*, B) *IL-6*, C) *IL-12b*, D) *TNF-α*, E) *NOS2*, and F) *pro-IL-18* in BV2 and MMC. Data analyzed via Student's t-test, ***p<0.001. Data represented as mean±SEM with 3-8 biological replicates from 2-3 independent experiments.

Figure. 4

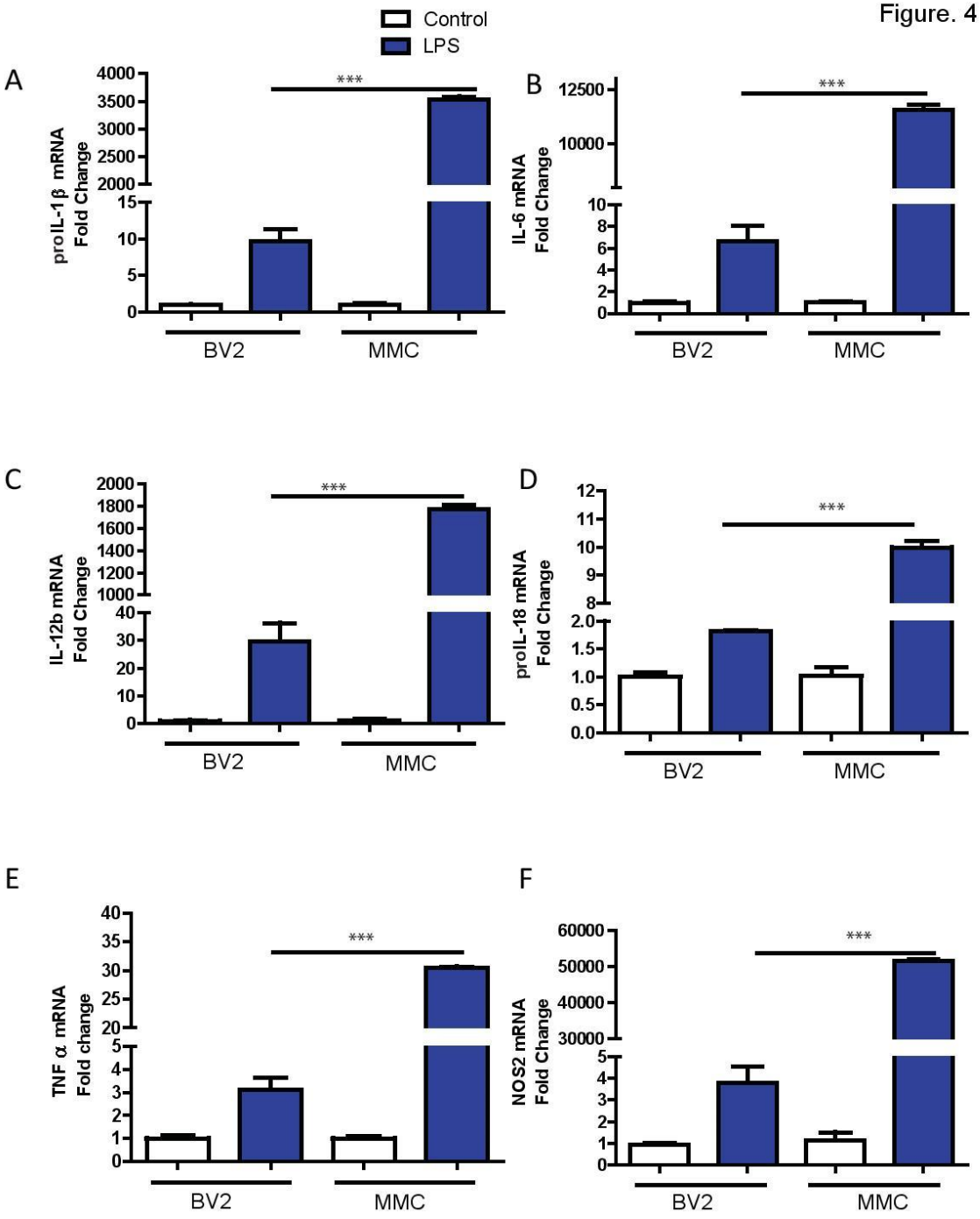
Control
LPS
A
pro IL-1β mRNA Fold Change
4000
3500
3000
2500
2000
15
10
5
0
***
BV2
MMC
B
IL-6 mRNA Fold Change
12500
10000
10
8
6
4
2
0
***
BV2
MMC
C
IL-12b mRNA Fold Change
2000
1800
1600
1400
1200
1000
40
30
20
10
0
***
BV2
MMC
D
proIL-18 mRNA Fold Change
12
11
10
9
8
2.0
1.5
1.0
0.5
0.0
***
BV2
MMC
E
TNF α mRNA Fold change
40
35
30
25
20
5
4
3
2
1
0
***
BV2
MMC
F
NOS2 mRNA Fold Change
60000
50000
40000
30000
5
4
3
2
1
0
***
BV2
MMC

Figure 4: LPS-stimulated pro-inflammatory response is weaker in BV2s compared to MMCs. A-F) qRT-PCR analysis of levels of A) *pro-IL-1β*, B) *IL-6*, C) *IL-12b*, D) *pro-IL-18,* E) *TNF-α*, and F) *NOS2* in BV2s and MMCs 6 h after LPS treatment. Data analyzed via ANOVA with Tukey post-hoc analysis, ***p<0.001. Data represented as mean±SEM with 2-3 biological replicates from 2-3 independent experiments.

Figure. 5

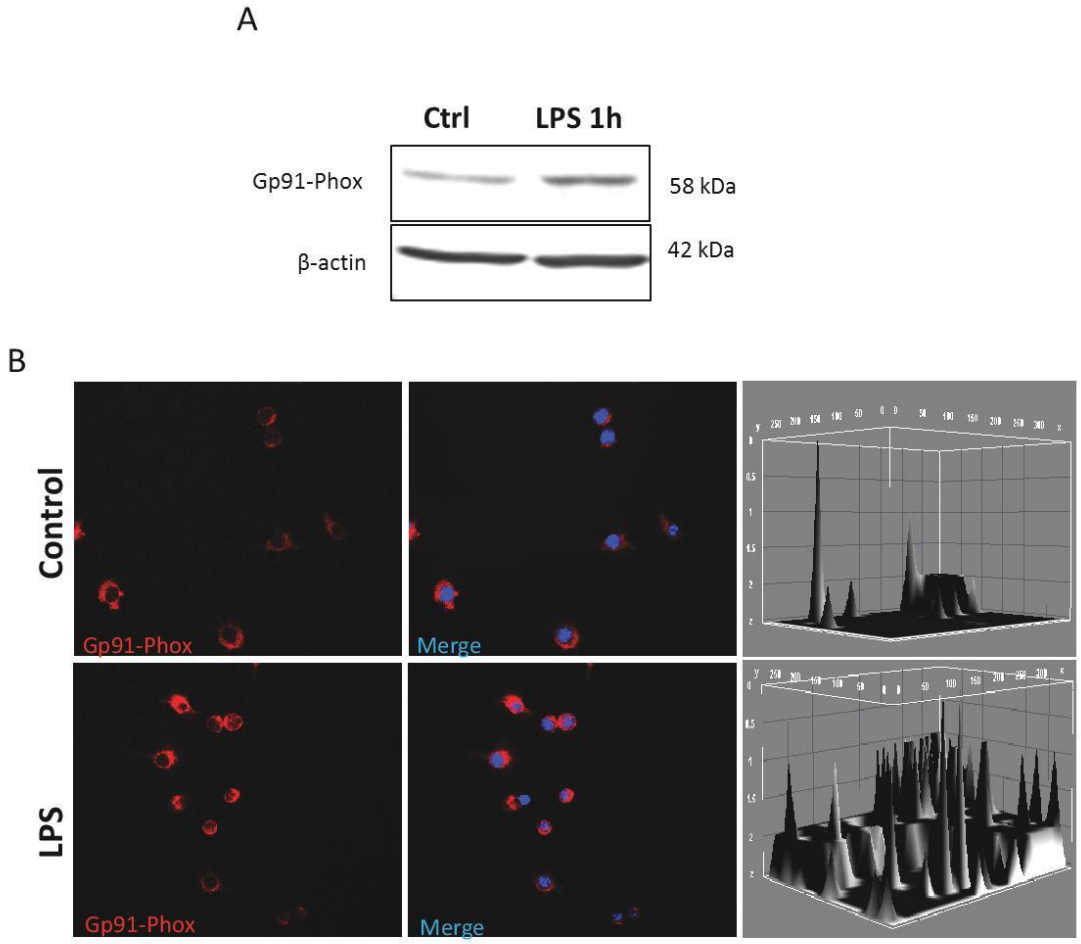

Figure 5: LPS induces gp-91phox in MMC. A) Western blot and B) ICC analysis reveal increased gp91-phox in MMCs following LPS exposure for 1 h.

Figure. 6

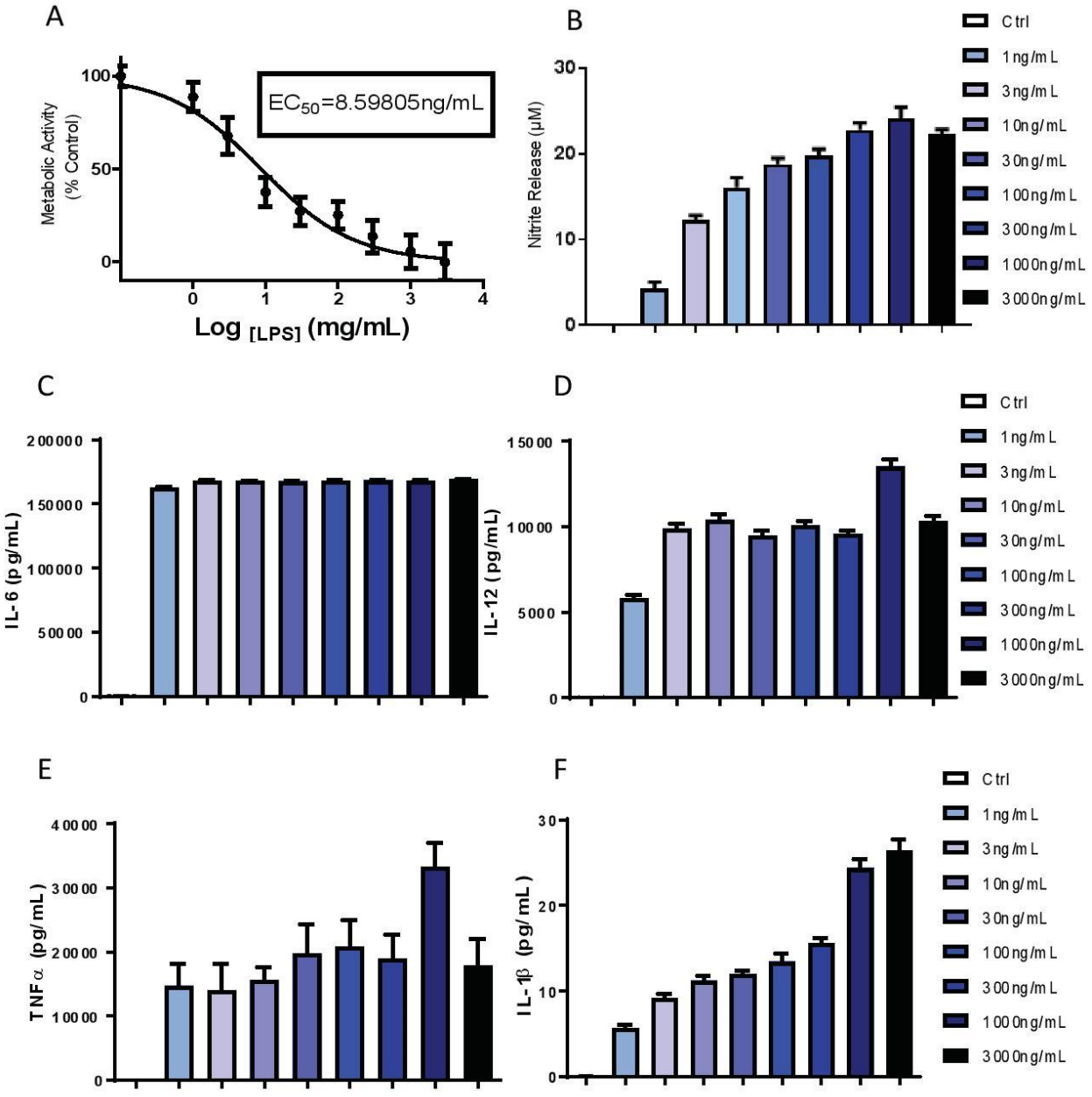
A
Metabolic Activity (% Control)
EC50=8.59805ng/mL
Log [LPS] (mg/mL)
B
Nitrite Release (μM)
Ctrl
1ng/mL
3ng/mL
10ng/mL
30ng/mL
100ng/mL
300ng/mL
1000ng/mL
3000ng/mL
C
IL-6 (pg/mL)
D
IL-12 (pg/mL)
E
TNFα (pg/mL)
F
IL-1β (pg/mL)

Figure 6: MMCs respond to LPS in a dose-dependent manner. A) MTS assay performed on MMCs after treatment with 1, 3, 10, 30, 100, 300, 1000 and 3000 ng/mL LPS for 24 h reveals dose-dependent decrease in metabolic activity. B) Griess assay performed on MMCs after treatment with 1, 3, 10, 30, 100, 300, 1000 and 3000 ng/mL LPS for 24 h demonstrating dose-dependent increase in nitrite release. C-F) Luminex assay performed on MMCs after treatment with 1, 3, 10, 30, 100, 300, 1000 and 3000 ng/mL LPS for 24 h demonstrating increase in secreted C) IL-6, D) IL-12, E) TNF-α, and F) IL-1β. Data analyzed via ANOVA with Tukey post-hoc analysis. Data represented as mean±SEM with 8-32 biological replicates from 3-4 independent experiments.

Figure. 7

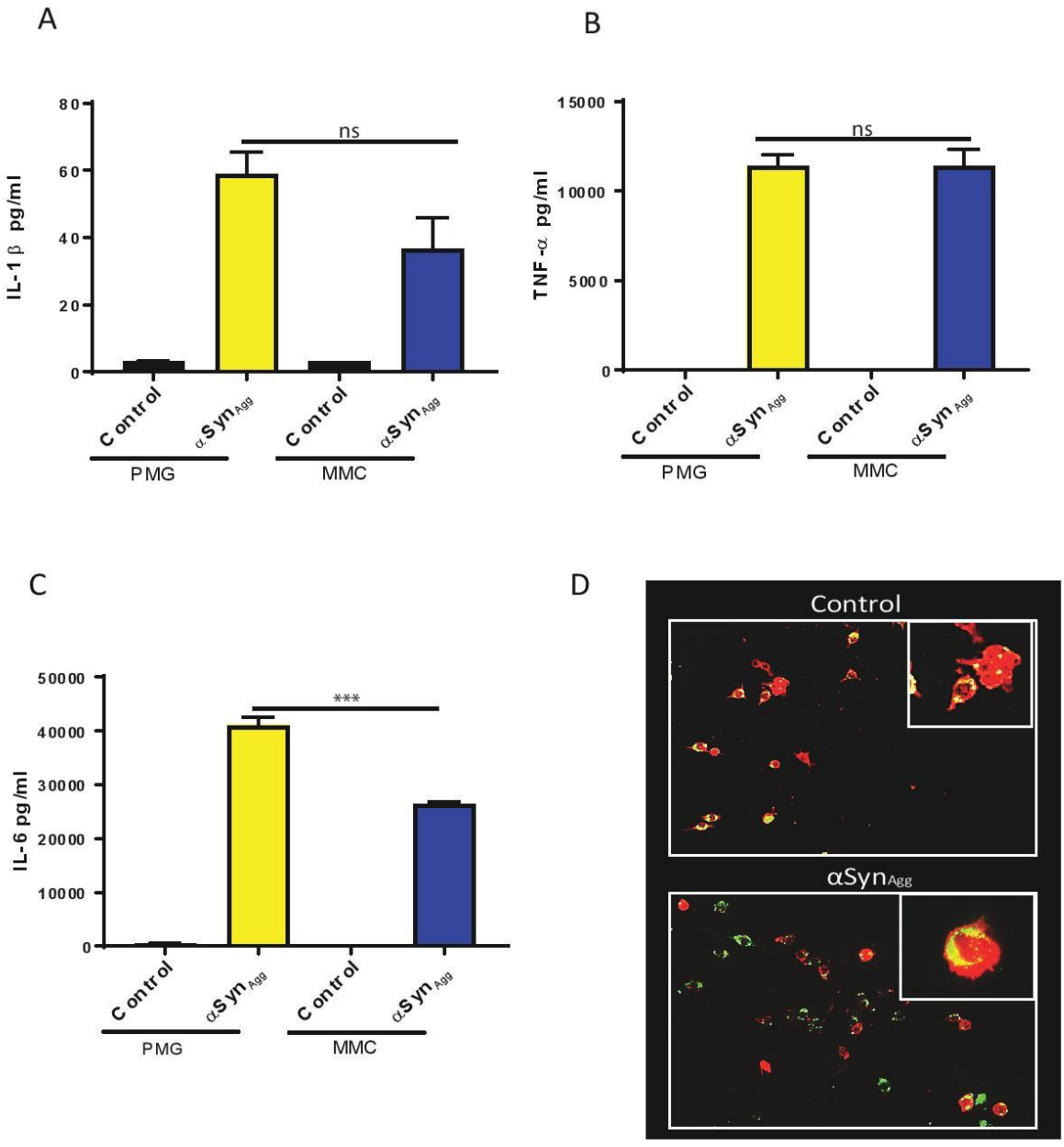
A
IL-1 β pg/ml
80
60
40
20
0
ns
Control
αSynAgg
Control
αSynAgg
PMG
MMC
B
TNF -α pg/ml
15000
10000
5000
0
ns
Control
αSynAgg
Control
αSynAgg
PMG
MMC
C
IL-6 pg/ml
50000
40000
30000
20000
10000
0
***
Control
αSynAgg
Control
αSynAgg
PMG
MMC
D
Control
αSynAgg

Figure 7: αSyn_{Agg} induces comparable pro-inflammatory response in MMCs and PMG. A-C) Luminex analysis of levels of secreted A) IL-1β, B) TNF-α and C) IL-6 in MMCs and PMG 24 h after αSyn_{Agg} treatment. D) Phagocytic activity assay demonstrating that 24-h αSyn_{Agg} treatment intensified phagocytic activity in MMCs. Data analyzed via ANOVA with Tukey post-hoc analysis, ***$p<0.001$. Data represented as mean±SEM with 3-5 biological replicates from 2-3 independent experiments.

Figure. 8

A

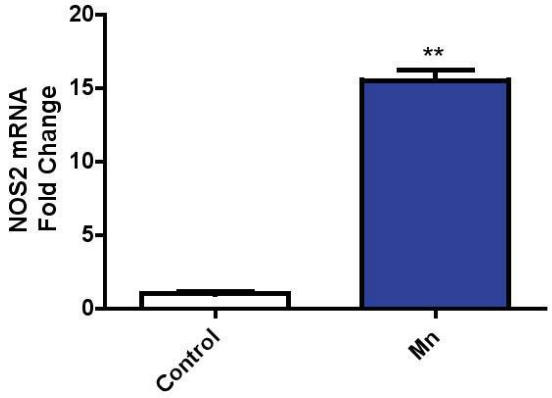
NOS2 mRNA
Fold Change
20
15
10
5
0
**
Control
Mn

B

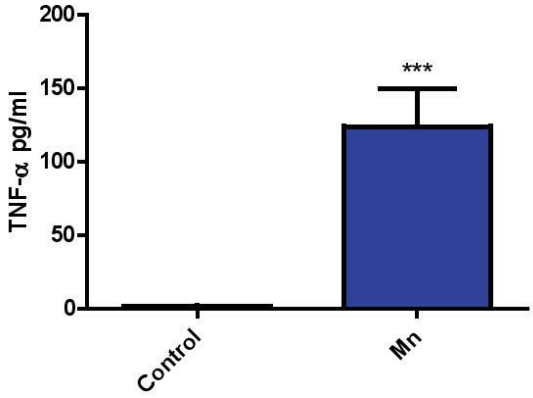
TNF-α pg/ml
200
150
100
50
0
***
Control
Mn

C

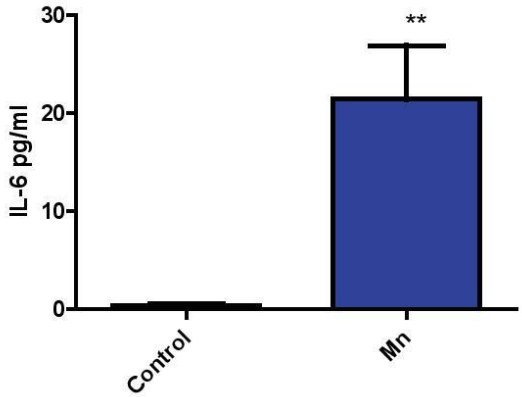
IL-6 pg/ml
30
20
10
0
**
Control
Mn

Figure 8: Mn activates MMCs producing inflammatory factors. A) qRT-PCR analysis of levels of *NOS2* in MMCs 24 h after 100-μM Mn treatment. B-C) Luminex analysis of levels of secreted B) TNF-α and C) IL-6 in MMCs and PMG 24 h after Mn treatment. Data analyzed via Student's t-test, **p<0.01, ***p<0.001. Data represented as mean±SEM with 3-5 biological replicates from 2 independent experiments.